ELECTROFABRICATION OF Ni-BASED ALLOY COATINGS FOR BETTER CORROSION PROTECTION AND WATER ELECTROLYSIS

Thesis

Submitted in partial fulfilment of the requirements for the degree of

DOCTOR OF PHILOSOPHY

by

AKSHATHA R SHETTY

(Reg. No: 155032CY15F01)

DEPARTMENT OF CHEMISTRY

NATIONAL INSTITUTE OF TECHNOLOGY KARNATAKA

SURATHKAL, MANGALURU-575025

February, 2021

DECLARATION

By the Ph.D. Research Scholar

I hereby declare that the Research Thesis entitled '**Electrofabrication of Ni-based alloy coatings for better corrosion protection and water electrolysis'** which is being submitted to the National Institute of Technology Karnataka, Surathkal in partial fulfilment of the requirements for the award of the Degree of Doctor of Philosophy in Chemistry is a *Bonafide report of the research work carried out by me.* The material contained in this Research Thesis has not been submitted to any University or Institute for the award of any degree.

Akshatha R Shetty

Register No. 155032CY15F01

Department of Chemistry

Place: NITK-Surathkal

Date:

CERTIFICATE

This is to certify that the Research Thesis entitled "**Electrofabrication of Ni-based alloy coatings for better corrosion protection and water electrolysis**" submitted by Mrs. Akshatha R Shetty (Register No: 155032CY15F01) as the record of the research work carried out by her, is *accepted as the Research Thesis submission* in partial fulfilment of the requirements for the award of degree of Doctor of Philosophy.

Prof.A.Chitharanjan Hegde
Date:
Research Guide

Chairman- DRPC
Date:

ACKNOWLEDGEMENT

I would like to express my deep gratitude to my research guide Prof. A. Chitharanjan Hegde, Dept. of Chemistry NITK, Surathkal for giving me opportunity to carry out my research work under his guidance. His timely advice, patience guidance, enthusiastic encouragement and useful critiques helped me to grow in all direction. His guidance helped me in all the time of my research and writing of this thesis. I could not have imagined having a better advisor and mentor than him for my Ph.D. work.

Beside of my advisor, I would like to thank my Research Progress Assessment committee members Dr.Darshak R Trivedi Dept.of Chemistry and Prof.Sitaram Nayak, Dept.of Civil engineering for their insightful comments and encouragement. This helped me to gain knowledge in various research perspectives.

My sincere thanks to National Institute of Technology Karnataka, Surathkal for providing all facilities and institute fellowship to carry out my research work.

I would like to thank Prof A Nityananda Shetty and Prof D Krishna Bhat Dept.of Chemistry who gave me permission to access their laboratory equipments.

My Sincere thanks to Head of the department Dr. Arun M Isloor and all faculty members of department of Chemistry, NITK Surathkal for their support during my research journey.

My special thanks to fellow labmates Dr. Sandhya Shetty, Dr. Liju Elias, Miss Cindrella Nishmitha Gonsalves, Mrs. Neethu R, Mr.Yathish and Miss Harshini for always standing by my side and sharing a great relationship as compassionate friends. I will always cherish the warmth shown by them.

A special mention of thanks to my friends Miss Viprabha K, Mr. Harsha Bantwal, Mr. Rajula Rajkumar, Mr.Aranganathan, Mr. Meenakethan Sethi and all my batchmates and many more for their constant support and cooperation during my stay. Their timely help and friendship shall always be remembered.

I acknowledge Mrs. Shamila Nandini, Mr. Prashanth, and Mr. Pradeep, who were always ready to give their timely help whenever required. I must thank office and non teaching staff for their kind support throughout my tenure at NITK.

My deep and sincere gratitude to my Dad Mr. Ramesh Shetty and Mom Mrs. Shantha R Shetty, who formed part of my vision and taught me good things that really matter in life. Their eternal support, infallible love and support has always been my strength. Their patience and sacrifice will remain my inspiration throughout my life. Special thanks to my brother Mr.Akshay Shetty for his continuous love, affection and moral support in throughout my life journey.

I owe my deepest gratitude to my better half and best friend Mr. Pramod K Shetty, for his eternal support, love, affection, encouragement and understanding of my goals and aspirations.

My heartfelt regards goes to my father- in- law Mr. Krishna Shetty, mother-in- law Mrs Sujatha Shetty and brother-in-law Mr.Vinod Shetty for their love and moral support. Above all, I humbly thank God Almighty, who showered the choicest of his blessing to complete this endeavour.

Thank you,

Akshatha R Shetty

ABSTRACT

This thesis titled, ‘*Electrofabrication of Ni-based alloy coatings for better corrosion protection and water electrolysis* ‘details a comprehensive approach for improving the corrosion resistance and electrocatalytic activity of (Ni-Co) and (Ni-Mo) alloy coatings through different advanced electrodeposition techniques. Inherent poor properties of alloy coatings, like corrosion resistance and electro catalytic activity of conventional (Ni-Co) and (Ni-Mo) alloy coatings have been improved by taking the advent of artificial convection of mass transport, by inducing ultrasound and magnetic field effect, during electrodeposition. The properties of sonoelectrodeposited (Ni-Co) coatings are improved further by developing them in multilayers, and by pulsing the ultrasound to go ON and OFF periodically, parallel to the process of deposition. The magneto-electrodeposited (Ni-Co) alloy coatings of higher corrosion resistance were developed by superimposing the magnetic field (B), in both intensity and direction (parallel and perpendicular), while depositing. The corrosion resistance property of electrodeposited (ED), sono-electrodeposited(SED), magnetoelectrodeposited (MED) and multilayer alloy coatings were evaluated in 5% NaCl solution through electrochemical AC and DC methods.The experimental investigation on corrosion behavior of all coatings demonstrated that magnetoelectrodeposited (Ni-Mo-Cd) alloy coating, represented as $(\text{Ni-Mo-Cd})_{6.0/0.3\text{T}}$ is the most corrosion resistant, compared to other coatings.

The electrocatalytic activity of electrodeposited (Ni-Co) and (Ni-Mo) alloy coatings, developed at different current densities (c.d.) were evaluated by alkaline water electrolysis in 1.0 M KOH, using them as both anode and cathode. Electrocatalytic efficacy, in terms of hydrogen evolution reaction (HER) and oxygen evolution reaction (OER) have been studied by measuring quantitatively the amount of H_2 and O_2 evolved. Effect of addition of nanoparticle into the alloy matrix found to increase the electrocatalytic activity of both (Ni-Co) and (Ni-Mo) alloy coatings, and results are discussed.The electro-catalytic efficacy of electrodeposited alloy coatings, having different configurations demonstrated that $(\text{Ni-Mo-CeO}_2)_{2.0\ \text{Adm}^{-2}}$ and $(\text{Ni-Mo})_{2.0\ \text{Adm}^{-2}}$ coatings are the most active electrode materials for HER and OER, respectively. The electrocatalytic kinetic parameters of HER and OER, corresponding to different alloy/composite coatings were evaluated through cyclic voltammetry (CV) and chronopotentiometry (CP) methods. A mutually opposite electrocatalytic activity of both (Ni-Co) and (Ni-Mo) alloy coatings towards HER and OER, with deposition c.d.'s was observed. It was attributed to the change in composition of the alloys, in terms of their constituting metals content, in the deposit.The changed property of alloy coatings, both corrosion and electrocatalytic activity was found to have a close relationship with their composition, phase structure, surface morphology and roughness, confirmed by EDX, XRD, SEM and AFM analyses, respectively. The experimental data are compared, and results are discussed with Tables and Figures, and a note for future work is mentioned at the end.

Keywords: Electrodeposition, (Ni-Co) and (Ni-Mo) alloys, Sono-electrodeposition, magnetoelectrodeposition, corrosion study, electro-catalytic activity

1.11.1 Activation Polarization 23
1.11.2 Concentration Polarization 25
1.11.3 Ohmic Polarization 27
1.12 CORROSION 27
1.12.1 Corrosion Mechanism 28
1.12.2 Corrosion Prevention 29
1.12.3 Corrosion Evaluation Technique 30

CHAPTER 2

LITERATURE REVIEW, SCOPE AND OBJECTIVES 35
2.1 INTRODUCTION 35
2.2 ELECTROCATALYSIS 38
2.2.1Electrochemical water splitting 38
2.3 ELECTRODE MATERIALS FOR WATER ELECTROCATALYSIS...... 38
2.3.1 Electrodeposition as a Tool for Synthesis of Electrode Materials 39
2.4 Ni-Co ALLOY 41
2.4.1 Magnetoelectrodeposition 43
2.4.2 Sonoelectrodeposition 45
2.4.3 Electrocatalytic Study 46
2.5Ni-Mo ALLOY 47
2.5 SCOPE AND OBJECTIVES 50
2.5.1 Scope 50
2.5.2 Objectives 51

CHAPTER 3

RESEARCH METHODOLOGY 53
3.1 INTRODUCTION 53
3.2 MATERIALS AND METHODS 53

3.2.1Chemicals and Materials....53
3.2.2 Surface Cleaning....55
3.2.3 Optimization of Bath....55
3.3 DEVELOPMENT OF ELECTRODEPOSITED ALLOY COATINGS....56
3.3.1 Development of Monolayer Coatings....56
3.3.2 Magnetoelectrodeposition....57
3.3.3 Sonoelectrodeposition....58
3.4 ELECTRODEPOSITION OF COMPOSITE COATINGS....60
3.5 CHARACERIZATIONS OF ALLOY COATINGS....61
3.5.1 Corrosion Study....61
3.5.2 Electrocatalytic Study....61
3.6 GENERAL CHARACTERIZATIONS....63
3.7 INSTRUMENTS/EQUIPMENTS USED FOR THE PRESENT STUDY....64

CHAPTER 4

DEVELOPMENT OF HIGH PERFORMANCE OF Ni-Co COATINGS THROUGH MAGNETOELECTRODEPOSITION....67
4.1INTRODUCTION....67
4.2 OPTIMIZATION OF Ni-Co ALLOY BATH....68
4.3 ELECTRODEPOSITION AND CHARACTERIZATION OF Ni-Co ALLOY COATINGS....69
4.3.1 Compositional Analysis....69
4.3.2 Surface Morphology....71
4.3.3 X-RAY Diffraction Study....72
4.3.4 Corrosion Study....73
4.4 MAGNETO-ELECTRODEPOSITION OF Ni-Co ALLOY COATINGS....76
4.4.1 Potentiodynamic Polarization Study....77

4.4.2 ImpedanceStudy........80
4.5 XRD STUDY........82
4.6 SURFACE STUDY........85
4.6.1 SEM Study........85
4.6.2 AFM Study........88
4.7 DISCUSSION........90
4.7 CONCLUSIONS........92

CHAPTER 5

DEVELOPMENT OF MULTILAYER Ni-Co ALLOY COATINGS FOR BETTER CORROSION PROTECTION BY SONOELECTRODEPOSITION METHOD........93
5.1 INTRODUCTION........93
5.2 SONOELECTRODEPOSITION........95
5.3 SONOELECTODEPOSITION OF MONOLAYER Ni-Co ALLOY COATING........99
5.4 CHARACTERIZATION OF Ni-Co ALLOY COATINGS........101
5.5 RESULTS AND DISCUSSION........102
5.5.1 Optimization of c.d. and p.d........102
5.5.2 SEM Study........105
5.5.3 XRD Study........106
5.5.4 Corrosion Study........107
5.6 SONOELECTODEPOSITION OF MULTILAYER Ni-Co ALLOY COATING........110
5.6.1 Corrosion Study........110
5.8 COMPARISION OF CORROSION BEHAVIORS OF MONOLAYER AND MULTILAYER ALLOY COATINGS........113
5.9 SEM STUDY OF MULTILAYER COATING........115

5.10 CONCLUSIONS..117

CHAPTER 6

ELECTROCATALYTIC BEHAVIOR OF Ni-Co ALLOY COATINGS AND ITS DEPEDENCY ON DEPOSITION CURRENT DENSITY..........................119

6.1 INTRODUCTION..119

6.2 MATERIALS AND METHODS...120

6.3 RESULTS AND DISCUSSION...122

  6.3.1 Electrodeposition of Ni-Co Alloy Coatings..122

  6.3.2 Atomic Force Microscopy Study 123

  6.3.3 Corrosion Stability...124

6.4 ELECTROCATALLYTIC STUDY..127

  6.4.1 Hydrogen Evolution Reaction...127

  6.4.2 Oxygen Evolution Reaction...130

6.5 MECHANISM OF HER AND OER REACTIONS.....................................133

6.6 CONCLUSIONS..134

CHAPTER 7

EFFECT OF CNT ON ELECTROCATALYTIC BEHAVIOR OF Ni-Co ALLOY COATINGS...137

7.1 INTRODUCTION..137

7.2 MATERIALS AND METHODS...138

7.3 RESULTS AND DISCUSSIONS...139

  7.3.1Compositional Analysis 139

  7.3.2 Surface Analysis..140

  7.3.3 XRD Study...142

  7.3.4 Corrosion Stability...143

7.4 WATER ELECTROLYSIS...145

7.4.1 Hydrogen Evolution Reaction..145

7.4.2 Oxygen Evolution Reaction...148

7.5 MECHANISM OF HER AND OER REACTIONS..151

7.6 COMPARISON OF ELECTROCATALYTIC ACTIVITY..........................152

7.6 CONCLUSIONS 153

CHAPTER 8

ELECTRODEPOSITION AND CHARACTERIZATION OF Ni-Mo ALLOY COATINGS...156

8.1 INTRODUCTION..155

8.2 EXPERIMENTAL..156

8.3 RESULTS AND DISCUSSIONS..156

8.3.1 Surface Morphology and Compositional Analyses..................................156

8.3.2 XRD Study..158

8.3.3 Corrosion Stability...159

8.4 ELECTROCATALYTIC STUDY...161

8.4.1 Hydrogen Evolution Reaction...161

8.4.2 Oxygen Evolution Reaction...164

8.6 MECHANISM OF HER AND OER...167

8.7 CONCLUSIONS 168

CHAPTER 9

EFFECT OF ADDITIVES ON ELECTROCATALYTIC BEHAVIOR OF Ni-Mo ALLOY COATINGS..172

9.1 INTRODUCTION...171

9.2 ELECTRODEPOSITION OF Ni-Mo COMPOSITE COATINGS...............172

9.3 RESULTS AND DISCUSSION 173

9.3.1 Compositional Analysis 173

9.3.2 SEM Analysis 174

9.3.3 XRD Study..176

9.3.4 AFM Analysis..177

9.3.5 Corrosion Study 178

9.3.5 Hydrogen Evolution Reaction...180

9.3.6 EIS Study 182

9.3.7 Mechanism of HER Reaction..186

9.4 CONCLUSIONS 186

CHAPTER 10

MAGENETOELECTRODEPOSITION OF (Ni-Mo-Cd) ALLOY COATINGS OF HIGH CORROSION RESISTANCE...190

10.1ELECTRODEPOSITION OF Ni-Mo ALLOY COATINGS........................189

10.1.1Induced Codeposition of Ni-Mo Alloy 189

10.1.2 Potentiodynamic Polarization Method 190

10.1.3 Electrochemical Impedance Study 191

10.2 ELECTRODEPOSITION OF (Ni-Mo-Cd) ALLOY COATINGS.............192

10.2.1 SEM Study..193

10.2.2 Composition Study...194

10.2.3 XRD Study..195

10.2.4 AFM Study 196

10.2.5 Corrosion Study 196

10.3 MAGNETOELECTRODEPOSITION OF Ni-Mo-Cd ALLOY COATINGS

10.3.1 Introduction...199

10.3.2 Magnetic Field Induced Discussion..201

10.3.3 MED of Ni-Mo-Cd Alloy Coating...203

10.3.4 Effect of Induced Magnetic Field 204

10.4 CHARACTERIZATION OF MED (Ni-Mo-Cd) COATINGS....................207

10.4.1 XRD Study..207

10.4.2 Corrosion Study 209

10.4.3 SEM Study..213

10.4.4 AFM Analysis 216

10.5 EFFECT OF INDUCED *B* ON Ni CONTENT...217

10.6 COMPARISON OF ED AND MED COATINGS...219

10.7 COMPARISON OF CORROSION BEHAVIORS.......................................220

10.8 CONCLUSIONS...222

CHAPTER 11

SUMMARY AND CONCLUSIONS

11.1 STRUCTURE OF THE THESIS..225

11.2 EXPERIMENTAL...226

11.3 SUMMARY..228

11.4 CORROSION STUDY OF ALLOY COATINGS…………………………230

11.4.1. Conventional Monolayer Alloy Coatings……………………………..230

11.4.2 Corrosion Behavior of MED, SED and SMD (Ni-Co)Alloy Coatings..231

11.4.3 Corrosion Behavior of (Ni-Mo), (Ni-Mo-Cd) and MED (Ni-Mo-Cd) Alloy Coatings……………………………………………………………..233

11.5 ELECTROCATALYTIC STUDY OF ALLOY COATINGS…………….235

11.6 CONCLUSIONS…………………………………………………………..240

11.7 SCOPE FOR FUTURE WORK…………………………………………….241

REFERENCES……………………………………………………………………243

RESEARCH PUBLICATIONS AND CONFERENCES ATTENDED………267

BIODATA…………………………………………………………………………271

A.LIST OF ABBREVIATIONS

AC	Alternate current
AFM	Atomic force microscopy
c.d.	Current density
CMMA	Composition modulated multilayer alloy
CMA	Composition multilayer alloy
CP	Chronopotentiometry
CR	Corrosion rate
CV	Cyclic voltammetry
CVD	Chemical vapor deposition
DBT	Dual bath technique
DC	Direct current
ED	Electrodeposition
EDL	Electrical double layer
EDX	Energy dispersive X-ray analysis
EIS	Electrochemical impedance spectroscopy
HER	Hydrogen evolution reaction
MED	Magneto electrodeposition
MHD	Magnetohydrodynamic
OCP	Open circuit potential
OER	Oxygen evolution reaction
p.d.	Power density
PVD	Physical vapor deposition
SBT	Single bath technique
SCE	Saturated calomel electrode
SED	Sono Electrodeposition
SEM	Scanning electron microscopy
SMD	Sonomultilayer deposition

wt.%	Weight percentage
XRD	X - ray diffraction
AC	Alternate current

A. LIST OF SYMBOLS

A cm^{-2}	Ampere per centimeter square
A dm^{-2}	Ampere per decimeter square
η_a	Anodic overpotential
i_{pa}	Anodic peak current density
β_a	Anodic Tafel slope
C_{dl}	Capacitance double layer
η_c	Cathodic overpotential
i_{pc}	Cathodic peak current density
β_c	Cathodic Tafel slope
R_{ct}	Charge transfer resistance
i_{corr}	Corrosion current density
E_{corr}	Corrosion potential
δ	Diffusion layer thickness
i_o	Exchange current density
i_L	Limiting current density
C_{B}	Concentration of ions
F_{L}	Lorentz force
B	Magnetic field intensity
R_{a}	Mean roughness
mA	Milliampere
mV	Millivolts
R_{P}	Polarization resistance
R_{q}	Root mean square roughness
R_{S}	Solution resistance
E°	Standard electrode potential
E	Potential

CHAPTER 1 INTRODUCTION

This chapter gives an overview of basic concepts of electroplating technology and various advanced methods of electrodeposition for enhanced alloy properties. It also gives a brief introduction to corrosion and corrosion measurement techniques, with a detailed account on water splitting application.

1.1 ELECTROPLATING TECHNOLOGY

Surface science is an interdisciplinary subject which deals with the study of interfaces of two phases, and finds applications in almost all fields of surface chemistry. Surface chemistry is related to chemical reaction that occurs at the interfaces, and has many applications in the fields, like heterogeneous catalysis, surface science and electrochemistry. Surface science is mainly concerned about the prevention of degradation of surface properties of materials, with effect of time. This can be achieved through an established method, called electroplating, or electrodeposition. The electroplating can be carried out in an aqueous electrolyte near ambient temperature (called aqueous solution electroplating), or in a fused metal salt at high temperatures (called fused-salt electroplating). Generally, by electroplating only surface properties can be modified, without changing the bulk properties. But modern electroplating technology enabled to improve not only the appearance but also to modify the material properties of the coatings. The electroplating can change the surface properties of electrodeposited coatings only if they are compact, nonporous, hard and adherent. Today, electroplating technology is responding in both revolutionary and evolutionary ways due to ever increasing demand in industry. Today, it has turned into an important means for developing nano/micro - structured materials, showing variety of functional properties. Some of the technological areas in which electroplating finds important place are: macro and micro - electronics, optics, opto-electronics, giant magnetoresistance (GMR) and sensors, to name few among many(Schwarzacher 2006).

Electroplating can be defined as the process of depositing the metal/alloy on to the surface of a substrate by electrochemical reduction of metal ions by passing direct current (DC) through their electrolyte solution. Electroplating is generally intended to impart additional surface properties to the substrate. The electrochemical cell is used to deposit material on the surface of electrodes. However, in the case of two electrode cell the reaction are controlled by the current applied between a working electrode (substrate) and a counter electrode (anode). In the three electrode system, a reference electrode is used to control or measure the potential of the working electrode, and deposition is carried out by controlling current/potential. Electroplating finds extensive applications in the field of electronics, protective coating industries, and many other surface engineering fields. Electrodeposition is a process governed by thermodynamics and kinetics aspects, through which the performance of coating materials can be improved/altered for various applications.

The process of electrodeposition is governed by the laws, introduced by Michael Faraday in 1833 and Walter J. Nernst in 1898 (Paunovic and Schlesinger 2000). Since then, techniques of metal and alloy deposition have developed enormously to meet various applications. The process and product of electrodepositions, in terms of the microstructure and their properties are principally governed by mass transfer process towards cathode. This process of mass transfer is mainly controlled by factors, such as current density (c.d.), pH, temperature, convection effect (inside the bath) and the chemistry of bath. There are number of industries, like automobile industry adopts different methods of coatings other than electroplating. They are basically vacuum techniques, like sputtering, chemical vapor deposition (CVD), physical vapour deposition (PVD), sputtering etc. These techniques are not so familiar to practice as electroplating, due to genuine reasons of economy and/or non-flexibility in fixing the conditions and non-reproducibility(Paunovic et al. 2006).

1.2 PRINCIPLES OF ELECTROPLATING

Electroplating is a process of deposition of thin and uniform layer of metal/alloy on the surface of a substrate in an electrochemical cell by passing electricity through the electrolyte solution. An electrochemical cell is schematically shown in Figure 1.1. The electrochemical cell consists of atleast two electrodes (cathode and anode) where electrochemical reaction occur,an electrolyte for conduction of ions and external power source of direct current (DC) to drive the reaction, and the external wire to provide the continuity of the circuit.

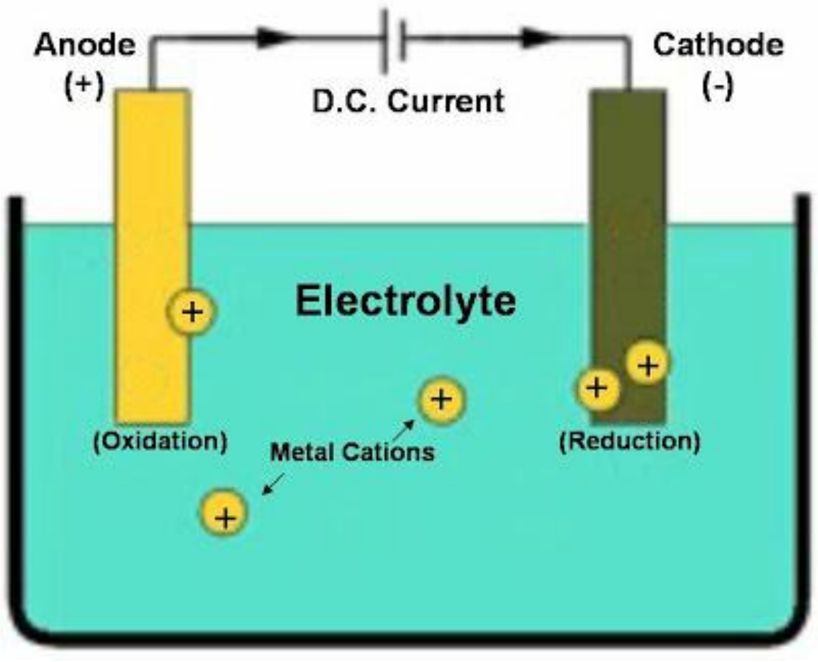

Figure 1.1-Basic components of DC electroplating

The cathode is the one at which reduction takes place (where metal/alloy is deposited); and anode (either a non-metallic conductor such as graphite, or coating metal itself) at which oxidation takes place.The primary purpose of anode is to complete the electrical circuit. As the metal cations are removed from solution as deposit, one or more balancing processes must takes place at the anode to remove anions and thereby maintaining the overall charge neutrality in solution. The anode may or may not fulfil the second function *.i.e.*, to provide a source of fresh metal ions to replace what has been removed from solution by deposition (reduction) at the cathode. When an electric current passed through an electrolyte, having metal ions electrochemical changes will take place at electrode surfaces at the expense of applied current. The cation move towards the cathode where they are discharged, and deposited as metal, or alloy, depending on bath chemistry.

$$M^{2+} + \ 2e^{-} \rightarrow M(lattice) \text{..........} \ (1.1)$$

At the same time, the depleted metal ions near the cathode are replaced by the ions coming from the dissolution of anode (if anode is coating metal).

$$M \rightarrow M^{2+} + 2e^{-} \text{...........................} (1.2)$$

Thus the depletion of metal ions near cathode is just replenished by the metal ions coming from anodic reaction, and thereby maintaining a constant metal ion concentration in the electroplating bath. Thus this overall redox process is known as electrolysis, where electrochemical reaction is taking place at the expense of applied current. However, in case of insoluble anodes such as graphite, stainless steel and platinum, oxidation of water takes place to liberate O_2.

$$2H_2O \rightarrow 4H^{+} + O_2 + 4e^{-} \text{...........} (1.3)$$

Generally, one can find following three main steps during process of electroplating (Paunovic et al. 2006)

i) *Ionic migration,* in electrolyte solution, is movement of hydrated ions towards the diffusion double layer on the cathode surface under the influence of applied potential as well as through diffusion and/or convection.

ii) *Electron transfer,* means that at the cathode surface the hydrated metal ion(s) enter(s) the diffusion double layer where water molecules of the hydrated ion are aligned by the weak field present in this layer. Subsequently, the metal ion(s) enter(s) the fixed double layer, where, due to the higher field present, the hydrated shell is lost. Then on the cathode surface the individual ion is neutralized and is adsorbed.

iii) *Incorporation,* means that the adsorbed atom wanders to a growth point on the cathode and is incorporated in the growing lattice of the electrodeposit.

Advantages of electrodeposited coatings over the coatings obtained from other methods are:

- Electrodeposited coatings have high hardness, good electrical and thermal conductivity, solderability and reflectivity.
- Electrodeposition being an atomistic deposition process, the crystal structures of electrodeposited coatings is fine, whereas in other processes the crystal structures are coarse.

- In electrodeposition the coating thickness can be controlled precisely and reproducibly, whereas in dip coating, like galvanization and other processes, the coating thickness cannot be controlled precisely.
- Thus electroplating is considered as the most reliable method of applying coatings of metals/alloys, having very high melting points such as copper, nickel, chromium, silver, iron, gold and platinum than any other methods.

1.3 ALLOY DEPOSITION

Concept of alloy plating has come into existence in the way of achieving better quality coatings, compared to simple single metal coatings. Chemical reactivity and corrosivity of electrodeposited alloys usually lies between that of the constituent metals. An alloy is usually more reactive than its nobler constituent and less reactive than its baser constituent. However, an exception to the general rule occurs with alloys which are inter-metallic compounds. With advancement of science and technology, many alloys and their composite coatings have been developed for better properties and performances. Electroplated alloy coatings generally satisfies most of the requisites of good electrodeposits, like good appearance, adhesion, hardness, resistance towards corrosion, thermal conductivity etc. Thus an electrodeposited alloy coating shows better properties as compared to either of the parent metals (Slavcheva et al. 2005).The most obvious requirement of alloy codeposition is that the two parent metals have deposition potentials that are close together. However, since there is no generalization covering the proximity of the potentials, this condition is not considered as the principle of alloy plating. Alloy plating can be classified into the following five types: a) Regular codeposition, b) Irregular codeposition, c) Equilibrium codeposition, d) Anomalous codeposition and e) Induced codeposition (Younes et al.2000).

a) Regular codeposition

This type of deposition is characterized by the process which is governed by simple diffusion theory. The regular co-deposition is most likely to occur in baths in which the equilibrium potentials of the metals are not far apart, and with metals that do not form solid solution. This deposition occurs in baths having either simple ions, or complex ions. The percentage of the more noble metal in the deposit is increased by those agencies that increase the metal ion content of the cathode diffusion layer, like increase in the total metal content of the bath, decrease of current density, elevation of bath temperature, and increased agitation of bath.

b) Irregular codeposition

In this type, the effect of plating variables on the composition of the deposit is much smaller than with the regular codeposition. It is mostly likely to occur in complex ion solution. It is related to systems in which deposition is not under diffusion-control. Deposition in these systems is controlled by irregularities of the potentials of metals in solution.

c) Equilibrium codeposition

This is characterized by the deposition from a solution, which is in chemical equilibrium with both of the parent metals. Cu-Bi and Pb-Sn alloys fall in this category. This is the only type of deposition in which the ratio of metal content in the deposit (plated at low current) is equal to their ratio in the solution. The alloys, which do not have equilibrium with the both parent metals, belong to regular or irregular plating systems.

d) Anomalous codeposition

This anomalous type of codeposition, as proposed by Brenner(Brenner 1963) is rather rare, and is frequently associated with the electrodeposition of Zn-M (where M stands for Ni, Co and Fe) alloys, and mutual alloys of iron group metals, like Fe-Ni, Fe-Co and Co-Ni etc. In electrodeposition of Zn-Ni group metal alloys, the wt. % Zn (less noble) in the deposit is much higher than in the bath. However, one would expect to obtain an electrodeposits of nearly pure Ni due to high thermodynamic stability ($E_{Zn}°$ = -0.76 V and $E_{Ni}°$ = -0.25 V). Actually, it is not the case, instead, under most practical conditions; the ratio of the less noble metal (Zn) to the noble metal (Ni) in the deposit is larger than in the bath. This phenomenon is known as *anomalous codeposition*. The phenomena deserve a considerable amount of study, since its explanation would greatly advance our knowledge of electroplating.

e) Induced codeposition

This type of codeposition occurs whenever a harder metals, like molybdenum, tungsten, vanadium and titanium which cannot be deposited alone from simple salt solutions. These metals which do not deposit on their own are called *reluctant* metals. However, these reluctant metals can be codeposited with other metals, like Fe, Ni, Co, Mo and W. Metals which stimulate the deposition of reluctant metals is called inducing metals. The deposition of Ni-Mo, Ni-Ti and W-Co alloys are other examples for this type of codeposition. The effects of the plating variables on the composition of the alloys of induced deposition are more vagaries and unpredictable than the effects on the composition of alloys of any of other types of codeposition.

1.3.1 Faraday's law of electrolysis

The subject of electroplating is based on two fundamental laws of electrochemistry, popularly called as Faraday's laws of electrolysis. It speaks about the extent of deposition/dissolution of a metal determined by the quantity of electricity passed.

i) Faraday's first law of electrolysis : The mass of the substance altered at an electrode during the electrolysis is directly proportional to the quantity of the electricity consumed at the electrode. Quantity of the electricity is the electric charge measured in coulombs.

$$m = \frac{QM}{ZF} \ldots\ldots\ldots\ldots\ldots \quad (1.4)$$

Where 'm' is the mass of the deposit, in grams produced at the electrode; and 'Q' is the electric charge (coulombs) required for the process; M is the molar mass of the substance; F = 96,485 C mol^{-1} is Faraday's constant; z is valance number of ions involved in the reaction.

ii) Faraday's second law of electrolysis: For a given quantity of electric current through different electrolytes, the mass of the metal (m) deposited/dissolved at an electrode is directly proportional to the electrochemical equivalent weight (z) of metal deposited/dissolved.

$$\frac{m_1}{m_2} = \frac{z_1}{z_2} \dots\dots\dots\dots \quad (1.5)$$

1.4 EFFECT OF VARIABLES ON PROCESS OF DEPOSITION

Electrodeposition is a very simple and inexpensive method to impart improved properties to wide range of base metals with great degree of accuracy and reproducibility. Saying that, electroplating is not just a simple dip and dunk process. It is probably one of the most complex processes because of the unusually large number of critical elementary phenomenon, or steps which control the overall process. The most important factors which can influence the process of electroplating are listed below (Luo et al. 2006).

1.4.1 Metal Ion Concentration

During electroplating, generally the metal salt concentration should be kept high as high current density (c.d.) allows high metal content in the solution. In general, a decrease in metal ion concentration decreases the crystal size and results in fine adherent coating films. The low free metal ion concentration, in a strong electrolyte solution of metal compounds can be achieved by addition of either a salt having a common ion, or a complexing agent as in cyanide baths of copper (Brenner A 1963; Parthasaradhy 1989).

1.4.2 Current Density

The current density (c.d.) which is the applied current divided by the surface area, expressed as $Adm^{-2}$is the most important parameter of electroplating, which controls the quality of deposit and the rate of deposition. In general, the raising of c.d. increases the proportion of the readily depositable metal in the deposit. It is an established fact that a periodic change in the cathode c.d. allows the growth of coating with periodic change in the composition, and hence the properties of coatings(Kanani 2004). Therefore, using c.d. as a tool it is possible to develop a cyclic multilayer alloy, or composition multilayer alloy (CMMA) coatings, with great degree of accuracy and reproducibility(Cohen et al. 1983). Variety of multilayer coatings of material properties can be developed from simple electrolytic bath by simple modulation of current. The property of coatings can be varied as function of both pulsing current and thickness of the each layer.

1.4.3 Temperature

The operating temperature is a vital parameter for the consistent performance of any electrolytic bath. Deviations of more than 5^0C from optimum temperature are sufficient to harm plate quality, deposition rate, and other properties. Baths can usually be formulated, however to operate satisfactorily at any given temperature, typically upto 60^0C.For protective coatings, the ability to use higher plating currents with increased deposition rates is of practical importance. While electroplating an alloy, the increase of bath temperature decreases the polarization of nobler metal relatively more than the polarization of less noble metal.

1.4.4 Agitation

The increase of agitation during deposition process has a same effect as the temperature. As can be expected, with bath agitation the effective thickness of diffusion layer diminishes; hence the diffusion rate will increase. This thickness will vary from species to species. A diffusion layer is not formed immediately on turning on the voltage/current. Agitation brings fresh nobler metal ions to the cathode film and decreases the cathode layer thickness, which lead to increase in proportion of nobler metal in the deposit. In case of deposition of alloys, an increase of agitation usually increases the amount of nobler metal in the alloy. The effect of agitation is likely to be less pronounced when the metal ions are in complex ion form, rather than with simple ions; and more pronounced in the case where two or more metals are associated with like anions rather than with unlike anions.

1.4.5 Polarization

Electrochemically, when metal deposition is accompanied by hydrogen evolution, it may be said that one deals with alloy plating in which hydrogen is codepositing element. This is so even when hydrogen is discharged as gas since the conditions for codeposition is met. Alloy plating of metals makes it into a process of production of hydrogen and two or more metals. The evolution of hydrogen during electrodeposition of an alloy has a significant effect on the polarization and composition of the alloy deposited. If a significant amount of hydrogen is evolved, the potential of the cathode during alloy deposition may be determined almost totally by the hydrogen evolution reaction. If, as it is usually the case, over potential for hydrogen evolution is high in the preceding case, the currents corresponding to the individual metals will be close to limiting values. Under these conditions, an increase in the current will increase the amount of hydrogen evolved, resulting in a poor efficiency for alloy deposition with a minor change in the composition of the alloy deposited. Though there are many other variables which can affect the structure and properties of electrodeposits, the above are of greater significance as far as the process and product of electrodeposition is concerned.

1.5 HULL CELL

The Hull cell is a test cell used to check the working conditions of electrolyte, under wide range of current density. This technique was followed to set plating conditions for a given electroplating bath. It gives the information about the effect of current over a range of c.d., effect of amount of salts and additives, pH and impurity of bath solution etc. Hull cell is named after the scientist Richard Hull, who introduced his invention to the industry in 1939.Hull cell, is a miniature plating tank in which the cathode is angled with respect to the anode. The bird view of Hull cell is as shown in Figure 1.2(a). As cathode is inclined to the anode, when a current is applied across the cell, the resulting current will vary along the length of the cathode, as current is a vector quantity. The current is highest on cathode where it is closest to the anode. In this way, one can assess the effect of range of c.d. on the nature of electrodeposit by singe test run. After single test run, the cathode is removed and inspected. At the highest current densities, the deposit may be burnt. At the lowest current densities, no deposition may be observed. Thus the Hull cell test allows the determination of the so-called ‘operating window’ of the c.d. range over which acceptable deposition can be obtained from the given bath.

The Hull cell is basically a trapezoidal container that holds 267 mL of solution in a depth of 48 mm of the cell. Today, Hull cell is made of an insulating material such as Perspex or PVC material, and is shown in Figure 1.2 (b). To carry out the test, the electrolyte is placed in the cell and an anode of 60 × 75 mm size and cathode of 75 × 100 mm (at slanting edge) are positioned as shown in Figure 1.2(a). Using Hull cell, a platter could alter the bath parameters, like chemical constituents, pH and temperature etc., without interrupting the production.

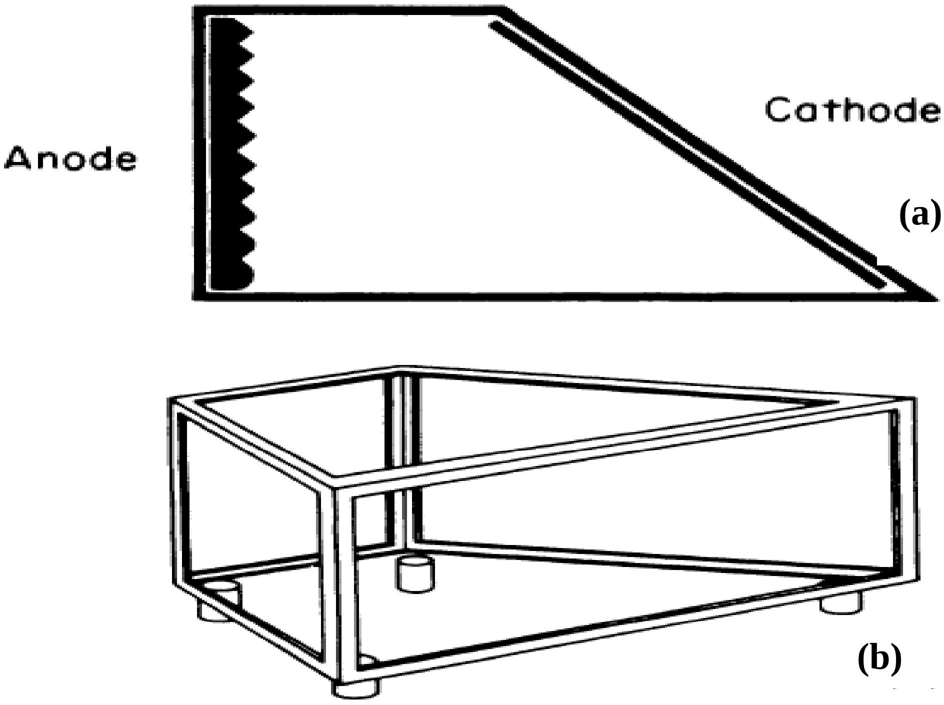

Figure 1.2- Hull cell: (a) top view (b) plan view of 267mL cell

Hull cell can be used to assess any factor that produces a change in the appearance of electrodeposits over a wide range of current densities. The test is simple and quick in execution. In practice, a certain amount of skill in the interpretation of data is required. The Hull cell test is complimentary to an analytical control method and is only method to control the concentration of addition agents (like brighteners, grain refiners, levellers, stress relievers etc.).Hull cell test is a valuable guide to determine the influence of any parameter on appearance of the deposit. It is used to assess the effect of c.d. on number of solution properties like brighteners, burning ranges, levelling, ductility, covering power, throwing power and current efficiency. By taking required electrolytic solution, the deposition can be carried out on cathode at definite cell current, such as 1 A, 2 A or 3 A etc. The corresponding current densities at definite distance from High Current Density (HCD) end can be obtained from Hull cell ruler, shown in Figure 1.3.

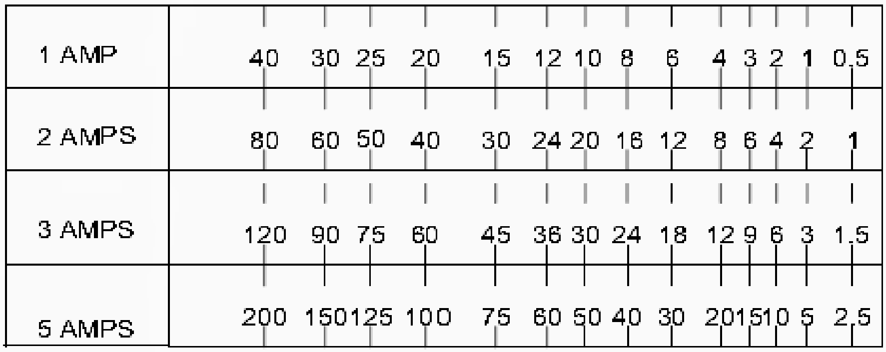

Figure 1.3- Hull Cell Ruler

The c.d. at a given point along the cathode panel can also be calculated using formula,

$$I = C(5.10 - 5.24\, log\, L) \dots\dots\dots (1.6)$$

Where 'I' is the c.d. in A dm^{-2} at any point on the cathode, 'C' is the cell current strength (I) used for the test, and 'L' is the distance in cm from HCD to the point on the cathode at which c.d. is desired to be calculated. Thus, Hull cell is an invaluable analytical tool for preventive maintenance and allowing platters to make corrections before problems to occur in production or to troubleshoot after they have occurred. Regular use of Hull cell saves the time, money and helps to avoid disasters in plating line. Hence Hull cell is one of the most trusted testing devices in modern electroplating even today, because of its simplicity and utility. Knowing the invaluable use of Hull cell, it is said that 'a plater without a Hull cell is like an electrician without a voltmeter (Dini 1993).

1.5.1 Structure of Cathode Diffusion Layer

Generally, in the process of electrodeposition, there will be formation of electrode-solution interface; and its origin is due to the formation of one inner Helmholtz layer containing solvent molecules and specifically adsorbed ions (Bockris 1998) .The structure of the cathode diffusion layer, or cathodic double layer, or electrical double layer (EDL) responsible for changing the properties of electrodeposited metal/alloy coatings is shown in Figure 1.4. According to this, outer Helmholtz plane reflects the imaginary plane passing through the centre of solvated ions at their closest approach to the surface.

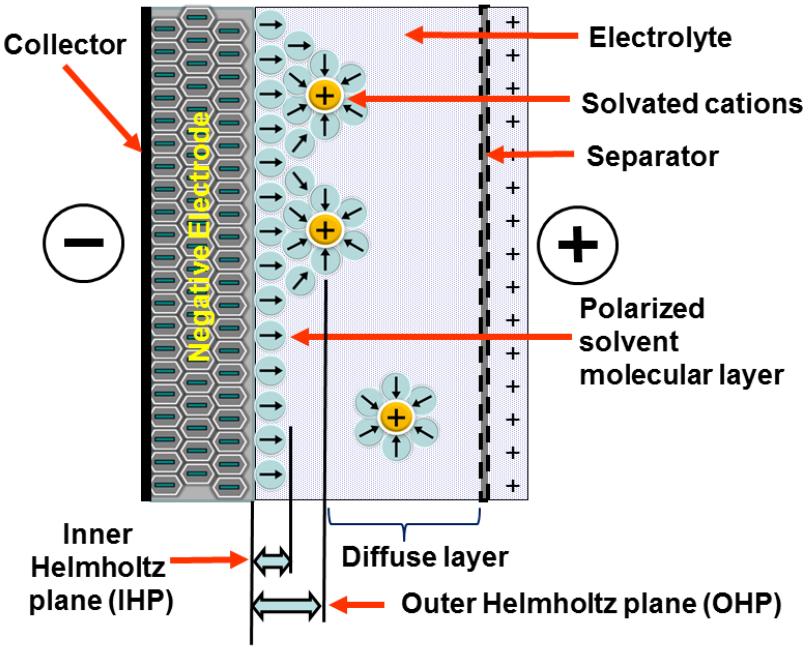

Figure 1.4 - Structure of electrical double layer at a metal/solution interface

The ions and unspecified solvated ions also adsorbed as atoms on the surface of cathode. Hence, there will be formation of double layer and forms electrode-solution interface. This layer is called *Helmholtz electrical double layer*. Transport of metal ions from the bulk solution to the cathode surface is primarily due to the convection and diffusion controlled process. The diffusion of ad-ions to form ad-atoms takes place within the electrolyte double layer, which forms spontaneously metal-solution interface. During electrodeposition process, adsorbed ions will be adsorbed as atoms towards the cathode surface, through the process of nucleation followed by crystal growth. The nucleation process is the result of diffusion of ions. Thus the crystal growth process begins, once the nuclei size reaches a critical size. This process is called electro-crystallization. Hence, phase structure, surface morphology and percentage composition of the electrodeposited coatings are principally determined by the process of nucleation and electro-crystallization. This in fact is mainly depends on the rate of mass transfer process taking place at that cathode diffusion layer. Hence to summarize, the properties of electrodeposited metal/alloy coatings can be changed substantially by modulating mass transport of metal ions towards cathode, by inducing some effects at the electrode-electrolyte (E-E) interface.

1.6 MODERN METHODS OF ELECTRODEPOSITION

Electrodeposition is well known method for tuning the shape of microcrystals, and to control the crystal lattice by changing the composition of coatings. A common method to manipulate crystal habit is to employ a growth medium containing additives that can preferentially adsorb on specific crystallographic planes. The properties of electrodeposited metal/alloy coatings can be improved drastically by changing the mass transport process towards cathode, due to the reasons explained in Section 1.5.1. Thus modulation of mass transport process, near cathode diffusion layer during deposition allows to synthesize new materials showing advanced properties (Tacken and Janssen 1995a). The development of such new materials is driven by following fundamental principles:

- Periodic modulation in mass transport process at cathode brings a periodic modulation in composition of the coatings deposited. This is the basic principle of electrodeposition as well.
- The material property can be increased substantially by increasing the surface area of the coatings, *i.e.*, by layering. The increase of material property with increase of the surface area is basis of nanotechnology.

Keeping in view of the above points, the corrosion resistance of conventional monolayer alloy coatings can be increased by multilayer coating approach. Such multilayer alloy coatings can be accomplished by any of the following methods, by brining modulation in mass transport process during deposition. It can be affected by altering periodically any one of the parameter mentioned below, during plating:

- Cathode current density
- Magnetic field intensity (magnetoelectrolysis, or magnetolysis)
- Agitation (Sono-electrodeposition, or sonoelectrolysis)
- Temperature

Since periodic variation of temperature between two limits, during plating is practically not possible; development of such multilayer coating is far from reality.

1.7 COMPOSITION MODULATED MULTILAYER ALLOY (CMMA) COATINGS

New class of materials with alternate layers, of few nanometer thicknesses of two or more metals/alloys are gaining interest due to their improved properties such as mechanical strength, micro hardness, giant magnetoresistance and corrosion resistance etc. They are generally known as composition modulated multilayer (CMM) materials (Krishnan et al. 2002). These materials basically consist of very thin sub-layers, a few nanometer in thickness, of different metals arranged in an alternate fashion. Schematic representation of CMM coating, having alternate layers of two metals/alloys is shown in the Figure 1.5.One of the reason for interest in multilayer coatings is their enhanced material properties, and today multilayer materials are being considered for protective coatings, as their benefit exceeds that for comparable bulk alloys. With two alternating phases, the resistance to plastic deformation and hardness increase as the individual layer thickness decreases.

Figure 1.5 - Schematic diagram of composition modulated multilayer coating

1.7.1 Methods of Production of CMM'S

There are two approaches to develop multilayer coatings, namely physical method (Dry process) and electrolytic method (Wet process).

a) Dry process

Physical vapor deposition (PVD), chemical vapor deposition (CVD), sputtering and molecular epitaxy techniques are few among many types of physical methods of development of multilayer coatings. Several coating systems have been prepared by PVD method, such as Si/Nb and Co/X where 'X' is either Au or Pd, or Cu. The above methods have several advantages for specific applications. But due to few limitations of above methods, such as high capital cost, high energy cost etc., an alternative method was found. Electrolytic deposition has fulfilled this need, despite of having its own limitations. In this regard, electrodeposition method, called wet process has drawn a great deal of interest among researchers.

b) Wet process

The processes of production of CMM material by electrochemical method, using aqueous electrolyte are called wet process.This process is more advantageous, and equally promising with the added advantage over dry process such as:

- The processing coat is lowand is applicable even to curved and recessed substrates.
- Simplicity of the facility for metal deposition and the mass production. Thick coatings can be deposited (>100 µm) with high deposition rates (upto about 5nm/minute).
- The depositions can be controlled precisely and reproducibly in intended way using advanced power sources.
- Being a cold process, the risk of inter diffusion between the layers is low.

In spite of above advantages, metal finishing processes have some disadvantages such as the range and quality of coating that can be produced is limited due to complicated bath chemistry. Due to high number of variables, process optimization and its control is little complicated. The electrodeposition of many important metals such as Al, Mg, W and Ti from aqueous bath is precluded (Tench et al. 1984),since the reduction potential of metal ion is lesser than that of hydrogen ions having lower current efficiency. Multilayer deposition may be accomplished by two methods, namely, Single Bath Technique (SBT), Dual Bath Technique (DBT).The most common technique for electrodeposition of CMMMs involves the use of a single electrolyte containing two or more metal ions. Pulsed currents or potentials are applied to preferentially reduce one of the metals, so as to form alternating layers of (nearly) pure metallic layers. By maintaining such a difference in metal-ion concentration, the noble material is plated under mass transfer controlled conditions, and the less noble component is deposited under kinetic control. During the period when the less noble component is discharged, the noble component is also co-deposited. However, since the noble metal is always reduced at the mass-transfer-limiting current, a nearly pure layer of the less noble component is obtained. Hence in SBT, it is possible to deposit alternate layers of alloys of same metals, but of different composition using same electrolyte by proper manipulation of deposition of c.d.

In SBT, Substrate is always remaining in the electrolyte and due to which the risk of mutual bath contamination due to substrate transfer is not possible. The major drawback of DBT is substrate transfer, which leads to bath contamination. It also includes different phenomena, such as dissolution, reaction displacement, outside pollution and formation of metal oxides during the intermediate rinsing which can adversely affect the properties of deposits. Hence, SBT technique preferred than Dual bath technique.

1.8 MAGNETOELECTROLYSIS

Magneto-electrodeposition, or magnetoelectrolysis is a method of electrodeposition under the influence induced magnetic field, *B*. The concept of magnetoelectrodeposition is relatively a new approach, and is a subject of interdisciplinary area providing ample opportunities for production of new materials showing unique properties. When magnetic field is applied parallel to the process of electrodeposition, the mass transport of electrolyte ions to the cathode surface is increased, and electrochemical reaction can be modified. The change in the dynamics of electrolyte, due to effect of applied magnetic field is called magnetohydrodynamic (MHD) effect. This MHD effect increases the convection inside the bath, among which the most important is Lorentz force due to the interaction between the magnetic and electric field (maximal when the magnetic field is imposed perpendicular to the direction of the cathodic current), and the paramagnetic force coming from the potential energy possessed by the magnetic dipoles placed in a magnetic field, which acts inside the diffusion layer during a strong concentration gradient in electroactive species due to the electrochemical reactions at the working electrode(Dalton et al. 2018) .The forces involved in magnetoelectrodeposition may be of electromagnetic origin (Lorentz force) and/or magnetic (paramagnetic) depending on the nature of the involved ions. The intensity of these convections varies depending on the relative orientation of the electric fields and imposed magnetic fields, and concentrations of ionic species in the solution.

Basically, magnetoelectrolysis covers four major aspects of electric/magnetic field interactions. They are: i) magnetic field effect on electrolyte properties, called magneto hydrodynamic (MHD) effect, ii) electrolytic mass transport, iii) to a smaller extent on electrode kinetics, and iv) quality of the deposit on cathode (Fahidy et al.,1983).In the recent years, there have been many studies, and numerous theories concerning Magnetoelectrochemistry have been formulated. Analysis of the published studies, investigating the influence of constant magnetic field on chemical reactions allowed finding several types of magnetic field effects. Firstly, electrodeposition, electropolymerization, and some organic reactions occur faster under constant magnetic field. The surface of metal and alloy coatings obtained in the presence of magnetic field is smoother, and their grains are finer. Uniform magnetic field, applied during electrodeposition, improves corrosion resistance of many coatings. Constant magnetic field also accelerates the transport of H^+ to the cathode surface and desorption of hydrogen bubbles. The limiting current density (i_L) of many metals are increased to a large extent as a result of induction of magnetic field during electrodeposition. The effects of constant magnetic field on the process of electrodeposition is not been fully investigated yet. However, experimental investigation revealed that constant magnetic field can be widely used in electrochemistry and electrodeposition industries, to achieve better performance of the coatings.

The magnetically assisted mass transfer, called *magnetoelectrolysis*, is viewed as having usually four levels of actions, as mentioned in the literature. They are effects on interface reaction kinetics, electrolyte properties, deposit structure and mass transport. The first three effects are connected with fundamental physics and can be elucidated through thermodynamics, surface sciences, etc. Although some aspects, like the weak modification of electrolyte properties at moderate magnetic induction, *i.e.*, when $B <$ 1T(Tesla), and the improvement in the quality of deposit were found today, a big effort in the direction of understanding the mechanisms are still to be made.

1.8.1 Lorentz Force

According to the classical theory of particle electrodynamics, a non-interacting charge 'q' moving with velocity 'v' in an electric field of density 'E' and a magnetic field intensity 'B 'experiences a force called, Lorentz force (F_L), and is given by relation,

$$F_L = q(E + v \times B)\ldots\ldots\ldots\ldots\ldots \quad (1.7)$$

Magnetohydrodynamic phenomena arise from the interaction of velocity fields with electromagnetic fields. Since the Lorenz force is capable of producing movement of charged particles, such as ions a magnetic field is applied during electrolysis gives rise to convection of the electrolyte. So, the electromagnetic body force, called Lorentz force results from the vector product of current density 'i' and magnetic induction, B.

$$F_L = i \times B\ldots\ldots\ldots\ldots\ldots\ldots\ldots\ldots \quad (1.8)$$

During electrolysis, this force acts on the moving ions and induces a convective flow of the electrolyte close to the electrode surface. The largest effect of this force, and consequently the largest MHD effect is achieved, when magnetic field is perpendicular to the direction of E. *i.e.*, when the external magnetic field is oriented parallel to the plane of the cathode surface. On the contrary, when a magnetic field is applied parallel to the direction of E. *i.e.*, when the external magnetic field is oriented perpendicular to the plane of the cathode, causes induction of additional convection in the diffusive layer at the electrode surface through the MHD effect. The additional convection enhances creation of laminar flow at the electrode surface, and subsequently a decrease of the diffusive layer thickness. The effect of additional convection during deposition is responsible for change of alloy composition, phase structure and microscopic surface structure; and they may throw effect on the electro-catalytic properties of alloy coatings as well(Mohanta et al.1978). Change in the quality of electrodeposit, due magneto-electrodeposition is affected due to change in the thickness of EDL, limiting current density (i_L) of ions and the rate of mass transfer process. Hence, induced magnetic field exert a strong influence on the composition, phase structure, surface morphology of the coatings by changing the flow patterns of electrolyte.

1.9 SONOELECTROLYSIS

As early as 1930's, the effect of ultrasound in the electrolysis of water was tested, and in 1950s, there was considerable interest in using the effect of ultrasound in electrodeposition, especially in electrodeposition of Ni and Cr. Analytical applications of sonoelectrodeposition was found in the 1960s. In the 1980s, sonoelectrochemistry is focused on studies of polymerization of styrenes and thiophene and also organic sono-electrosynthesis. However, from 1990's subject of sonoelectrochemistry grown as part of applied sciences. Now one can find several review articles on sonoelectrochemistry highlighting its specific applications, in many organic synthesis and electrodeposition (Moriguchi 1934). Ultrasound is defined as the sound with a frequency that is beyond the range of human hearing, and this is generally considered to be above 20 kHz. The part of sonic spectrum which ranges from 20 kHz to 10 MHz is called ultrasound and is mainly divided into three categories ; power ultrasound (20-100 kHz), high-frequency power ultrasound (100 kHz-1 MHz) and diagnostic ultrasound (1-20 MHz)(Peters 1996).When *power ultrasound* is applied to a liquid electrolyte, a number of well-known effects occur that can influence an electrochemical process. In particular,microjetting, or microstreaming can improve the mass transport,thereby thinning of diffusion layers (or Nernst diffusion layer) and generate localized heating. Such benefits have been used to enhance two widely used electrochemical metallization processes,namely, electroplating and electroless plating, which are employed in key industrial sectors(Ma et al. 2012; Peters 1996). This particular phenomenon can effectively used to improve the properties of electrodeposited coatings.

1.10 WATER SPLITTING REACTIONS

Due to ever increasing energy demand in the world against rapidly depleting natural fuels, researchers are looking for production hydrogen energy using simple and efficient electrode materials (Kasai 2014).In this direction, water splitting reaction is a suitable step for renewable energy production, using transition metal-based electrode materials (Wang et al. 2015).Hydrogen and oxygen are considered as good energy carrier as a fuel due to the following reasons: i) it is perceived as a clean fuel, emits almost nothing other than water at the point of use, ii) it can be produced using any energy sources, with renewable energy being most attractive, and iii) it works with fuel cells and together, they may serve as one of the solutions to the sustainable energy source to the ever growing energy cost. Platinum and oxides of ruthenium, iridium are used as best electrode material for HER and OER respectively. However, their high cost impedes them from wide industrial scale applications. Therefore transition metal based alloy materials are the most suitable alternative material for water splitting reactions.

1.10.1 Hydrogen Evolution Reaction

Hydrogen is a cleaner form of energy carrier with high energy density and is considered to be an alternative energy source for fossil fuels. Water splitting and steam reforming are the two methods for hydrogen production. In steam forming process, lot of environment damage will occurs due to the release of green-house gases. Hence, this method is not preferred for production of hydrogen. Hence, alkaline water splitting is a best tool to produce hydrogen, even though it is expensive method. Since, its production uses renewable energy sources and has some advantages, like high degree of purity, simple and green process. Though platinum is the most established electrode material for production of hydrogen, its high cost and scarcity limits its applications in water electrolysis. Hence, iron group metals such as Fe, Co,Ni; and harder metals, like W and Mo are used as best electrode material for hydrogen evolution reaction (HER). In alkaline solution, HER follows three step mechanism, and is as follows:

a) Hydrogen adsorption(Volmer reaction)

$$H_2O + M + e^- \leftrightarrow MH_{ads} + OH^- \dots\dots (1.9)$$

b) Hydrogen desorption(Heyrovsky reaction)

$$MH_{ads} + H_2O + e^- \leftrightarrow M + H_2 + OH^- \dots (1.10)$$

c) Chemical recombination (Tafel reaction)

$$MH_{ads} + MH_{ads} \leftrightarrow 2M + H_2 \dots\dots\dots (1.11)$$

As per equations, Volmer reaction produces adsorbed hydrogen metal surface (MH_{ads}) due to the interaction between metal surface (M) and water molecule. Subsequently, adsorbed hydrogen will reacts with water and it releases hydrogen (Heyrovsky reaction). Finally, adsorbed hydrogen reacts themselves and produces hydrogen (Tafel reaction). The Tafel values decide type of reaction mechanism undergone by the metal surface for hydrogen evolution.

1.10.2 Oxygen Evolution Reaction

The oxygen evolution reaction (OER) is anodic half-cell reaction in electrochemical water splitting, leading to the generation of oxygen gas in the process of electrolysis. Precious metal oxides, such as ruthenium and iridium oxides show the best OER activities, but their scarcity and high costs limited the scalable applications. Hence, other metals have been targeted for development of electrode materials, as OER catalysts. In alkaline media, oxides of elements of first row of the transition metals in the periodic table were found to be the good electrocatalysts for OER(Grimaud et al. 2016). During electrolysis, cathode part involves hydrogen evolution reaction (HER) and the anode part proceeds with oxygen evolution reaction (OER), or oxidation of some chemical fuels. One of the disadvantages of OER is its sluggish kinetics, which made it not suitable for practical use. In acidic media, OER is a four electron-proton coupled reaction, and releases one oxygen molecule. In alkaline media, reaction involves between hydroxide ions, and leads to the formation of oxygen molecule with same number of electrons involved. OER requires a higher energy (higher overpotential) to overcome the kinetic barrier of OER to occur. In the past several decades, the electrocatalytic OER has been extensively studied; and various electrocatalysts have been designed to improve both electrode kinetics and their stability under different electrolyte environments(Suen et al. 2017).Thus transition-metal based, or their oxides based electrode materials have been studied extensively as better electrocatalyst for OER. In acidic and alkaline condition the oxygen evolution reaction is given as below (Eqns. 1.12 and 1.13).

In Acidic condition,

$$2H_2O \rightarrow O_2 + 4H^+ + 4e^- \dots\dots\dots (1.12)$$

In Alkaline condition,

$$4OH^- \rightarrow 2\,H_2 + 2H_2O + 4e^- \ldots\ldots\ldots (1.13)$$

The Ni associated metal atoms such as Mo, Co, Fe and Pt are used as better electrocatalysts for oxygen evolution reaction, as absorptivity of Ni atoms coupled with electronic structure of participating atoms helps the OER.

1.11 ELECTROCHEMICAL POLARIZATION

Electrochemical polarization (usually referred as polarization) is the change in Electrode potential due to the flow of a current. There are three types of polarization(Mc Cafferty 2010) they are:

1) Activation polarization.
2) Concentration polarization
3) Ohmic polarization

The degree of polarization is measured by the quantity, called *overvoltage* (over potential), η is given by the following equation:

$$\eta = E - E_0 \ldots\ldots\ldots\ldots\ldots\ldots (1.14)$$

Where, E is the electrode potential for some condition of current flow and E_o is the electrode potential for zero current flow, also called as open-circuit potential (OCP) or rest potential.

1.11.1 Activation Polarization

When some step in the half cell reaction controls the rate of charge flow, the reaction is said to be under activation or charge transfer control, and activation polarization results. Hydrogen evolution on a metal surface occurs, in three major steps:

$$2H^+ + 2e^- \rightarrow H_2 \uparrow \quad \ldots\ldots\ldots\ldots\ldots\ldots\ldots. (1.15)$$

First H^+ reacts with an electron from the metal to form an adsorbed hydrogen atom, H_{ads}, at the surface.

$$H^+ + e^- \rightarrow H_{ads} \quad \ldots\ldots\ldots\ldots\ldots\ldots\ldots\ldots. (1.1.6)$$

Two of these adsorbed atoms must react in the second step to form the hydrogen molecule

$$H_{ads} + H_{ads} \rightarrow H_2 \ \ldots\ldots\ldots\ldots\ldots\ldots\ldots\ldots. (1.17)$$

A third step requires sufficient molecules to combine and nucleate a hydrogen bubble on the surface. Any one of the above steps can control the rate of reaction and cause activation polarization. The relationship between activation polarization or overpotential η, and the rate of the reaction in terms of anodic and cathodic current density, abbreviated, respectively as i_a and i_c is given by,

$$\eta_a = \beta_a \, log \frac{i_a}{i_o} \quad \ldots\ldots\ldots\ldots\ldots\ldots\ldots\ldots.(1.18)$$

For anodic polarization, and

$$\eta_c = \beta_c \, log \frac{i_c}{i_o} \quad \ldots\ldots\ldots\ldots\ldots\ldots\ldots\ldots.(1.19)$$

For cathodic polarization,

Here, β_a and β_c are Tafel constants for anodic and cathodic reaction, respectively, and i_o is the exchange current density, corresponding to OCP, or overvoltage equal to zero. It is corresponding to the half-cell electrode potential $E_{H^+/H2}$, where reaction is at equilibrium. The rate of discharge of H^+ (forward) exactly balances the rate of ionization of H_2 (reverse). The presence of overpotential suggests the presence of energy barriers (activation energies) $\Delta G_f{}^*$ and $\Delta G_r{}^*$ corresponding to forward and reverse reaction, is given by,

$$\Delta G_f{}^* - \Delta G_r{}^* = \Delta G_{H^+/H_2} = nFe_{H^+/H_2} \ldots\ldots\ldots\ldots.(1.20)$$

On further substitution, one will arrive at the most celebrated equation of electrochemistry known as Butler-Volmer equation.

1.11.1.1Butler-Volmer equation

The Butler-Volmer equation is one of the most fundamental relationships in electrochemical kinetics. It describes how the electrical current on an electrode depends on the electrode potential, considering that both cathodic and anodic reaction occurs on the same electrode. Butler-Volmer dependence of the electrode current (i) on activation polarization overpotential (η), where $\eta = (E - E_{equ})$ is given by relation,

$$i = i_c - i_a = i_o \left\{ e^{\left(\frac{\alpha_a nF}{RT}(E-E_{equ})_f\right)} - e^{\left(\frac{\alpha_c nF}{RT}(E-E_{equ})_r\right)} \right\} \ldots\ldots\ldots\ldots.(1.21)$$

Where E and E_{equ} are the electrode potentials (volts) under conditions of non equilibrium and equilibrium, respectively. i_a and i_c are cathodic and anodic current density, i_o exchange current density, T is the absolute temperature in Kelvin, n is a number of electrons involved in the electrode reaction, F is Faraday constant, R is universal gas constant. α_c is cathodic charge transfer coefficient, and α_a is anodic charge transfer coefficient (both are dimensionless quantity). This form of Butler-Volmer equation is valid when the electrode reaction is controlled by electrical charge transfer at the electrode, not by the mass transfer to or from the electrode surface, from or to the bulk electrolyte. Nevertheless, the utility of the Butler-Volmer equation in electrochemistry is very wide, and it is often considered to be central in the phenomenological electrode kinetics.

1.11.2 Concentration Polarization

At high rates of cathodic reaction, cathodic reduction rates deplete the adjacent solution for dissolved species being reduced. The concentration profile of H^+ ions (in place of M^{+n} ions) is shown schematically in Figure 1.6. Here, C_B is the H^+ concentration of the uniform bulk solution, and δ is the thickness of the concentration gradient in solution. The half-cell electrode potential (HCE) $E_{H^+/H2}$ of the depleted surface is given by the

Nernst equation as the function of H^+ concentration

$$E_{H^+/H_2} = E^{\circ}{}_{H^+/H_2} + \frac{2.303RT}{nF} log \frac{[H^+]^2}{H_2} \dots\dots\dots\dots (1.22)$$

It is apparent that the HCE potential E decreases as H+ is depleted at the surface. This decrease in concentration amounts to the concentration polarization (η_{conc}) and is given by equation 1.23, as a function of current density(Jones 1996).

$$\eta_{conc} = \frac{2.303RT}{nF} \log\left[1 - \frac{i_c}{i_L}\right] \dots\dots\dots\dots\dots.. (1.23)$$

The plot of above equation, in Figure 1.7 (a) shows that η_{conc} is low until a limiting current density, i_L is approached. Limiting current density is the measure of maximum reaction rate that cannot be exceeded because of a limited diffusion rate of H^+ ions in solution. The limiting current density i_L is given by relation,

$$i_L = \frac{nFDC_B}{\delta} \dots\dots\dots\dots. (1.24)$$

Where D is diffusion coefficient of the reacting species, (it may be H^+ ions or any other species). δ is the diffusion layer thickness, C_B is the concentration of the electroactive (limiting) species in the bulk of the electrolyte. Hence, it may be noted that i_L increases with the increase of bulk concentration (C_B), D and high solution agitation, but decreases with δ, as shown in Figure 1.7 (b).

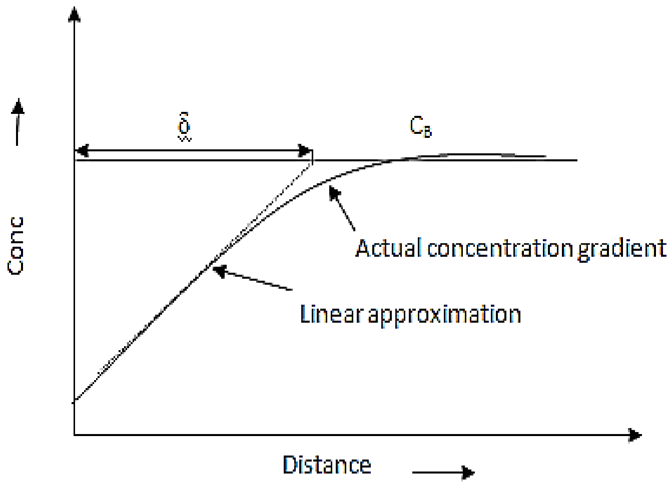

Figure 1.6 – Concentration of H^+ *in solution near a surface controlled by concentration polarization*

The concentration polarization for anodic oxidation, i.e. for corrosion, can usually be ignored due to an unlimited supply of metal atoms at the interface.

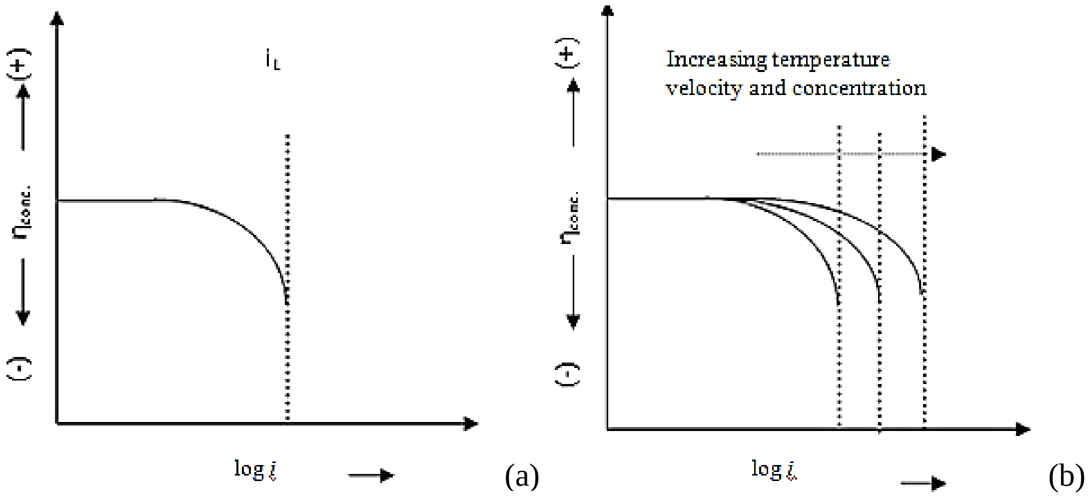

Figure 1.7 – Cathodic concentration polarization: (a) plotted vs. reaction rate or current density, and (b) effect of solution conditions

Some concentration polarization of the anodic reaction is possible at very high corrosion rates or during intentional anodic dissolution by impressed currents (e.g.

electrochemical machining or electrorefining), when rates are limited by transport of soluble oxidation products away from the surface.

1.11.3 Ohmic Polarization

Ohmic polarization results from the pure resistance of elements along the current path within the solution. To minimize error due to such circuit elements, called iR drops, Luggin-Haber capillary tube is generally used. This method alleviates the problem of keeping the reference electrode directly at the electrode-electrolyte interface. The Luggin’s tube, generally used in all electrochemical work. The Luggin capillary and salt bridge connecting the cell and the reference electrode do not carry the polarizing current, and it serves the purpose of reducing the ohmic resistance gradient through the electrolyte between the working electrode and auxiliary/contour electrode. Ohmic polarization is observed either in the region of ionic conductivity, where current is transported by the movement of ions through the electrolyte from the anode to cathode or in the electronic conductivity region. The term iR solution is usually negligible for high-conductivity solutions, such as most aqueous solutions, but can be a problem for low-conductivity solutions, such as organic media, and for some soils. If the iR drop is due to the existence of a surface film on a metal, such as an oxide, hydroxide, oxyhydroxide or salt film, then they are usually understood to be the part of system and the electrode potential is considered to be that for the total system metal/film/solution(McCafferty 2010).

1.12 CORROSION

Corrosion is a natural electrochemical phenomenon, in which pure metal is converted into its most stable oxide or hydroxide form due to its interaction with the environment. Corrosion essentially involves oxidation and reduction reaction. *i.e.*, chemical interaction occurs at the interface of metal and environment. Hence, corrosion is the result of interfacial interaction of the metal with the environment to which it is exposed. Most common examples of corrosion are tarnishing of the silver, brown coloured layer on iron substrate, green deposit formation on copper or brass, loss of shine on aluminium material. In other words, corrosion is the consumption, or dissolution of materials with environment due to the irreversible reaction of materials interfaces with environment. Electroplating is one of the best method to protect the base metal from the effect of corrosion. Credentials of electroplating largely depend on many factors, such as coating thickness, corrosion susceptibility and nature of exposed environment. The rate of corrosion of electrodeposited coatings depends on the composition, surface morphology and phase structure of the materials, alongside the environmental factors such as temperature, nature of reagents and type of corrosive products formed etc.

1.12.1 Corrosion Mechanism

During corrosion, the metal atom from metal surface undergoes oxidation by leaving metal ions into the medium and this step is called anodic reaction. This anodic reaction may be represented as, $M \rightarrow M^{n+} + ne^{-}$.The electrons so left on the metal surface is going to be consumed by the constituent of the environment (either H^{+} ions, or free O_2present) to comply with the conservation of charge to undergo reduction. This reaction is called cathodic reaction. Thus corrosion is a redox process due to effect of both metal and medium (environment).

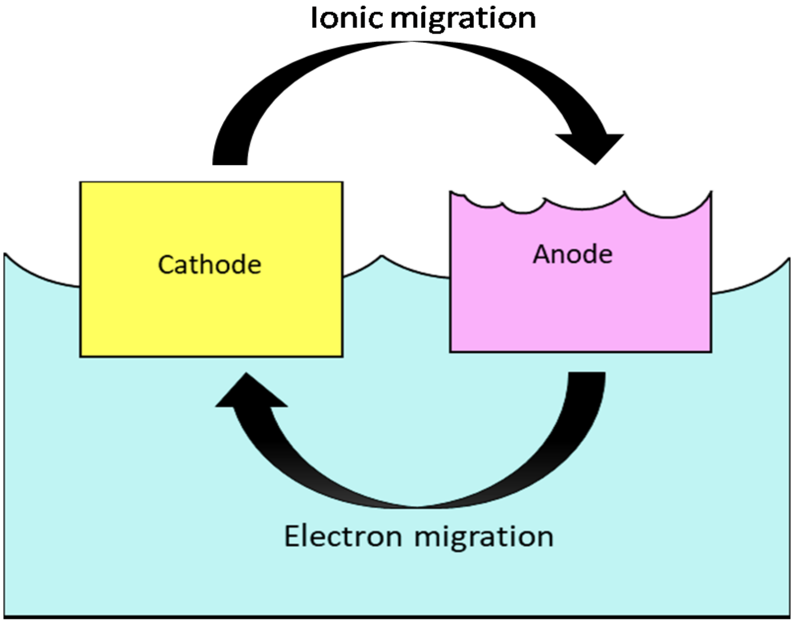

Figure 1.8-Schematic representation of a corrosion process

The process of corrosion may be shown schematically in Figure 1.8. Two reactions, *i.e.*, anodic and cathodic reactions are combined together to form a cell, involving both ionic and electron migrations as shown in Figure 1.8 (Stansbury and Buchanan 2000).Generally, in corrosion process anodic reaction is very simple, where metal atom is transformed into metal ions. But complexity of corrosion lies in the type of cathodic reaction involved. It is determined by several factors, depending on the nature of reducible species present in the environment to which the metal is exposed.

1.12.2 Corrosion Prevention

Corrosion can be prevented by different approaches such as electroplating, applying paint, oil or grease, sacrificial anode method, cathodic protection method etc. One natural way of controlling the corrosion is by use of passive metals. Few metals, like aluminium, chromium and titanium attain a natural passivity, due to interaction of metal with the environmental air, and they form a barrier of thin oxide layer on their surface, which prevents corrosion. Another approach to prevent corrosion is through metallic coating, wherein four types are common. They are: electroplating, mechanical plating, electroless plating and hot dipping. Among these methods, electroplating is the most promising method to control the corrosion of base metal, in terms of both appearance and durability. To achieve higher corrosion stability, binary alloy coatings are extensively used to meet various applications. Nickel and its alloys are found to be the promising materials of today, and are used for wide variety of applications. The majority of which require corrosion and heat resistance, including aircraft gas turbines, steam turbine power plants, medical applications, nuclear power systems, and the chemical and petrochemical industries. Hence, alloy of Ni-based Fe group metals often, have a high hardness, high internal tension and high magnetic properties. In addition to that Ni-based alloy coatings are more compatible for the production of composition modulated multilayer coatings, to achieve better efficacy of corrosion protection. Moreover, Ni-based alloy coatings stay light and brittle with very good corrosion resistant ability, and hence they can be used for decorative purposes as few of them can be coloured. Electrochemical methods of corrosion analyses may be classified into two types depending on the current used. They are:

- Potentiodynamic polarization, or Tafel’s extrapolation method (DC method)
- Electrochemical impedance spectroscopy (EIS), or Alternate Current (AC) method

1.12.3 Corrosion Evaluation Technique

Electrochemical methods of corrosion evaluation are currently gaining popularity among corrosion engineers, primarily due to the rapidity with which these measurements can be made, and secondly the long term corrosion studies, such as weight loss methods will take several days, or weeks to complete. In this regard, electrochemical methods are very quick and precise, and can be completed within few hours. The quickness of electrochemical measurement is of utmost importance, especially for those metals/alloys which are highly corrosive in nature. The traditional weight loss method takes long time, apart from inherent inaccuracy involved in the method. In this regard, electrochemical methods of corrosion analyses are very rapid and results are more accurate. Among electrochemical methods, electrochemical impedance spectroscopy (EIS) method and potentiodynamic (PD) polarization method, or Tafel extrapolation method and are two important techniques used for evaluating the corrosion performance of given material in a known medium (Johnson and Pohlman 1983). The basic principles of EIS and potentiodynamic polarization methods are given below.

1.12.3.1Electrochemical Impedance Spectroscopy

Electrochemical impedance spectroscopy (EIS) method is one of the most accurate characterization techniques available to check the corrosion resistance of a material, and widely used by all researchers. EIS method is a non-destructive type, which uses a three electrode system, controlled by the Potentiostat/Galvanostat. Impedance (an AC analogue of DC resistance) involved in any electrochemical reaction can be studied using set procedure. Modern electrochemical equipments enabled to acquire the data of impedance (Z) over a wide range of frequencies. The EIS method involves applying of AC potential to an electrochemical cell, and then to measure its current response in the cell. Then the value of time dependant resistance, called impedance (Z), written as $Z = V_{(t)}/R_{(t)}$may be determined over a range of AC frequency. EIS method is the most sought after technique to understand the mechanism of corrosion, electrochemical reactions in fuel cells, batteries or any electrodic reaction, in general.EIS has been used to study the corrosion behaviour of the materials. To make EIS measurements, AC voltage of small amplitude (between 5 to 50 mV) is applied at the interface of the test specimen over a range of frequencies of 10 mHz to 100 KHz. When sinusoidal potential excitation is made, the response to this potential is an AC current signal. This current signal can be analyzed as a sum of sinusoidal functions. The excitation potential or AC voltage can be expressed as a function of time, given by:

$$E_t = E_o \sin(\omega t) \ldots\ldots\ldots\ldots\ldots\ldots\ldots..(1.25)$$

Where, E_t= Potential at time t,E_o= amplitude of voltage and ω=radial frequency

The relationship between radial frequency ω (expressed in radians/second) and frequency *f* (expressed in Hertz) is:

$$\omega = 2\pi f \ \ldots\ldots\ldots\ldots\ldots\ldots\ldots\ldots.(1.26)$$

The response to the AC voltage is given by

$$I_t = I_o \sin(\omega t + \varphi) \ldots\ldots\ldots\ldots(1.27)$$

Where, I_t= response current, I_o= amplitude of current and φ = phase shift

For AC current, the Ohm's law can be represented as given below:

$$Z = \frac{E_t}{I_t} = \frac{E_o \sin(\omega t)}{I_o \sin(\omega t + \varphi)} = Z_o \frac{\sin(\omega t)}{\sin(\omega t + \varphi)} \ldots\ldots\ldots\ldots\ldots\ldots..(1.28)$$

It may be noted here that impedance Z is AC analogue of DC resistance. For applied AC, the behaviour of pure resistor is same as DC. But in the circuit elements, like capacitor and inductor, the current phase leads and lags by 90° respectively. This leads to the concept of capacitive and inductive reactance.

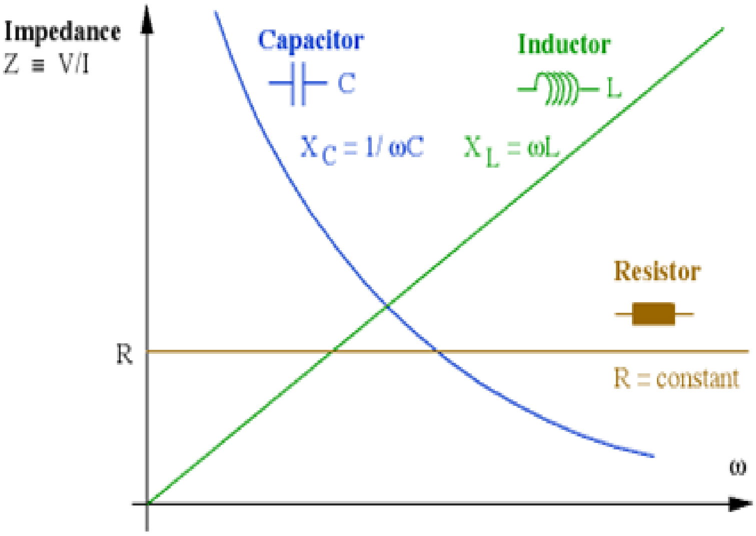

Figure 1.9-Impedance response of C, L and R to AC over range of frequency

The impedance response of a capacitor (C), inductor (L) and resistor (R) to AC, over range of frequency is shown in Figure 1.9. In EIS method, Nyquist plot is one of the popular approach for evaluating ac impedance data. This approach is also known as Cole-Cole plot or a complex impedance plane diagram, as is shown in Figure 1.10. Here, the imaginary component of impedance (*Z''*) is plotted versus the real component of impedance (*Z'*) at each excitation frequency.

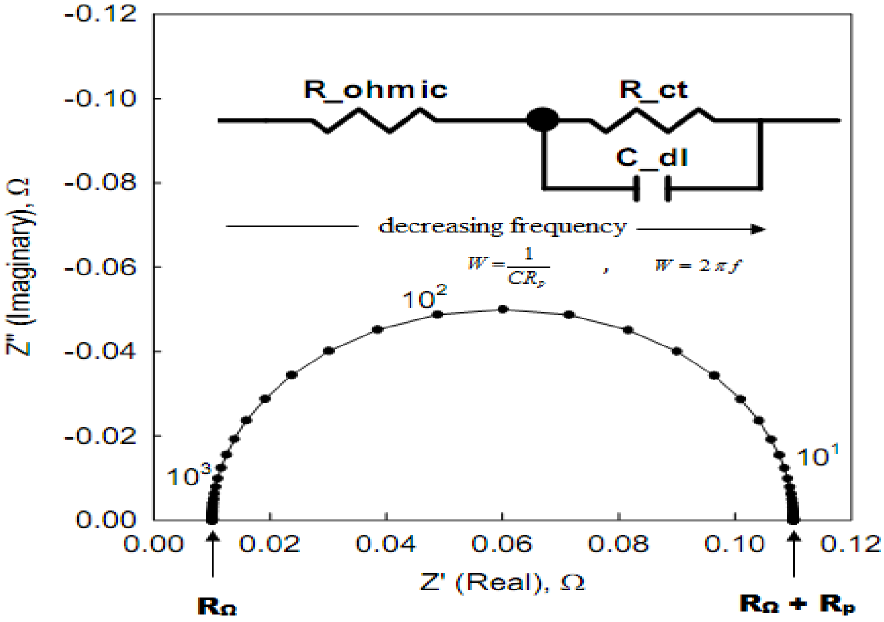

Figure 1.10-Representative Nyquist plot showing frequency dependent impedance response, having solution resistance R_s *and polarization resistance* R_P.

At high frequencies only the uncompensated resistance contributes to the real portion of impedance, while at very low frequencies the polarization resistance (R_P) contributes to the value of impedance. On the other hand, the ohmic resistance, or solution resistance (R_Ω) will be constant to all frequencies. This is consistent with the fact that R_p can also be measured by the DC technique while R_Ω cannot. The polarization resistance can be used to calculate the corrosion rate of test electrode in a given medium.

Advantages of AC technique over DC technique

i) AC impedance spectroscopy techniques use very small excitation amplitudes, usually in the range of 5-10 mV peak-to-peaks. Excitation amplitudes of this order perturb the electrochemical test system to a minimal, and thus reduces errors caused by the measurement technique itself.

ii) Since AC impedance measurements provide data on both electrode capacitance and charge transfer kinetics, the technique can provide valuable mechanistic information.

iii) The AC impedance technique does not involve potential scan, and hence can be applied even to low conductivity solutions, but DC techniques are subject to serious potential control errors.

iv) Although AC impedance measurements offer a great deal of information, it requires in depth knowledge in the field to interpret the data and extract meaningful results from famous Nyquist plots and Bode's phase angle and magnitude plots.

1.12.3.2 Potentiodynamic polarization study

Potentiodynamic polarization method is commonly used find the corrosion rates of a test material, interms of its potential and current (E-I) relationship. A typical potentiodynamic polarization behaviour (Tafel's plot) of test specimen is shown in Figure 1.8. In this method, both anodic and cathodic reactions are allowed to take place by applying the potential, on dipping the test specimen in aqueous corrosive environment. However, the corrosion rate is determined by Tafel extrapolation method. A potentiodynamic polarization experiment typically starts at a potential about 250 mV negative to the OCP, and scans upward through the potential of zero current (which might be different than the original OCP) to a value that is about 250 mV positive to the original OCP. The line describing the behaviour in the Tafel region can be extrapolated to the corrosion potential to determine the corrosion rate. The rate of polarization in a potentiodynamic scan is typically between 0.1 and 1 mV s^{-1}. The linear portion of the curve in cathodic direction from OCP is called anodic Tafel slope, represented by β_a. The slope of the linear portion of the polarization curve towards anodic side is called cathodic Tafel slope, represented by β_c. The curve shows that for an active metal, as the electrode potential is made more negative, or as the solution becomes more oxidizing, the metal dissolution increases. The cathodic branch of the polarization curve is the solid line at more negative potential than the

OCP; a cathodic current to the metal specimen is measured. As the potential is made more negative, the rate of the reduction reaction increases. The total anodic and cathodic polarization curves corresponding to hydrogen evolution and metal dissolution are superimposed as dotted lines. To determine the corrosion rate from such polarization measurements, the Tafel region is extrapolated to the corrosion potential, as shown in Figure 1.8.

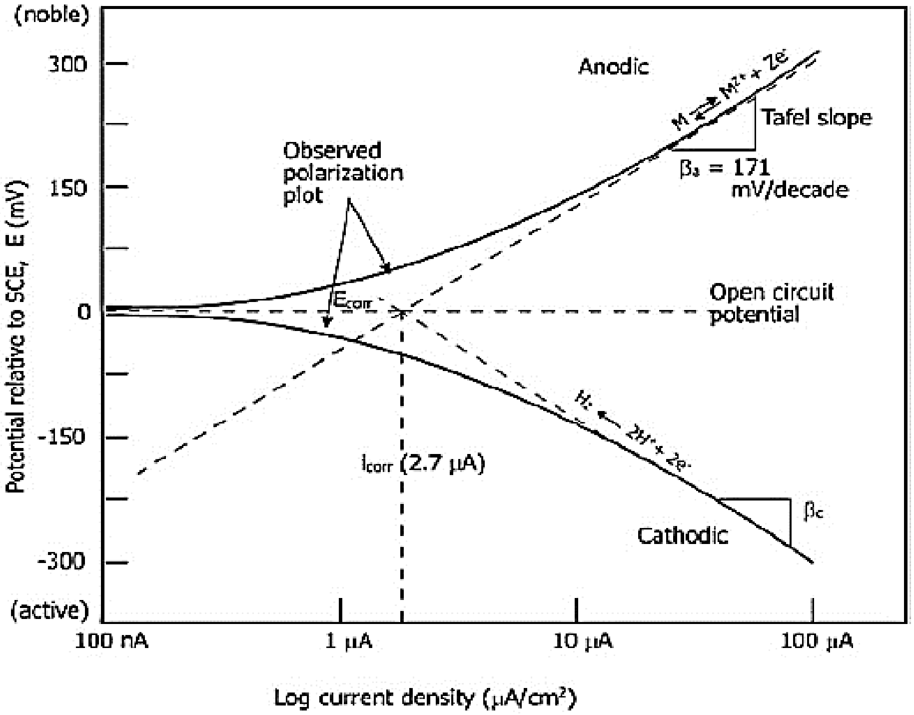

Figure 1.8 – A typical potentiodynamic polarization plot showing different corrosion parameters, like corrosion current ($i_{corr,}$) corrosion potential (E_{corr}),anodic slope (β_a) and cathodic slope (β_c)

The corrosion rate (CR) of a test specimen may be calculated, knowing corrosion current (i_{corr}), obtained from potentiodynamic polarization study, using the Eqn. (1.29).

$$CR = K \times \frac{E}{D} \times i_{Corr} \quad \ldots\ldots\ldots\ldots\ldots\ldots\ldots\ldots\ldots\ldots\ldots\ldots\ldots\ldots\ldots\ldots\ldots. \quad (1.29)$$

Here, CR is expressed of milli meter per year (mmy^{-1}), Where K=0.00327 E = Equivalent weight of the alloy, D= density of alloy under study and, i_{corr} =corrosion current density in μAcm^{-2}

CHAPTER 2 LITERATURE REVIEW, SCOPE AND OBJECTIVES

This chapter covers the literature review on electrodeposited Ni-based alloy coatings, of both binary and ternary alloys and their applications in both corrosion prevention and electrocatalytic activity. Advancement in the area of modern methods of electrodeposition, namely magneto-electrodeposition and sono-electrodeposition were also reviewed. Based on the available information in the field of electrodeposited Ni-based alloy coatings, the scope and objectives of the thesis is stated, at the end of chapter.

2.1 INTRODUCTION

Electroplating is the most time-tested method to protect the active metal surface from the effect of corrosion, in addition to impart a decorative look. Electroplating bath generally composed of different constituents, namely metal salts, brighteners, additives, complexing agents etc. Prior to electrodeposition, the prepared electrolyte is filtered for removal of insoluble impurities. Electroplating is intended to improve a wide range of surface properties, not inherently belongs to the base material. The different benefits of electroplating include increased corrosion resistance, improved hardness, superior strength, resistance to wear, improved ductility. Nickel is considered in electroplating since it provides superior ductility, corrosion resistance, and hardness. Electro nickel plating can also improve a product's brightness and external appearance. Also, Nickel is versatile in nature and readily forms an alloy with most of the metals. Nickel is one of the most common metals in electroplating, as electroplated Ni-based alloy coatings can provide superior ductility, corrosion resistance, and hardness, brightness and aesthetic appearance. Even though electrodeposition of single metal Ni has its own advantages, compared to many other non-noble metals, electrodeposited Ni-based alloy coatings were found to exhibit much better property, compare to its single metal coating. Nickel and its alloys are found to be the promising materials of today, and are used for wide variety of applications, the majority of which require corrosion and heat resistance, including aircraft gas turbines, steam turbine power plants, medical applications, nuclear power systems, and the chemical and petrochemical industries.

In this regard, Ni can be alloyed with other metals, like Co and Mo to achieve better properties of their coatings. These Ni- M (where M = Co or Mo) alloy coatings were found to show a wide variety of applications, in areas such as aerospace, military/defense, electronics/electrical, industrial motors, manufacturing, micro-tools, micro-sensors, electronic imaging, electrochemical energy conversion etc.

The electrodeposited metal/alloy/composite coatings are widely used for the corrosion protection of the base material. The coatings provide a layer that changes the surface characteristics of the bulk material onto which it is deposited. They provide a barrier between the corrosive environment and the substrate. Several protective metallic coatings like Cu, Bi, Zn, Sn, Cd etc. have been reported to protect easily corrodible substrates (Brenner 1963). Copper and nickel are examples for cathodic coatings, which are chemically less active than steel. In salt solution, the metallic coatings provide a durable, corrosion resistant layer. Such protective coatings of a given thickness need much longer time to deteriorate than an equivalent thickness of the steel substrate, due to its less reactivity than steel (Brooman 2000).The metallic protective coatings can serve either as noble coatings, which provide only barrier protection, or as sacrificial coatings, in addition to barrier protection which can also provide cathodic protection. From corrosion protection point of view, not only metallic coatings but also their alloy coatings show better resistance towards corrosion. Many electrodeposited alloy coatings based on Zn, Ni, Fe etc. have been reported for their good corrosion protection efficiency, in different environments (Masdek and Alfantazi 2010). The Ni and its alloy coatings are found to be the promising materials of today, and are used for wide variety of applications including aircraft gas turbines, steam turbine power plants, medical applications, nuclear power systems, and the chemical and petrochemical industries (Akiyama and Fukushima 1992; Brooman 2000).Alloys of iron-group metals (Fe, Co, and Ni) with other metallic or non-metallic elements such as P, Mo and W, are widely used in industries owing to their unique properties like high corrosion resistance, (Akiyama and Fukushima 1992),(Donten et al. 2000)(Sakai et al. 2006) high hardness(Mahalingam et al. 2007), brilliant luster for decorative purposes(Brenner 1963) ,electrocatalytic activity for hydrogen evolution(Paseka and Velicka 1997),(Burchardt 2000) and interesting magnetic properties. The alloy coatings such as Ni-Co(Wang et al. 2005) Ni-Mo(Donten et al. 2000; Sakai et al. 2006), are being considered to replace conventional hard chromium deposits(Gawne and Ma 1988), as they are remarkably hard compared to pure nickel coatings(Brenner 1963) .

Recently, electrodeposition of Ni-based alloys with transition metals such as Mo or W has taken importance due to their enhanced surface performance properties. Apart from the Ni- based alloys, their composite coatings are also reported to be effective in terms of corrosion resistance(Spyrellis et al. 2009). The composites of Ni and its alloys obtained through the incorporation of various nanoparticles like Al_2O_3(Webb and Robertson 1994), (Steinbach and Ferkel 2001), TiO_2 (Li et al. 2002),CNT (Xu et al. 2016)etc., are found to show enhanced material properties in terms of corrosion resistance. Since the electrodeposited composite coatings can impart the combined advantages of metal/alloy and hard nanoparticle inclusions, nanocomposite coatings show properties superior to their metal/alloy counterpart(Li et al. 2017).Further, the corrosion resistance of the alloy coatings can be enhanced through modern methods of electrodeposition such as multilayer, sono-electrolysis and magnetoelectrolysis approaches. A wide variety of binary and ternary alloys have been electroplated as multiple-layer films through CMM approach, including Ni-Co, Zn-Ni, Ag-Pd, Cu-Ni-Fe, Cu-Ag, Cu-Co, Cu-Pb, Cu-Zn, Ni-P/Ni-Co-P, and Ni/Ni-P to name a few (Simunovich et al. 1994)(Yogesha et al. 2011). The CMMA coatings were found to have manyfold improvement in corrosion resistance compared to their monolayer counterparts(Roy 2009). Fahidy (1983) reported the importance of magnetoelectrolysis in various applications, later many reports came on the magnetic field effects on electrodeposition. Many researchers utilized MED to improve the material properties of the electrodeposited alloy coatings (Taniguchi et al. 2000),(Aaboubi and Msellak 2017).

2.2 ELECTROCATALYSIS

Electrocatalysis is the term used to indicate the catalysis of electrode reactions. This can be accomplished by the action of the electrode material, or alternatively by the action of species in solution, or both (Trasatti 1972). A number of phenomena which may have little in common are grouped together under the term electrocatalysis. However, it can be distinguished into homogeneous and heterogeneous to avoid this generalization of electrocatalysis. Heterogeneous electrocatalysis is more a function of the electrode material and electrode kinetics, and it refers ‘electrocatalysis’ in practical fields (Pletcher 1984).

2.2.1Electrochemical Water Splitting

The energy crisis and environmental concerns intensified the need for searching a clean and renewable alternate energy for the future(Chen et al. 2016).In this regard, researchers are looking forward to use abundant, renewable and cleanest fuel *i.e.*, hydrogen, as a promising alternate energy carrier in the future(Reddy et al. 2016) Hydrogen has been promoted as the ideal clean energy source with zero-emission (Luo et al. 2016; Prather 2003)and having excellent energy storage density (Pu et al. 2016). Water is the most abundant source of hydrogen, free from carbon(Zeng and Zhang 2011) and its splitting into H_2 and O_2 is the best choice for H_2 production. Whereas the water electrolysis is tedious process, suffers from practical over potentials due to sluggish electrode kinetics (Reddy et al. 2016)

2.3 ELECTRODE MATERIALS FOR WATER ELECTROCATALYSIS

The role of electrocatalysts is to reduce the overpotential as far as possible. Under acidic conditions, the best electrocatalysts are precious metals, platinum at the cathode and IrO_2or RuO_2 at the anode(Roger et al. 2017).However, the wide applications of these noble metals have been hindered due to their scarcity and high costs. Hence,extensive research has already been devoted to this area for the development of non-Pt materials as electrocatalysts(Cardoso et al. 2015). At the same time, under basic conditions, the first-row transition metals (and their alloys) and oxides make excellent HER and OER catalysts, respectively. In general, the HER catalysts fall into three categories: *i)* noble metal (Pt) catalyst, *ii)* transition metal (mainly including Fe, Co, Ni, Cu, Mo and W) based electrodes and *iii)* non-metals (mainly including B, C, N, P, S and Se) based materials(Safizadeh et al. 2015; Zou and Zhang 2015).Most of the non-precious HER electrocatalysts reported to date are based on these twelve transition elements and non-metals. An ideal HER electrocatalyst should have some essential requirements, like *i)* low hydrogen overvoltage at industrial current density, *ii)* no potential drift with time, *iii)* good chemical and electrochemical stability: long lifetime and no release of process-deleterious products, *iv)* high adhesion to the support, *v)* low sensitivity to poisoning by impurities, *vi)* low sensitivity to current shut down (short-circuit) or modulation, *vii)* no safety or environmental problems in the manufacture process, *vii)* easy to prepare at a low cost/lifetime ratio (Roger et al. 2017; Safizadeh et al. 2015). The highest abundance and the lowest price of Ni and Fe making them more desirable to make economically viable electrocatalysts (Gong et al. 2014).

2.3.1 Electrodeposition as a Tool for Synthesis of Electrode Materials

Numerous research works on the HER activity of various elements like Cu, Au, Mo, Pd, Rh, Fe (Pentland et al. 1957), Ni(Lasia and Rami 1990), RuO_2(Thiemig and Bund 2008)etc. were reported during the last decades. Whereas, the prepared cathodes either in the form of pure metal or in alloyed form are not found to be necessarily better than steel cathodes (using commercially for alkaline HER).Whereas, compared with the bulk materials, the alloy/composite coatings were found to show improved electrocatalytic activity and decrease in overvoltage, due to increase in effective surface area of the cathode. Although there are several methods available for the fabrication of coatings, the cost effectiveness and simplicity of electrodeposition making it more attractive and reliable(Mirkova et al. 2011), (Luo et al. 2016).A variety of coatings such as metal, alloy or composite can be developed with high precision through electrodeposition, and also it allows to have a close control over the desired properties of the deposits. It also allows the convenience of producing the deposits of desired composition, porosity (large area surfaces), low-temperature growth and the possibility to control film thickness, morphology and phase structure by adjusting the electrical parameters and the composition of electrolytes (Correia et al. 1999; Zheng et al. 2012). The interesting advantages of electrodeposition over other coating techniques (like, plasma or thermal spraying, thermal decomposition, in-situ activation etc.) are: *i)* simple setup, *ii)* easy to develop non-crystalline phases, *iii)* control over composition of the coating, *iv)* suitable for scalability and *v)* low cost(Aal and Hassan 2009).Moreover, it can improve the adherence of the deposits on the substrate surface and enhance the electrocatalytic activity and stability. Many literature reports are there on the electrodeposited metal/alloy/composite electrocatalysts.

Many reports are there on the efficiency and cost effectiveness of electrodeposited coatings (metal/alloy/composite) as electrode materials for electrocatalytic water splitting reactions. Arul Raj accompanied with Vasu reported many electrodeposited Ni- based binary and ternary alloys as cathode materials for alkaline HER (Raj and Vasu 1990),(Raj and Vasu 1992).They observed the electrodeposited Ni-Mo alloy coating as the best towards alkaline HER with low overpotential(Raj 1993; Raj and Vasu 1992).The same research group also reported the codeposited Ni- based ternary alloys such as Ni-Mo-Fe, Ni-Mo-Cu, Ni-Mo-Zn, Ni-Mo-Co, Ni-Mo-W, Ni-Mo-Cr as electrode material for alkaline HER(Raj 1993).Thereafter many alloy and composite electrodes developed using electrodeposition technique were reported as efficient materials for HER (Kaninski et al. 2009; Low et al. 2006; Lupi et al. 2014; Shervedani et al. 2008). Herraiz-Cardona et al. (2011) developed porous electrodes through galvanic codeposition to enhance the HER efficiency through increasing the effective surface area, and they succeeded in depositing porous Ni-Co alloy electrode. Later, numerous publications came on the electrodeposited Ni- based alloys (Subramanya et al. 2015; Ullal and Hegde 2014; Vargas-Uscategui et al. 2015; You et al. 2015)and composites (Danilov et al. 2016; Kuang et al. 2013), oxides/hydroxides (Trotochaud et al. 2014), heterostructures (Gong et al. 2013; Zou and Zhang 2015) etc., as efficient electrode materials for alkaline HER. Based on this, a literature of Ni-Co and Ni-Mo alloy is detailed in the following sections.

2.4 Ni-Co ALLOY

Nickel is versatile in nature and readily it forms alloy with most of metals such as Co, Fe, Zn and Alloys of iron group metals, Fe, Ni and Co, are known as very good magnetic materials since 1921.Electrodeposited Ni-Co have been widely employed in industry due to their good corrosion and wear resistance, high mechanical strength, moderate thermal conductivity and outstanding electrocatalytic and magnetic properties (Karimzadeh et al. 2019). The Ni-Co alloy system has variety of application due to their better corrosion resistance, electrocatalytic and magnetic properties(Gu et al. 2006).Deposition of Ni and Co metals together is easier due to their nearer standard potential values ($E°_{Co} = -0.27$ V and $E°_{Ni} = -0.25$ V vs. SHE).The deposition involved is either normal or anomalous. The physical and mechanical properties of the Ni-Co alloy system depends on the composition of the deposited metal on the substrate(Tian et al. 2011).Current density is a major factor and controls the rate of deposition, surface morphology, phase structure and composition.Idris et al. (2013) prepared Ni-Co coatings through electrodeposition method. The influence of cathodic current density at constant pH on microstructure of the coatings was studied. The homogeneous surface morphology is obtained for all current densities coatings confirm that current density has a large effect on thickness of the coatings. The effect of current density and pH on electrodeposition of Ni-Co sulphate alloy system was studied. It was found the efficiency of alloy deposition increases with increase of sulphate concentration in the bath. The current plays an important role for change of surface morphology from in the deposit. With increase of current density a gradual refinement of the particles size was observed.This was attributed to increase of nuclear density with increase of overpotential. This is responsible for improvement in corrosion resistance of the materials(Abd El-Halim and Khalil 1986).

Wang group synthesized Ni-Co alloy coating through normal electrodeposition method. They have studied the effect of cobalt content on surface morphology and phase structure of the deposited coatings. Results revealed that with increase of cobalt content, a wear and hardness property of the coating also increases. And it was found to be was maximum at 49% of cobalt. They concluded that Co rich alloys better than Ni rich alloys towards corrosion resistance of the system(Wang et al. 2005).Zamani et al. (2016) studied the effect of cobalt content on Ni-Co alloy system through electrochemical impedance spectroscopy method.It was found that with increasing the cobalt content up to 45% in alloy coating, the grain size decreased and consequently, hardness and strength of the alloy increased. Further enhancement of cobalt content up to 55% led to a little decrease in hardness and strength. The maximum ductility was observed for Ni–25%Co coating due to relatively small grain size and compact structure. Khorsand et al. (2016) fabricated the super hydrophobic films with enhanced corrosion resistance by one step electrodeposition method. The corrosion study was done by using potentiodynamic polarization and electrochemical impedance spectroscopy techniques in NaCl medium. Results revealed that super - hydrophobic samples are found to be more corrosion resistant then normal coatings.Bouzit et al. (2017) synthesized chloride sulphate bath for deposition of Ni-Co alloy on copper substrate. This result showed the effect of current density composition, surface morphology and phase structure to elucidate the formation of mechanism of coatings. The EDX analysis revealed that deposition follows anomalous behaviors. And, rough and smoother surface structure is obtained at lower (1 and 2 A dm^{-2}) and higher (3 and 4 A dm^{-2}) current densities respectively and is confirmed by SEM analysis. Imanian synthesized Ni-Co composite coating reinforced with ZnO particles by pulsed or direct current electrodeposition method(Imanian Ghazanlou et al. 2019). The effects of electrodeposition parameters such as stirring rate, average current density, and ZnO particles concentration on the microhardness of electrodeposited composite coating reinforced with nano and micro ZnO particles are investigated. Incorporation of ZnO nanoparticles in the Ni-Co matrix by PC-electroplating method improved the corrosion and wear resistances of coating to more than those obtained using ZnO microparticles by DC method. Results revealed that improved corrosion resistance of the system due to the incorporation of ZnO nanoparticles through pc electroplating technology. Li et al. (2020) developed Ni-Co alloy system through normal electrodeposition method. The results showed effect of deposition potential which controls the microstructure and Co content of Ni-Co alloy. Nano crystal structure could be obtained with a grain size in the range of 3.1–4.0 nm. Comparison in the corrosion behavior of the coatings showed that the change of Co content had an effect on the corrosion resistance of Ni-Co alloy.The best corrosion resistance was found for Ni-25%Co with corrosion potential is -0.370 V and corrosion current is 2.6×10^{-6} A/cm^2.

2.4.1 Magnetoelectrodeposition

The superimposition of external magnetic field on the process of can offer better results on the nature of electrodeposit, through MHD effect arising from Lorentz force (Fahidy 1983; Ragsdale et al. 1998). Many reports are there on the magnetic field induced convection due to Lorentz force operating on moving charged species in an electromagnetic field (Ganesh et al. 2005a; Monzon and Coey 2014; Tacken and Janssen 1995). The magnitude of Lorentz force ($F_L = qvB \sin\theta$) is maximum when it is applied perpendicular ($\theta = 90^{o}$) to the applied current density or velocity of the moving charged species (Monzon and Coey 2014a). This enhanced mass transport due to MHD convection can reduce the polarization resistance as well as the ohmic drop due to bubble resistance through the easy detachment of generated gas bubbles from the electrode surface(Kiuchi et al. 2006) The reduction in cell overvoltage by superimposing external magnetic field is irrespective of the nature of the electrode material, provided all other conditions maintained as the same. Therefore by proper design of the electrode material and superimposition of an external magnetic field of optimal strength can offer efficient electrolysis of water by minimizing the polarization effects. Wassef and Fahidy 1976 reported a detailed study on the magnetic field effects on water electrolysis. Thereafter many researchers have succeeded in using the magnetic field as a tool to improve the electrochemical reaction kinetics(Aaboubi and Msellak 2017; Devos et al. 1998; Matsushima et al. 2006).

Devos et al. (1998) reported that a magnetic field could change the surface morphology and the preferred orientation of the nickel grain due to an increase of the diffusion flux of specific inhibiting species. For nickel, the variation in the pH near the cathode surface due to MHD convection occurs parallel to the substrate plane. Waskaas and Kharkats (1999) have reported the Mechanism of Influence of Magnetic Fields on Electrochemical Processes and also the effect of magnetic field on the polarization of nickel or cobalt systems. The more striking effect on magneto electrodeposition is limiting current. Thus, increase in limiting current changes the surface morphology of electrodeposits. Cobalt is an element with excellent ferromagnetic properties. It is highly corrosion resistant material and easy to handle. In this regards, effect of magnetic field on electrodeposition of cobalt have been studied (Krause et al. 2004).Guan and Nelson (2005) studied the effect of magnetic field on ternary Co-Ni ternary alloys as hard magnetic materials for microelectrochemical systems. Results revealed that with the application of magnetic field in parallel and perpendicular direction the residual stress developed inside the coatings got reduced. This increases the rate of transport of electroactive species to or from the electrode. Hence, Cobalt and Cobalt based alloys have been used in magnetic storage systems and other magnetic application. Ganesh et al. (2005) have studied the effect of magnetic field upto 1T on grain refinement, during electrodeposition of Ni-from sulphamate bath at constant current density (1mAcm^{-2}). It was further observed the magnetic field effect increases the mass transfer rate with decrease of concentration polarization. Further, visible convection and magnetic properties of nickel caused by the Lorentz force was reasoned to be responsible for the preferential orientation of nickel. The increase in the mass transfer rate of Ni ions is due to magnetic field-induced convection. This increases the rate of Ni deposition leading to the formation of fine-grained deposit. And hence surface properties of the coatings. Bund and Ispas (2005) investigated the influence of a parallel (with respect to the surface of the working electrode) static magnetic field on the electrochemical reaction, the morphology and the magnetic properties of electrochemically deposited nickel layer and they found that the layers prepared in the magnetic field had a considerably higher properties as compared to normal coatings.

Wu et al. (2010) prepared Ni-Co alloy nanostructure solvothermally under external magnetic field. The results showed that saturation magnetization is higher for nanostructure under the influence of magnetic field as compared with the absence of magnetic field effect. The difference in magnetic properties between Ni and Co is responsible for change of properties of the Ni-Co nanostructure. Tian et al. (2011) produced Ni-Co films with different compositions, microstructure and magnetic properties by electrodeposition method. The effect of cobalt ion concentration was studied. With increase of cobalt content from 22.42% to 56.09%, saturation magnetization (Ms) moves up from 144.84 kA m^{-1} to 342.35 kA m^{-1} and hence increases the corrosion resistant of the materials..Li et al. (2016) have reported that the modification in surface morphology, structure of Co-Ni-P was attributed to polarized and diffusion acceleration effect under magnetic field. Results revealed that surface roughness was decreased with the application of magnetic filed through annealing process which inturn increases the surface properties. Fang et al. (2017) developed Ni-Co alloy coating by the application of perpendicular magnetic field with different magnetic field intensities. It was found that magnetic field greatly improved the surface smoothness of the coating and hence corrosion resistance. Along with this, magnetic field plays a important role in change of grain size, orientation and little lattice structure of deposited alloy coatings.(Jiang et al. 2019) produced Ni-Co and Ni-Co-SiC composite coatings through magnetic field induced jet electrodeposition method. Under the influence of magnetic field coating has showed a proper uniform growth and distribution of nanoparticle into the matrix and Ni-Co-SiC composite coating exhibited a single-phase solid solution structure, and its adhesion increased to 33.2 N, which was 2.65 times that of the Ni-Co alloy coating. The corrosion current density of the composite coating was 4.768 μAcm^{-2}, which was sufficient to protect sintered NdFeB magnets.

2.4.2 Sonoelectrodeposition

Chung and Chang (2009) investigated the effect of pulse frequency and current density on cobalt content of the deposited Ni-Co alloy coating. Results showed that smoother morphology can be obtained with increase and decrease of pulse frequency and current density respectively. Hence, enhances corrosion resistant of materials. El-Feky et al. (2013) developed Ni-Co alloy coating on a copper foil substrate using galvanostatic technique and ultrasound waves. The applied ultrasound wave was found to produce fine and smooth crystals leading to higher hardness of Ni-Co alloys. The microhardness of the Ni-Co alloys was varied between 4860–7530 HV. The surface morphology of coatings was changed from granular to fine due to application of ultrasound waves. This results in formation dense, nanocrystalline and shiny more corrosion resistant Ni and Ni-Co alloys.Mahboob et al. (2017) synthesized Ni-Co based catalysts by using the effect of ultrasound. Results showed that ultrasonic power and time controls the limited growth of particle with avoid of particle agglomeration. It has lot of effect on surface morphology, specific surface area, particle size distribution and hence increases the catalytic performance of the materials. Chuang et al. (2020) studied the effect of mechanical properties on Ni-Co coating through ultrasound assisted electroplating process. Under ultrasonic agitation, coating obtained is of good deposition quality, with higher hardness, resistance to wear and corrosion, lower surface roughness and finer grain sizes.AFM revealed that high frequency, lower power ultrasound electroplating process resulted in smoother and brighter film morphologies, with the lowest roughness values measured at 2.3 nm and results in increased mechanical properties. The Corrosion analyses revealed that films with smaller grains and smoothest surfaces posses good corrosion resistant value.

2.4.3 Electrocatalytic Study

Gonzalez-Buch et al. (2013) developed Ni and Ni-Co electrodes materials at higher current density. Results revealed that surface roughness got decreased with increase of cobalt content and also, coating with Co content of 43 at. % showed highest intrinsic activity for HER. This is attributed to synergistic effect between Ni and Co. And also, EIS study showed that electrocatalysts with Co contents around 40–60 at.% will have highest intrinsic catalytic activities with increased electrocatalytic activity.Lupi et al. (2014) studied the effect of third component like Mo on electrocatalytic behavior of Ni-Co alloys. The values of exchange current density for Ni–Co alloys without Mo, are an average of about 4.1×10^{-6}Acm^{-2}, while by using in situ activation, these values are about 3.5×10^{-4} Acm^{-2}. Therefore, exchange current density presents a value nearly one hundred-fold higher when molybdate ions are present in solution. Hence, catalytic activity is also enhanced with the addition of third component to the Ni-Co alloy matrix.Liu et al. (2015)synthesized a new family of catalyst including Co-CoO/N-rGO and Ni-NiO/N-rGO for oxygen evolution and hydrogen evolution reaction. Both of them showed good electrocatalytic activity.

The possible synergetic effect among transition metals, metal oxides, and graphene was systematically studied, making them simultaneously highly active for the OER, ORR, or HER. One of the advantage is to replace noble-metal-based catalysts for clean Production of renewable energy sources.Sun et al. (2017) fabricated mesoporous Ni-Co alloys by electroless deposition for hydrogen evolution reaction in alkaline medium. A series of Ni-Co electrocatalysts have been synthesized with variation of Ni and Co content. Results showed that optimal $Ni_{58}Co_{42}$ catalyst exhibits a highly ordered mesoporous structure with a narrow pore size distribution of 3–5 nm and has a high BET surface area of 106 $m^2\ g^{-1}$. Owing to the synergetic combination of Ni and Co, as well as the enlarged exposure of catalytically active sites and improved transport of mass and charge from the unique ordered mesoporous structure, the $Ni_{58}Co_{42}$ catalyst shows outstanding HER electrocatalytic activity. Liu et al. (2019) developed Ni-Co-Sn electrode for HER and OER by electrodeposition method. The microstructure and electrocatalytic performance of the developed coating was tuned with change of pH during electrodeposition. Hence, by controlling the pH the active site and electrocatalytic properties of Ni-Co-Sn coating effectively controlled. The Ni-Co-Sn electrode prepared at pH = 5.0 showed the best catalytic activities and stability toward both the HER and OER in alkaline solution.Darband et al. (2019) prepared Ni-Co nanocones though two step electrodeposition method for hydrogen evolution reaction. The enhanced electrocatalytic activity is attributed to the synergy effect between Ni, Co and rough active edge of the nanosteps on nanocones helps to increase of active site for fast transport of ions.

2.5 Ni-Mo ALLOY

Huang et al. (2015) prepared Ni-Mo alloy coating by current technology. Results showed that coating obtained at different duty cycle and pulse frequency posses different corrosion resistance values. The Ni-Mo coating showed better corrosion resistant having 30.2 Wt% of Mo. With lower duty cycle, the current efficiency decreases which is due to reduction in reaction inhibited by molybdate in cathode interface. Increasing the frequency in the range from 10-1000 Hz leads to increase in the Mo content in PC-plated coatings. The maximum Mo content (30.2 wt.%) in the coating occurred at a current density of 10 A/dm^2, a duty cycle of 0.7, and a frequency of 1000 Hz. As the pulse frequency is increased, it can reduce the surface roughness and enhance the Mo content of the coating which further improves corrosion resistance.Laszczynska et al. (2016) developed Ni-Mo-ZrO_2 composite coating by normal electrodeposition method. The influence of deposition parameters on composition of coatings was studied. XRD study revealed that crystallite size of the coating got decreased with increase of molybdenum and ZrO_2 content in the deposit and helps for improvement of corrosion resistant of materials. Along with this, presence of nanoparticle in the matrix enhances the corrosion property of the deposited material. Hence added nanoparticle is acts like barrier for corrosion propagation in the material.

Laszczynska et al. (2017) investigated corrosion resistance and passive film formation ability of Ni-Mo alloy coating in 0.5M NaCl medium. The coating was exposed to corrosive medium for 3 hours. After that increase of Polarization resistance is observed for a coating containing Mo content of 21-28 Wt%. This indicates that in the course of longer contact with corrosive media, formation of passive film on the coating surface started to control the corrosion rate.Wasekar et al. (2019) prepared Ni-Mo alloy by electrodeposition method .The influence of Mo content on grain size, hardness, corrosion and wear resistance of the coating has been studied.Increase in duty cycle and current density increased Mo content in the coatings only up to a certain limit due to mass transport effects. However, higher Mo contents can be obtained at lower current density, Corrosion current and passive current density increased with Mo content. The uniform corrosion rate depends on the grain size whereas passivation was largely controlled by Mo content in the coatings. Increase in Mo content decreased the wear rate. Hence, Ni-Mo coatings can also be viewed as a suitable alternative for conventional HCr coatings for wear and corrosion resistance applications.Iragar et al. (2020) studied the effect of corrosion on Ni-Mo alloy coatings. Results revealed that coating having lower wt% of Mo was found to be more corrosion resistant as compared to other coating. They have studied the corrosion of materials by using potentiodynamic polarization and electrochemical impedance spectroscopy techniques.Meng et al. (2020) developed Ni-Mo-TiO_2 composite coatings for improved carrion corrosion.Results revealed that compact, crack-free NiMo/TiO_2 nanocomposite coatings exhibit much nobler E_{corr}, lower i_{corr} and larger R_{ct} values than those of the Ni-Mo alloy coating. Among all Ni-Mo/TiO_2 nanocomposite coatings, deposited from a bath containing 40 mg/L TiO_2 nanoparticles, shows the best corrosion resistance.

Xia et al. (2014) synthesized Ni-Mo-Cu electrode for hydrogen evolution reaction using constant current electrodeposition method. Results showed that introduction of Cu to the alloy matrix enhances the surface roughness and which presents more activity for HER as compared to Ni-Mo electrode system. The prepared Ni–Mo–Cu alloy coating electrode exhibits lower overpotential, lower activation energy and better stability toward the HER than Ni–Mo alloy electrode. The HER efficiency observed for the Ni–Mo–Cu alloy coating electrode can be explained by a synergistic combination of its electrocatalytic components and the increased surface area.Xu et al. (2016) prepared Ni-Mo coating by electrodeposition method. The catalytic activity of the coating was investigated by using steady state polarization and electrochemical impedance spectroscopy methods. The various chemical composition of Ni-Mo coating obtained on a substrate was characterized for its electrocatalytic behavior. The coating of 19.59 at% of Mo showed better catalytic activity due to the presence of cauliflower like rough surface structure. Steady-state polarization and EIS study revealed that increase of electrocatalytic activity is due to increase of exchange current density and real electrode surface area of the deposited coating respectively.Gao et al. (2017) synthesized self supported porous Ni-Mo alloy sphere for efficient and durable catalyst for both HER and OER in alkaline media. The best electrocatalysts obtained at a current density of 20mA cm^{-2}, low overpotential of - 63 mV for the HER and 335 mV for the OER.The porosity of the microsphere leads to the access of more surface area, as well as active sites for the electrocatalytic reaction, and the porous structure with open channels providing convenient paths for fast electron/mass transport and electrolyte penetration resulting in rapid electrode reaction kinetics as well as gas release. Moreover, the synergetic effect of Ni and Mo also promotes the HER catalytic activity of the porous Ni–Mo electrode.

Abuin et al. (2019) developed Ni-Mo alloy for hydrogen evolution reaction. The influence of different variables such as electrolyte composition, power supply conditions on electrocatalytic activity and stability was studied. The maximum catalytic activity was observed for coating with Mo content in 19–24 at. % range. These alloys are characterized by amorphous structure by desorbing hydrogen atom from the surface easily. Hence, enhances the electrocatalytic activity.Toghraei et al. (2020) developed adequate and inexpensive electrocatalysts Ni-Mo-P/NF for electrochemical hydrogen production. The optimized Ni-Mo-P/NF electrode not only exhibits better catalytic activity than the Ni-Mo/NF and Ni-P/NF control electrodes but also has better HER activity than most of the other binary and ternary alloys. The high catalytic active surface area of Ni-Mo-P/NF along with the synergistic effect of Mo, P, and Ni in improving the inherent catalytic activity of the electrode is known to be responsible for its excellent HER activity. The lower values of charge transfer resistance of different coatings further proves the faster hydrogen evolution kinetics of Ni-Mo-P/NF in comparison with Ni-Mo/NF and Ni-P/NF.

2.5 SCOPE AND OBJECTIVES

2.5.1 Scope

Even though Ni-based alloy coatings can be achieved using other technique, like chemical vapor deposition and physical vapor deposition and hot dipping methods, electrodeposition method is the most preferred one because of its cost and ease of fabrication. Since, properties of the electrodeposited coatings can be controlled by changing electrolyte composition and operating parameters, such as current density, pH, temperature etc, it is a better option for development of alloy coatings at less cost.The literature review of Ni-M (where M = Co and Mo) alloy coatings, focusing on their corrosion resistance and electrocatalytic efficiency for alkaline water electrolysis revealed that the alloying of Ni with other metals, like Co and Mo, using baths of different compositions may open a new avenue for development of coatings, showing different material properties. The literature survey revealed that the physico-mechanical properties of conventional monolayer alloy coatings can be improved greatly with the advent of many modern methods of electrodeposition, like magnetoelectrodeposition and sonoelectrodeposition etc. Superposition of magnetic field and ultrasound field effects can bring a remarkable change on the process and properties of alloy coatings, which is unattainable by conventional methods. Thus literature review of Ni-M (M = Ni and Mo) alloy coatings, focusing on corrosion resistance and electrocatalytic behavior for alkaline water splitting reaction revealed that the noble Ni can be alloyed with harder metals, like Co and Mo to impart many promising properties to the coatings, by proper manipulation bath composition and operating variables. In this direction, two new electrolytic baths of Ni-Co and Ni-Mo alloys have been planned to optimize to get coatings and their corrosion resistance and electrocatalytic activities can be further improved by modern electrodeposition methods. The main limitation of Ni-Mo bath to develop coatings of high corrosion resistance, due to inherent induced type of deposition can be resolved by addition of small amount of Cd into the bath. The addition of a third metal into a binary alloy bath was found to bring a large change on the corrosion resistivity of binary alloy coating. The effect can be made more pronounced under condition of superimposed magnetic field.

Therefore from the literature review it was derived that:

1. The corrosion resistance of alloy coatings can be increased substantially by tailoring the composition, phase structure and morphology of the coatings by proper manipulation of deposition current density.
2. The corrosion resistance and electro catalytic activity of alloy coatings can be altered by superimposition of magnetic field/ultrasound effect parallel to the process of electrodeposition, which is unattainable by conventional method.
3. The electrocatalytic activity of the alloy coatings can be improved by the incorporation of nanomaterials, *i.e.*, through composite electrodeposition.
4. The corrosion resistance of the binary alloys has been improved with the addition of third component into the binary system. The effect can be further increased to many fold with the advent of magnetoelectrodeposition.

2.5.2 Objectives

Guided by the available literature on production and properties of electrodeposited binary alloy coatings the following objectives are intended to achieve:

1. To optimize few electrolytic baths of Ni - based alloy coatings, like Ni-Co and Ni-Mo etc for deposition of bright, uniform, protective coatings of their alloys, showing highest corrosion resistance and electrocatalytic activity, using proper additives.
2. To characterize the electrodeposited Ni-based alloy coatings using EDX, SEM, AFM and XRD techniques and understand the influence of deposition current density (c.d.) on the properties of coatings.
3. To evaluate, and compare the corrosion stability of the electrodeposited alloy coatings by electrochemical methods, like electrochemical impedance spectroscopy (EIS) and potentiodynamic (PD) polarization techniques, in standard corrosion medium
4. To study the effect of frequency of ultrasound on the corrosion protection efficacy of monolayer alloy coatings, due to effect of change of composition and surface morphology of the coatings.
5. To develop multilayer alloy coatings of high corrosion performance, by periodic pulsing of ultrasound effect parallel to the deposition of electrodeposition.
6. To study the effect of applied magnetic field (B), in both intensity and direction on the composition, phase structure, surface morphology and crystallographic orientation, and hence corrosion behaviour of the alloy coatings.
7. To study the electrocatalytic behavior of electrodeposited alloy coatings, deposited at different c.d.'s using electrochemical techniques, like cyclic voltammetry (CV) and chronopotentiometry (CP) in 1 M KOH medium.
8. To study the effect of addition of nanoparticles into the alloy matrix on electrocatalytic behaviors of water electrolysis.
9. To study the effect of addition of Cd into the alloy bath, in terms of corrosion behaviour of the coatings at different c.d.'s; and effect of magnetic field (B) on electrodeposition of Ni- (in terms of intensity and direction).

This chapter details about the materials used and different experimental methods adopted for electrodeposition and characterization of Ni-based alloy coatings. The procedures adopted for the optimization of electrolytic baths, and deposition of alloys and their nanocomposite coatings are discussed, followed by a concise description of the characterization techniques used. The experimental procedure of sonoelectrodeposition and magneto-electrodeposition are described, with a note on the custom made set up, designed to study corrosion efficacy and electrocatalytic activity of electrodeposited alloy coatings.

3.1 INTRODUCTION

Electroplating is a process of electro-crystallization of metal atoms on to the surface of base metals to improve their surface properties. The deposition was carried out on a cathode surface from the pool of ions of electrolyte solution. The ultimate goal of electroplating is to produce plated materials having more chemical, physical and mechanical properties, and as a result they can be used for different applications. The product of electrodeposition is very sensitive of different factors, like chemistry of bath (purity, pH and temperature of the electrolyte), current density (c.d.), additives, agitation *etc.*Electroplating is probably one of the most complex processes known because of the unusually large number of critical elementary phenomena, or process steps involved. Generally, a practicable method for electrodepositing any metal/alloy/composite involves three steps. The first step is concerned with the surface preparation of the substrate to be plated. Second and the most important step involve the optimization of a suitable plating bath. This requires a practical knowledge of the electrochemistry of elements, the solubility of their salts, and the chemistry of their complexes. Finally, the third step involves direct deposition of the metal/alloy/composite coating from the optimal bath.

3.2 MATERIALS AND METHODS

3.2.1Chemicals and Materials

All the chemicals used for the study are of analytical chemical grade, and dissolved in distilled water. The copper is used as the base material for electrodeposition, for both corrosion and electrocatalytic study. Different chemicals used in the present study are listed in the Table 3.1.In the present study two binary alloy baths, namely Ni-Co and Ni-Mo are chosen. The deposition of alloys has been carried out on a substrate, and were subjected to study of corrosion and electrocatalytic behaviours. The corrosion and electrocatalytic behaviours of electrodeposited alloy coatings were studied in, respectively 5% NaCl and 1M KOH solution, as common medium for comparison purpose.

Table 3.1- List of chemicals used for the research work

Chemicals Name	Molecular Formula	Brand
Cobalt sulfate	$CoSO_4.7H_2O$	Merck, India
Nickel sulphate	$NiSO_{4.}6H_2O$	Merck, India
Sulphanilic acid	$C_6H_7NO_3S$	Merck, India
Ascorbic acid	$C_6H_8O_6$	Merck, India
Boric acid	H_3BO_3	Merck, India
Glycerol	$C_3H_8O_3$	Merck, India
Sodium molybdate	$Na_2MoO_4.\ 2H_2O$	Merck, India
Tri-Sodium citrate	$Na_3C_6H_5O_7$	Merck, India
Cadmium chloride	$CdCl_2$	Merck, India
Potassium hydroxide	KOH	Nice Chemicals, India
Sulphuric acid	H_2SO_4	Nice Chemicals, India
Sodium chloride	NaCl	Nice Chemicals, India
Sodium hydroxide	NaOH	Nice Chemicals, India
Nitric acid	HNO_3	Nice Chemicals India
Ammonium hydroxide	NH_4OH	Nice Chemicals, India
Titanium dioxide	TiO_2	Merck, India
Cerium dioxide	CeO_2	Merck, India
Multi-walled carbon nanotubes(MWCNT)	-	Merck, India

All electrodepositions are carried out at known constant pH, and variations, if any were adjusted using dilute solution of acid/base depending on the requirement. The nanoparticles, like TiO_2, CeO_2 and MWCNT were used, as they procured for electrocatalytic study.

3.2.2 Surface Cleaning

All substrates ($3.0\times3.0cm^2$) were pre-treated by mechanical polishing using emery dressed mops of gradually decreasing of grit size. The mechanically polished mirror surfaces were degreased with trichloroethylene (TCE), as solvent. The surface was electro-cleansed cathodically for 2 minutes, and then anodically for 30 seconds. The surface of the specimen was washed with running distilled water, followed by activation using 10% HNO_3.Finally, the specimen washed and rinsed with distilled water, and then taken for deposition.

3.2.3 Optimization of Bath

The Hull cell is an invaluable analytical tool in electroplating, to formulate the bath composition and current density to get satisfactory coatings. The electrolyte prepared (by dissolving the chemicals in distilled water using mechanical stirrer) was taken in Hull cell to optimize the bath conditions. The nickel plate was used as anode, and substrate as cathode. The DC power source was used, as the driving force for electrodeposition. By passing current of 1A through Hull cell set up for a given time (5 min), plating is allowed to take place on cathode surface. Then, on inspecting the coating patterns, deposited along the length of cathode, *i.e.*, from lower current end to higher current end, the current density corresponding to the satisfactory coating has been fixed, using Hull cell ruler as explained in Section 1.5(Parthasarathy 1992). Electrodeposition using Hull cell gives idea about the effect of range of current density on deposit patterns, in a given bath. Accordingly, bath composition and operating variables of Ni-Co and Ni-Mo alloy baths, of present study were arrived by Hull cell method. Hull cell set up used for optimization of an electrolytic bath is shown in Figure 3.1.It may be seen that cathode is placed inclined to the anode, which enables to find the effect of range of c.d. on the deposit patterns to fix the optimal c.d. using Hull cell ruler. To summarize, the electrolytic baths were optimized (for both composition and c.d.) using Hull cell method, and such optimized baths were used for further study.

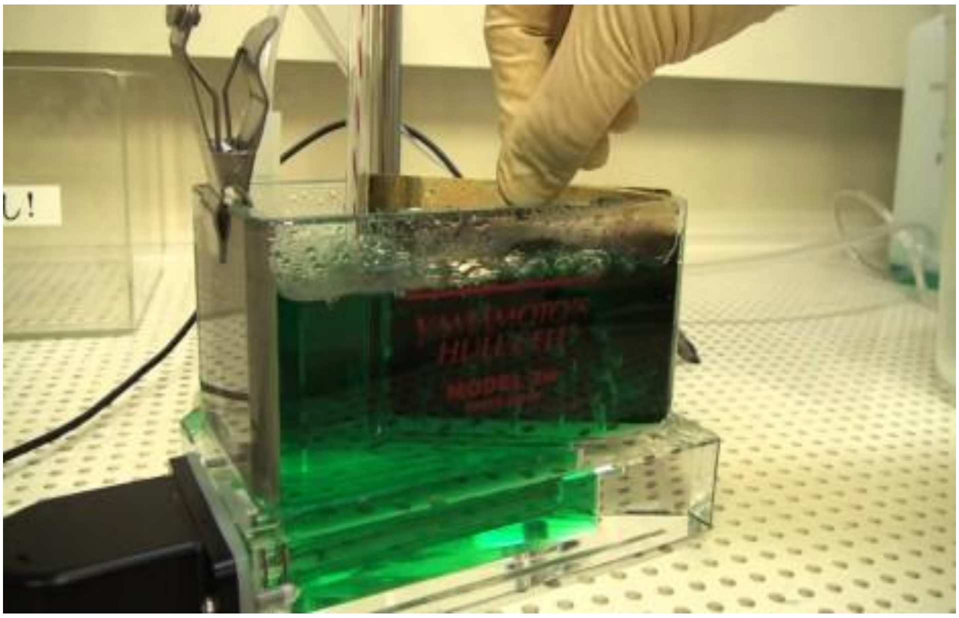

Figure 3.1-Experimental set up used for optimization of a bath using conventional Hull cell, where cathode is placed inclined to the anode

3.3 DEVELOPMENT OF ELECTRODEPOSITED ALLOY COATINGS

3.3.1 Development of Monolayer Coatings

Both monolayer and multilayer alloy coatings were developed using constant current, or direct current (DC) power source (Aplab-LD3202).All electrodepositions were carried out using a custom made PVC cell, having capacity 250 mL by keeping anode and cathode parallel. The optimized bath (arrived using Hull cell) was taken as the electrolyte. The substrate was mechanically polished and cleaned with trichloroethylene, then washed with water and pickled with 1:1 $HNO_{3.}$Diagrammatic representation of conventional (monolayer) electrodeposition, using DC power source is shown in the Figure 3.2, where pure Ni plate was used as anode, and polished substrate was cathode.

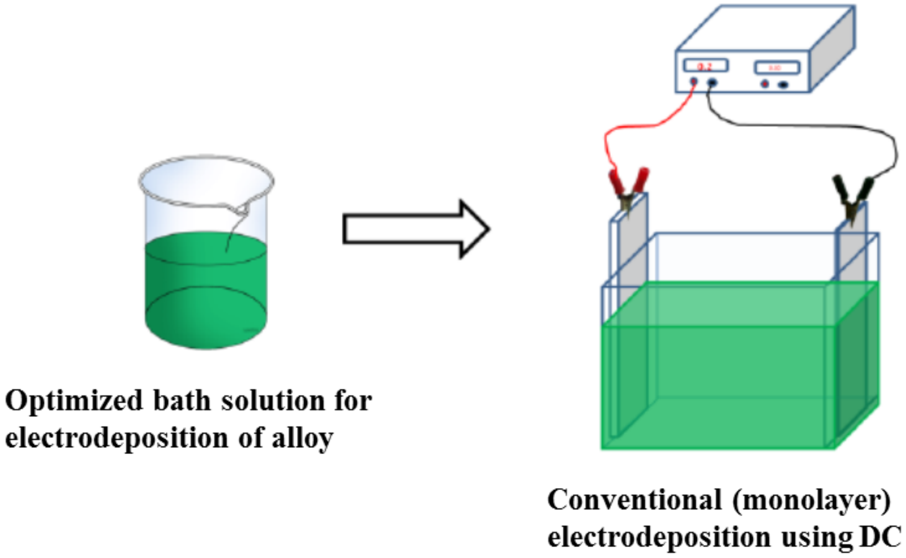

Figure 3.2-The experimental set up used for conventional electrodeposition using custom made PVC cell

The electrodes were kept in a parallel position at a distance of 5 cm in the optimized electrolyte solution. The nickel (Ni) plates, having same exposed surface area as cathode (3×3 cm^2) were used as anode. The pH of the bath was maintained using pH Meter (Systronics - 362) at desired value, by adding either HCl, or NH_4OH, depending on the requirement. The electrodepositions were carried out at different current densities by proper setting up of the power source. The property, like corrosion resistance of Ni-Co and Ni-Mo alloy coatings have been enhanced further, using modern techniques called sonoelectrodeposition (SED), magnetoelectrodeposition (MED). All electrodeposited alloy plates were washed with distilled water, and then dried and then desiccated. The desiccated alloy coatings were analysed for their surface morphology, composition, phase structure, corrosion and electrocatalytic performances.

3.3.2 Magnetoelectrodeposition

The magneto-electrodeposition, *i.e.*, electrodeposition under the effect of induced magnetic field was carried out using Electromagnet (Polytronics, Model: EM 100, India) in conjunction with DC power source (Aplab, LD3205, India). The magnetic field was applied both parallel and perpendicular to the direction of electric field. The magnetometer set up used for magnetoelectrodeposition of alloy coatings is shown in

Figure 3.4. The electrolytic bath was kept in centre of space between the poles to maintain a uniform magnetic field inside the bath.

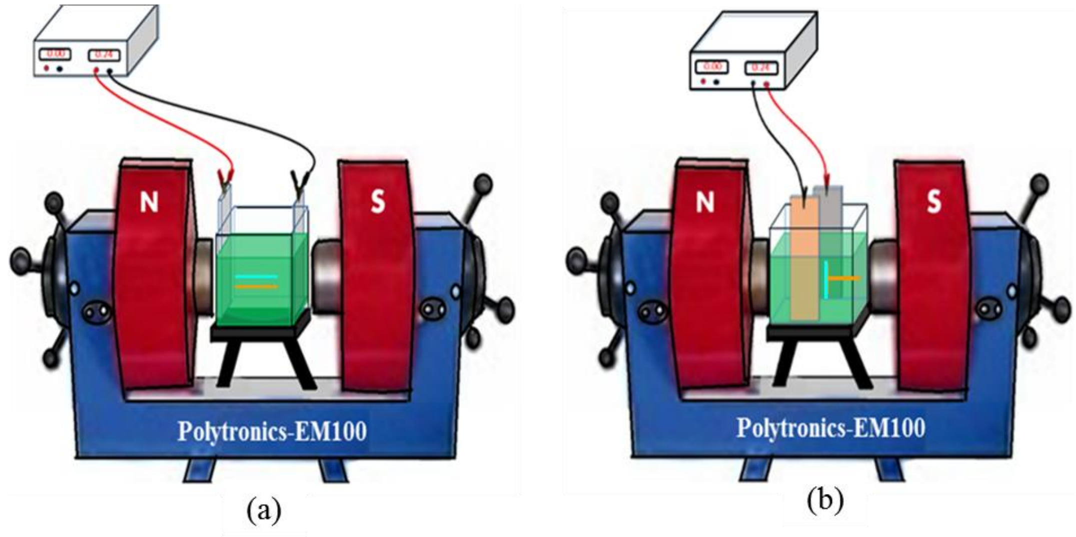

Figure 3.4 –The experimental set up used for magnetoelectrodeposition of alloy coatings under conditions, where direction of transportation of ions are: a) parallel to B, and b) perpendicular to B

Magneto-electrodepositions were carried out by inducing the magnetic field, in the range of 0.1- 0.4 T (Tesla), simultaneous to the effect of given c.d. Change in intensity of magnetic field, responsible for the change in the convection process at the cathode layer brings change in the composition, and hence properties of alloy coatings. Magnetoelectrodeposition of alloy coatings were carried out by applying the magnetic field of different intensity, both parallel and perpendicular to understand the effect of *magnetoconvection* on the product and performance of alloy coatings. Magneto-electrodeposited alloy coatings were rinsed with water, dried in hot air and desiccated, until further testing.

3.3.3 Sonoelectrodeposition

The effect of ultrasound on the process and product of electrodeposition was studied, using ultrasound generator (SONIC, Vibra-Cell TM VC 750, 20kHz), having maximum power density of 750W, and cylindrical sono-electrode (rod) of 13mm tip diameter. Sonoelectrodeposition (SED), *i.e.*, electrodeposition under the effect of sonication was carried out by superimposing the ultrasound effect, parallel to the process of electrodeposition. Basically, ultrasound effect benefits the electrodeposition by improving the convection, or mass transport of metal ions towards the cathode.

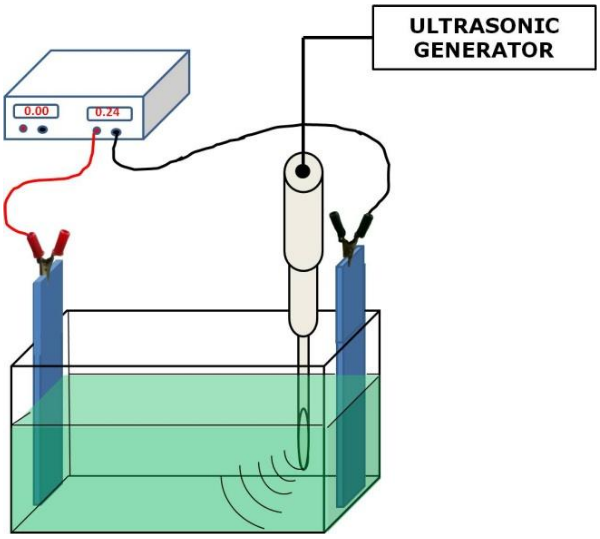

Figure 3.3- The set-up used for sonoelectrodeposition of alloy coatings in a custom made PVC cell, having optimal electrolyte, DC power source and ultrasound generator

This benefit has been used advantageously in development of both monolayer and multilayer alloy coatings. Monolayer sonoelectrodeposition was accomplished under condition of constant current density and power density, whereas in multilayer sonoelectrodeposition, power density was made to modulate between two values, keeping current density constant. Monolayer sonoelectrodeposition was carried out from an optimized bath, by placing ultrasonic horn at a distance of 1 cm from cathode (inside the bath). Monolayer sonoelectrodeposited alloy coatings were carried out at different power densities, measured in Wcm^{-2} in conjunction with DC power source. The experimental set up used for sonoelectrodeposition of alloy coating is shown in Figure 3.3.

Having taken the principle of electrodeposition that - ‘periodic modulation in the mass transport process at the diffusion layer brings a periodic change in the composition of electrodeposited coatings, a multilayer alloy coatings were developed by pulsing the power density between two values, keeping the current density constant. Accordingly, multilayer alloys having nano/micro layers have been developed by making the ultrasound generator to go ON and OFF periodically during electrodeposition. Periodic ON and OFF of the ultrasound generator, at a given power density allowed the development of multilayer coatings, having alternatively different compositions (depending on the amplitude of modulation); and different thickness of layers (depending on the duration of modulation).

3.4 ELECTRODEPOSITION OF COMPOSITE COATINGS

The effect of addition of different nanoparticles on the corrosion and electrocatalytic behaviours have been tested, by adding known amount of nanoparticles into the optimized baths of Ni-Co and Ni-Mo. Effect of different nanoparticles, like TiO_2 and CeO_2 including MCNT were tested by adding known amount of nanoparticles into the optimized bath.. As the solubility of nanoparticles were very less in the plating bath, the solution was stirred overnight for particle dispersion using a magnetic stirrer. The stepwise illustration of the composite electrodeposition process is shown in Figure 3.5.Electroplating was performed in 400 mL capacity plating setup, consisting of a copper rod and nickel plate as cathode and anode, respectively.

Figure 3.5 - The schematic of composite electrodeposition for electrocatalytic study of Ni-Mo-TiO_2 *nanocomposite coating for electro-catalytic study*

The composite coating was developed at given c.d. (obtained as optimal for alloy coatings towards alkaline HER) for the same deposition time of 600 s, using set up shown in Figure 3.5. The Ni-M nanocomposite coatings electrodeposited on copper substrates, were then subjected to further study to see the relative effect of these nanoparticles on corrosion and electro-catalytic behaviours.

3.5 CHARACTERIZATIONS OF ALLOY COATINGS

Electrodeposited alloy coatings were subjected to different type of analysis to understand their relative performances.

3.5.1 Corrosion Study

The corrosion performance of all electrodeposited alloy (including composite) coatings were evaluated using controlled Potentiostat/Galvanostat (VersaSTAT^3, Princeton Applied Research,USA).All electrochemical experiments were performed in a three electrode cell, using platinised platinum, as counter electrode; and saturated calomel electrode(SCE), as reference electrode. The corrosion tests were carried out at room temperature by exposing a 1cm^2 surface area of the alloy coatings in 5% NaCl solution, as representative corrosion medium. The corrosion behaviours of alloy coatings were studied by electrochemical impedance spectroscopy (EIS) and potentiodynamic polarization methods. The Nyquist plots were drawn, using data corresponding to AC frequency in the range of 100 kHz-10mHz, with perturbing sine wave of 10mV amplitude. The corrosion rates were calculated by Tafel extrapolation methods, by scanning the test electrode in a potential ramp of ±250mV, at scan rate of 1mV/sec. The value of cathodic slope (β_c) and anodic (β_a) slopes were determined using Tafel plots. The corrosion data, like corrosion current density (i_{corr}), corrosion potential (E_{corr}) and corrosion rate (CR) in millimetre per year (mm y^{-1}) was calculated using the Eqn. (3.1).

$$CR = (K \times i_{Corr}) \frac{E}{D} \dots\dots\dots\dots\dots\dots\dots\dots (3.1)$$

Where, constant K=0.00327 defines the unit of corrosion rate (mm y^{-1}), i_{corr} is the corrosion current density in μA cm^{-2}, D is the density of the alloy and E is the equivalent weight of the alloy.

3.5.2 Electrocatalytic Study

The electrocatalytic behavior of the alloy coatings were studied in a customized tubular glass set up, using Potentiostat/Galvanostat. Prior to this, the deposition was carried out in a glass beaker of 400 mL capacity, consisting of a copper rod and nickel plate as cathode and anode, respectively (Figure 3.6).

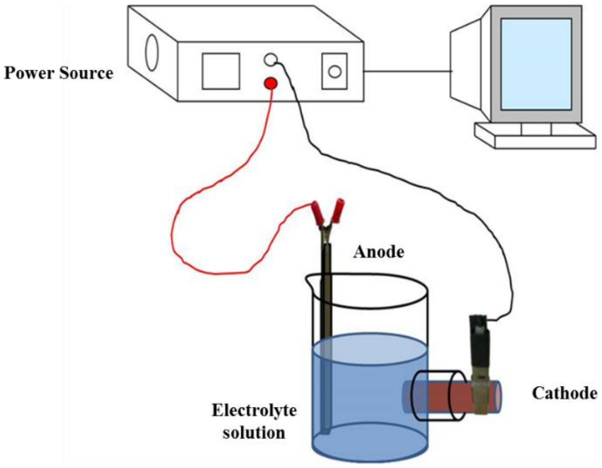

Figure 3.6-Customized glass set up for electrodeposition of alloy coatings on the cross sectional surface area of copper rod, taking the optimal bath as the medium of deposition

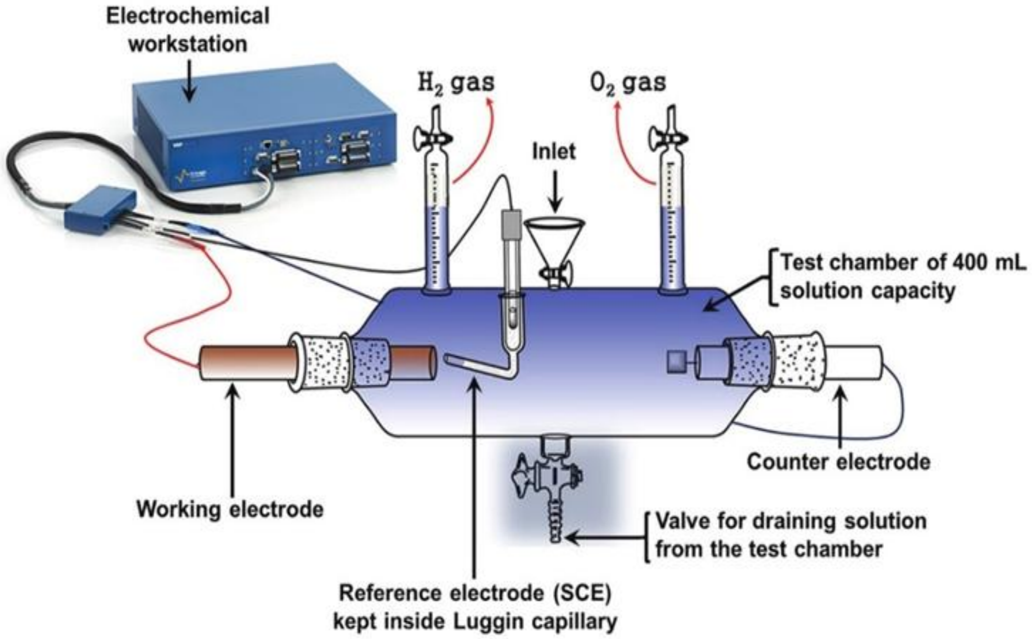

Figure 3.7-Tubular glass set up (electrolyzer) used for studying the electrocatalytic behaviour of electrodeposited alloy coatings, fitted with working electrode, counter electrode and reference electrode. Graduated burette on the top enables the quantitative measurement of H_2 and O_2 evolved at cathode and anode, respectively during alkaline water electrolysis

The electrodeposition was carried out for duration of 600 s, keeping copper rod and Ni plate at a distance of 5cm apart as shown in Figure 3.6. Electroplating was performed using 400 mL capacity bath, consisting of a copper rod and nickel plate as cathode and anode, respectively. Similarly, The Ni-M nanocomposite test electrode was prepared on copper plates rod by composite electrodeposition method using optimal Ni-M plating bath, containing known amount of nanoparticles. The composite coating was developed at given c.d. (obtained as optimal for alloy coatings towards alkaline HER) for the same deposition time of 600 s, as shown in Figure 3.5.To enable the quantitative evaluation of electro catalytic activity of electrodeposited alloy coatings, as anode and cathode material in water electrolysis a specially made tubular glass set up is used. The schematic representation of the tubular glass set up is shown in the Figure 3.7. The glass set up consists of alloy coated copper rod is used as working electrode, platinum as counter electrode and saturated calomel electrode (SCE) as reference electrode. The efficacy of electrocatalytic activity of alloy coatings, as cathode and anode material for water electrolysis were evaluated quantitatively by measuring the volume of H_2 and O_2 collected in the graduated burettes provided in the setup, as shown in Figure 3.7.The electrocatalytic kinetic parameters were studied using cyclic voltammetry (CV) and chronopotentiometry (CP) techniques. The CV and CP study were carried out using Potentiostat/Galvanostat (VersaSTAT^3, Princeton Applied Research) to understand the underlying reaction mechanism involved in the evolution of gases.

3.6 GENERAL CHARACTERIZATIONS

Apart from evaluating the corrosion and electro catalytic performances of electrodeposited alloy coatings, other characterizations were also made in order to establish their structure-property relationships. In this regard, electrodeposited alloy/composite coatings were characterized using various instrumental methods. The surface morphology of the deposited coatings were characterized by Scanning Electron microscopy (SEM) using EVO18 from Carl Zeiss, Germany. The coatings developed on the substrate with a dimension of 1.0×1.0 cm^2 was mounted directly on sample holder using carbon tape for analysis. The phase structure and composition of alloy coatings were analyzed using X-ray diffraction (XRD) study (Rigaku- miniFlex 600) and Scanning Electron Microscopy (SEM), interfaced with Energy Dispersive X-ray spectroscopy (EDS) facility (Oxford EDS(X-act), respectively. The phase structure of the sonoelectrodeposited (SED) and magnetoelectrodeposited (MED) alloy coatings and the incorporation of nanoparticles into the alloy matrix were also confirmed through XRD analysis (Model: Rigaku Miniflex 600, with CuK$_\lambda$ radiation as the X–ray source). The surface roughness of the coatings was measured using Atomic Force Microscopy (AFM, Innova SPM Atomic Force Microscope). In X-ray diffraction techniques, the phases of the coatings were analyzed by passing radiation Cu K$_\alpha$ (λ=1.54A°) at a scan rate of 2° per minute. Further, crystallite size was calculated by Debye Scherrer's equation:

$$D = \frac{K\,\lambda}{\beta C \cos\theta} \ldots\ldots\ldots\ldots\ldots\ldots\ldots\ldots\ldots.(3.2)$$

Where D - crystallite size, K-Debye coefficient, β_C-FWHM (Full Width at Half Maximum) and θ -Bragg's angle

3.7 INSTRUMENTS/EQUIPMENTS USED FOR THE PRESENT STUDY

The various instruments/equipments used for the present investigation, with their model number and purpose of use are tabulated in Table 3.2.

Table 3.2- The list of various instruments/equipments used for the present investigation

Name of the instrument/equipment	Model No. and manufacturer/supplier	Purpose used for
Electronic Weighing Balance	SC-391, Scientech, India	For weighing the salts for bath preparation, and also for weighing the plated samples
pH Meter	EQ-611, Equiptronics, India	To adjust the plating bath pH
Magnetic stirrer	EQ-771, Equiptronics, India	To attain homogeneous mixing of the plating bath before plating
Bench Polisher	BPP/A, Sugama Machine Tool, India	Primary mechanical polishing of the substrates
DC Power source	Aplab-LD3202, India	Conventional electrodeposition
DC Power Analyzer	Agilent-N6705, Agilent Technologies, USA	Electrodeposition for Electrocatalytical study

Electromagnet	EM 100, Polytronics, India	For the development of MED coatings
Sonicator	SONIC, Vibra-Cell TM VC 750,20kHz	For the development of SED coatings
SEM	EVO18 from Carl Zeiss, Germany	Surface morphology analysis
EDS	Link ISIS-300 Micro-analytical System, Oxford Instruments, UK	Elemental composition analysis
XRD	Rigaku Miniflex 600, USA	Phase structure analysis
Potentiostat/Galvanostat	VersaSTAT^3 (Princeton Applied Research)	Corrosion and electro-catalytic study

CHAPTER 4 DEVELOPMENT OF HIGH PERFORMANCE OF Ni-Co COATINGS THROUGH MAGNETOELECTRODEPOSITION

This chapter details the optimization of a new Ni-Co alloy bath for development of its alloy coatings for better corrosion resistance. The corrosion resistance of alloy coatings was further improved by superimposition of magnetic field (B), both parallel and perpendicular to the direction of B. The improved corrosion resistance of magnetoelectrodeposited (MED) alloy coatings were attributed to the change in the composition of alloy, affected due to the magnetoconvection effect at cathode layer during deposition. The pronounced effect of perpendicular B, compared to parallel B on the properties of alloy coatings were explained on the basis of Lorentz force (F_L) coupled magnetohydrodynamic effect, and results are discussed.

4.1 INTRODUCTION

The electrodeposition of Ni-Co alloy coatings gained tremendous attention of researchers due to their wide spread applications, and ease of fabrication. However, electroplating variables such as current density(c.d.), temperature, concentration of additives, pH value of bath are of great importance in electrodeposition process(Pan et al. 2007). The Ni-Co alloys were extensively used as recorder head materials in computer hard drives, surface finishing industries as printed circuit boards; corrosion resistant coatings in aerospace, medical applications, nuclear power systems; and in magnetic devices as anticorrosive coatings. Current density is an important variable and no study of the alloy deposition is complete without detailed data on its variation. Moreover, the effect of c.d. is less consistent or predictable than that of other operating variables, with respect to the variation in composition of the electrodeposited alloy. Hence, to begin with detailed study on effect of c.d. on composition of Ni-Co alloy coating was undertaken. It is appropriate to recall here that the standard electrode potentials (E°) of nickel(Ni) and cobalt(Co) are relatively close together, *i.e.,* Ni = - 0.23V and Co = -0.28V, and difference of their electrode potential value is about 0.05V. It is well known that Ni-Co electroplating follows anomalous codeposition, where less noble metal (cobalt) is preferentially deposited, compared to the more noble metal (nickel). This phenomenon of preferential deposition of less noble metal (Co), compared to more noble metal (Ni) was attributed to the formation hydroxide of less noble metal on the surface of substrate. The hydroxide film so formed suppresses the deposition of more noble metal, as envisaged by Brenner. Thus the inherent limitation of anomalous type of codeposition of Ni-Co alloy coating was tried to alleviate using the advantage of magnetic field effect. The advantages of magnetic field in electrodeposition was reviewed extensively by Fahidy (Fahidy 1983). It has been described that magnetic field primarily effects the transport of ions towards cathode, and consequently alters the thickness of electrical double layer (EDL). This change in mass transport process is responsible for the change in morphology of the deposit (Ganesh et al. 2004).Thus, change in the thickness of the double layer is responsible for bringing a large change in properties of the alloy coatings. Thus, corrosion performance of Ni-Co alloy coatings can be improved, by altering the mass transport process at the electrode-electrolyte interface. This can be brought by taking the advantage of magnetic field effect, called magnetoelectrodeposition, and the effect is called magnetohydrodynamic(MHD) effect (Fahidy 1983). Thus the superposition magnetic field develop a new route for developing material of better corrosion properties. The effect on deposit characteristic mainly dependant on intensity and direction (parallel and perpendicular) of applied magnetic field. Therefore, this chapter is unfolding into two parts. In the first part, optimization of Ni-Co bath using conventional direct current (DC) method is explained. In the second part how magnetic field can be used beneficially to improve the corrosion resistance property of Ni-Co alloy coatings.

4.2 OPTIMIZATION OF Ni-Co ALLOY BATH

A new Ni-Co electrolytic bath was optimized by standard Hull cell method (Parthasaradhy 1989).The composition and operating variables of the optimized bath is given in Table 4.1. The electrolytic bath was prepared by dissolving cobalt sulphate, nickel sulphate, Sulphanilic acid. Ascorbic acid and boric acids were used as antioxidant and buffer, respectively. Glycerol was used as brightener. The effect of composition and operating parameters on the deposit character was assessed through visual observation of Hull cell panels, after deposition.

Table 4.1 - Composition and operating parameters of Ni-Co alloy bath used

Bath composition	Amount, g/L	Operating parameters
Cobalt sulfate	14.0	pH : 3.4
Nickel sulphate	131	Temperature : 298 K
Sulphanilic acid	0.74	Anode : Nickel
Ascorbic acid	2.4	c.d. range: 1.0 A dm^{-2} - 4.0 A dm^{-2}
Boric acid	30.0	
Glycerol	14 mL/L	

The Hull cell study revealed that the current density plays a vital role on the appearance and composition of the alloy coatings. The current density range at which satisfactory deposition taking place was determined by carrying out the Hull cell experiment. A slight increase of pH was observed, after each deposition. The bath pH = 3.4 was maintained during deposition. A slight increase of pH after each deposition was adjusted by addition of either NaOH, or HCl into the bath, depending on the requirement. The electrodeposition was carried at different current densities, maintaining the bath temperature as 298K. Electrodeposited alloy coatings were analyzed for their corrosion behaviour in 5% NaCl solution. The Ni-Co alloy coatings deposited at different c.d.'s are conveniently represented as $(\text{Ni-Co})_x$ where x - represents the c.d. at which the deposition was made from the optimized bath.

4.3 ELECTRODEPOSITION AND CHARACTERIZATION OF Ni-Co ALLOY COATINGS

4.3.1 Compositional Analysis

The change in the wt. % of Ni and Co with c.d., in the present Ni-Co alloy deposition is reported in Table 4.2. The change in the wt. % of constituting metals of the alloy, *i.e.*, Ni and Co with increase of c.d. is shown in Figure 4.1. It is well known that Zn-Fe group metal alloys, like Zn-Ni, Zn-Co and Zn-Fe, and mutual alloys of Fe group metals, like Ni-Co, Ni-Fe follow peculiar anomalous type of codeposition. The anomalous type of codeposition is characterized by the behaviour that less noble metal deposits preferentially compare to the more noble metal of the alloy(Brenner 1963). It may be seen that only at lower current density limit, *i.e.*, at 1.0 A dm^{-2}, wt. % of Co in the deposit is higher than the wt.% Ni (noble metal) in the deposit. It evidences the fact that Ni-Co bath follows anomalous type of codeposition. But as the c.d. increased, wt. % Co in the deposit is less than the wt. % Ni in the deposit. It indicates that bath follows normal type of codeposition at high c.d. limit. *i.e.*, noble metal deposits preferentially. This peculiar behaviour of the bath, where anomalous type of codeposition is changed to normal type with increase of c.d. may be attributed to the very low transition current density of Co, affected due to low concentration of Co in the bath. It may be recalled that transition current density is the current density at which wt.% metal in the deposit is equal to that in the bath. Due to very low concentration Co salt in the bath, the transition c.d. of Co is obviously very less.

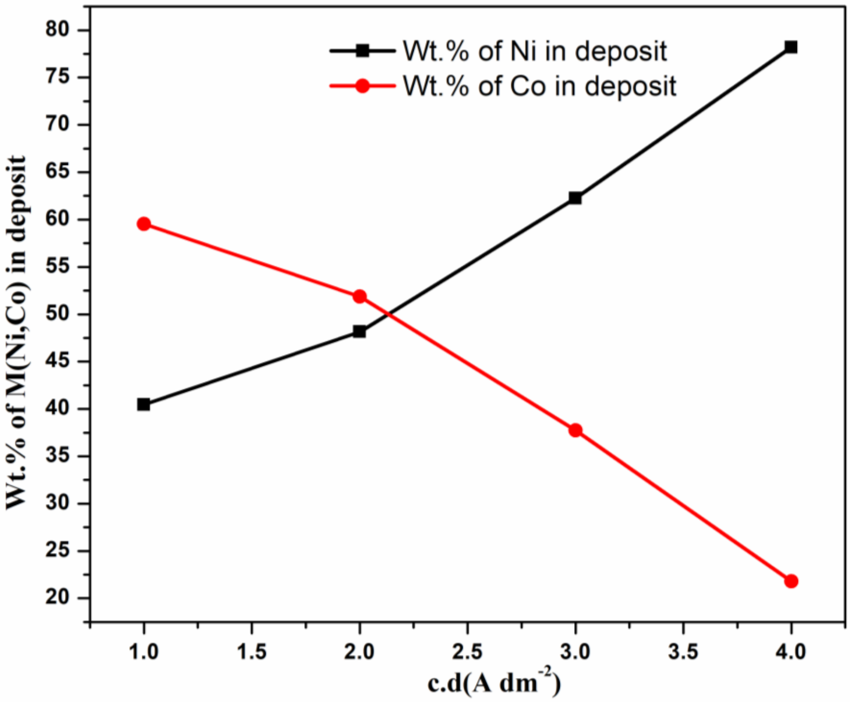

Figure 4.1- Change of wt.% of Ni and Co in the Ni-Co alloy deposit with applied c.d.

Hence, towards high c.d., the bath followed normal type of codeposition with preferential deposition of nobler Ni, instead of Co. The decrease of Co content in the deposit with increase of current density may also be explained in terms of the fundamental concept involved in the process of deposition. Since in the bath [Co^{2+}] ions very small compared to [Ni^{+2}] ions, Co is under diffusion control, and Ni is controlled kinetically. Hence, increase of current density is more beneficial for deposition of the species, controlled kinetically than the one controlled by diffusion. Therefore, on increasing the current density, discharge of Ni^{+2} ions is more favoured, with transfer of electrons. This in turn decreased the Co content of the alloy(Bahadormanesh and Dolati 2010).

4.3.2 Surface Morphology

The surface morphology of Ni-Co alloy coatings at different c.d.'s is shown in the Figure 4.2. It may be observed that the surface morphology of the alloy coating changed drastically with c.d., as shown from Figures 4.2(a) till 4.2(d).

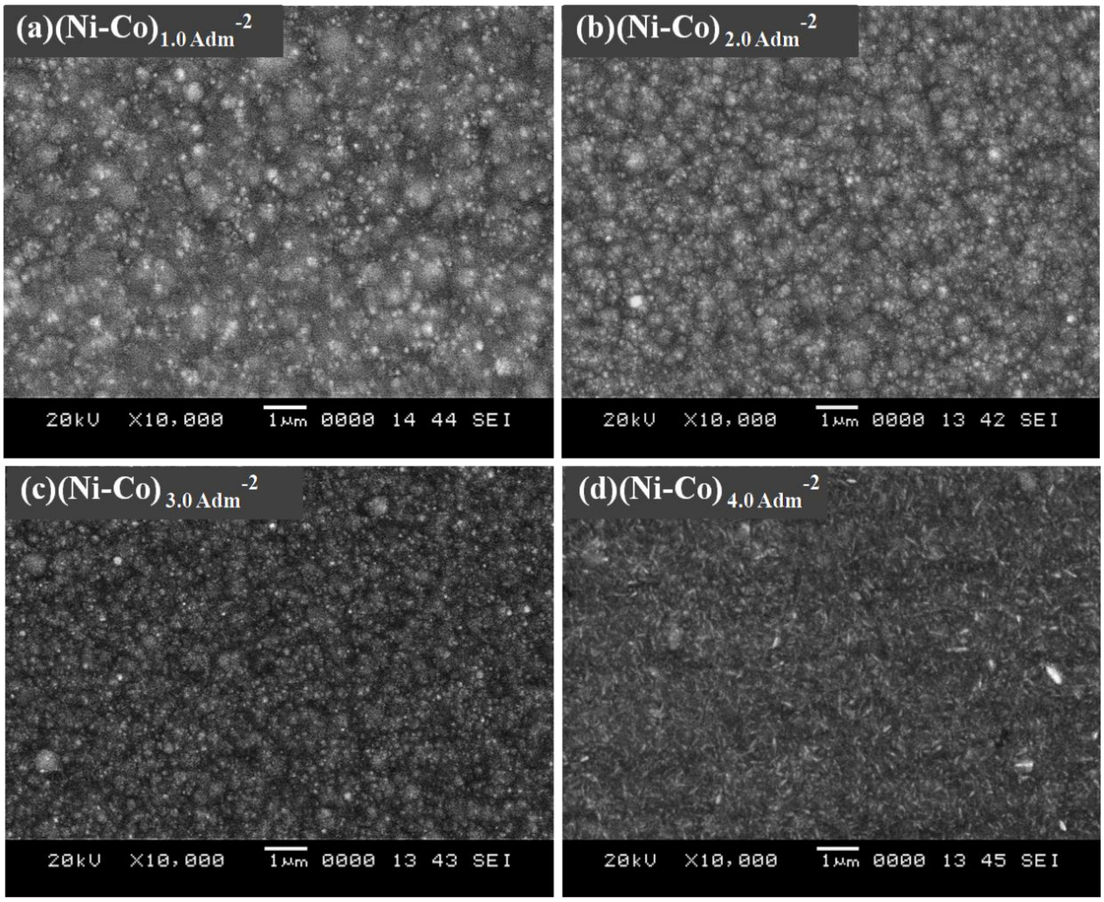

Figure 4.2 –Surface morphology of Ni-Co alloy coatings deposited from the optimized bath corresponding (a) (Ni-Co)$_{1.0\ A\ dm^{-2}}$ *(b)* (Ni-Co)$_{2.0\ A\ dm^{-2}}$ *(c)* (Ni-Co)$_{3.0\ A\ dm^{-2}}$ *and (d)* (Ni-Co)$_{4.0\ A\ dm^{-2}}$

Change in the microstructure of alloy coatings with c.d. clearly indicates that applied c.d. bears a close relationship with both composition and morphology of the coatings. The uniformity of the coating was found to be increased with increase of deposition. *i.e.* The granular structure of alloy coatings, corresponding to lower c.d. has changed to more uniform and fine grained structure as shown in Figure 4.2d. This is attributed to decrease of cobalt content with increase of current densities. With increase of current density, surface roughness value decreases. In addition, a large change in surface roughness of the alloy coating with c.d. was confirmed by Atomic Force Microscopy (AFM) also. Thus, surface study of the Ni-Co alloy coatings confirmed that c.d. has vital role on the microstructure of the alloy coatings.

4.3.3 X-RAY Diffraction Study

The phase structure of the electrodeposited Ni-Co alloys, developed under varying conditions of current densities were studied by X-ray diffraction (XRD) analysis. Identification of different phases of the electrodeposited alloy coatings, corresponding to different c.d.'s were obtained from the peak profiles of the X-ray reflections plotted as a function of 2θ. The X-ray diffraction pattern of Ni-Co alloys deposited at different c.d.'s in range of 1.0- 4.0 A dm^{-2} is given in the Figure 4.3.The peaks at 43.3^0 is corresponding to fcc structure of (200) plane of NiO(Pavithra and Hegde 2013). Other three peaks at 44.7^0, 51.8^0 and 76.4^0 are corresponding to (111), (200) and (220) planes of fcc structure of Ni (JCPDS 04-0850). One more distinct peak at 73.9^0 belongs to (311) plane of reflection corresponding to $CoNiO_2$(JCPDS10-0188).Increase or decrease in Intensity of the peaks with c.d. without any significant change in the diffraction angle indicates that Ni-Co alloy coatings form a single phase solid solution of Co in Ni with slightly different compositions, without change in the phase structures(Cullity 1956). The plane of reflections(112) and (311) corresponding to Ni-Co alloy(Pavithra and Hegde 2013).

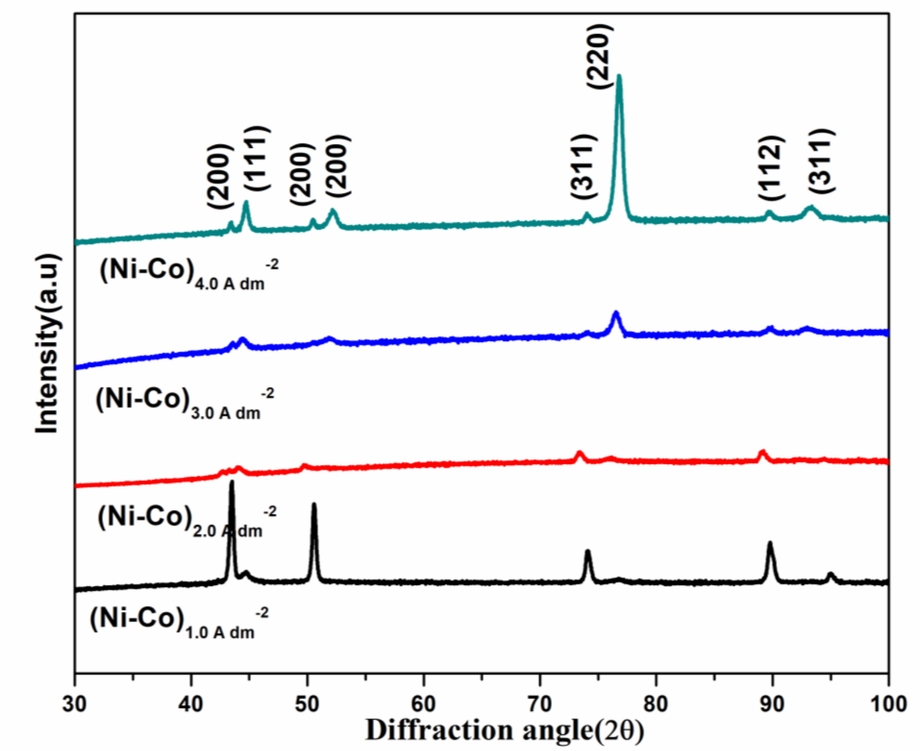

Figure 4.3- X-ray diffraction patterns of Ni-Co alloy coatings deposited at different current densities from the optimized bath

The increase of intensity of peak corresponding to (220) plane with increase of c.d.'s may be attributed to the change in the phase composition of alloy. In other words, the Ni content of the alloy increased with c.d. supported by composition data shown in Table 4.2.The average grain size of alloy coating was found to be 32 nm, calculated from full width at half maximum (FWHM)of all peaks using Debye-Scherrer formula(Subramanya et al. 2015),given by Eqn. (4.1).

$$D = \frac{K\lambda}{\beta \cos \theta} \qquad \ldots\ldots\ldots\ldots\ldots\ldots\ldots\ldots\ldots\ldots \qquad (4.1)$$

Where D= crystallite size (nm), λ= 1.5406 A°(Cu K_α radiation) is the wavelength of X-ray used, K=0.9(Debye coefficient), β = full width at half maximum (FWHM) in radian and θ = Bragg's angle(Degree).

4.3.4 Corrosion Study

The electroplated Ni-Co alloy coatings, deposited at different c.d.'s were subjected to corrosion study by conventional potentiodynamic polarization and Electrochemical impedance spectroscopy (EIS) methods.

4.3.4.1. Potentiodynamic polarization study

The corrosion behavior of Ni-Co coatings deposited at different c.d.'s was evaluated by subjecting them to polarization study, using three electrode system where electroplated specimens is the working electrode. The potentiodynamic polarization study was done in a potential range ± 250 mV at a scan rate of 1 mVSec^{-1}. Corrosion rates (CR's) were calculated by Tafel's extrapolation method and corresponding plots are shown in the Figure 4.4.

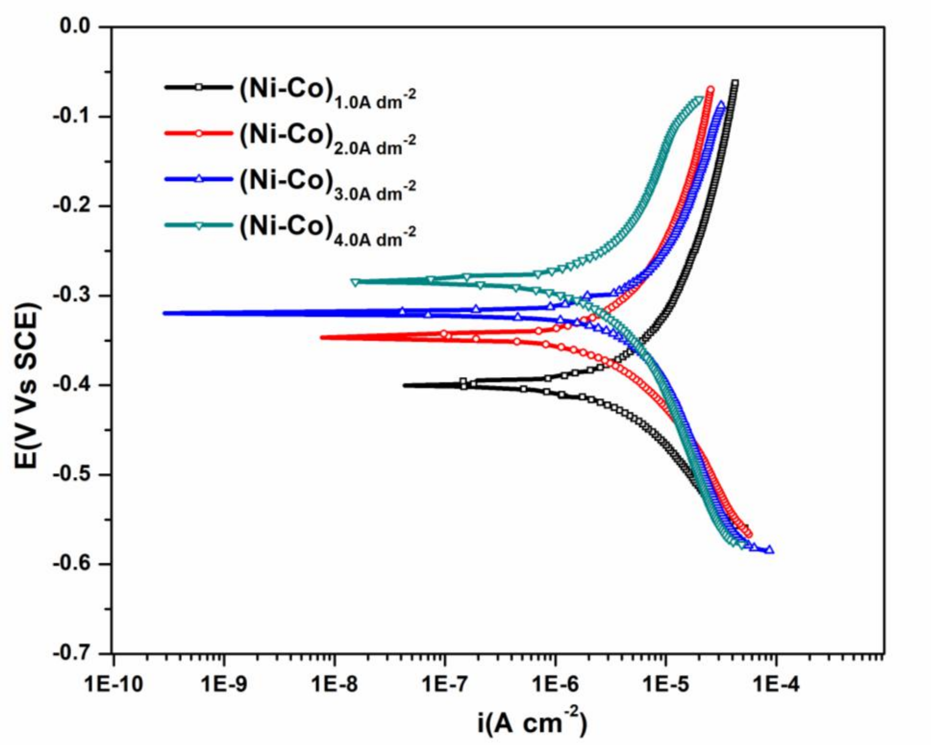

Figure 4.4- Potentiodynamic polarization curves of Ni-Co coatings deposited at different current densities

The values of observed corrosion potential (E_{corr}), corrosion current density (i_{corr}) and CR's are reported in Table 4.2. The corrosion data revealed that the optimized bath, given in the Table 4.2 could produce bright coating at c.d. = 4.0 Adm^{-2}, showing minimal corrosion rate (22.4×10^{-2}) mm y^{-1}, compared to those produced at other c.d.'s. This least CR of Ni-Co alloy coating may be attributed to the presence of highest Ni (noble metal) content of the alloy, which prevented the corrosion most efficiently(Srivastava et al. 2006).

Table 4.2- Corrosion data for electrodeposited Ni-Co alloy coating developed at different c.d.'s using optimal bath

Coating configuration	Wt.% Ni in the deposit	Wt.% Co in the deposit	$-E_{corr}$ (mV vs SCE)	i_{corr} (μA cm^{-2})	CR×10^{-2} (mm y^{-1})	R_{ct} (ohm)
$(Ni\text{-}Co)_{1.0\ A\ dm^{-2}}$	40.45	59.55	410	24.4	41.1	73
$(Ni\text{-}Co)_{2.0\ A\ dm^{-2}}$	48.14	51.86	346	14.6	24.6	289
$(Ni\text{-}Co)_{3.0\ A\ dm^{-2}}$	62.26	37.74	314	17.62	23.42	549
$(Ni\text{-}Co)_{4.0\ A\ dm^{-2}}$	78.20	21.80	287	20.81	22.4	787

4.3.4.2 EIS study

Electrochemical Impedance spectroscopy(EIS) study was made to evaluate the barrier properties, electrical double layer capacitance and charge transfer resistance(R_{ct}) of the electrodeposited Ni-Co alloy coatings (Yuan et al. 2009).In EIS, the most versatile approach to evaluate the behaviour of test electrode is Nyquist plots. This commonly considers the plotting data of real impedance (Z') vs imaginary impedance (Z'') with provision to distinguish the contribution of charge transfer resistance (R_{ct}) and solution resistance (R_S).The Nyquist plots of Ni-Co coatings deposited at different c.d.'s are as shown in the Figure 4.5. The existence of single semicircle for all Ni-Co alloy coating configuration showed that single charge transfer process is involved in corrosion process (Ullal and Hegde 2014). The capacitive loop found at higher frequency limit indicates that the corrosion protection of the coatings is due to double layer capacitance (C_{dl}). Further, an increase in the radius of semicircle with c.d. indicated that CR bears a close relation with c.d., employed for its deposition. The maximum diameter of the capacitive loop at optimal c.d. (4.0 A dm^{-2}) demonstrated that the $(Ni\text{-}Co)_{4.0\ A\ dm^{-2}}$ is the most corrosion resistant, compared to other coatings. The Nyquist ECE fitting corresponding to a coating at optimal c.d. (4.0 A dm^{-2}) is given in inset of Figure 4.5 and charge transfer resistant values corresponding to all deposited coatings were given in Table 4.2.

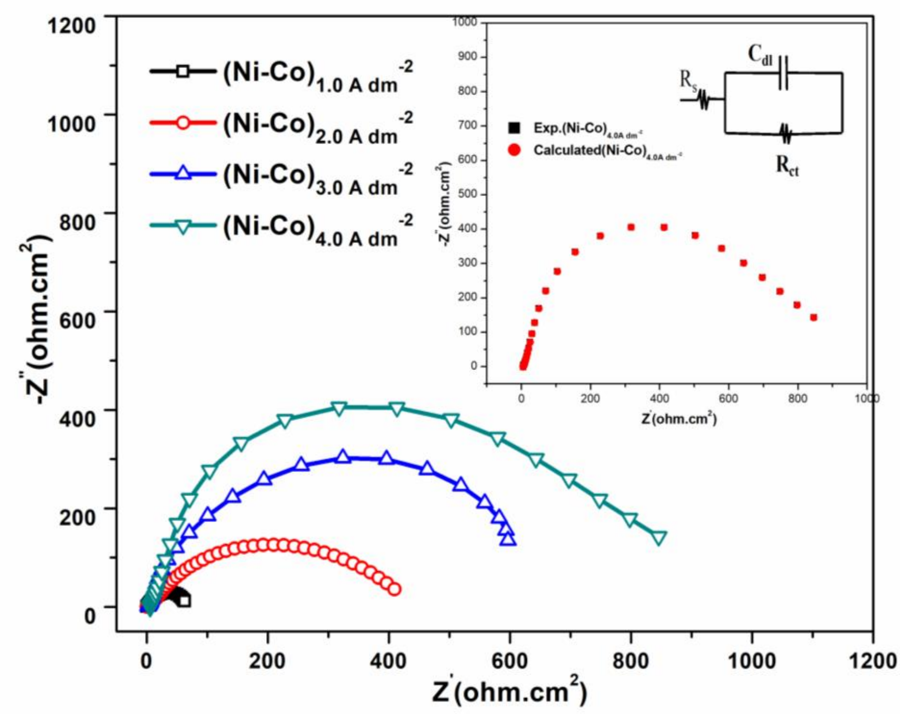

Figure 4.5-Nyquist plots of Ni-Co alloy coatings obtained at different c.d.'s

4.4 MAGNETO-ELECTRODEPOSITION OF Ni-Co ALLOY COATINGS

The composition, phase structure and surface morphology of alloy coatings can be improved/altered substantially, when magnetic field (*B*) is induced parallel to the process of electrodeposition and such process of electrodeposition is called magnetoelectrodeposition. Keeping this in mind, magnetoelectrodeposition of Ni-Co alloy coating was attempted to improve its corrosion resistance property. The experimental set up used for magnetoelectrodeposition of Ni-Co alloy coatings are shown in Figure 4.6. The magneto-electrodeposition was carried out using Electromagnet (Polytronics, Model: EM 100, India) in conjunction with DC power source (Aplab, LD3205, India). The magnetic field was applied both parallel and perpendicular to the direction of electric field. The optimal bath (Table 4.1) was kept in centre of space between the poles to maintain a uniform magnetic field inside the bath. Magnetoelectrodeposition were carried out by inducing the magnetic field, in the range of 0.1- 0.4 T (Tesla), parallel to the effect of c.d. = 4.0 Adm^{-2}. The intensity of magnetic field, responsible for change of convection process has varied, and its effect on the composition, and hence properties of alloy coatings were tested.

Magnetoelectrodeposition of Ni-Co alloy coatings were accomplished on a copper substrate using the same optimized bath (Table 4.1). The magnetic field *B* was applied, both parallel and perpendicular to the direction of electric field as shown in Figures 4.6 (a) and 4.6 (b), respectively. All experimental conditions, like bath composition and operating parameters, except c.d. were kept constant for magnetoelectrodeposition. Magnetoelectrodeposition of Ni-Co alloy coatings were carried out in a custom made cell, placing in the space between two poles of the Electromagnet as shown in Figure 3.4(Chapter 3). The pure nickel strip was used as anode, with same exposed area as that of cathode. The cathode and anode were placed parallel 5 cm apart during deposition. All coatings were cleaned using distilled water, followed by air drying. The magneto electrodeposited Ni-Co alloy coatings were analysed for the composition, phase structure and surface morphology.

Magnetoelectrodeposition of Ni-Co alloy coatings were carried out under different conditions of *B*, and their corrosion performances were evaluated by potentiodynamic polarization and EIS methods. Here for convenience, electrodeposited and magnetoelectrodeposited Ni-Co alloy coatings are represented as ED (Ni-Co) and MED (Ni-Co) alloy coatings, respectively. Further magnetoelectrodeposited Ni-Co alloy coatings are conveniently represented as $(\text{Ni-Co})_{4.0/\text{BT/Per or para,}}$ where subscript represent the c.d. and magnetic field intensity (B=0.1, 0.2, 0.3 and 0.4) (depending on the direction).

4.4.1 Potentiodynamic Polarization Study

The potentiodynamic polarization behavior of the MED Ni-Co coatings, corresponding to different of magnetic field intensity (*B*), both parallel and perpendicular are shown in Figures 4.6 and 4.7.The corrosion rates (CR’s) of magnetoelectrodeposited Ni-Co alloy coatings were evaluated by Tafel’s extrapolation method, and are reported in Table 4.3.

Table 4.3- Effect of magnetic field intensity (*B*) on deposit characters of Ni-Co alloy electrodeposited from optimized bath at 303K

Coating configuration	Wt. % Ni in the deposit	Wt. % Co in the deposit	$-E_{corr}$ (mV vs SCE)	i_{corr} (μA cm^{-2})	$CR\times10^{-2}$ (mm y^{-1})	R_{ct} (ohm)
$(Ni\text{-}Co)_{4.0/0.1T/Par}$	87.86	12.14	269	14.6	14.8	7554
$(Ni\text{-}Co)_{4.0/0.2T/Par}$	86.65	13.35	228	7.9	8.4	9436
$(Ni\text{-}Co)_{4.0/0.3T/Par}$	84.13	14.87	287	3.3	3.4	11258
$(Ni\text{-}Co)_{4.0/0.4T/Par}$	84.71	14.29	271	7.2	7.7	10346
$(Ni\text{-}Co)_{4.0/0.1T/Per}$	83.77	16.23	202	4.0	4.4	11642
$(Ni\text{-}Co)_{4.0/0.2T/Per}$	82.32	17.68	187	2.2	2.4	15611
$(Ni\text{-}Co)_{4.0/0.3T/Per}$	79.51	20.49	172	2.0	2.1	23338
$(Ni\text{-}Co)_{4.0/0.4T/Per}$	80.32	19.68	222	4.3	4.6	19289
$(Ni\text{-}Co)_{4.0\ A\ dm^{-2}}$	78.20	21.80	287	20.81	22.4	787

From the corrosion data, it is clear that the corrosion rates of MED Ni-Co alloy coatings decreased sequentially with increase of *B* till 0.3 T, and increased thereafter (in both parallel and perpendicular *B*). From the corrosion data, reported in Table 4.3, it may be noted that superimposition of *B* on the process of electrodeposition increased the Ni (noble metal) content of the alloy drastically. *i.e.* wt.% of Ni is changed from 78.20% to 87.86%. Thus decrease of CR of MED Ni-Co alloy coatings may be attributed to its increased Ni content. It is interesting to note that CR of MED Ni-Co alloy coating decreased with increase of intensity of *B*. The decrease CR with intensity of *B* is due to the increase of Co content of the alloy, under given bath condition. The increase of cobalt content with increase of *B* is reasoned by the fact that Co is magnetically more active than Ni. In other words, magnetic moment of cobalt is greater than nickel(Carlin and De Jongh 1986).Thus it may be summarized that decreased CR of MED Ni-Co alloy coating is due to the varying metal contents of the alloy, affected due to applied magnetic field intensity. It may be noted that CR's of MED (Ni-Co) alloy coatings, under both parallel and perpendicular *B* decreased with intensity of *B* only up to 0.3T. This decrease of CR is due to change in composition of the alloy, affected due to magneto-convection. However, when magnetic field *B*, higher than its limiting value (of the bath) is applied it throws an adverse effect on the deposit characters, due to increase of hydrogen evolution reaction (HER) at optimal c.d. Therefore, at higher limits of induced *B* (at 0.4T), the coatings was found to be more porous, and hence showed more CR, in both parallel and perpendicular *B*, and hence showed higher CR value (Table 4.3). Thus, it may be summarised that MED $(Ni\text{-}Co)_{4.0/0.3T/Per}$ coating exhibits the least corrosion rate (2.1×10^{-2} mm y^{-1}), compared to $(Ni\text{-}Co)_{4.0\ Adm^{-2}}$ with CR = 22.4×10^{-2} mm y^{-1}, and MED $(Ni\text{-}Co)_{4.0/0.3T/Par}$ with CR=3.4×10^{-2} mm y^{-1}.

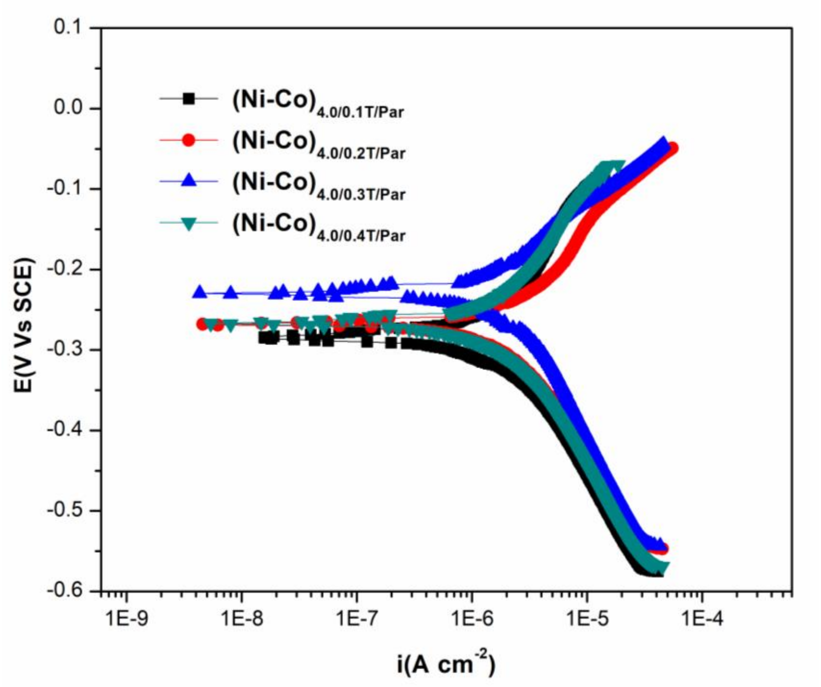

Figure 4.6-Potentiodynamic curves of MED Ni-Co alloy coatings obtained from optimized bath under different conditions of applied magnetic field (parallel)

The less CR of MED $(Ni\text{-}Co)_{4.0/0.3T/Per}$ compared to that of MED $(Ni\text{-}Co)_{4.0/0.3T/Par}$ may be attributed to the additional magneto convection effect, due to Lorentz force (F_L). In case of parallel B, the Lorentz force on the charge density in the diffusion layer which gives rise to a non-electrostatic field parallel to the working electrode surface which induces motion of the solution near the interface. The magneto convection effect is maximum in case of perpendicular B, as the net effect of both non-electrostatic and electrostatic force (Ebadi et al. 2010).

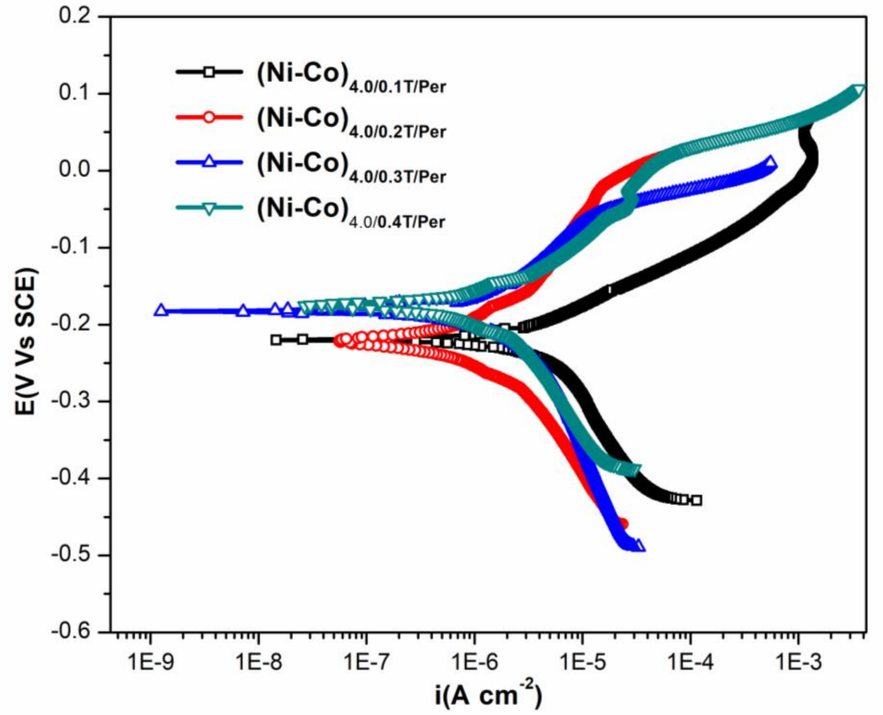

Figure 4.7-Potentiodynamic curves for MED Ni-Co alloy coating obtained from optimized bath under different conditions of applied magnetic field (perpendicular)

4.4.2 Impedance Study

EIS is a non-destructive method for studying the interfacial interaction of test material very accurately, by giving valuable information on reactions involving transfer of electrons at the electrode surface. This technique gives information on Ohmic conduction, charge transfer, interfacial charging, mass transfer at the electrode-electrolyte interface (Yuan et al. 2009).Therefore, impedance behaviour of MED (Ni-Co) alloy coatings, under effect of both parallel and perpendicular B were studied, and are shown in Figures 4.8 and 4.9, respectively. It may be seen that in both parallel and perpendicular *B*, axial radius of the semicircle keeps increasing with the intensity of *B*, till 0.3 T and then decreased. The ECE circuit for (Ni-Co)$_{4.0/0.3T/Par}$ and (Ni-Co)$_{4.0/0.3T/Per}$ are given in inset of Figure 4.8 &4.9 respectively,and charge transfer resistance values for all Magnetoelectrodeposited coatings were reported in the Table 4.3.

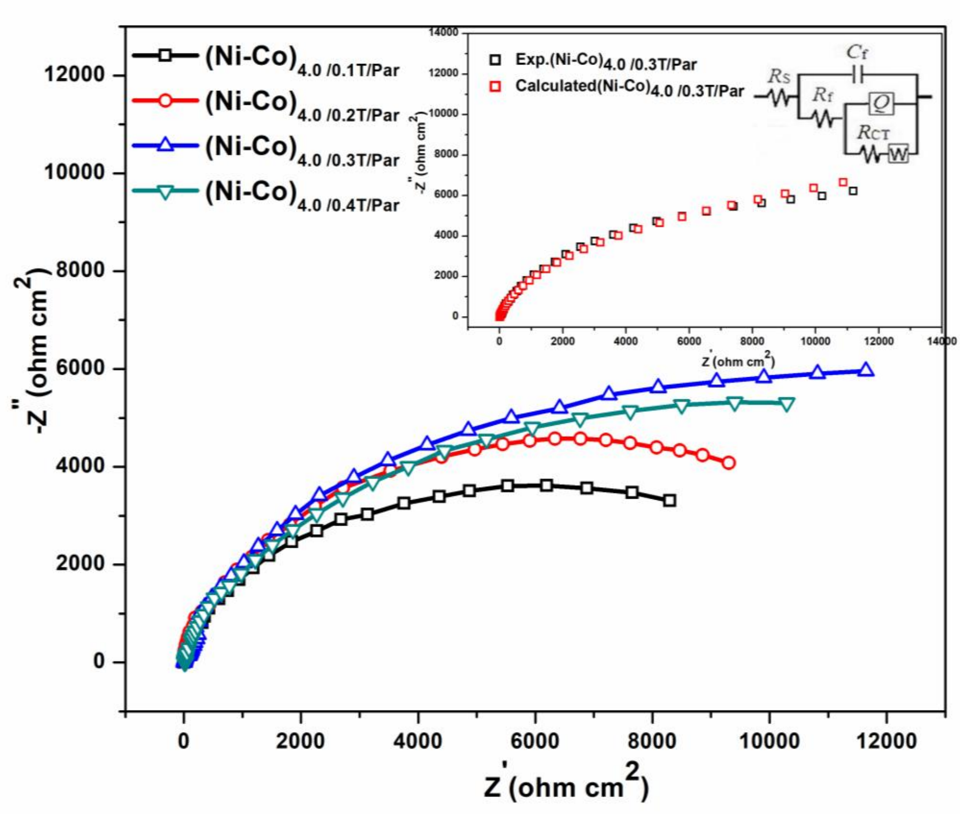

Figure 4.8-Nyquist response for MED Ni-Co alloy coating obtained from optimized bath under different conditions of applied magnetic field (parallel)

The Table 4.3, clearly suggests that the charge transfer resistance(R_{ct}) of MED coatings increases with intensity of *B*. But at high intensity of *B*, the value of R_{ct} was found to be decreased once again, due the reason explained in previous Section. 4.3. On comparing the axial radii of semicircles, corresponding to MED (Ni-Co) alloy coatings of different configurations (both in intensity and direction of *B*), it may be concluded that MED (Ni-Co)$_{4.0/0.3T/Per}$ coating is found to be the most corrosion resistant, due to increase of Co content of the alloy. The increase of Co in the deposit may be attributed to the magnetic field limited convection of Co ions in the bath, and are supported by composition and corrosion data, reported in Table 4.3.

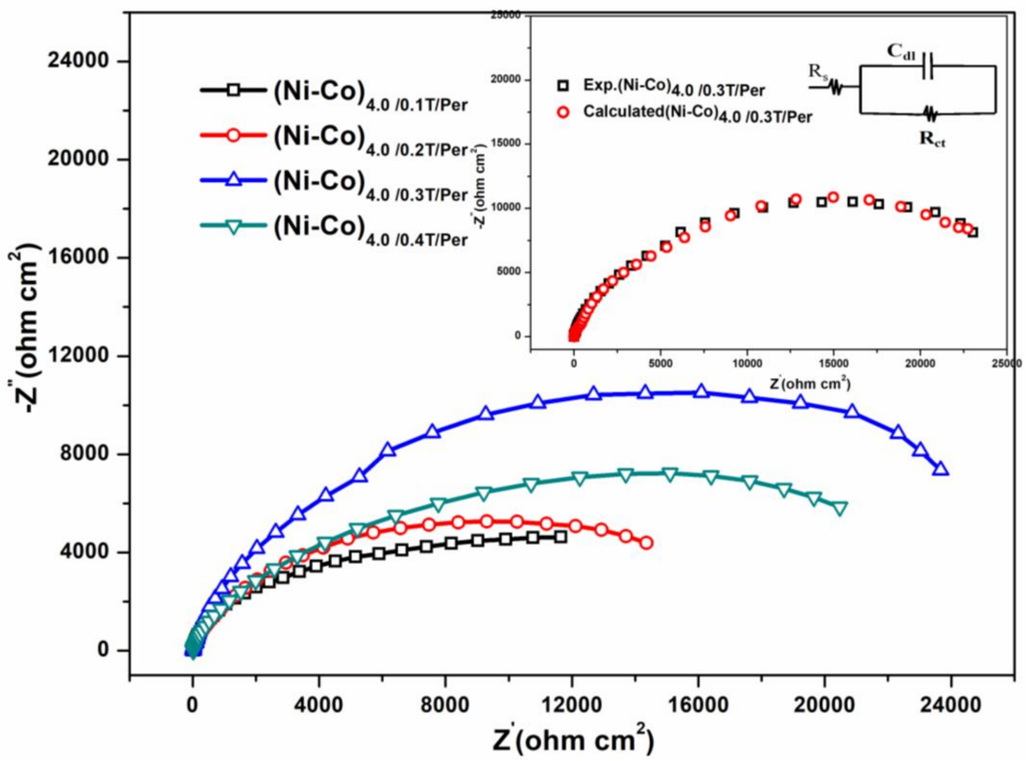

Figure 4.9-Nyquist response for MED Ni-Co alloy coating obtained from optimized bath under different conditions of applied magnetic field (perpendicular)

4.5 XRD STUDY

The XRD patterns for MED Ni-Co alloy coating obtained at different field strength, under parallel and perpendicular direction are given in the Figures 4.10 and 4.11.The peaks at 43.3^0 is corresponding to the plane (200) of NiO fcc structure. The three distinct peaks at 44.7^0,51.8^0 and 76.4^0 for the planes, respectively for (111),(200) and (220) were observed for fcc Ni structure (JCPDS 04-0840).One more distinct peak (311) at corresponds to $CoNiO_2$ structure (JCPDS10-0188). It may be noted that XRD patterns of all MED Ni-Co alloy coatings remains same, regardless of the intensity and direction of *B*. However, the intensity of reflection was found to be changed with change in the composition of the alloy. Thus XRD study of MED Ni-Co alloy coatings, under both parallel and perpendicular *B*, reveals that applied magnetic field has vital role on the composition of the alloy, but not with the phase structure of alloy. This confirms that fact that magneto electrodeposition of Ni-Co alloy coating is diffusion controlled, or magnetic field controlled, without change in the crystallinity of the deposit.

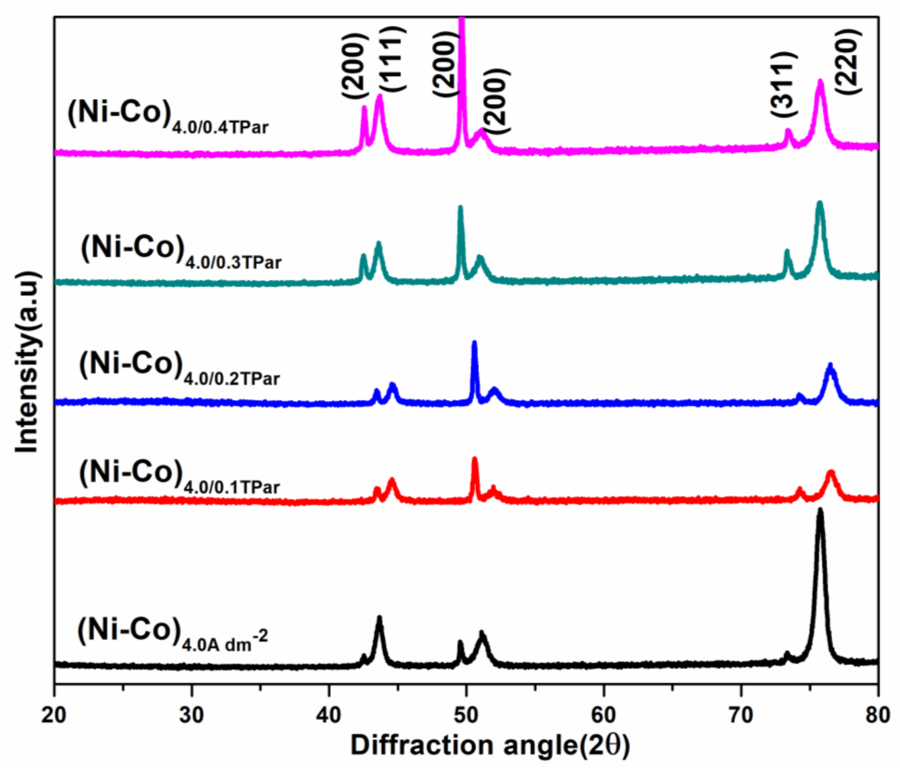

Figure 4.10-XRD patterns of Ni-Co alloy coating obtained at different magnetic field strength (parallel)

The constancy of phase structure of Ni-Co alloy coatings with direction and intensity of *B* may be explained as follows: From the literature and phase diagram of Ni-Co alloys, it is known that the electrochemically deposited Ni-Co alloy can form a solid solution of Co in a nickel matrix (up to 25 wt.% Co)(Obradovic et al. 2001). In the present study, Ni-Co alloy containing less than 25 wt. % Co forms a single phase solid solution of Co in Ni with slightly different compositions and very similar diffraction patterns. It may be recalled that in solid solution the chemical components (metals) remain in a single homogeneous phase in all proportions of constituents(Cullity 1956).The key point to the interpretation of the powder XRD patterns of alloys is that each phase produces its own pattern independently of the presence or absence of any other phase.

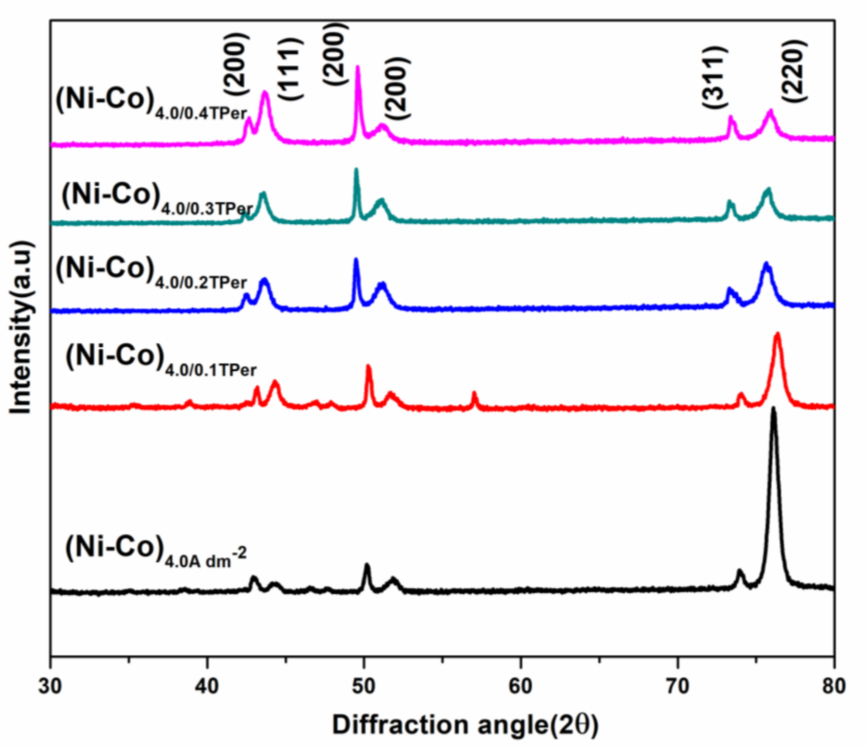

Figure 4.11-XRD patterns of Ni-Co alloy coating obtained at different magnetic field strength(perpendicular)

Thus a single phase alloy produces a single pattern, when Ni and Co completely soluble in the solid state (to form solid solution), then solid phase forms a continuous solid solution is of the substitutional type. It varies in composition, but not in crystal structure, from pure Ni to pure Co, which must necessarily have the same structure. The lattice parameter of solid solution also varies continuously from that of pure Ni to that of pure Co. Since all alloys in a system of this kind consist of the same single phase, their powder patterns appear quite similar, the only effect of a change in composition being to shift the diffraction line positions in accordance with the change in lattice parameter. Therefore, Ni-Co alloy coatings electrodeposited at different *B*= 0.1 to 0.4T formed a solid solution of Co in Ni lattice. Hence, all alloy coatings formed the solid solution of Co in Ni, with slightly different compositions, but with very similar diffraction patterns.

The average grain size of MED Ni-Co alloy coatings deposited under parallel and perpendicular conditions of *B*, calculated using Eqn. (4.1) was found to be in the range of 26 nm and 20 nm, respectively. This reduction in grain size on the application of perpendicular *B* is due to the fact that the rate of reaction is accelerated, which improves the nucleation and mass transfer process(Ebadi et al. 2010), which in turn responsible for improved corrosion resistance of MED alloy coatings, under perpendicular *B*(Bakhit and Akbari 2013; Srivastava et al. 2006).It may also be seen that finer grains (produced through higher nucleation rate and lower rate of grain growth) were produced under magnetic field effect, compared to the effect of only electric field (c.d.). Refinement of grain size of MED coatings, due to induced *B* is further confirmed by the increased charge transfer resistance of EIS curves, observed by increasing diameter of semicircles(Hassani et al. 2008).Basically, MED coatings blocks the active growth sites for corrosion and decreases the activation energy for nucleation.

4.6 SURFACE STUDY

4.6.1 SEM Study

The surface morphology of MED Ni-Co alloy coatings, developed under different conditions of *B* have been examined under SEM, and are shown in Figures 4.12 and 4.13. A clear difference in microstructure of MED alloy coatings was observed, when *B* is varied from 0.1T to 0.4T, in both parallel and perpendicular conditions. Numerous observations are reported in the literature of the magnetic field effect on the surface deposit pattern are contradictory since morphological characteristics of the deposit crystal structure cannot be related in a straightforward manner to the imposed magnetic flux density. There is, nevertheless, ample evidence for the beneficial effect of an imposed uniform magnetic field on surface evenness and firmness under carefully chosen experimental conditions(Fahidy 1983). In this regard, the present MED Ni-Co alloy coating do not show much difference in the surface microstructure with change of intensity of *B.* i.e. when *B* is changed from 0.1 T to 0.4 T, in both parallel and perpendicular *B*, as shown in Figures 4.12 and 4.13.However, MED (Ni-Co)$_{4.0/0.3T/Per}$ coating, showing the least CR was found to be the smoothest and uniform, compared all other coatings as shown in Figure 4.13. Hence, with increase of magnetic field intensity the surface roughness decreases(Fang et al. 2017) .The increase of CR at *B*=0.4T is attributed to increase of hydrogen evolution reaction at higher magnetic field intensity.

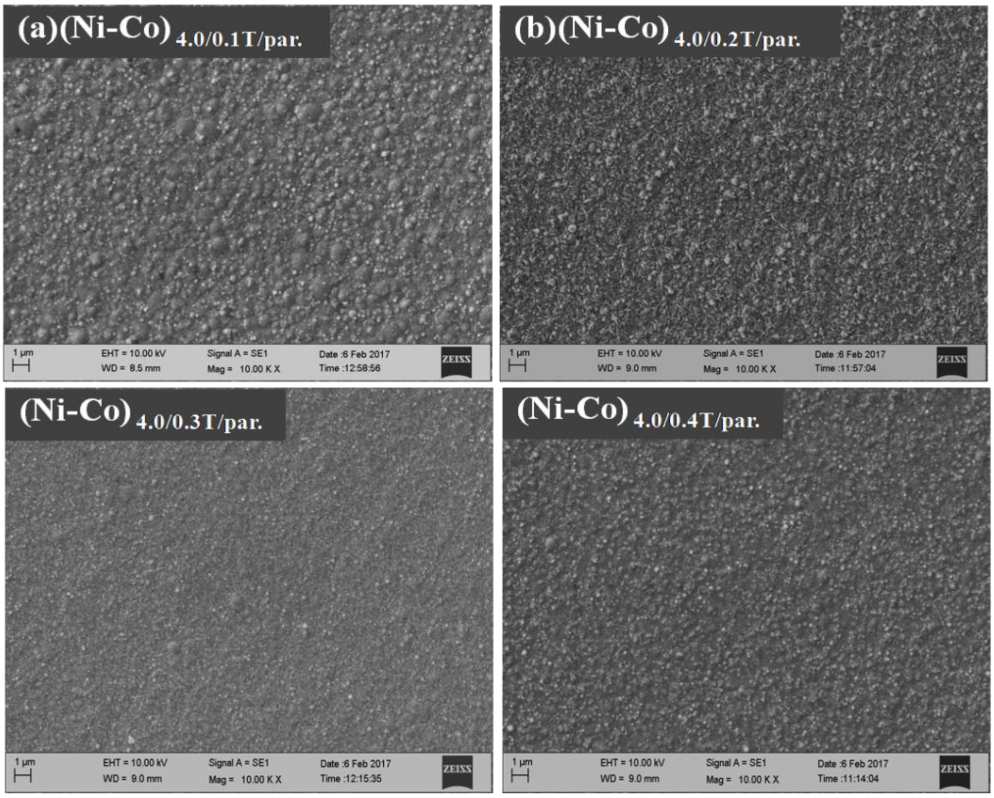

Figure 4.12- Surface morphology of MED Ni-Co alloy coatings developed under different conditions at magnetic field intensity (parallel), from the optimal bath

The evolution of excessive hydrogen at higher intensity of *B* is indicated by the formation of bubbles on the surface of coatings as may be seen in Figures 4.12 and 4.13. The surface morphology of MED Ni-Co alloy coatings, under optimal conditions of both parallel and perpendicular *B* is shown, in comparison with ED Ni-Co alloy coatings (optimal) is shown in Figure 4.14. It may be noted that ED Ni-Co alloy coatings, where *B*=0 T exhibits a rough surface, compare to MED Ni-Co alloy coatings, under both parallel and perpendicular conditions. This may be attributed to the excessive evolution of hydrogen during conventional codeposition process(Brenner 1963)(Elias and Hegde 2017).

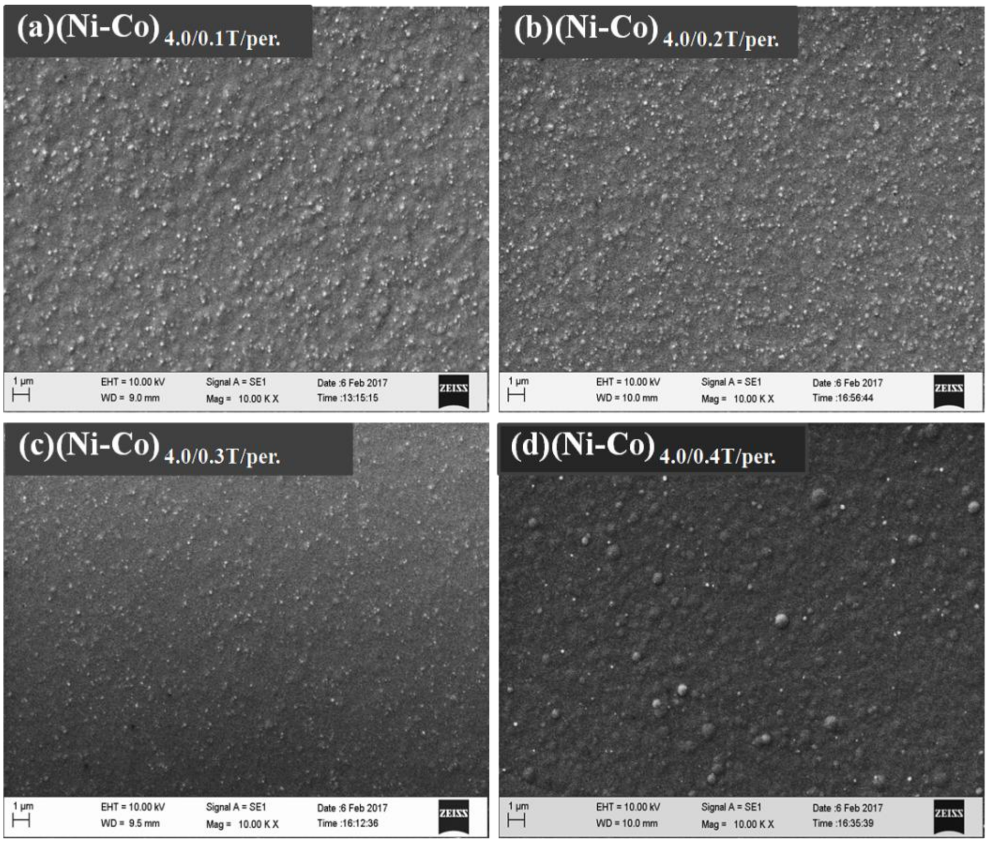

Figure 4.13- SEM images of MED Ni-Co coatings developed under different conditions of magnetic field intensity (perpendicular) from optimized bath

When *B* is oriented perpendicular to the electrode surface, the magneto convection effect will be maximum. As a result, change in surface morphology of the coating, due to perpendicular field is maximum, compared to the effect of parallel field. This amounts to state that the Lorentz force acting, under condition of perpendicular *B* is responsible to increase the mass transfer process towards cathode (Peipmann et al. 2010a),(Hinds et al. 2001).This in turn is responsible for decrease in diffusion layer thickness in the vicinity of the electrode(Uhlemann et al. 2005). Hence, the surface has become more flat in the case of perpendicular direction coating as compared to parallel coating and without magnetic field effect. Hence, the application of magnetic field smoothens the surface of the deposited alloy, which in turn responsible for better corrosion resistance.

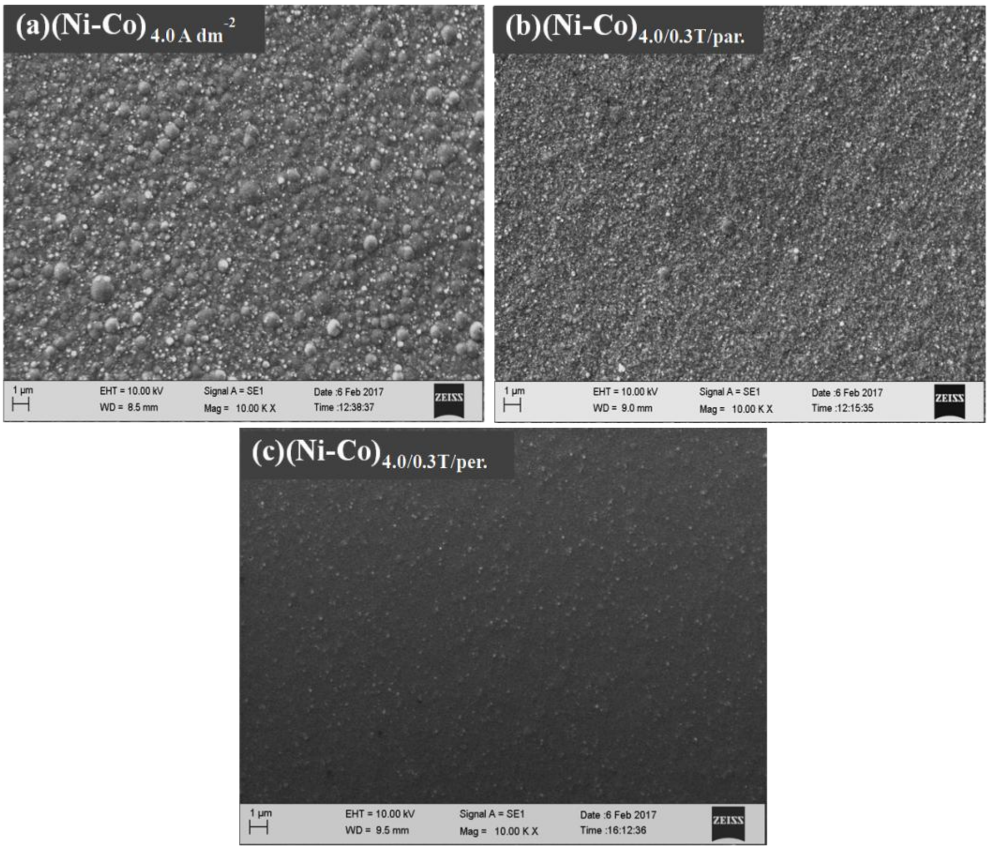

Figure 4.14- Comparison of surface microstructure of MED Ni-Co alloy coatings, under optimal conditions of both parallel and perpendicular B, in comparison with ED Ni-Co alloy coatings deposited from the same bath

4.6.2 AFM Study

The surface roughness of alloy coatings were studied using three dimensional Atomic Force Microscopy (AFM) techniques. The AFM image of Ni-Co alloy coatings, corresponding to three optimal conditions, *i.e.* ED $(\text{Ni-Co})_{4.0\ \text{Adm}^{-2}}$, MED $(\text{Ni-Co})_{4.0/0.3\text{T/par}}$ and $(\text{Ni-Co})_{4.0/0.3\text{T/per}}$ are shown, respectively in Figures 4.15 (a), (b) and (c). The surface roughness of the alloy has reduced substantially, when magnetic field *B* is induced during deposition as may be seen in Figure 4.15. Analysis of the experimental data of AFM study revealed that the average roughness of alloy coatings corresponding to $(\text{Ni-Co})_{4.0\text{Adm}^{-2}}$,$(\text{Ni-Co})_{4.0/0.3\text{T/par}}$ and $(\text{Ni-Co})_{4.0/0.3\text{T/per}}$ are, respectively 24.0, 14.9 and 7.63 nm.

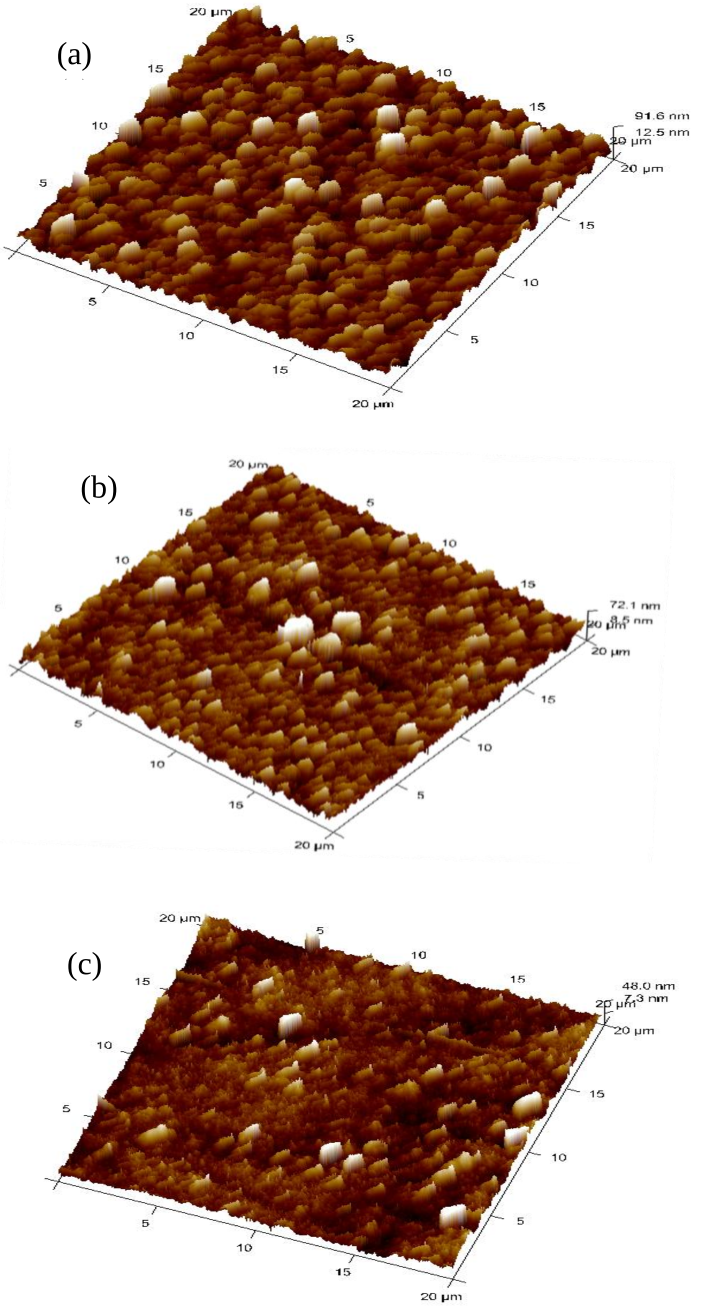

Figure 4.15- AFM image of Ni-Co alloy coatings at optimal conditions of electrodeposition :(a)ED (Ni-Co)$_{4.0Adm}^{-2}$,(b) MED (Ni-Co)$_{4.0/0.3T/par}$ and (c) (Ni-Co)$_{4.0/0.3T/per}$ alloy coatings deposited from same bath, at constant current density of 4.0 A dm^{-2}

At the same time, a decrease of surface roughness was found on superimposition of magnetic field, as shown in the Figures 4.15(a),(b) and (c), and corresponding data are reported in Table 4.4.

Table 4.4- The surface roughness data of ED (Ni-Co)$_{4.0A\ dm^{-2}}$, MED (Ni-Co)$_{4.0/0.3T/par}$ and (Ni-Co)$_{4.0/0.3T/per}$ alloy coatings obtained at constant current density of 4.0 A dm^{-2}

Coating configuration	R_a(nm)	R_q(nm)
(Ni-Co)$_{4.0Adm^{-2}}$	24.0 nm	30.8 nm
(Ni-Co)$_{4.0/0.3T/par}$	14.9 nm	20.9 nm
(Ni-Co)$_{4.0/0.3T/per}$	7.63 nm	10.7 nm

4.7 DISCUSSION

The MED approach adopted for improving corrosion resistance property of ED Ni-Co alloy coating was driven by the following incentives. The factor responsible for improved corrosion resistance of MED Ni-Co alloy coatings is by increasing wt. % Co in the deposit, and is discussed as below.

The effects of plating variables on the composition of the deposit are determined by changes in the concentrations of metal ions in the cathode diffusion layer (CDL), and are predictable from simple diffusion theory, and schematically as shown in Figure 4.16. Accordingly, the limiting current density (i_L) is the measure of maximum reaction rate that cannot be exceeded because of a limited diffusion rate of metal ions in solution. In the region of the limiting current, when the electrode process is mass-transfer controlled, the value of the current density is given by Eqn. (4.2)

$$i_L = \frac{nF\,D_z C_B}{\delta} \quad \text{....................} \ (4.2)$$

Where, n is the valency of the metal ions and F is the Faraday constant (96400 C), D is the diffusion coefficient of the reacting species, C_B is the concentration and δ is the thickness of electrical double layer (EDL).

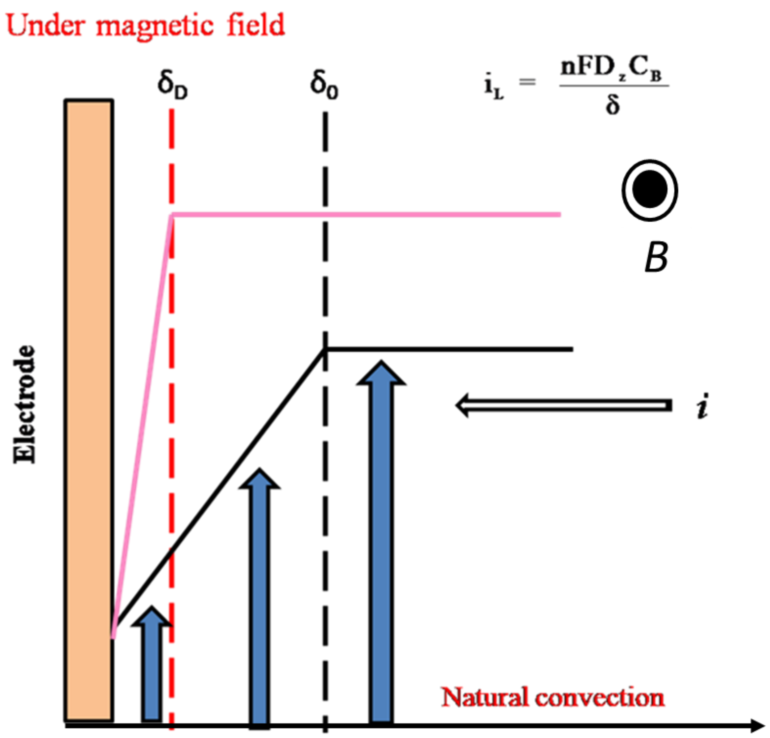

Figure 4.16-Schematic representation showing the decrease of diffusion layer thickness (δ) due to increase of limiting current density on superimposition of magnetic field B

The $(Ni\text{-}Co)_{4.0/0.3T/per}$ coating obtained in a perpendicular direction was found to be more corrosion resistant as compared Ni-Co alloy coatings of other configurations. This may be attributed to the combined effect of Lorentz force and non-electrostatic force, due to application of magnetic field. The Lorentz force is maximal when field is applied perpendicular to the direction of flow of ions, which is responsible for macro-MHD to decrease the thickness of diffusion layer near to the electrode. It may be noted that thickness of cathode film decreased from δ_0 to δ_D, as the mode of the coating is changed from ED to MED type. Further, an increase of i_L for deposition of Co, due to inducing of magnetic field is shown schematically in Figure 4.16, supported by the Eqn. (4.1). Increase of Co content of the alloy, due to increase of its i_L is responsible for increased corrosion resistance of Ni-Co alloy coatings. Further increase of B, both parallel and perpendicular caused the mass transport of cobalt ions to diminish, and to increase the evolution of hydrogen bubbles. Evolution reaction under magnetic field which gave larger cobalt crystallites prevented the appearance of holes attributed to hydrogen evolution reaction. Hence, improvement in corrosion behavior of the material was observed.

4.7 CONCLUSIONS

In an effort to optimise a sulphate bath of Ni-Co alloy, and to improve its corrosion resistance behaviour using the benefit of magnetic field, applied parallel to the process of deposition, following conclusions are drawn:

1. The corrosion rates of Ni-Co alloy coatings can be decreased drastically with advent of magnetoelectrodeposition (MED) by inducing the magnetic field B parallel to the process of electrodeposition.
2. Drastic improvement in corrosion resistance of MED Ni-Co alloy coating is attributed to an increase of Co content of alloy due to an increase of its limiting c.d. (i_L), affected due to magneto convection effect.
3. Under optimal conditions, MED coatings exhibits eleven-time better corrosion resistance compared to conventionally electrodeposited (ED) coatings, using same bath, deposited for same time.
4. The constancy of XRD patterns of MED Ni-Co alloy coatings, regardless of the direction and intensity of B is due to formation of solid solution of Co in a nickel matrix. Only shift of diffraction line positions takes place due to change in the composition of alloy, keeping the phase structures constant.
5. The roughness, and hence CR’s of Ni-Co alloy coatings were found to be decreased due to magnetoelectrodeposition, supported by SEM and AFM analyses.
6. The improved corrosion resistance of MED Ni-Co alloy coatings, in relation to its conventional alloy coatings were attributed to their changed composition, phase structure and surface morphology, supported by EDX, XRD and SEM study, respectively.

CHAPTER 5 DEVELOPMENT OF MULTILAYER Ni-Co ALLOY COATINGS FOR BETTER CORROSION PROTECTION BY SONOELECTRODEPOSITION METHOD

This chapter details the development of composition modulated multilayer alloy (CMMA), or simply multilayer Ni-Co alloy coatings using the effect of ultrasound. The first part of the chapter explains the sono-electrodeposition of monolayer Ni-Co alloy coatings for better corrosion protection. The second half of the chapter details the development of Ni-Co alloy coatings in multilayers to achieve better corrosion resistance of substrate. Multilayer Ni-Co alloy coatings were developed by periodic pulsing of the power density of ultrasound effect, parallel to the process of deposition. The composition and thickness of individual layers have been optimized by proper modulation of ON and OFF period of ultrasound effect. The deposition conditions, like pulsing power density (p.d.) and degree of layering have been optimized for the highest performance of coating against corrosion, evaluated by electrochemical testing methods.

5.1 INTRODUCTION

The Ni and Ni-based alloys have been widely used in variety of corrosion resistant applications including aircraft gas turbines, nuclear power plant system, and chemical, petrochemical industries (Gorobets et al. 2008).The deposition of Ni–Co alloy coatings has been widely used for recorder head materials in computer hard drives and in surface finishing industries for items such as printed circuit boards, wear resistant coating, corrosion resistance layers, electroformed laser mirrors and decorative coating(Bagotzky et al. 2003).And also, the Ni-Co alloy have been considered as an important engineering materials, because of their unique properties such as high mechanical strength, good wear resistance and anticorrosive performance(Kritzer et al. 2000).Recent advances in nanostructured materials have been led by the development of new synthetic methods that provide control over size, morphology, and nano/microstructure(Bang and Suslick 2010).Accordingly, a new class of materials having alternate layers of alloys of different composition/phase structure, called composition modulated multilayer alloy (CMMA)coatings have been practiced for achieving improved material’s properties(Wilcox and Gabe 1993).The

CMMA coatings, or simply multilayer alloy coatings having thin layers of alloys of same metals, but of different composition exhibit a wide range of applications owing to their unique technological properties different from their pure metals and their homogenous alloys. This multilayer alloy coating can be electrodeposited from the same bath having both metal ions by periodic modulation of the cathodic current density (c.d.) between two set values; and such deposition allows the growth of coatings, having periodic modulation in their composition. The properties of multilayer alloy coatings can be tuned by several factors, including the layer thickness, the overall thickness, the chemical composition of individual layer, and the periodicity of layers(Thangaraj et al. 2009).

In reality, the principle of multilayer alloy coating technique is based on the two fundamental aspects of electrochemistry. They are: i) periodic modulation in mass transport process near cathode allows the growth of the coatings with periodic modulation in their composition, and ii) The property of any coatings can be increased substantially by increasing its surface/interfacial area, *i.e.* by layering. The modulation in mass transport towards cathode can be affected by different approaches, like by pulsing the cathode current density (c.d.), power density (p.d.) of ultrasound (in case of sonoelectrodeposition) during process of deposition. There are several reports on electrodeposition of multilayer alloy coatings by pulsing the cathode c.d.'s, using single bath technique(Thangaraj et al. 2009). In this direction, our group has done an extensive work on development of multilayer Zn-M (M - Ni, Co and Fe) alloy coatings(Elias et al. 2016; Yogesha and Hegde 2010)and mutual alloys of transition metals for improved corrosion protection. A significant improvement in the corrosion resistance of multilayer alloy coatings were found, compared to their monolayer counter parts, deposited from the same bath using continuous current, or direct current (DC).

Thus from the literature on applications of sonochemistry, it was found that mass transport of metal ions towards cathode can be improved drastically, sometimes surprisingly by the irradiation of power ultrasound during process of deposition. The peculiar cavitation effect can be used beneficially to modulate the mass transport (by modulating the power density of the sonicator probe) for development of coatings of high corrosion resistance. But, to the best of authors knowledge till dated no work has been reported on the use of power ultrasound for developing multilayer Ni-Co alloy coatings for better corrosion protection. Accordingly, in the present study, the corrosion protection efficacy of monolayer Ni-Co alloy coating has been tried to enhance (to many fold of its magnitude) by multilayer coating approach, using acoustic cavitation effect as the tool(Pollet 2012). The improved corrosion resistance of sonoelectrodeposited multilayer Ni-Co alloy coatings are analyzed in the light of changed homogeneity of the coating (in terms of morphology, composition and phase structure) due to cavitation effect.

5.2 SONOELECTRODEPOSITION

It is well known that when power ultrasound is superimposed on an electrochemical reaction, contained inside the liquid medium many peculiar processes are going to take place inside it. Among these, microjetting, or microstreaming is the most important one. This can improve the mass transport, thereby thinning of diffusion layers (or Nernst diffusion layer) and generate localized heating. Such benefits have been used to enhance two widely used electrochemical metallization processes, namely, electroplating and electroless plating, which are employed in key industrial sectors (Ma et al. 2012; Peters 1996). Generally, the power ultrasound can be used in two basic ways to bring about changes in a material synthesis, and they are: *i)* Direct mechanical transmission of vibration from the transducer onto a solid to induce vibrations in the surface of the material, and *ii)* Indirect transmission of energy *via* cavitation induced in a fluid by the transmission of acoustic vibrations. Each of these has a relevance to electrochemistry since *i)* can be taken to represent induced vibrations at a solid electrode surface, and *ii)* can be taken to represent sonication of an electrolyte. In many cases, both will occur simultaneously and influence the overall electrochemical processes. Interestingly, the effect of such ultrasonication in electrochemical process are not derived directly from ultrasound itself, as acoustic wavelengths are much larger than molecular dimensions; instead it is due to molecular level interaction between ultrasound and the chemical species takes place, in the form of acoustic cavitation. *i.e.,* the formation, growth and implosive collapse of bubbles in liquids. An extraordinary reaction condition, created due to power ultrasound irradiation is attributed to the peculiar acoustic cavitation effect, responsible for changed mass transport process, *i.e.* diffusion process. The phenomenon of acoustic cavitation effect may be explained as shown schematically in Figure 5.1. According to this, when an ultrasonic wave passes through liquid, fluctuating pressures are rapidly setup, as a result of the alternate periods of compression and rarefaction associated with the wave as shown in Figure 5.1a. During the compression cycle, the liquid is subjected to a sufficiently positive pressure which pushes the molecules of the liquid together, whilst during the following rarefaction cycle; the liquid is subjected to an equal but negative pressure which pulls the molecules of the liquid away from each other. Increasing the amplitude of the wave leads to an increase in the magnitude of the positive and negative pressures, making the bubble to grow continuously to reach its maximum size as shown in Figure 5.1 b.

Thus liquids when irradiated with ultrasound, the alternating expansive and compressive acoustic waves create bubbles (cavities), and make the bubbles to oscillate. The oscillating bubbles can accumulate ultrasonic energy effectively while growing to a certain size (typically tens of μm). The increase of ultrasound intensity affects the molecular structure of the molecules. During this process, inter molecular force between the molecules reaches an optimum value. But, a point reached where the intermolecular forces are not able to hold the molecular structure intact. These results in the formation of bubbles, called cavities and the process are called cavitation. There are two types of cavitation, *i.e.,* stable and transient. Stable cavitation in which bubbles will vibrate about their mean position in compression and rarefaction cycle. In the case of transient cavitation bubbles will grow over one acoustic cycle a stage is reached doubled their initial size leads the explosion of bubbles violently and makes the movement of ions easier towards the cathode surface. Under the right conditions, a bubble can overgrow and subsequently collapse, releasing the concentrated energy stored in the bubble. within a very short time (with a heating and cooling rate of $>10^{10}$ K^{-1}). This cavitational implosion is very localized and transient with a temperature of ~ 5000 K and a pressure of ~1000 bar (Chen et al. 2011).

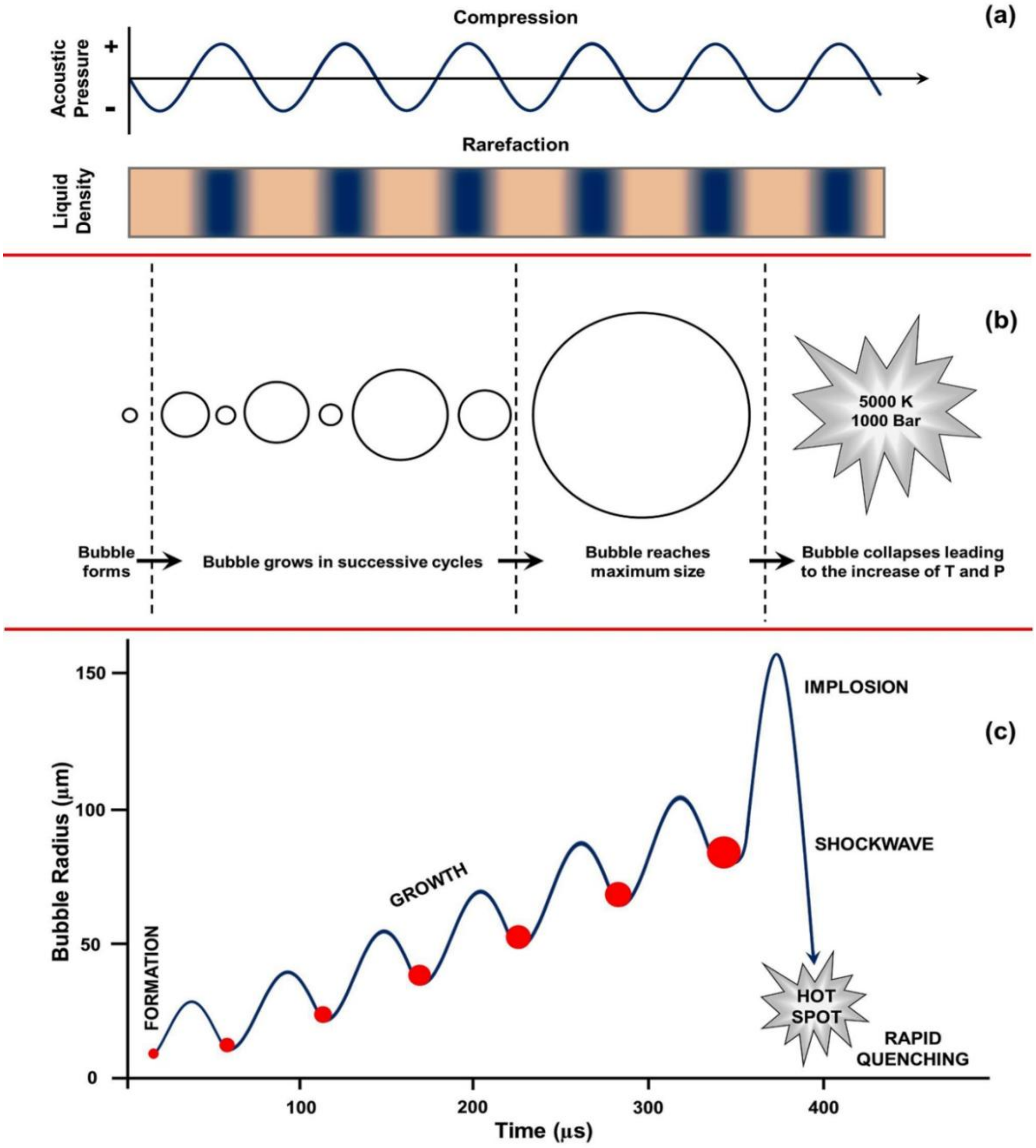

Figure 5.1- Schematic representation showing the effect of power ultrasound in liquid medium: a) acoustic compression and rarefaction, and hence the variation in the liquid density, b) successive growth of bubble leading to its maximum size and then its collapse c) Rapid quenching leading to the formation of 'hot spot'.

Thus it is well accepted fact that in sonochemistry, the cavitation bubble collapse leads to near adiabatic heating of the vapour that is inside the bubble, creating the so-called *hot-spot* in the fluid (Figure 5.1c). Because of this ultrasound's *extraordinary* effects, enormous amount of research work has been carried out, especially using high power ultrasound (20 kHz -2 MHz) (Banks and Compton 2003). The power ultrasound effect was used as tool in various chemical processes, to meet several industrial applications (Pollet and Ashokkumar 2019). In addition, when ultrasound intensity is higher than that of threshold intensity, it may create shock waves and microstreaming effect. This leads to decrease the diffusion layer thickness by increasing of mass transport process, which eventually allows a drastic change in the product and performance of sono-electrodeposited coatings (Banks and Compton 2003).

Thus benefit of ultra-sonication of electrolytic bath of Ni-Co alloy, can be effectively used to reduce the double layer thickness, and to increase the limiting current density of Co(less noble metal) in the bath. In this direction, optimised acid sulphate bath of Ni-Co alloy, given in Table 4.1 (Chapter 4) is used to demonstrate the advent of sonoelectrodeposition to improve the Co content, and hence the corrosion resistance property of Ni-Co alloy coatings, through both monolayer and multilayer approach. The bath chemistry and operating parameters of the bath are given in Table 4.1. The pH of the bath was measured to be equal to 3.5 by proper addition of either NH_4OH or HCl, depending on the requirement, using Micro pH Meter (Systronics-362).All electrodeposition of Ni-Co alloy coatings (both monolayer and multilayer) were carried out at room temperature (298 K) on the known surface area of the copper plate (7.5 cm ×3.0 cm), using an experimental set up as shown schematically in Figure 5.2. Ni-Co alloy deposition was carried out using an electrochemical cell (having cathode, anode, electrolyte), and a power source of direct current (DC) [DC Power Analyser, Aplab-LD3202, India)] coupled with a programmable power ultrasound generator (ultrasonicator) [SONIC Vibra-cell^{TM} VC 750, 20 kHz, maximum power 750 W, with probe of 13 mm tip diameter]. The copper plates (cathode) were polished metallurgically to get the mirror finish, degreased with trichloroethylene, and then pickled in 1:1 HNO_3. All depositions were carried out on known surface area (3 cm × 3 cm) of the cathode, masking the remaining portion by cellophane tape. Pure nickel plate, having same exposed surface area as that of cathode was used, as anode. The cathode and anode were placed parallel 5 cm apart during deposition. All depositions were carried out for a constant duration (600 sec), for comparison purpose.

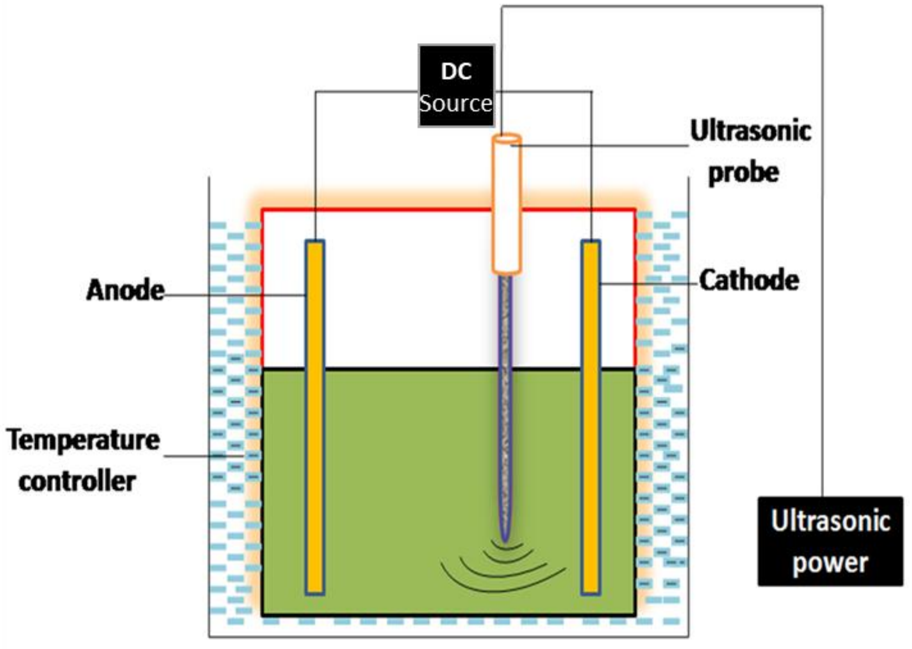

Figure 5.2 -Schematic representation for sonoelectrodeposition assembly, having tuneable DC power source and ultrasonic power source

5.3 SONOELECTODEPOSITION OF MONOLAYER Ni-Co ALLOY COATING

Monolayer and multilayer Ni-Co alloy coating were carried out using the power source, coupled with ultrasonicator (Figure 5.2).The constant current power source and ultrasonicator were set to source the desired current density (c.d.)and power density continuously to develop sonoelectrodeposition of monolayer Ni-Co alloy coating; and constant current power source and pulsing ultrasonicator, to go ON and OFF periodically were used to develop sono-multilayer electrodeposition of Ni-Co alloy coating. The current and ultrasound patterns used for development of conventional electrodeposition (ED) and sonoelectrodeposition of both monolayer and multilayer Ni-Co alloy coatings are shown in Figure 5.3. The constant current, or DC used for the electrodeposition of monolayer Ni-Co alloy coating (without the use of ultrasound effect) is shown in Figure5.3a. The constant current and ultrasound effect were used for the sonoelectrodeposition of monolayer Ni-Co alloy coating, shown in

Figure5.3b. The constant current and ultrasound pulses were used for development of multilayer Ni-Co alloy coating, as shown schematically in Figure5.3c.

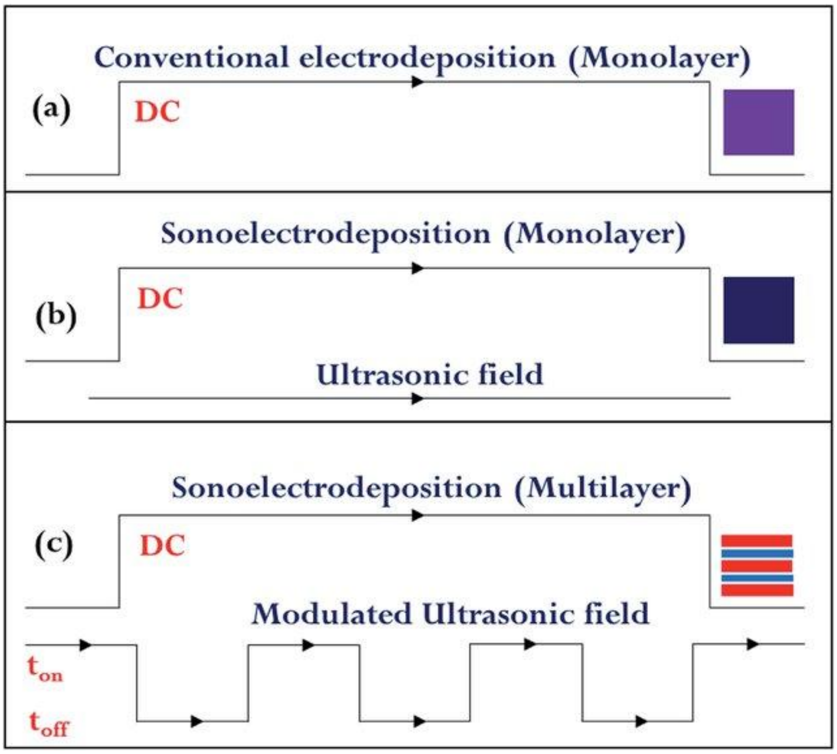

Figure 5.3–Schematic representation of current and ultrasound patterns used for electrodeposition of Ni-Co alloy coatings at: a) constant c.d. for monolayer, b) constant c.d. and p.d. for monolayer, and c) constant current and pulsing p.d. for multilayer alloy; The cross sectional view of corresponding coatings are given on the right

The cross sectional views of corresponding coatings are given on the right, in Figure 5.3. Multilayer Ni-Co alloy coatings with required number of layers were developed (at constant c.d.) by setting up of the ultrasonicator to go ON and OFF periodically, for definite T_{ON} and T_{OFF} time as shown in Figure5.3c. Monolayer Ni-Co alloy coating was accomplished by conventional method, using DC at 4.0 Adm^{-2}. Sonoelectrodeposition of monolayer Ni-Co alloy coating was carried out using both constant c.d. and power density (p. d.). Multilayer Ni-Co alloy coating was carried out at constant c.d. and by pulsing the p.d. (parallel to the process of electrodeposition).The p.d. is expressed in Wcm^{-2}.Here, c.d. acts as the driving force for migration, and then reduction of metal ions. The superimposition of ultrasound during deposition brings about the cavitation effect, responsible for modulation of the mass transfer process at cathode interface. Thus, periodic modulation of p.d. (as the sonicator probe turns ON and OFF) brings about a periodic modulation in the mass transfer process. This in turn, allows the growth of alloy coatings (in layered manner) having periodic modulation in their composition. In other words, periodic pulsing of the sonicator probe allowed the deposition of Ni-Co alloy coatings to take place in multilayers.

Thus monolayer Ni-Co alloy coatings were deposited from optimized bath at constant c.d. of 4.0 Adm^{-2}. Sonoelectrodeposited monolayer Ni-Co alloy coatings were developed at constant c.d. of 4.0 Adm^{-2}, at different p. d., like 0.6, 0.9, 1.2Wcm^{-2} The corrosion data of sonoelectrodeposited monolayer Ni-Co alloy coatings revealed that (Ni-Co)$_{1.2\ \mathrm{W\ cm}^{-2}}$coatings is the most corrosion resistant. Hence, 1.2 Wcm^{-2} was chosen as the p. d. for pulsing ultrasound effect. Taking 1.2 Wcm^{-2} , as the pulsing p. d., sonoelectrodeposition of multilayer Ni-Co alloy coatings of different configuration (having different number of layers) were developed by pulsing the ultra-sonicator, periodically. All electrodeposition were conducted for 600 s, for comparison purpose. The corrosion protection efficacy of alloy coatings were evaluated by conventional electrochemical methods. The Ni-Co alloy coatings are represented conveniently as (Ni-Co)$_{4.0\ \mathrm{Adm}^{-2}}$, (Ni-Co)$_{4.0/X\ \mathrm{Wcm}^{-2}}$ and (Ni-Co)$_{Y/Z/n}$ [where X =0.6,0.9,1.2] ; Y and Z are different power densities, ON and OFF time of ultrasound irradiation in seconds, and 'n' represents number of layers formed in total deposition time (600 secs),respectively.

5.4 CHARACTERIZATION OF Ni-Co ALLOY COATINGS

Sonoelectrodeposited Ni-Co alloy coatings (both monolayer and multilayer) were subjected to corrosion study by conventional three electrode assembly, using Potentiostat/Galvanostat. Saturated calomel electrode (SCE) has been used as the reference electrode, and platinum electrode as the counter electrode. The corrosion tests were carried out in 5% NaCl solution, as common corrosion medium at 298K, taking 1.0 cm^2 exposed surface area of the coatings. Potentiodynamic polarization study was carried out in a potential ramp of ±250 mV around equilibrium potential, at scan rate of 1 mVs^{-1}.Electrochemical impedance spectroscopy (EIS) study was made using 10 mV perturbing AC voltage, and corresponding Nyquist plots are analyzed. The corrosion rates(CR’s), expressed in mmy^{-1} were determined by Tafel’s extrapolation method. The electrochemical corrosion parameters, responsible for improved corrosion resistance of sonoelectrodeposited multilayer Ni-Co alloy coatings, in relation to its monolayer and conventional monolayer alloy coatings were analysed. Further, all electrodeposited Ni-Co alloy coatings, without and with effect of ultrasound were further analysed for their surface morphology, composition and phase structures. The characterization of Ni-Co alloy coatings developed from the optimized bath (Table 4.1) is given in Chapter 4 (without the effect of ultrasound).

5.5 RESULTS AND DISCUSSION

5.5.1 Optimization of c.d. and p.d

Hull cell method, studied over wide range of c.d. from 1.0 Adm^{-2} to 4.0 Adm^{-2} was used to set the optimal condition for deposition of bright, uniform and the most corrosion resistant Ni-Co alloy coatings, using bath shown in Table 4.1. Experimental results revealed that at optimal c.d. of 4.0 Adm^{-2}, bath produced alloy coating showing the least corrosion rate (CR) of 22.4×10^{-2} mm y^{-1}, as reported in Table 4.2(Chapter 4). Keeping this c.d. as the optimal, sonoelectrodeposition of Ni-Co alloy coatings were carried out at different p.d.’s (0.6, 0.9 and 1.2 Wcm^{-2}) and their CR’s were evaluated. Experimental data, reported in Table 5.1, demonstrated that CR’s of Ni-Co alloy coatings decreased drastically with increase of p.d., and reaches its minimum value of 7.9×10^{-2} mm y^{-1} at 1.2 Wcm^{-2} as reported in Table 5.1.Further, the compositional analyses of alloy coatings showed that cobalt content of (Ni-Co)$_{4.0\ \mathrm{Adm}^{-2}}$and (Ni-Co)$_{4.0/1.2\ \mathrm{Wcm}^{-2}}$ alloy coatings are 21.80 wt. % and 43.48 wt. %, respectively.

Hence, drastic decrease of CR of (Ni-Co)$_{4.0/1.2\ \mathrm{Wcm}^{-2}}$ coating, compared (Ni-Co)$_{4.0\ \mathrm{Adm}^{-2}}$ is attributed to its increased Co content, consequent to its increased limiting c.d. affected by induced ultrasonication(Shetty et al. 2016). This may be explained as follows: When power ultrasound is applied to liquid media, a range of processes occur which can create unusual physical and chemical conditions; these include acoustic steaming, turbulent convection, microstreaming in the presence of oscillating bubbles and cavitation as shown in Figure 5.4(a) (Tudela et al. 2015) These processes provide an increased mass transport regime in which thickness of Nernst's diffusion layer reduces, leading to an increase of the limiting c.d.(i_L) of cobalt ions, in accordance with Fick's law of diffusion(Banks and Compton 2003), given by Eqn. (4.1) in Chapter 4.The diffusion layer model shown in Figure 5.4(b) allows a naive description of the mass transport at the electrode interface by assuming a laminar sub-layer close to the surface (in the close proximity of cathode) and an approximately linear concentration gradient across a thin layer adjacent to the electrode.

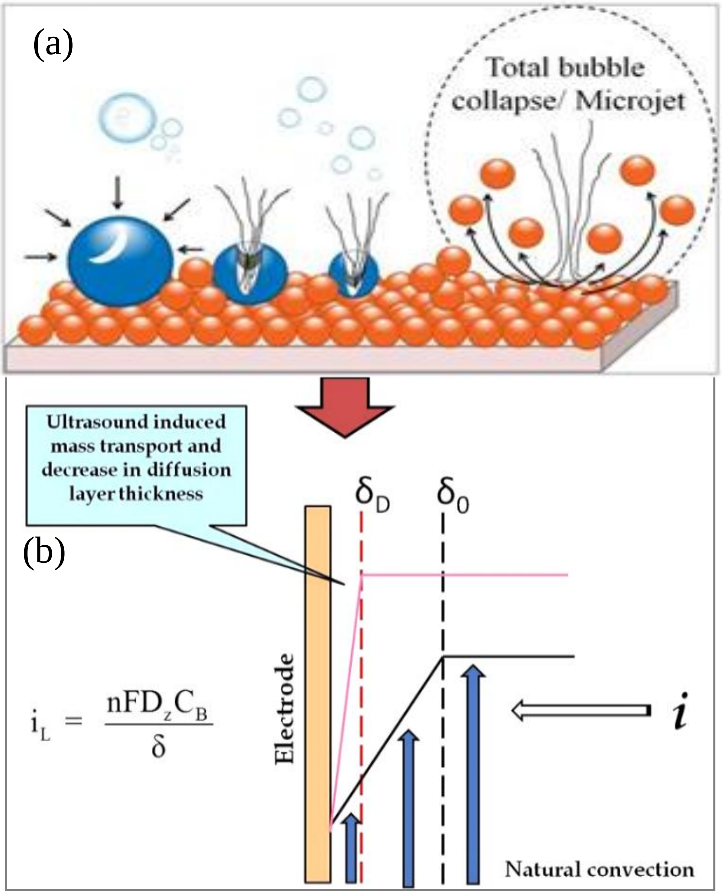

Figure 5.4 – A model showing the ultrasound induced turbulence at electrode-electrolyte interface leading to: a) Acoustic cavitation collapse on the electrode surface leading to the microstreaming, and b) Increase of limiting c.d. by decreasing the diffusion layer thickness.

The acoustic microstreaming is brought about by the momentum being absorbed by the liquid media, in the form of sound waves which manifests itself as turbulent flow in the direction of the applied sound field. Thus, the acoustic cavitation induced turbulence on the surface of cathode is reduces the thickness of diffusion layer, leading to an increase of limiting current density (i_L) of Co^{+2} ions. Therefore, it may be summarized that decreased CR's of sonoelectrodeposited Ni-Co alloy coatings is attributed to increased Co content of the coating, consequent to its increased limiting c.d., affected by cavitation induced ultra-sonication.

It is important to note that under the effect of ultrasound, the wt. % Co in the deposit increased drastically with the induced power density. The increase of wt. % Co with p. d. of the ultrasound is listed in Table 5.1. A drastic increase in the wt.% Co in the deposit with p. d. may be attributed to an increase of limiting c.d. (i_L) of Co by thinning of EDL(Del Campo et al. 1999), as shown in Figure 5.4(b). The variation in the thickness of EDL is mainly associated with the geometry of sonoelectrode, and the p.d. of induced ultrasound. Hence, it may be noted Co content of the alloy has increased drastically with power density, in relation conventionally electrodeposited Ni-Co alloy, developed without the effect of ultrasound.

Table 5.1- Corrosion data of sono-electrodeposited Ni-Co alloy coatings under different conditions of p.d.'s from the optimized bath, at 4.0 Adm^{-2} (optimal)

p.d. (W cm^{-2})	wt. % Ni in the deposit	wt. % Co in the deposit	$-E_{corr}$ (mV vs SCE)	i_{corr} (μA cm^{-2})	CR×10^{-2} (mm y^{-1})
$(Ni\text{-}Co)_{0\ W\ cm^{-2}}$	78.20	21.80	229.7	20.8	22.4
$(Ni\text{-}Co)_{0.6\ W\ cm^{-2}}$	68.68	31.32	215.4	9.3	10.4
$(Ni\text{-}Co)_{0\ .9\ W\ cm^{-2}}$	62.19	37.81	241.2	8.3	9.0
$(Ni\text{-}Co)_{1.2\ W\ cm^{-2}}$	56.52	43.48	247.1	7.4	7.9

5.5.2 SEM Study

The surface topography of Ni-Co alloy coatings, deposited at different p.d's areas shown in the Figure 5.5, in comparison with that of conventional Ni-Co alloy (where p. d. = 0 Wcm^{-2}). It may be noted on increasing the p.d. from 0 W cm^{-2} to 1.2 Wcm^{-2}, the Co content of the alloy increased from about 21.8 wt.% to 43.48 wt.%. It may be attributed to action of cavitation and ultrasonic microstreaming generated by ultrasonic vibration(Walker and Walker 1977).The decrease of Ni content may be reasoned by the fact that nickel ion being a smaller in size compared to cobalt ions, kinetic movement of Ni ions towards the cathode leads to creation of bubbles, during ultrasonic streaming.

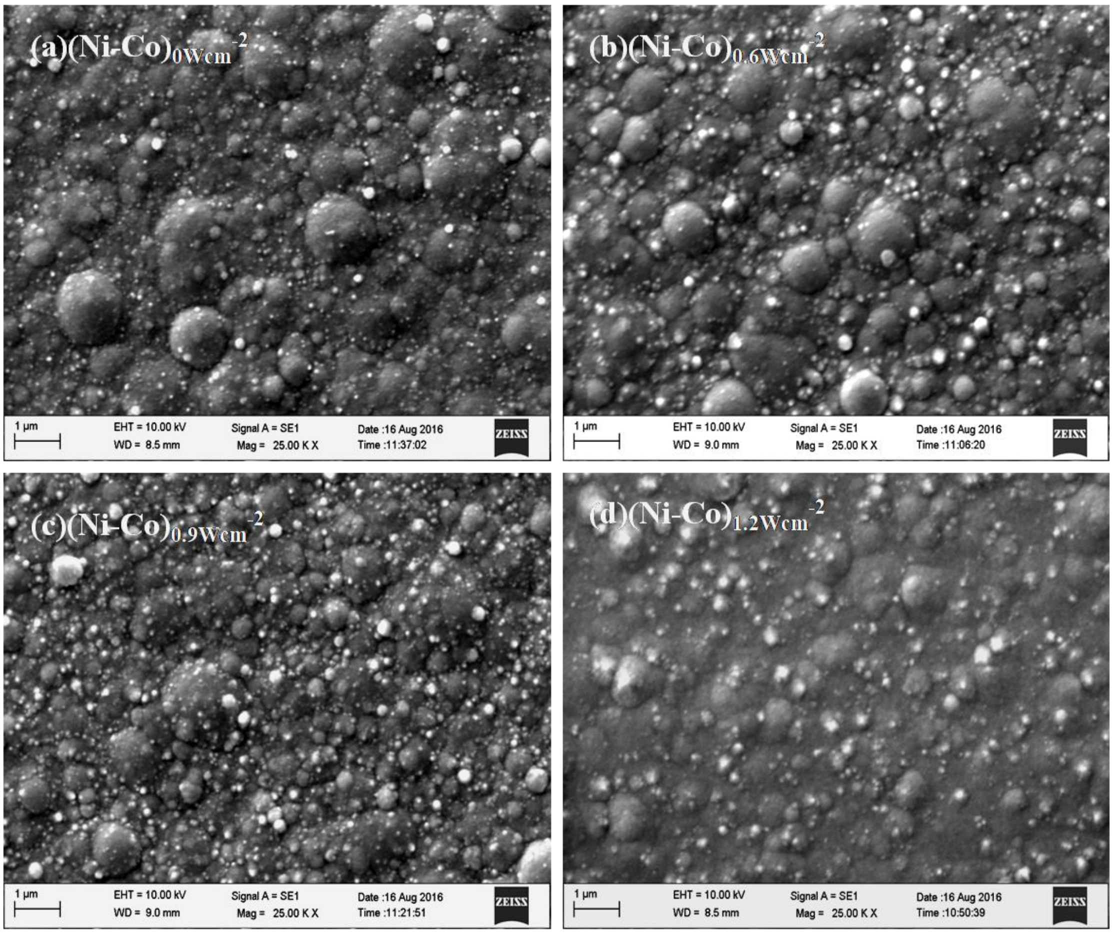

Figure 5.5-Surface morphology of Ni-Co alloy coatings deposited under different conditions of power densities: a)(Ni-Co)$_{0W\ cm^{-2}}$,b)(Ni-Co)$_{0.6\ W\ cm^{-2}}$,c)(Ni-Co)$_{0.9\ W\ cm^{-2}}$ and*(d)(Ni-Co)$_{1.2\ W\ cm^{-2}}$, from the optimized bath*

Thus a large difference in the surface morphology of sonoelectrodeposited Ni-Co alloy coatings, with p. d. may be attributed to an increase of Co content of the alloy, affected due to ultrasonic streaming effect.

5.5.3 XRD Study

The XRD patterns of sonoelectrodeposited Ni-Co alloy coatings obtained at different p.d.'s(from 0 Wcm^{-2} to 1.2 Wcm^{-2}) are shown in the Figure 5.6.It may be noted that the orientations of all phases are same in all coatings developed in both presence and absence of ultrasonic field effect. However, the intensity of reflection corresponding to (220) phase of fcc Ni structure (JCPDS 04-0850) decreased drastically with increase of p.d. as shown Figure 5.5.The intensity of distinct peak of conventional Ni-Co alloy, observed at 76.4^0 for (220) plane decreased with increase of p. d.

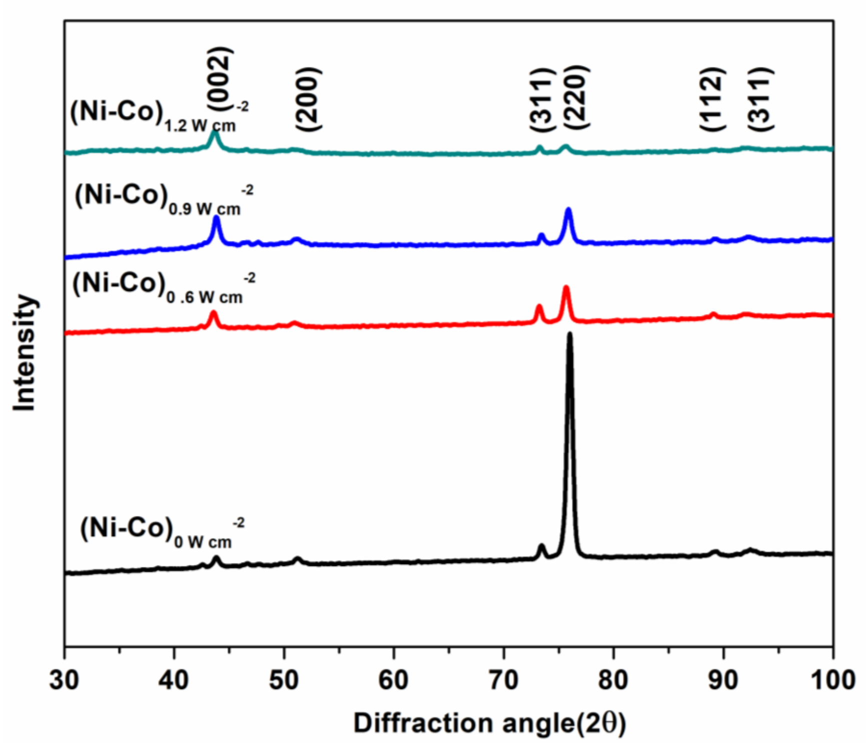

Figure 5.6-XRD patterns showing the crystallographic orientation of sonoelectrodeposited Ni-Co alloy coatings at different p.d. from optimized bath at same c.d. of 4.0 A dm^{-2}

The plane (112) and (311) reflections at higher angles are corresponding to the Ni-Co alloy. The wt. % Co in the deposit was found to be increased, or wt.% Ni decreased when the ultrasound field is applied, which is evidenced by plane of reflection (002)(JCPDS 05-0727). Hence, from XRD study it may be inferred that p.d. has vital role on the composition. However, there is no change in the phase structure of the alloy coatings due to formation solid solution of Co in Ni matrix. Since all sonoelectrodeposited Ni-Co alloy coatings forms solid solution, consisting of same single phase, their powder patterns appear quite similar. However, change in composition of the alloy increases the intensity of diffraction peaks, as a mark of change in lattice parameters.

5.5.4 Corrosion Study

The sonoelectrodeposited Ni-Co alloy coatings obtained at different power densities were subjected to corrosion study, by potentiodynamic polarization and electrochemical impedance study.

5.5.4.1 Potentiodynamic polarization study

The potentiodynamic polarization method was used to study the corrosion behaviour of Ni-Co alloy coatings, and CR’s were evaluated by Tafel extrapolation method. The Ni-Co alloy deposited at 4.0 Adm^{-2} showed the least CR, and hence it has been considered as optimal c.d. for sonoelectrodeposition. Then, sonoelectrodeposition of Ni-Co alloy coatings were carried out at different p. d. (0, 0.6, 0.9 and 1.2 Wcm^{-2}) and their CR’s were evaluated, and are reported in Table 5.1. The corrosion data reported in Table 5.1 demonstrate that (Ni-Co) $_{1.2\text{Wcm}^{-2}}$ alloy coating exhibits the least CR compared to all other coatings. The least CR (7.9×10^{-2} mm y^{-1}) of (Ni-Co)$_{1.2\ \text{Wcm}^{-2}}$ alloy coating may be attributed to highest Co content of the alloy, evidenced by EDX analysis (reported in Table 5.1) due to effect of induced ultrasonic effect. A comparison of Tafel’s plots of sono-electrodeposited Ni-Co alloy coatings, deposited at different p.d.’s are shown in Figure 5.7, in relation to that of conventional Ni-Co alloy coating

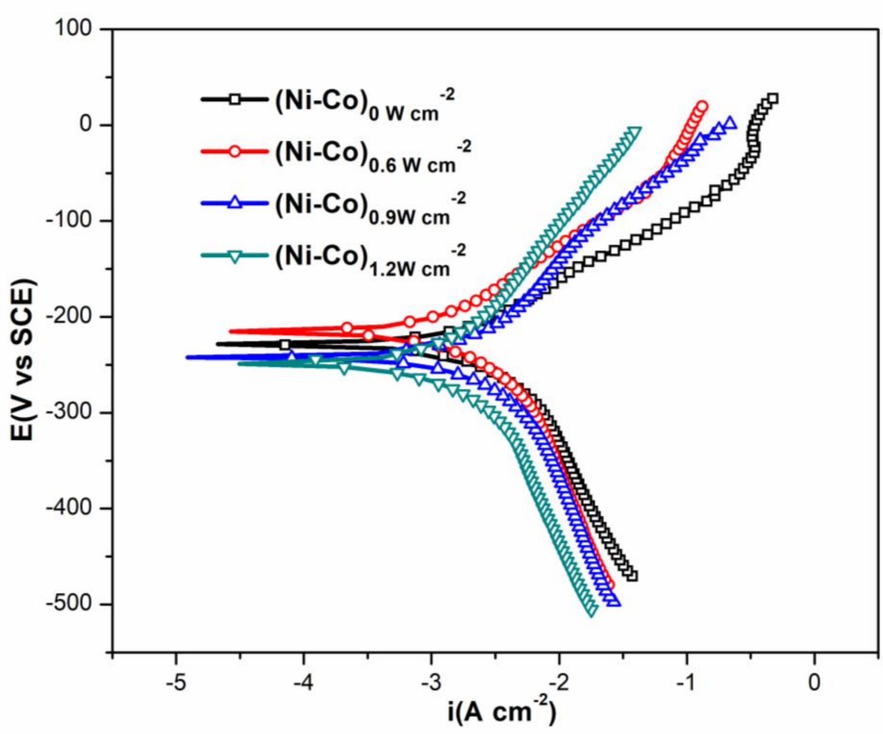

Figure 5.7- Potentiodynamic polarization behaviour of sonoelectrodeposited Ni-Co alloy coatings, deposited different p.d., at same c.d. (4.0 Adm^{-2}) from the optimized bath

5.5.4.2 Electrochemical impedance spectroscopy study

EIS is a non-destructive method for studying the interfacial interaction of test material very accurately. The ability of the technique to segregate various processes, like Ohmic conduction, charge transfer, interfacial charging, mass transfer etc, and made it as an elegant technique for electrochemical study. Electrochemical impedance response is more commonly represented by popular Nyquist’s diagrams. The impedance response of sonoelectrodeposited Ni-Co alloy coatings, deposited at different p. d. are shown in Figure 5.8.The impedance responses showed incomplete depressed semicircle in the studied frequency range, in addition to an increase of axial radius of the semicircle with increase of p.d. was found. Nature of Nyquist plots clearly shows that the charge transfer resistance (R_{ct}) of the coatings has increased progressively with of p.d. used for deposition. The impedance response of (Ni-Co)$_{1.2Wcm^{-2}}$alloy coatings is characterized by high polarization resistance (Rp) as shown in Figure 5.8, indicates that this particular coating is more corrosion resistant compared to all other coatings, including its conventional alloy coating.

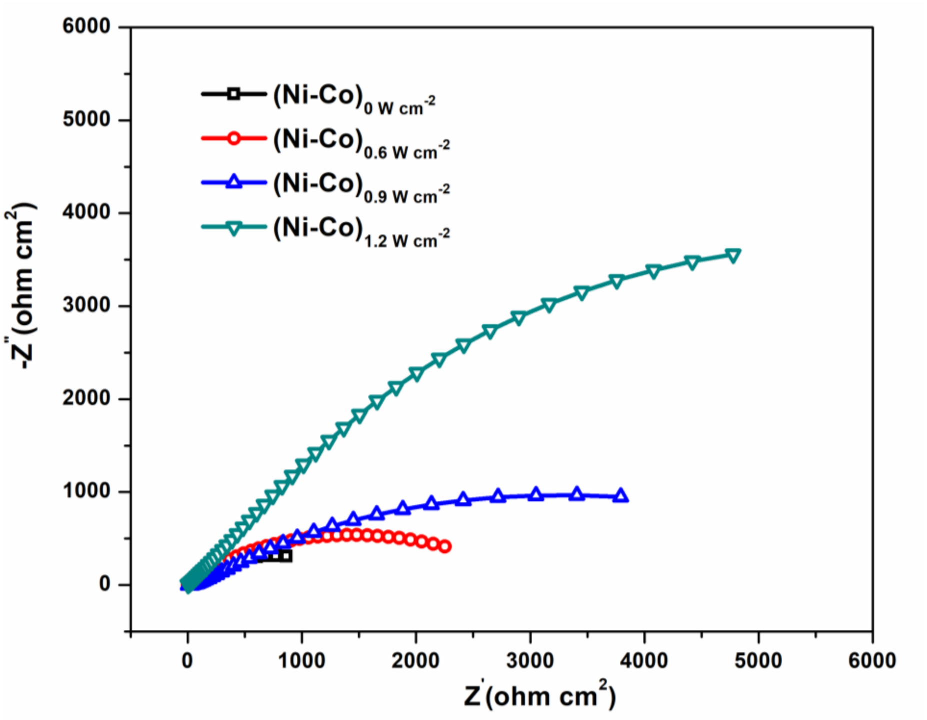

Figure 5.8- EIS response of sonoelectrodeposited Ni-Co alloy coatings, deposited different p.d., at same c.d. (4.0 Adm^{-2}) from optimized bath

Comparison of SEM images of Ni-Co alloy coatings, shown in Figure 5.5 clearly demonstrates that (Ni-Co)$_{0\ Wcm^{-2}}$ alloy coating is more rougher than other coatings, deposited under effect of ultrasound; and the surface roughens was found to be decreased with increase of p. d. Further, decreased surface roughness due to ultrasonic effect may be attributed to an decreased concentration gradient at the interface due to cavitation effect (Banks and Compton 2003).The XRD peaks shown in Figure 5.6, clearly shows the change of only composition of the alloy, without phase change on superimposition of ultrasound deposition. It may be noted that intensity of (220) phase decreased drastically, as effect of induced ultrasound inside the bath. This change of intensity of XRD peak may be attributed to the increased wt. % Co in the alloy *.i.e.*, from 23.80 wt.% to 43.48 wt.%. The corrosion data of sonoelectrodeposited Ni-Co alloy coatings, reported in Table 5.1 shows that (Ni-Co)$_{4.0/1.2\ Wcm^{-2}}$ alloy coating is the most corrosion resistant, compare to other sonoelectrodeposited coatings. Hence, (Ni-Co)$_{4.0/1.2\ Wcm^{-2}}$ alloy coating has been selected for development of its multilayer coatings. *i.e.*, multilayer Ni-Co alloy coatings was developed by sourcing c.d. = 4.0 Adm^{-2} and by pulsing p. d. = 1.2 Wcm^{-2} to go ON and OFF periodically, during deposition. The coating configurations of multilayer Ni-Co alloy coating were optimized further (in both numbers and thicknesses) to minimize the CR by exploiting the principle of nanostructured multilayer alloy coatings. The experimental results are reported as below.

5.6 SONOELECTODEPOSITION OF MULTILAYER Ni-Co ALLOY COATING

Based on the preliminary corrosion study of (Ni-Co)$_{4.0\ \mathrm{Adm}^{-2}}$ and (Ni-Co)$_{4.0/1.2\ \mathrm{Wcm}^{-2}}$ coatings (showing the least CR),(Ni-Co)$_{4.0/1.2\ \mathrm{W\ cm}^{-2}}$ coating has been chosen for development of its multilayer coatings. Accordingly, multilayer (Ni-Co)$_{4.0/1.2\ \mathrm{Wcm}^{-2}}$ alloy coatings, having 10, 30, 75, 100, 150 and 300 layers have been developed by pulsing the ultrasound probe to go ON and OFF periodically, for T_{ON} and T_{OFF} for 30, 10, 4, 3, 2 and 1second each, respectively.

5.6.1 Corrosion Study

The corrosion behaviour of sonoelectrodeposited multilayer Ni-Co alloy coatings was evaluated by potentiodynamic polarization and electrochemical impedance methods, and is described below.

5.6.1.1. Potentiodynamic polarization study

The potentiodynamic polarization behavior of sonoelectrodeposited multilayer Ni-Co alloy coatings, having different number of layers are given Figure 5.9, and corresponding CR's are reported in Table 5.2.From corrosion data, it may be noted that CR's of multilayer coatings decreases with increase in number layers up to 150 layers, and then started increasing at 300 layers. This increase of CR at 300 layers may be attributed to the homogeneity of the coating, affected due to very short ON and OFF time of sonication, *i.e.*, due to very short pulsing period of sonication, no modulation in mass transport has taken place. Hence, no change in the composition of alloy has affected.

Table 5.2- Corrosion data of sonoelectrodeposited multilayer Ni-Co alloy coatings having different number of layers (at optimal c.d. of 4.0 A dm^{-2} and p.d. of 1.2Wcm^{-2}) in comparison with its monolayer counter parts deposited from the same bath

Coating configuration	Number of layers	T_{ON} (Sec)and T_{OFF}(Sec)		$-E_{corr}$ (mV vs SCE)	i_{corr} (µA cm^{-2})	CR×10^{-2} (mm y^{-1})	R_{ct} (Ohm)	C_{dl} (µF)
		T_{ON}	T_{OFF}					
(Ni-Co)$_{4.0\ Adm^{-2}}$	monolayer	-	-	229	20.8	22.4	887	997
(Ni-Co)$_{4.0/1.2\ W\ cm^{-2}}$	monolayer	-	-	247	7.4	7.9	4309	549
Corrosion data of multilayer Ni-Co alloy coatings under optimal c.d. and p.d.								
(Ni-Co)$_{30/30/10}$	10	30	30	301	5.6	6.0	4545	281.2
(Ni-Co)$_{10/10/30}$	30	10	10	326	4.1	4.5	5300	125.2
(Ni-Co)$_{4/4/75}$	75	4	4	257	3.9	4.2	7950	54.8
(Ni-Co)$_{3/3/100}$	100	3	3	254	2.3	2.5	8210	51.8
(Ni-Co)$_{2/2/150}$	150	2	2	276	1.4	1.5	15400	40.9
(Ni-Co)$_{1/1/300}$	300	1	1	270	1.6	1.8	11270	45.8

In otherwords, multilayer coating tends to become monolayer(Yogesha et al. 2012).Hence, it may be concluded that CR of sonoelectrodeposited multilayer alloy coatings decreased with increase in number of layers, only up to certain optimal level (150 layers), and then started decreasing due to interlayer diffusion.

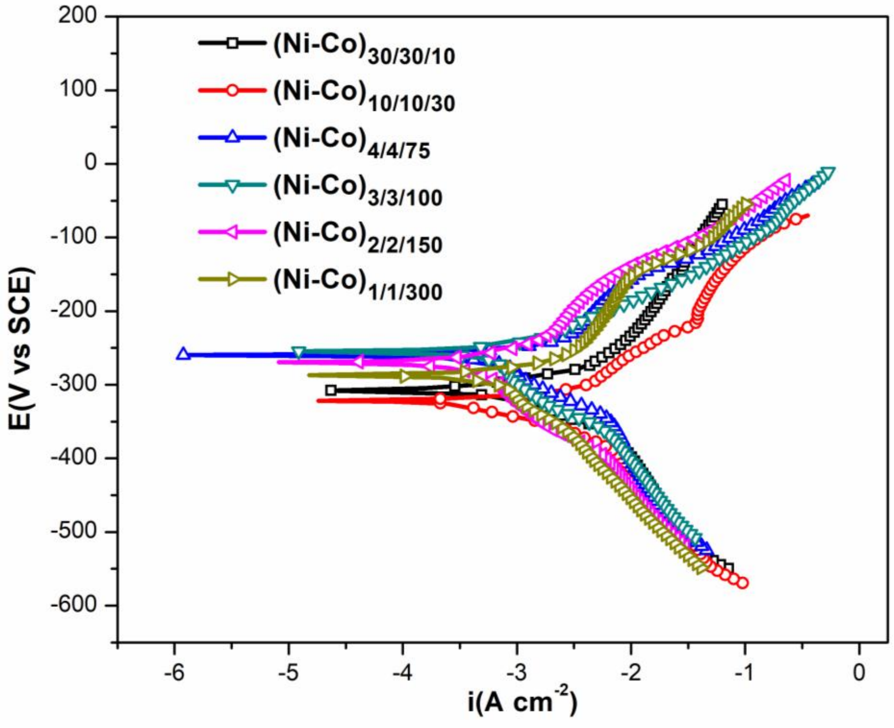

Figure 5.9-Potentiodynamic polarization behaviour of sonoelectrodeposited multilayer Ni-Co alloy coatings having different number of layers, deposited from the optimal bath

5.6.1.2 Electrochemical impedance study

EIS is a powerful diagnostic tool for studying the interfacial interaction of the test specimen through popularly called Nyquist diagram. It provides valuable information on the reactions, involving the transfer of electron in terms of charge transfer resistance (R_{ct}) and double layer capacitance (C_{dl}) values(Tudela et al. 2015).Accordingly, the impedance response of sonoelectrodeposited multilayer Ni-Co alloy coatings, having different number of layers are shown in Figure 5.10.It may be noted that all coatings exhibited an impedance response with incomplete depressed semicircles. Further, the axial radius of the semicircles were found to be increased with number of layers, indicating their improved corrosion resistance. It is further supported by their R_{ct} values, reported in Table 5.2. It is important to note that R_{ct} value increased with number of layers upto 150 layers, and then decreased, in compliance with the C_{dl} values, reported in Table 5.2. The least C_{dl} value corresponding to $(Ni\text{-}Co)_{2/2/150}$ coating suggests that it is most resistant to corrosion, consequent to less flow of current through it. Thus, the corrosion study, from both potentiodynamic polarization and impedance spectroscopy methods demonstrated that $(Ni\text{-}Co)_{2/2/150}$ alloy coating is the most corrosion resistant compared to all other coatings. Hence it has been considered as the optimal configuration of the sonoelectrodeposited multilayer Ni-Co alloy coating, from the optimal bath given in Table 4.1.

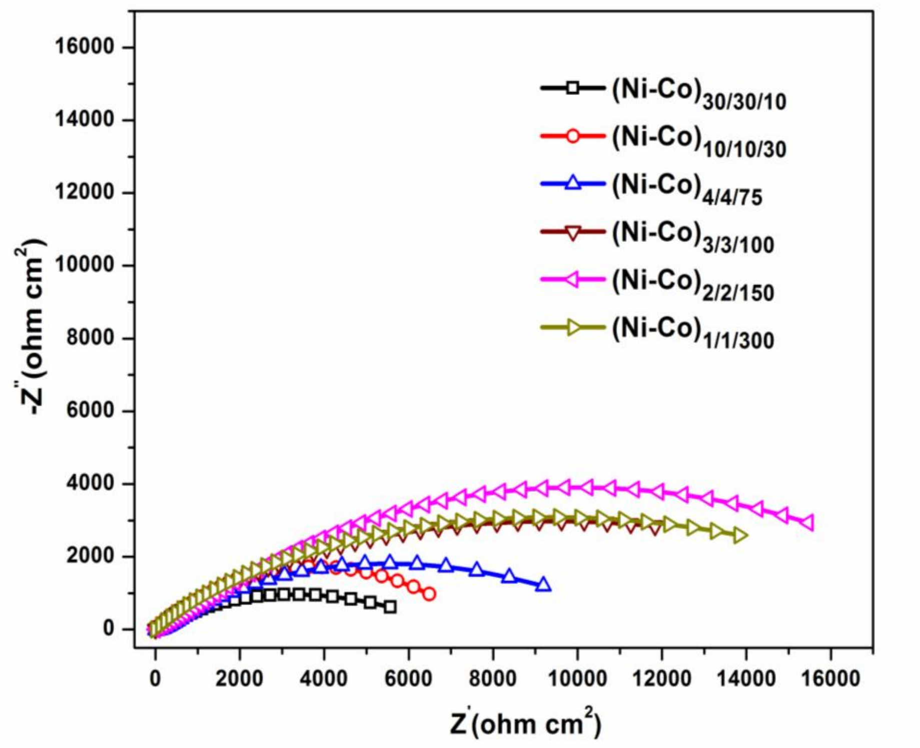

Figure 5.10 - Nyquist plots of sonoelectrodeposited multilayer Ni-Co alloy coatings having different number of layers, deposited from the optimal bath

5.8 COMPARISON OF CORROSION BEHAVIORS OF MONOLAYER AND MULTILAYER ALLOY COATINGS

Based on the CR values of monolayer and multilayer Ni-Co alloy coatings (developed from optimal bath) reported in Table 5.2, it may be inferred that sonoelectrodeposited multilayer Ni-Co alloy coating, having 150 layers, deposited with T_{ON} = 2 sec and T_{OFF} = 2 sec, is the most corrosion resistant, with least CR. Hence, $(Ni\text{-}Co)_{2/2/150}$ has been taken as the optimal configuration of multilayer coating for highest corrosion resistance. The comparison of Tafel's behaviour of conventional monolayer and sonoelectrodeposited multilayer Ni-Co alloy coatings (under optimal conditions), *i.e.*$(\text{Ni-Co})_{4.0\ \text{Adm}^{-2}}$ and $(\text{Ni-Co})_{2/2/150}$ were made, and is shown in Figure 5.11.

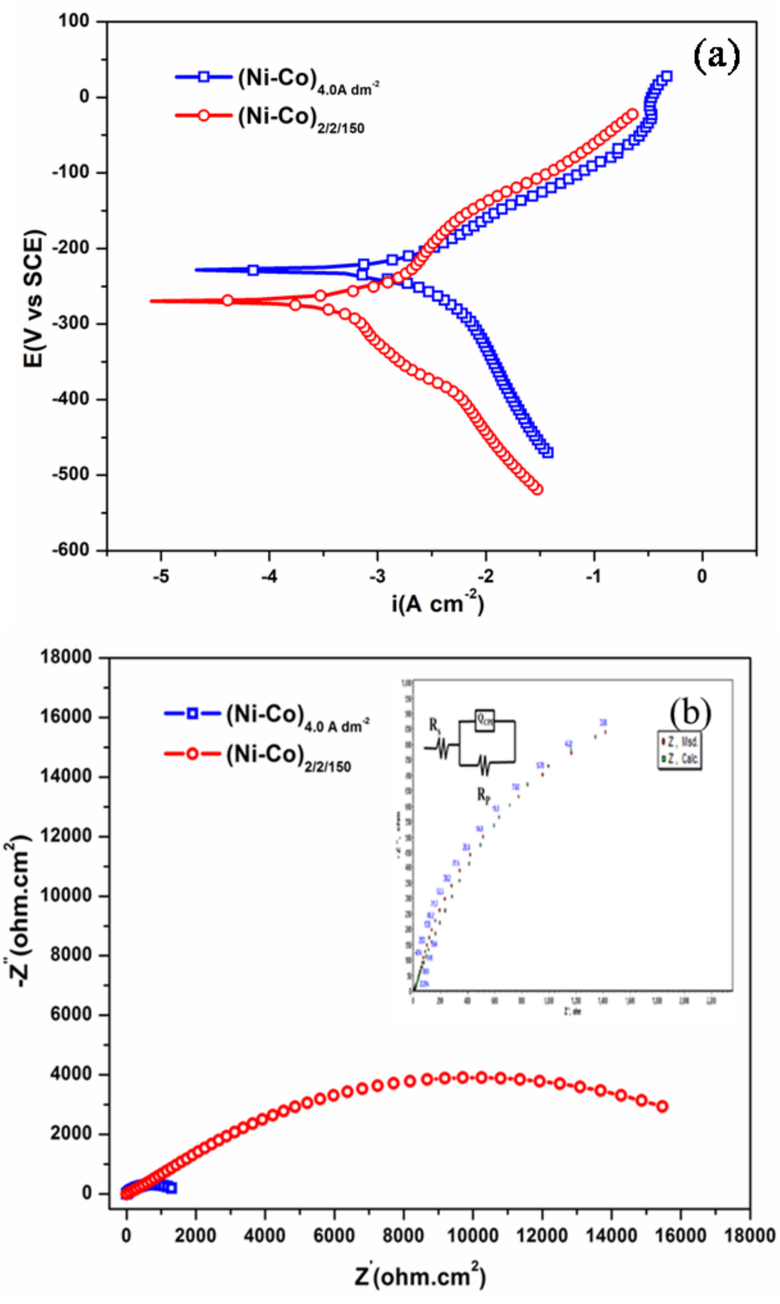

Figure 5.11-Comparison of corrosion behaviours of monolayer $(\text{Ni-Co})_{4.0\ \text{Adm}^{-2}}$ *(conventional) and sonoelectrodeposited multilayer*$(\text{Ni-Co})_{2/2/150}$ *alloy coatings through: (a) Tafel's plots, and (b) impedance response, deposited from same optimized bath for same duration of time*

The Tafel plots shown in Figure 5.11a, clearly shows large decrease of i_{corr} value indicating that $(\text{Ni-Co})_{2/2/150}$ is more corrosion resistant than $(\text{Ni-Co})_{4.0\ \text{Adm}^{-2}}$. It is further supported by its Nyquist plots shown in Figure 5.11b.The electrochemical equivalent (ECE) circuit corresponding to $(\text{Ni-Co})_{2/2/150}$ coating, shown in the inset of Figure 5.11b indicates that simulated simple ECE circuit, having R_P and constant phase element (CPE) agrees with the experimentally observed values, reported in Table 5.2.

5.9 SEM STUDY OF MULTILAYER COATING

Generally nanostructured multilayer alloy coatings exhibit special/improved properties due to effect of increased surface/interface arising from the exceptional thinness of the layers. Hence, they show large deviations from bulk behavior, and leads to promising mechanical strength, wear, elasticity, ductility, electrical, magnetic, optical and anti-corrosion properties(Ma et al.2012).Here, the decreased CR of sonoelectrodeposited multilayer Ni-Co alloy coating, compared to its conventional alloy coating may be attributed the increased interfacial surface area due to layering. Formation of coatings in multilayers, having alternate layers of alloys with two different compositions was confirmed by the following test as explained here.

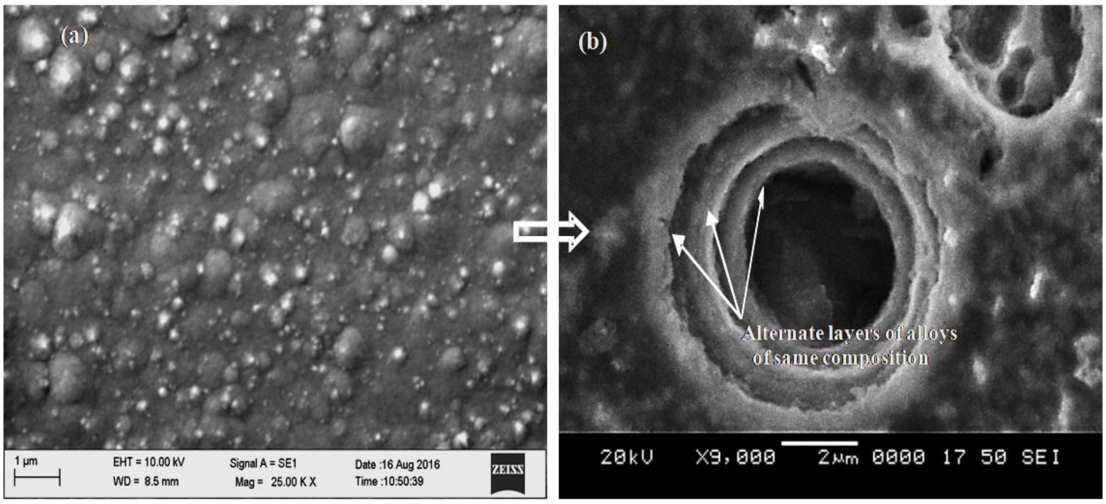

Figure 5.12- SEM micrograph of top surface of (Ni–Co) $_{30/30/10}$ *alloy coating: a) before acid test, and b) after acid test displaying the formation of layers, having differnet compositions*

A drop of 2N HCl has been treated on to the surface of electrodeposited copper, having (Ni-Co) $_{30/30/10}$ coating configuration. It is allowed to stay for about 60 second on the surface, for layers to dissolve partially. It is later washed, and then dried. Inspection of the treated surface under SEM confirmed the formation of Ni-Co alloy coatings in layered manner, due to effect of T_{ON} and T_{OFF}. The surface morphology of multilayer Ni-Co alloy coating before and after acid test, are shown in Figures 5.12(a) and (b), respectively. It confirms of formation of coatings in multilayers, and an existence of separating interface between the layers. Thus inspection of microscopic appearance of multilayer alloy coating, after corrosion test confirmed the formation of coatings in layers, separated by interfaces. The shape of vortexes (Figure 5.12b) confirmed the dissolution of layers of alloys of two different composition, (having 78.20 wt.% Ni deposited at p.d. = 0 Wcm^{-2}; and 56.52 wt.% Ni deposited at p.d. at = 1.2 Wcm^{-2}). i.e., only alternate layers of alloys have dissolved more preferentially than the other. In other words, the layer of one composition (having 21.80 wt.% Co, corresponding to $(Ni\text{-}Co)_{4.0\ Adm}{}^{-2}$ dissolved less preferentially compared to its adjacent layer (having 43.48wt.%Co, corresponding to $(Ni\text{-}Co)_{30/30/10}$). Thus, the interfaces formed due to periodic pulsing of sonicator, made the corrosion medium to spread laterally, instead of attacking the substrate directly. The increased corrosion protection of multilayer alloy coatings, compared to its monolayer counterpart , due to lateral spreading of the corrosive agent through interfaces rather than its direct attack towards the substrate (Wang et al. 2016). However, in case of monolayer alloy coatings, corrosive agent attacks the substrate directly, and is responsible for increased corrosion rate.

The decreased CR of multilayer Ni-Co alloy coating, compared to its conventional homogenous alloy coatings may be attributed the increased interfacial surface area due to layering. The formation of layered coating due to periodic pulsing of the ultrasound waves was confirmed by taking the cross-sectional view of coating under SEM. The cross-sectional view of multilayer Ni-Co alloy coating having 10 layers, with alternately varying composition (5 each), represented as $(Ni\text{-}Co)_{30/30/10}$ is shown in Figure 5.13.

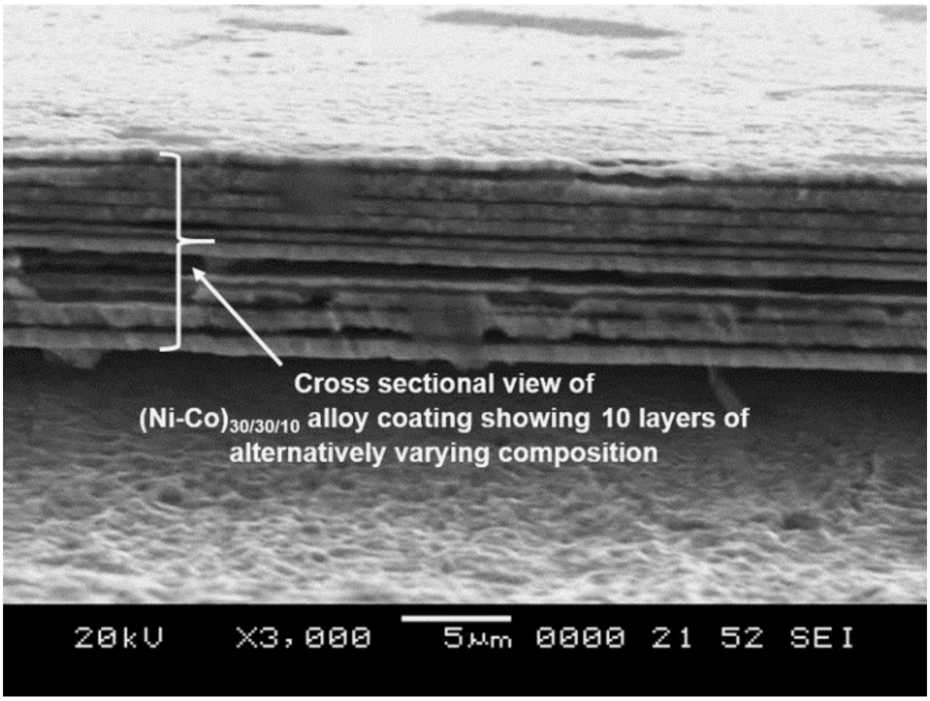

Figure 5.13- SEM cross-sectional view of multilayer Ni-Co alloy coating, represented as $(\text{Ni-Co})_{30/30/10}$ *displaying 10 layers, with alternately different compositions*

Clear demarcations on the cross section of the coating evidence the formation of layers, due to periodic pulsing of ultrasonic probe during deposition. In other words, periodic modulation of ultrasound waves during deposition allowed the formation of interfaces, separating two layers of alloys having different composition. Thus improved corrosion protection of multilayer Ni-Co alloy coating is due to nano/micrometric layering of alloys affected by periodic pulsing of the sonicator probe.

5.10 CONCLUSIONS

In an effort to improve the corrosion protection ability of monolayer Ni-Co alloy coatings by multilayer technique, using the benefit of sonoelectrodeposition, the following conclusions are made:

1. The corrosion rates of Ni-Co alloy coatings can be decreased drastically by sonoelectrodeposition by inducing the ultrasound effect, parallel to the process of electrodeposition.

2. The factors such as surface morphology, composition and phase structures, responsible for better corrosion resistance of the coatings were found to be controlled by the power density (p. d.) used for deposition, supported by SEM, EDX and XRD study, respectively.
3. Drastic decrease of CR of $(Ni\text{-}Co)_{4.0/1.2\ Wcm^{-2}}$ coating, compared $(Ni\text{-}Co)_{4.0\ Adm^{-2}}$ is attributed to its increased Co content of the alloy, consequent to its increased limiting c.d. (i_L), affected by induced ultrasonication.
4. Corrosion rates of multilayer Ni-Co alloy coatings decreased with number of layers only upto 150 layers, and then increased due to interlayer diffusion.
5. Improved corrosion resistance of sonoelectrodeposited multilayer Ni-Co alloy coating is due to formation alternative layers of alloys having two different compositions (21.8 and 43.48 wt.% of Co), formed due to periodic T_{ON} and T_{OFF} of sonication, parallel to the process of deposition.
6. Corrosion data showed that under optimal condition, CMMA $(Ni\text{-}Co)_{2/2/150}$ is about 3 times more corrosion resistant than sonoelectrodeposited $(Ni\text{-}Co)_{4.0/1.2\ Wcm^{-2}}$ coating and about 15 times more corrosion resistant than its conventional monolayer counterpart $(Ni\text{-}Co)_{4.0\ A\ dm^{-2}}$, deposited from the same bath for same duration.
7. The increased corrosion protection of multilayer Ni-Co alloy coatings, in relation to its monolayer alloy coatings is attributed to increased number of interfaces formed (due to layering) affected by periodic pulsing of ultrasound waves, during deposition.

CHAPTER 6 ELECTROCATALYTIC BEHAVIOR OF Ni-Co ALLOY COATINGS AND ITS DEPEDENCY ON DEPOSITION CURRENT DENSITY

This chapter introduces how electrodeposited Ni-Co alloy coatings can be used as stable and efficient bipolar electrode material for water electrolysis of hydrogen evolution reactions (HER) and oxygen evolution reactions (OER). The electrocatalytic performance of were evaluated quantitatively by measuring amount of hydrogen and oxygen liberated, when used as cathode and anode material, respectively. The electrocatalytic kinetic parameters of HER and OER were determined, taking 1M KOH as reaction medium using cyclic voltammetry (CV) and chronopotentiometry (CP) methods. The structure-property relationship of electrodeposited Ni-Co alloy coatings have been discussed, with support of evidences of XRD, SEM and EDX analyses.

6.1 INTRODUCTION

Hydrogen is generally considered as a secondary source of energy, and is a good energy carrier. Since it does not exist on earth as a gas and it should be separated from other compounds. In this regard, water splitting and steam forming are the two commonly used methods for hydrogen production(Shetty and Hegde 2017).The water splitting, or water electrolysis is preferred (though it is less expensive) over steam forming method as latter indirectly supports the global warming issues due to liberation of green-house gases. The water splitting reactions, using electric current produces gases of very high purity, and hence it has been extensively used for production of hydrogen.The electrocatalytic properties of the electrode materials mainly depends on density of active site of a material, and is controlled by electronic structure of the materials(Wu et al. 2004).Generally, platinum and other noble metal oxides, like IrO_2, RhO_2, PtO_2 and RuO_2 are used as best electrode material for hydrogen and oxygen evolution reactions respectively, but their prohibitive cost impedes their wide industrial scale application as good electrode material(Sapountzi et al. 2017).In this regard, the transition metals and their alloys are used as best electrode materials for water splitting reactions. Since, Ni and its alloys have been considered as efficient electrode materials due to their special properties, such as low cost, high-strength, good wear resistance and good electrocatalytic activity(Wang et al. 2005). The electrodeposited alloys of transition metals, like Ni, Co, Fe, Mo are proved to be the efficient electro catalysts towards water splitting reaction than bare Ni coatings, obtained under same condition(Fan et al. 1994), (Rosalbino et al. 2008).

In this direction, the Ni-Co alloy coatings electrodeposited from the optimized bath of Ni-Co (Table 4.1) has been subjected to electrocatalytic study. Ni-Co alloy coatings were accomplished on copper substrate from acid sulphate bath at different c.d.'s, and their efficacy for water electrolysis of HER and OER were studied. The performance of Ni-Co deposit, as efficient bipolar electrode material has been evaluated quantitatively, and electrocatalytic kinetic parameters were assessed by conventional cyclic voltametry (CV) and chronopotentiometry (CP) methods. The factors responsible for different electrocatalytic activity of Ni-Co alloy coatings, deposited at different c.d.'s were correlated with their composition, phase structure and surface morphology, evidenced through EDX, XRD and SEM analyses.

6.2 MATERIALS AND METHODS

The electrodeposition of Ni-Co alloy coatings was accomplished from the optimized sulphate bath, used in Chapter 4. The composition and its operating parameters are given in Table4.1. Electrodeposition of Ni-Co alloy coatings for electrocatalytic study was made in a specially made glass set up, shown schematically in Figure 4.1.

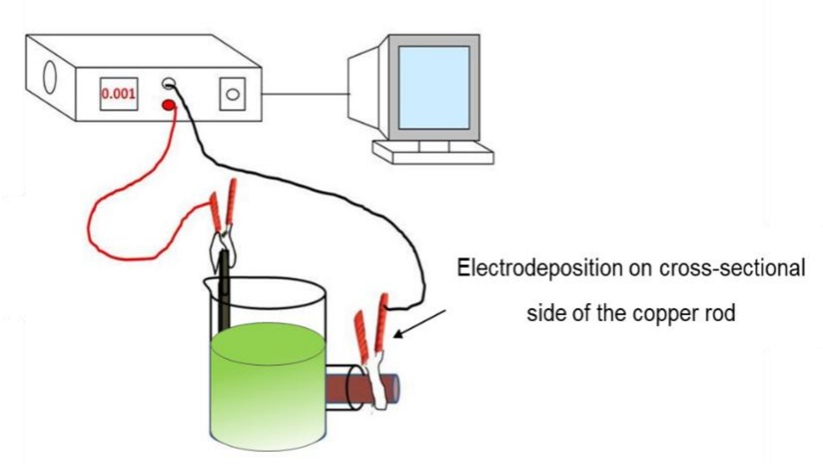

Figure 6.1- The glass set up used for electrodeposition of Ni-Co alloy coatings on the cross sectional surface of the copper rod

It should be noted that electrodepositions for electrocatalytic study were made on the cross-sectional side of the copper rod to fit into custom made glass set up to be used for quantitative measurement of hydrogen and oxygen gas evolved, as measure of their electro catalytic efficacy. The Ni-Co alloy deposition was carried out on the cross sectional surface area of copper rod at different c.d.'s using DC Power Analyzer (N6705A, Agilent Technologies, USA) for constant time (10 min), for comparison purpose. The pure nickel strip was used as anode for electrodeposition with same exposed area as that of cathode. After electrodeposition, all plating are cleaned using distilled water, followed by air drying. The deposited coatings were further analysed for the composition, phase structure and surface morphology. The electrocatalytic activity of deposited Ni-Co alloy coatings was studied using a specially designed electrolyzer, shown in Figure 6.2. The electrolyzer was equipped with three electrodes, in which platinized platinum is used as counter electrode, saturated calomel electrode (SCE) as reference electrode and copper rod as working electrode. A Luggins capillary with KCl Bridge was used to minimize the ohmic polarization. The electrolytic cell fitted with graduated burettes on top (Figure 6.2), enables quantitative measurement of hydrogen and oxygen gases, liberated during water electrolysis.

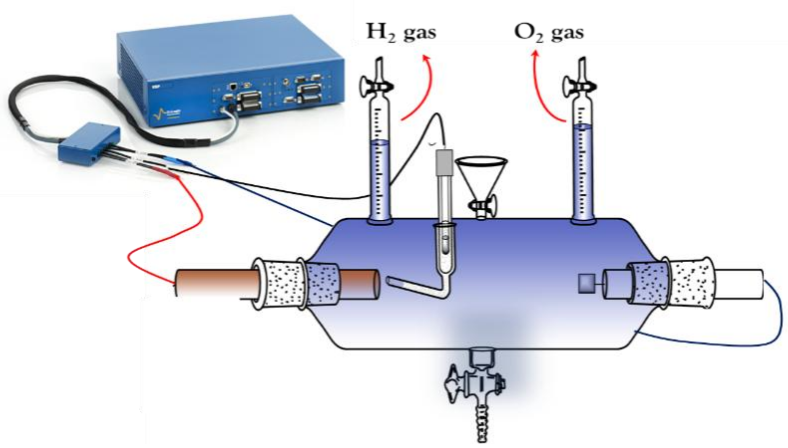

Figure 6.2- Schematic representation of custom made electrolytic cell, having three electrodes used for studying the electro catalytic efficiency of Ni-Co alloy coatings. The graduated burettes provided on the top enables the quantitative measurements of H_2 and O_2 gas evolved

The electrodeposited Ni-Co alloy coatings, deposited at different c.d.'s were used as both anode and cathode (as bipolar) in alkaline water electrolysis. The electrocatalytic activity of all Ni-Co alloy coatings, corresponding to different c.d.'s were studied in a 1M KOH medium. Kinetic parameters of electrocatalysis of Ni-Co alloy coatings were studied through cyclic voltammetry (CV) and chronopotentiometry (CP) using potentiostat/galvanostat.

6.3 RESULTS AND DISCUSSION

6.3.1 Electrodeposition of Ni-Co Alloy Coatings

The Ni-Co coatings have been accomplished on a copper substrate at different c.d.'s, like 1.0 Adm^{-2}, 2.0 Adm^{-2}, and 3.0 Adm^{-2} and 4.0 Adm^{-2}; and then they were characterized using SEM, EDX and XRD techniques. The detailed characterization of Ni-Co alloy coatings, deposited at different c.d. are reported in Chapter 4. The wt.% Ni in the deposit is found to vary drastically with the c.d. employed for its deposition. Literature review supports the fact that surface morphology and porosity of the electrode materials play an important role on their electrocatalytic behaviours. It was found that that the surface roughness of the Ni-Co alloy coatings decreased drastically with increase in the deposition c.d., alongside the increase of its Ni content. The Ni-Co alloy deposited at 1.0 Adm^{-2}, having 59.55wt. % of Co exhibited rough structure, whereas coating deposited at 4.0 Adm^{-2}, having 21.80 wt. % of Co displayed smooth surface. A drastic decrease in the grain size of the alloy coatings was attributed to decrease in its cobalt content. Surface morphology of the coating deposited at 1.0 Adm^{-2} was found to be more rough and porous, compared those at other c.d's. Hence, increased surface roughness resulted in increased active sites, or active surface area. Consequently, this resulted in enhanced electrocatalytic properties (Subramanya et al. 2015).As the c.d. increased the structure of the deposit changes from nodule to fibrilar due to decrease in wt.% of Co in the deposit(Correia and Machado 2000).The phase structure binary Ni-Co coatings, deposited at different c.d.'s were analyzed by XRD techniques, and were discussed in Chapter 4.

6.3.2 Atomic Force Microscopy Study

The AFM is a powerful means to characterize the microstructure of the coatings, in terms of their average roughness. Accordingly, a three dimensional AFM image of the Ni-Co alloy coatings corresponding to (Ni-Co)$_{1.0\ \mathrm{Adm}^{-2}}$ and (Ni-Co)$_{4.0\ \mathrm{Adm}^{-2}}$(extreme representatives) have been taken, and are shown in Figures 6.3(a) and 6.3(b).Experimental data revealed that the average roughness of (Ni-Co)$_{1.0\ \mathrm{Adm}^{-2}}$, and (Ni-Co)$_{4.0\ \mathrm{Adm}^{-2}}$ are, respectively 32.0 and 24.0 nm, as reported in Table 6.1. Further, a decrease of surface roughness was found to be increased with deposition c.d.as reported in Table 6.1, and as observed in Figure 6.3.

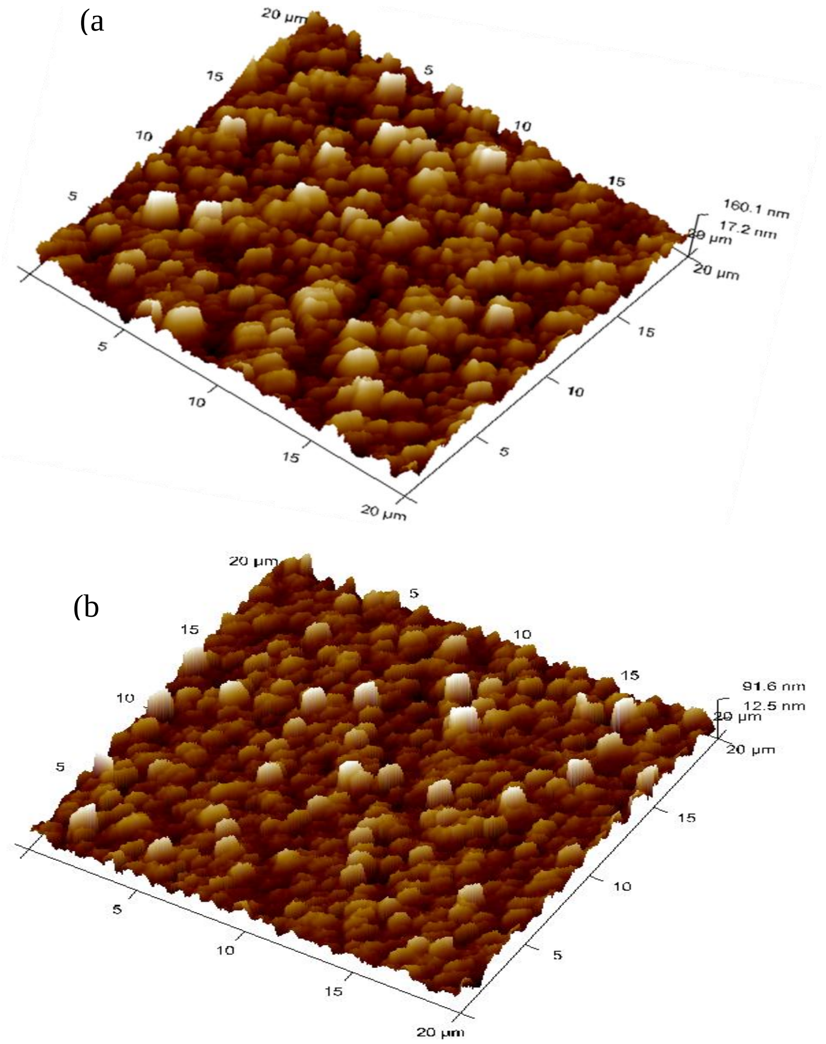

Figure 6.3 - AFM image of Ni-Co alloy coatings deposited at, a) 1.0 Adm^{-2}, and b) 4.0 Adm^{-2} from same optimized bath for same duration (10 min)

Table 6.1- The AFM data on average roughness and surface roughness of (Ni-Co)$_{1.0\ Adm^{-2}}$and (Ni-Co)$_{4.0\ Adm^{-2}}$ alloy coatings obtained at extreme conditions of current density (1.0 Adm^{-2} and 4.0 Adm^{-2})

Coating configuration	R_a(nm)	R_q(nm)
(Ni-Co)$_{1.0\ Adm^{-2}}$	32.0 nm	40.6 nm
(Ni-Co)$_{4.0\ Adm^{-2}}$	24.0 nm	30.8 nm

6.3.3 Corrosion Stability

The corrosion stability is an important aspect of electrode materials, while validating its use as good electrocatalyst. Hence, electrochemical corrosion stability of all Ni–Co alloy coatings are tested for their corrosion behaviour in 1M KOH medium. The corrosion rates (CR's) of alloy coatings were calculated through Tafel extrapolation method, and corresponding corrosion data are reported in Table 6.2. The potentiodynamic polarization curves of Ni–Co alloy coatings deposited at different c.d.'s is as shown in the Figure 6.4. It was found that the corrosion stability of Ni–Co alloy coatings decreases with increase of c.d., and it was found that corrosion stability of all Ni–Co alloy coatings were within the tolerable limit to use for electrocatalytic applications(Subramanya et al. 2015). The electrocatalytic kinetic parameters, like exchange current density (i_o) and cathodic slope (β_c), were deduced from the linear part of semi-logarithmic polarization plots. Apparent i_o values were deduced on extrapolation of Tafel plots to zero current potential. Accordingly, i_o , β_c, and overpotentials (η_c and η_a) values were listed in the Table 6.3. The data derived from Tafel plots can be used to describe the electrocatalytic activity of the electrodes, interms of exchange current density (i_o) Tafel slopes and overpotential values.

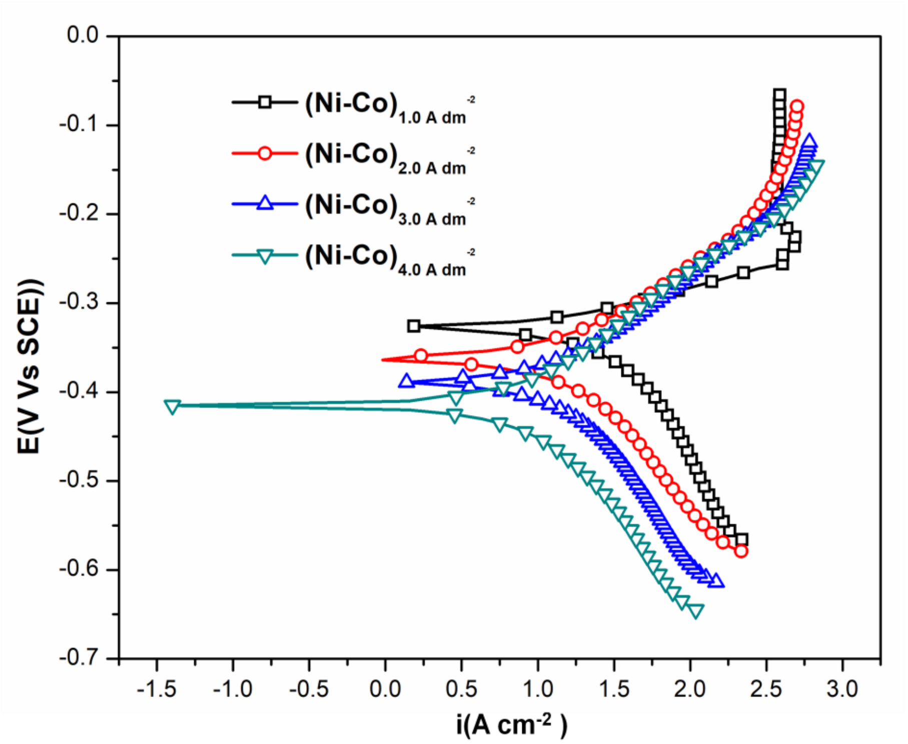

Figure 6.4-Potentiodynamic polarization response of Ni-Co alloy coatings deposited at different current densities, studied in 1M KOH solution

It is known that smaller the value of Tafel's slope better is the electrocatalytic character, as small change of overpotential brings faster exchange of electrons. Hence evolution of hydrogen gas takes place more readily. The process is favoured by higher value of charge transfer coefficient(α) (Manazoglu et al. 2016). As the wt. % of Co in the deposit is more at 1.0 Adm^{-2}, HER is more favoured. Since, it shows lowest values for β_c and η_c and highest value for α, i_o proving that it is electro-catalytically more active for HER than rest of the coatings developed at higher c.d.'s. The better performance of (Ni-Co) $_{4.0\ \mathrm{A\ dm}^{-2}}$ for OER may be explained in the same line, due to highest value of anodic overpotential (η_a).

Table 6.2- Corrosion data of Ni-Co alloy coatings, deposited at different current densities studied in 1M KOH medium

Coating configuration	Wt. % Ni in the deposit	Wt. % Co in the deposit	$-E_{corr}$ (mV vs SCE)	i_{corr} (μA cm^{-2})	CR×10^{-2} (mm y^{-1})
(Ni-Co)$_{1.0\ A\ dm^{-2}}$	40.45	59.55	320	19.4	25.5
(Ni-Co)$_{2.0\ A\ dm^{-2}}$	48.14	51.86	360	20.2	23.42
(Ni-Co)$_{3.0\ A\ dm^{-2}}$	62.26	37.74	360	15.1	17.2
(Ni-Co)$_{4.0\ A\ dm^{-2}}$	78.20	21.80	410	14.0	15.0

Table 6.3- Electrocatalytic kinetic parameters for Ni-Co alloy coatings deposited at different current densities, studied in 1M KOH medium

Coating configuration	β_c (mV dec^{-1})	α (symmetry factor)	i_o (mA cm^{-2})	η_c (mV Vs SCE)	η_a (mV Vs SCE)
(Ni-Co)$_{1.0\ A\ dm^{-2}}$	120	0.24	1.397	400	300
(Ni-Co)$_{2.0\ A\ dm^{-2}}$	128	0.23	1.307	450	346
(Ni-Co)$_{3.0\ A\ dm^{-2}}$	148	0.20	1.172	500	349
(Ni-Co)$_{4.0\ A\ dm^{-2}}$	155	0.19	1.064	510	352

6.4 ELECTROCATALYTIC STUDY

6.4.1 Hydrogen Evolution Reaction

The steady state equilibrium is one of the simplest techniques to study the water splitting ability of the electrocatalysts. Hence, the Ni-Co coatings obtained at different c.d.'s was subjected to electrocatalytic study of HER in 1M KOH medium. The experimental data were investigated through cyclic voltammetry (CV) and chronopotentiometric (CP) techniques, and are discussed in the following sections.

6.4.1.1 Cyclic voltametry study

The electrocatalytic behavior of Ni-Co coatings have been studied for HER, using it as cathode. The CV study was made in a potential range of 0.0V to -1.6V, at 50mV/sec scan rate for 30 cycles. The CV curves of Ni-Co alloy coatings deposited at different c.d.'s are as shown in the Figure 6.5.It was observed that peak cathodic c.d. at -1.6V decreased with increase in number of cycles, and finally reached a stable value. The decrease in peak c.d. attributed to resistance offered by the hydrogen molecules formed on the surface of cathode.

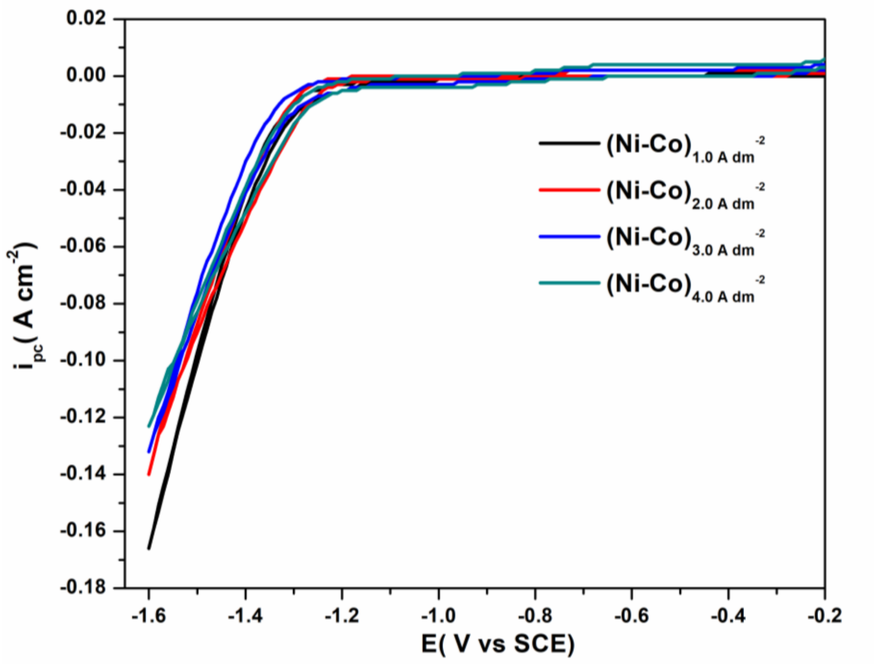

Figure 6.5-CV curves for HER on the surface of Ni-Co coatings, deposited at different c.d's from the same optimized bath.

A stable and reproducible CV curves followed at the end, indicated a state of equilibrium between attachment and detachment of hydrogen gas on the electrode surface.The c.d. corresponding to this equilibrium is called cathodic peak current density denoted by $i_{pc,}$ and the potential at which desorption of hydrogen gas started is called onset potential. The CV curves shown in Figure 6.5 indicates that Ni-Co coating, deposited at 1.0Adm^{-2} showed the highest cathodic current density with least onset potential for HER, as compared to other coatings. Thus, the better electrocatalytic activity of Ni-Co alloy (1.0Adm^{-2}) may be attributed to high wt.% of Co in the deposit by providing more number of active sites for evolution of hydrogen. And also ascribed to synergic combination of Ni and Co atoms at this concentration(Perez-Alonso et al. 2014). Further, it is important to note that HER of Ni-Co alloy coatings bears a close relationship surface roughness. As the surface roughness increases the reactive sites for evolution of hydrogen gas also increases. Further, due to the high cobalt content of the coating (Ni-Co)$_{1.0\ \mathrm{Adm}^{-2}}$ coating showed better electrocatalytic activity. And metallic Co content in the deposit accelerated the proton discharge reaction. This is due to the increase of exchange current density and charge transfer coefficient values. In addition to this, an important factor responsible for enhanced electrocatalytic activity of Ni-Co alloy coatings is due to synergistic effect low hydrogen overpotential of Ni and high hydrogen adsorption of Co(Herraiz-Cardona et al. 2011).

6.4.1.2 Chronopotentiometry study

The Ni-Co coatings, deposited at different c.d.'s were also subjected to chronopotentiometry analysis by monitoring potential change as a function of time keeping current as constant, between test electrode and reference electrode. The CP curves of Ni-Co coatings at different c.d.'s (at constant current of -300mAcm^{-2}) for duration of 1800s are as shown in the Figure 6.6.The electrocatalytic behaviour of Ni-Co coatings were assessed on the basis of the amount of hydrogen liberated for initial 300s. The quantity of hydrogen evolved, corresponding to coatings deposited at 1.0 Adm^{-2}, 2.0 Adm^{-2}, 3.0 Adm^{-2}, 4.0 Adm^{-2} were shown in Table 6.4. Experimental data shown in Table 6.4 demonstrated that Ni-Co (1.0 Adm^{-2}) alloy coatings in which maximum amount of hydrogen gas evolved, compared to coatings at other c.d.

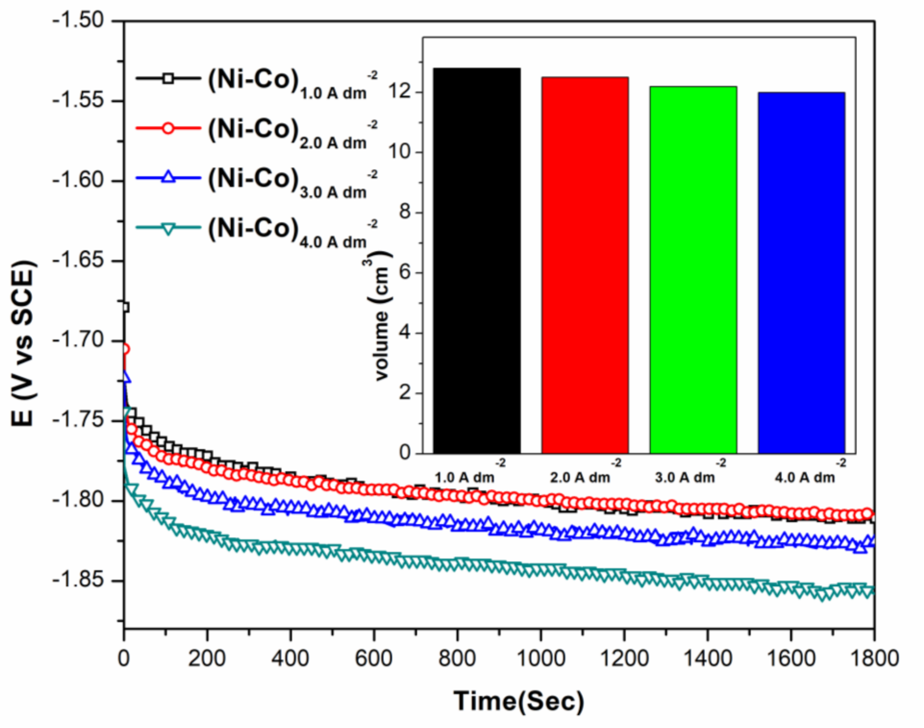

Figure 6.6 - Chronopotentiograms for Ni-Co coatings, deposited at different current densities at impressed cathodic current of -300 mAcm^{-2}, showing different degrees of responses for HER

Table 6.4-Hydrogen evolution parameters for Ni-Co alloy coating obtained at different c.d.'s

Coating configuration	Cathodic peak c.d.(i_{pc}) (Acm^{-2})	Onset potential for H_2 evolution (V vs SCE)	Volume of H_2 Evolved in 300s(cm^3)
$(Ni\text{-}Co)_{1.0A\ dm^{-2}}$	-0.165	-1.23	12.8
$(Ni\text{-}Co)_{2.0A\ dm^{-2}}$	-0.140	-1.24	12.5
$(Ni\text{-}Co)_{3.0A\ dm^{-2}}$	-0.130	-1.25	12.2
$(Ni\text{-}Co)_{4.0A\ dm^{-2}}$	-0.121	-1.26	12.0

Thus CP curves supported the fact that Ni-Co alloy coatings, deposited at 1.0 Adm^{-2} are the best electrode material for HER, in compliance with CV study. From the nature of CP curves, shown in Figure 6.6, it is clear that initially there is sudden decrease of potential with time in all coatings. This is due to fact that in the beginning of electrolysis, evolution of hydrogen takes place faster. However, after some time equilibrium is established between H_2 gas and H^+ ions, indicating a constant potential as shown in Figure 6.6.

6.4.2 Oxygen Evolution Reaction

The electrocatalytic behavior of Ni-Co alloy coatings, at different c.d.'s was studied for OER, using it as anode, in the same line as for HER. The experimental studies were carried out using CV, CP and results are discussed below.

6.4.2.1 Cyclic voltametry

The cyclic Voltammetric techniques have been applied for Ni-Co coatings at different c.d's in the potential window of 0 to 0.75 V at a scan rate of 50mVsec^{-1} for 30 cycles and corresponding voltamograms are as shown in the Figure 6.7.Since oxygen evolution activity on Ni-Co coatings depends on redox pair prior to the onset of oxygen evolution which decides the electrochemical properties. This is supported by CV of electrodeposited pure Ni exhibiting anodic and cathodic peaks at 0.362 and 0.265 V respectively in 1M KOH medium and is corresponding to the NiOOH/$Ni(OH)_2$ transition(Ullal and Hegde 2014).From the graph, it is clear that the Ni-Co alloy deposited at c.d.4.0 Adm^{-2} showed better OER activity compared to those at other c.d. The mechanism proposed involves initial adsorption of OH^- ion from electrolyte solution onto the electrode surface followed by electron transfer process within the system leads to the liberation of oxygen(Lyons and Brandon 2008; Peters 1996).The peak current shifts towards lower positive potential with increase in deposition c.d.

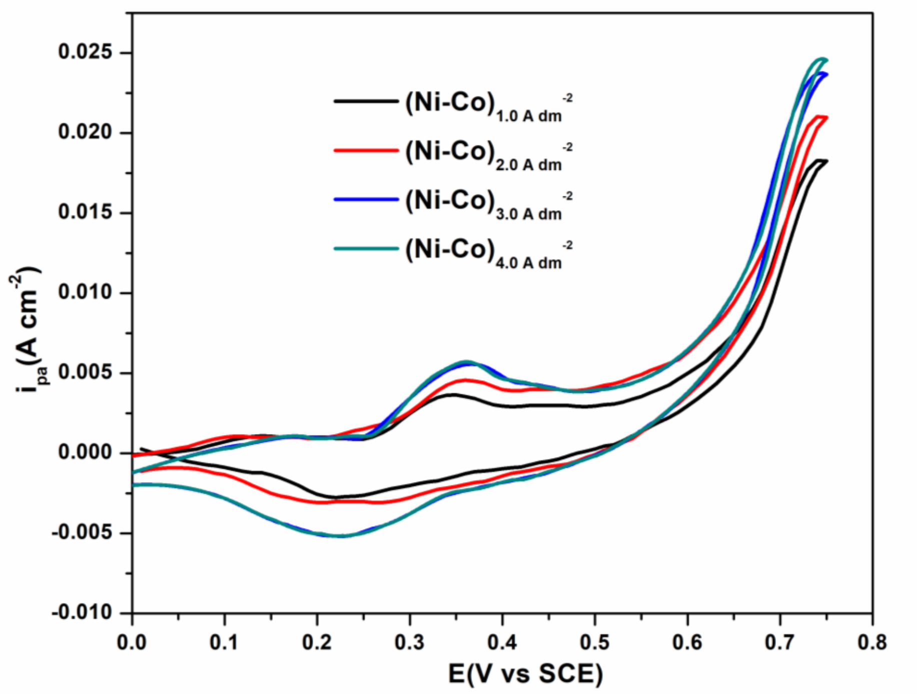

Figure 6.7-Cyclic voltagrams for OER on the surface of Ni-Co alloy coating, deposited at different c.d.'s

Further, the intermediate anodic and cathodic peaks obtained in the voltagrams of Ni-Co alloys (Figure 6.7) indicates that formation and reduction of NiOOH layer. In this potential range the semiconductor layer NiO(H_2O) formed is found to be responsible for better OER activity due to enhanced adsorption of OH^- ions(Elias and Hegde 2015).Beyond this potential range, the OER activity is limited, due to lack of formation of semiconducting NiO(H_2O) layer. Hence, the highest electrocatalytic activity of Ni-Co alloy deposited at 4.0 Adm^{-2} towards OER is attributed to its high Ni content, resulting to better OH^- adsorption.

6.4.2.2 Chronopotentiometry

CP study for evolution of OER on the surface of Ni-Co alloy coatings were carried out at a positive current +300mAcm^{-2}, and corresponding electrochemical responses are shown in Figure 6.8. It may be observed that initially the potential has increased drastically, and then remained almost constant indicating the establishment of an equilibrium between adsorbed OH^- and liberated O_2.The amount of O_2 liberated in the initial 300s on different coatings were measured and is reported in Table 6.5.It was found that the coating deposited at 4.0 Adm^{-2} showed the highest amount of O_2 evolved confirming its highest electrocatalytic activity for OER.

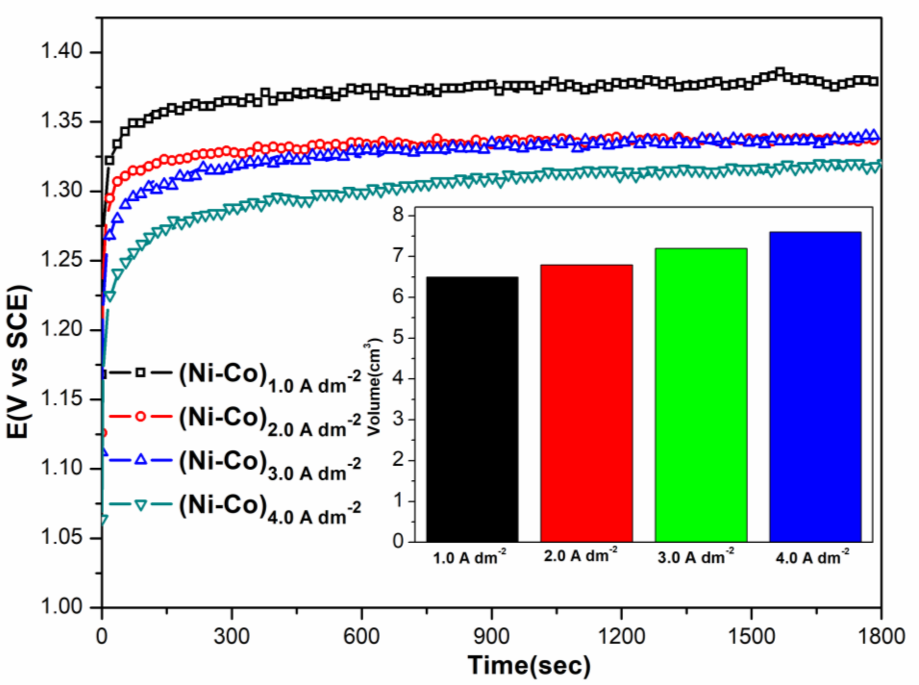

Figure 6.8-Chronopotentiograms of Ni-Co alloy coatings deposited at different c.d.'s, showing different degrees of responses for OER

Table 6.5- Electrochemical parameters of chronopotentiometric study for OER on the surface of Ni-Co alloy coatings deposited at c.d.'s

Coating configuration	Anodic peak c.d. (A cm^{-2})	Onset potential for O_2 evolution (V vs SCE)	Volume of O_2 Evolved in 300s(cm^3)
(Ni-Co)$_{1.0\ A\ dm^{-2}}$	0.017	0.56	6.5
(Ni-Co)$_{2.0\ A\ dm^{-2}}$	0.020	0.53	6.8
(Ni-Co)$_{3.0\ A\ dm^{-2}}$	0.023	0.51	7.2
(Ni-Co)$_{4.0\ A\ dm^{-2}}$	0.024	0.49	7.6

This is attributed to highest wt. % Ni in the deposit, supported by EDX study. The highest Ni content of the alloy is found to be responsible for increased OH^-

adsorption, and hence OER. Thus from the data reported in Tables 6.4 and 6.5, it may be noted that(Ni-Co)$_{1.0\ \mathrm{A\ dm}^{-2}}$ and (Ni-Co)$_{4.0\ \mathrm{A\ dm}^{-2}}$ coatings produced the highest volume H_2 and O_2 gases, when they are used, respectively as cathode and anode during alkaline water electrolysis. This mutually opposite electro catalytic activity of Ni-Co alloy coatings towards HER and OER, which changes with deposition c.d.'s, is attributed to the change in composition of the alloy, in terms of their Ni and Co content.

6.5 MECHANISM OF HER AND OER REACTIONS

The experimental results of investigations of both CV and CP study revealed that Ni-Co alloy deposited at 1.0 Adm^{-2} and 4.0 Adm^{-2}(from the bath taken)are considered as best electrode materials for HER and OER, respectively evident from volume of H_2 and O_2 evolved shown in Tables 6.4 and 6.5, respectively.

The mechanism of HER on the surface of Ni-Co alloys is given as below.

1. Hydrogen adsorption(Volmer reaction).

$$H_2O + M + e^- \leftrightarrow M - H + OH^-$$

2. Hydrogen desorption (Tafel reaction)

$$M - H + M - H \leftrightarrow 2M + H_2 \uparrow$$

The schematic representation for adsorption, desorption reaction responsible for HER is shown in Figure 6.9(a). Ni-Co alloy coatings deposited at 1.0 Adm^{-2} is considered to be best for HER due to its highest cobalt content, increased surface roughness is responsible for increased HER. Further, Tafel's cathodic slope (β_C) values of different Ni-Co coatings was found to be in the range of 118 mVdec^{-1} (Table 6.2).From data, it may be concluded that HER on Ni-Co coating follows Volmer-Tafel mechanism(Subramanya et al. 2015).Similarly, most favoured OER on the surface of coating, deposited at 4.0 Adm^{-2} can also be explained through a mechanism, shown in the Figure 6.9(b).As the nickel content in the alloy increases, the ability of formation to form semiconducting layer on the surface also increases. Hence, adsorption of OH$^-$ leading to the formation NiOOH on the surface, which inturn increases the liberation of oxygen on this surface.

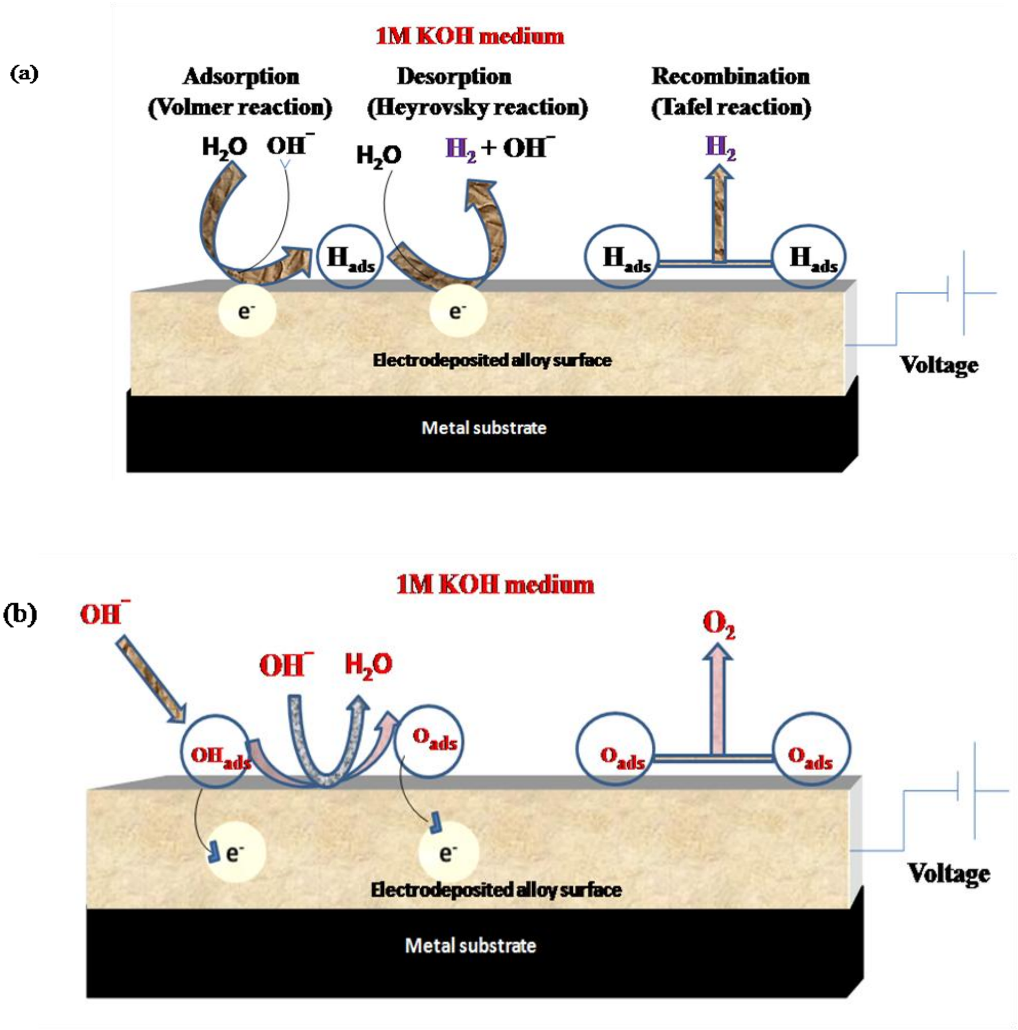

Figure 6.9-Schematic representation showing the mechanism for a) Hydrogen evolution reaction and b) Oxygen evolution reaction on the surface of Ni-Co alloy coatings deposited at 1.0 Adm^{-2} and 4.0 Adm^{-2}

6.6 CONCLUSIONS

The Ni-Co alloy coatings electrodeposited from the optimal bath was found to exhibit the electrocatalytic activity for water splitting reaction of HER and OER. The experimental results of investigation demonstrated the following facts, as conclusions.

1. Electrodeposited Ni-Co alloy coatings can be used as an active and stable electrode material, both as anode and cathode for alkaline water splitting applications.

2. Experimental results demonstrated that electrocatalytic activity of alloy coating is highly dependent on its composition, depending on the c.d. at which they are deposited.
3. Quantitative measurement of H_2 and O_2 gases, evolved at cathode and anode revealed that Ni-Co alloy coatings deposited at lowest and highest c.d.'s are good electrode materials for HER and OER, respectively.
4. The mutually opposite electrocatalytic activity of Ni-Co alloy coatings towards HER and OER, which changes with deposition c.d.'s is attributed to the change in composition of the alloy, in terms of their Ni and Co content.
5. The highest electrocatalytic activity of the Ni-Co alloy coatings were attributed to the change of composition and surface roughness, supported by EDX and AFM analysis.
6. The HER on the surface of Ni-Co alloy coatings was found to follow Volmer-Tafel mechanism, supported by Tafel's slope values.

CHAPTER 7 EFFECT OF CNT ON ELECTROCATALYTIC BEHAVIOR OF Ni-Co ALLOY COATINGS

The present chapter details the effect of addition of carbon nanotube (CNT) on the electrocatalytic behavior of Ni-Co alloy coatings. The Ni-Co-CNT composite coatings were developed, and their electro catalytic efficacy for hydrogen evolution reaction (HER) and oxygen evolution reaction (OER) of water electrolysis have been studied. The improved electrocatalytic behaviors of Ni-Co-CNT coatings were analyzed in the light of its changed surface structure and porosity. Electrocatalytic ability and stability of the composite coatings were tested in 1M KOH using cyclic voltametry and chronopotentiometric techniques.

7.1 INTRODUCTION

Nowadays there is ever increasing demand for renewable energy sources as remedy for global warming crisis. In order to fulfill the energy demands, there is alternative need of new energy strategy which will reduce the environmental issues, like acid rain, global warming etc(Bianchini and Barbaro 2009).Therefore, researcher are trying to find new materials which is more ecofriendly, abundant and cleaner in nature, compared to fossil fuels. In this direction, Ni and Ni-based alloy/composite coatings have been tried widely for water splitting reactions. As carbon nanotubes (CNTs) is an excellent material having good mechanical characteristics, high tensile strength, high elastic modulus, high thermal and electrical conductivity, it has been used in many application(Li et al. 2006). Ni-CNT composite coatings were widely used in plating technology owing to their excellent tribological properties, mechanical strength, wear and corrosion resistance properties(Chen et al. 2003).Improved properties of CNT interposed electrodeposited coatings may be attributed to its remarkable properties, such as high strength and elastic modulus, good flexibility, and unique conductivity(Wang et al. 2002; Zimmerman et al. 2002).

In this direction, the effect of addition of a third phase element, *i.e.,* carbon nanotubes (CNT) into the binary alloy bath of Ni-Co have been tried, with intention of improving the corrosion resistance property of its electrodeposited Ni-Co alloy coatings. The experimental investigation revealed that electrodeposited Ni-Co-CNT composite coatings, developed on dispersing the CNTs homogeneously in the optimized bath exhibits better electrocatalytic activity for alkaline water splitting reaction. The improved electrocatalytic activity of Ni-Co-CNT coatings was attributed to the changed composition, porosity and phase structure of the composite coatings, confirmed by various analytical methods of characterization.

7.2 MATERIALS AND METHODS

The electrodeposition of Ni-Co-CNT alloy coatings were accomplished on a copper substrate using optimized bath of Ni-Co alloy, having dispersed with CNT nanoparticles. The composition and operating parameters of the bath, used in the present study is given in Table 7.1.

Table 7.1-Bath composition and operating parameters used for electrodeposition of Ni-Co-CNT coatings

Bath composition	Amount(g/L)	Operating parameters
Cobalt sulfate	14.0	pH - 3.5
Nickel sulphate	131	Temperature - 303 K
Sulphanilic acid	0.75	Anode – Nickel
Ascorbic acid	2.5	c.d. range- 1.0 Adm^{-2}- 4.0 Adm^{-2}
Boric acid	30.0	
Glycerol	15 mL	
CNT	0.25	

The electrolyte was prepared in distilled water, and reagents used here were of LR grade (Merck, Mumbai, India). The electrolyte, after addition of CNT nanoparticles was sonicated, and kept overnight for homogeneous dispersion of CNT nanoparticles. All depositions were carried out at 303K with constant agitation, following the same experimental procedure described in Chapter 6.

7.3 RESULTS AND DISCUSSIONS

Preliminary Hull cell study of Ni-Co-CNT bath revealed that a sound deposit of Ni-Co-CNT coating is likely to take place in the c.d. range of 1.0 - 4.0 Adm^{-2}. Accordingly, electrodeposition of Ni-Co-CNT alloy coatings were carried out at different c.d.'s, *i.e.*, at 1.0 Adm^{-2}, 2.0 Adm^{-2}, 3.0 Adm^{-2} and 4.0 Adm^{-2}. The deposited coatings were later analyzed for change of composition, surface morphology and phase structure due to addition of CNT's, using EDX, SEM, AFM and XRD techniques. Improvement in the corrosion resistance property of Ni-Co-CNT alloy coatings were evaluated by electrochemical AC and DC methods, and results are discussed below.

7.3.1 Compositional Analysis

The variation in the wt.% of Ni, Co and carbon (C)content of the alloy coatings with increase of their deposition current densities (c.d.'s) are shown in the Table 7.2.From the composition data, it is clear that wt.% Ni in the deposit has increased, and carbon increased with growth of deposition c.d. The comparison of composition data of alloy coatings, corresponding to Ni-Co bath (Table 4.1) and Ni-Co-CNT bath (Table 7.2) reveals that addition of CNT nanoparticles has role in changing its metal contents (Ni and Co) substantially. This observation may be explained by the deposition principle of mutual alloys of iron group metals. During deposition, increase of c.d. increases the electrostatic force of attraction of metal ions. Hence, at high c.d. wt.% of more readily depositable metal (Ni) increased (Pavithra and Hegde 2013). In addition, as CNT is conductive in nature its codeposition with metal ions do take place to form the composite coating, and it is confirmed by the C content of alloy, as reported in Table 7.2. At lower limits of c.d., the wt.% of C is high in Ni-Co alloy matrix as may be seen from the data in Table 7.2. The high C content of Ni-Co-CNT alloy coatings, at lower limits of c.d.is contributing for its better electrocatalytic activity(Daneshvar-Fatah and Nasirpouri 2014).

Table 7.2-The change in the wt.% of Ni, Co and C in Ni-Co-CNT electrodeposits at different current densities deposited from the same bath

Coating configuration	wt.% of Ni	wt.% of Co	wt.% of C
$(\text{Ni-Co-CNT})_{1.0\ \text{A dm}^{-2}}$	56.68	28.54	14.78
$(\text{Ni-Co-CNT})_{2.0\ \text{A dm}^{-2}}$	58.86	26.96	14.18
$(\text{Ni-Co-CNT})_{3.0\ \text{A dm}^{-2}}$	70.86	15.10	14.04
$(\text{Ni-Co-CNT})_{4.0\ \text{A dm}^{-2}}$	75.1	14.87	10.05

7.3.2 Surface Analysis

7.3.2.1 SEM study

Electrocatalytic activity of electrode materials is a function of its composition and surface morphology. Generally, the mechanism of water splitting involves the adsorption of ions onto the surface, surface structure and porosity plays important role on electro catalytic performance. Hence to decode the dependency of electro catalytic activity with surface structure and porosity of the coatings, SEM study of Ni-Co-CNT deposit, corresponding to different c.d.'s was made. The surface morphology of Ni-Co-CNT alloy coatings, shown in Figure 7.1.It clearly indicates that porosity and surface roughness of the composite coatings decreases drastically with deposition c.d. It may be noted that the porous and globular structure of Ni-Co-CNT alloy coating is changed into more homogeneous as c.d. increased from 1.0 Adm^{-2} to 4.0 Adm^{-2}.

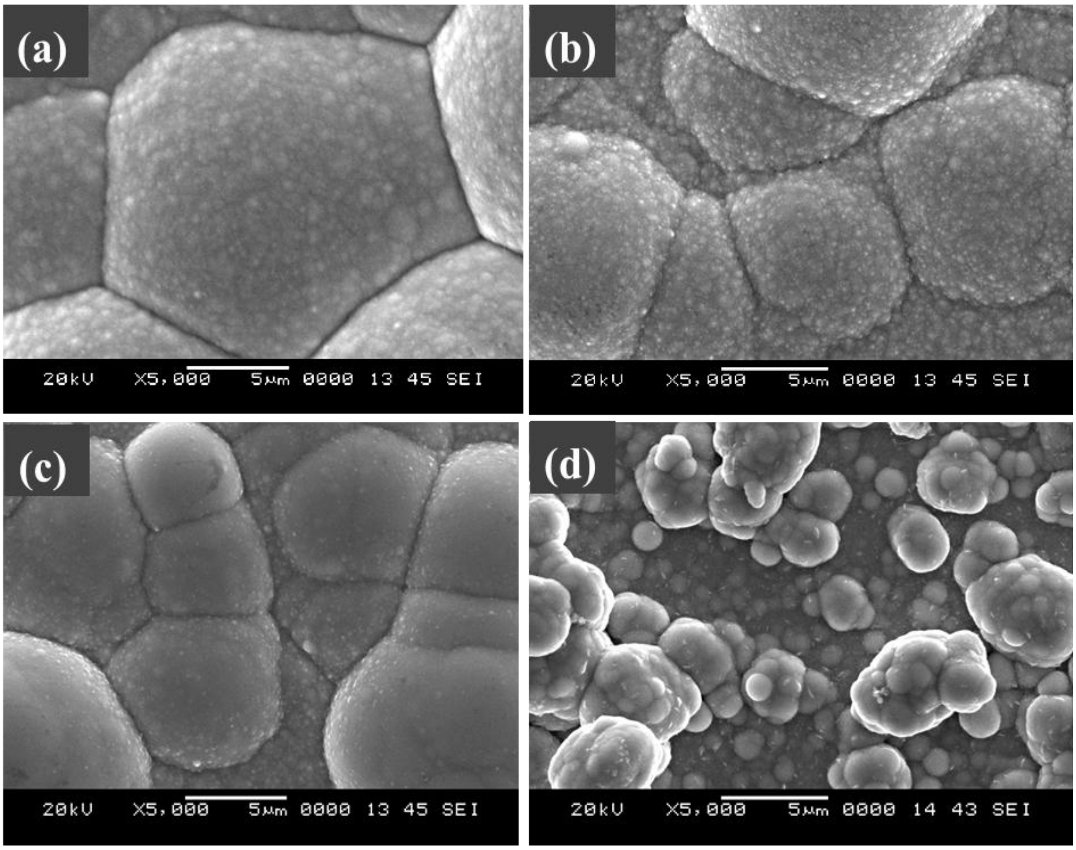

Figure 7.2-Surface morphology of Ni-Co-CNT coatings deposited at different current densities: a) (Ni-Co-CNT)$_{1.0\ Adm^{-2}}$*, b) (Ni-Co-CNT)*$_{2.0\ Adm^{-2}}$*, c) (Ni-Co-CNT)*$_{3.0\ Adm^{-2}}$*, and d) (Ni-Co-CNT)*$_{4.0\ Adm^{-2}}$

7.3.2.2 AFM Analysis

The AFM analysis gives valuable information about the surface properties of materials, particularly surface average roughness. Accordingly, the AFM image of Ni-Co-CNT composite coatings, deposited at 1.0 Adm^{-2} and 4.0 Adm^{-2} (only extreme cases) are shown in Figures 7.3(a) and 7.3(b), respectively. From the image, it is clear that surface roughness of the composite coatings decreased drastically when deposition c.d. is increased from 1.0 Adm^{-2} to 4.0 Adm^{-2}, and calculated surface roughens was found to be, respectively 60.3nm and 39.3 nm.

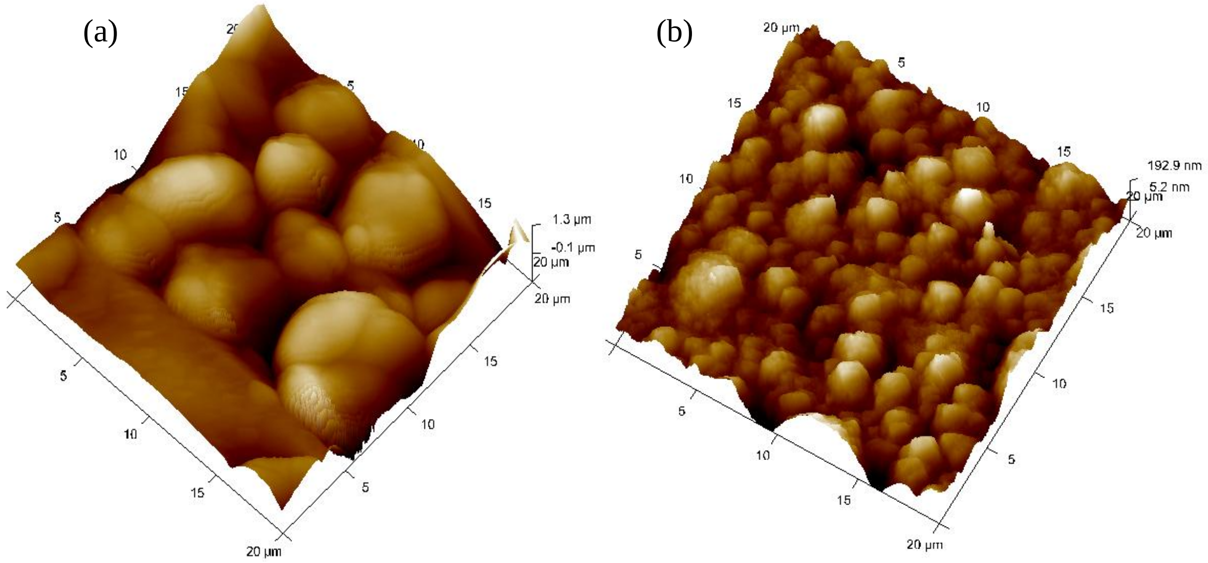

Figure 7.3-AFM image of Ni-Co-CNT coatings deposited at two extreme situations of c.d.'s: a) $(Ni\text{-}Co\text{-}CNT)_{1.0\ Adm^{-2}}$*, and b)* $(Ni\text{-}Co\text{-}CNT)_{4.0\ Adm^{-2}}$ *displaying a drastic difference in the surface roughness and porosity*

7.3.3 XRD Study

To validate the structure-property relationship of electrodeposited Ni-Co-CNT composite coatings, the change of phase structures was tried to link with their improved electro catalytic behaviours. In this direction, the phase structure and grain size of binary Ni-Co-CNT coatings were studied by XRD techniques. The XRD patterns recorded for Ni-Co-CNT alloy coatings, at different c.d.'s are shown in Figure 7.4. It may be seen that three distinct peaks at 44.7^0, 51.8^0 and 76.4^0 for the planes (111),(200) and (220), respectively are for fcc structure of Ni (JCPDS 04-0850), and one distinct peak at 73.9^0 corresponds to (311) plane is of $CoNiO_2$(JCPDS10-0188). It may also be noted that with increase of c.d., the intensity of peak corresponding to (220) plane at 76.4^0 increases, due to increase in the wt.% Ni in the deposit; and contrary to this, wt.% Co in the deposit decreased, which reflected as decrease of intensity of peak corresponding to the plane (311) at 73.9^0, as may be seen in Figure 7.4. The carbon peak, corresponding to CNT, interstice in the alloy matrix has also been noted in the Figure 7.4 (shown by arrow mark). The grain size was determined using Debye-Scherrer formula (Chapter – 6), and it was found that Ni-Co-CNT coating matrix possess an average grain size of 35nm.

Further, it may also be noted that except the intensity of peak, there is no change in the phase structure of the Ni-Co-CNT coatings with change of c.d. It is due to the fact that Ni-Co alloy forms single phase solid solution of cobalt in Ni (Chapter - 4) even in the presence of CNT.

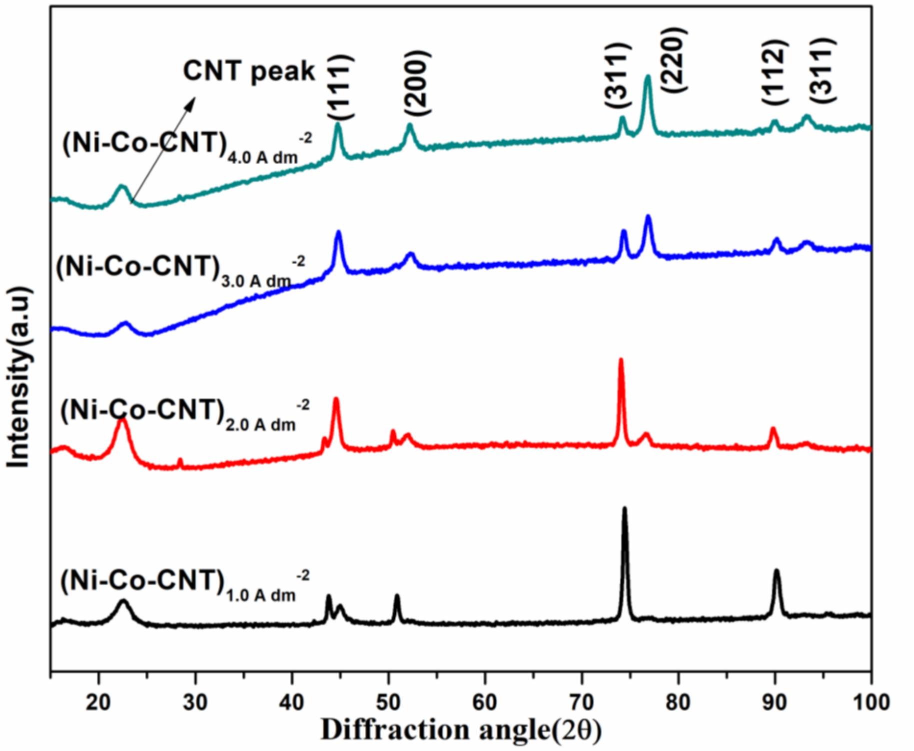

Figure 7.4- XRD patterns of Ni-Co-CNT coatings deposited at different current densities

7.3.4 Corrosion Stability

The corrosion study of materials to be used as electrode materials is of vital importance to verify their long term stability in the working conditions. Hence, corrosion behavior of electrodeposited Ni-Co-CNT composite coatings have been studied in 1M KOH medium, by potentiodynamic polarization method. Tafel's response of Ni-Co-CNT coatings, deposited at different c.d.'s is shown in Figure 7.5. The corrosion rates (CR's) were calculated by Tafels extrapolation method. The CR's of Ni-Co-CNT composite coating deposited at 1.0, 2.0, 3.0 and 4.0 Adm^{-2} was found to be 14.5× 10^{-2}, 11.6 ×10^{-2}, 6.7× 10^{-2} and 5.7 × 10^{-2} mm y^{-1} respectively. The corrosion rate values are found be in the range of acceptable limit of its tolerance to work as electrode. The Tafel's can be used to explore many valuable information as far as their electrocatalytic characters are concerned. Accordingly, electrocatalytic kinetic parameters, like exchange current density (i_o) and Tafel's cathodic slope (β_c) were deduced from the linear part of semi-logarithmic polarization plots, shown in Figure 7.5. Apparent i_o values were derived by extrapolation of Tafel's plots to equilibrium (zero current) potential. Accordingly i_o, β_c, and overpotential (η_c and η_a) values are tabulated in Table 7.3.From the data reported in Table 7.3, it is clear that Ni-Co-CNT coating obtained at a current density of 1.0 Adm^{-2} was found to be electrocatalytically more active towards HER, as (Ni-Co-CNT)$_{1.0\ \text{Adm}^{-2}}$ coating possess lower β_c, and lower overpotential(η_c) values and higher i_o values. It is guided by the fact that material having high value of exchange current density is considered to be electrocatalytic more active(Gonzalez-Buch et al. 2013).

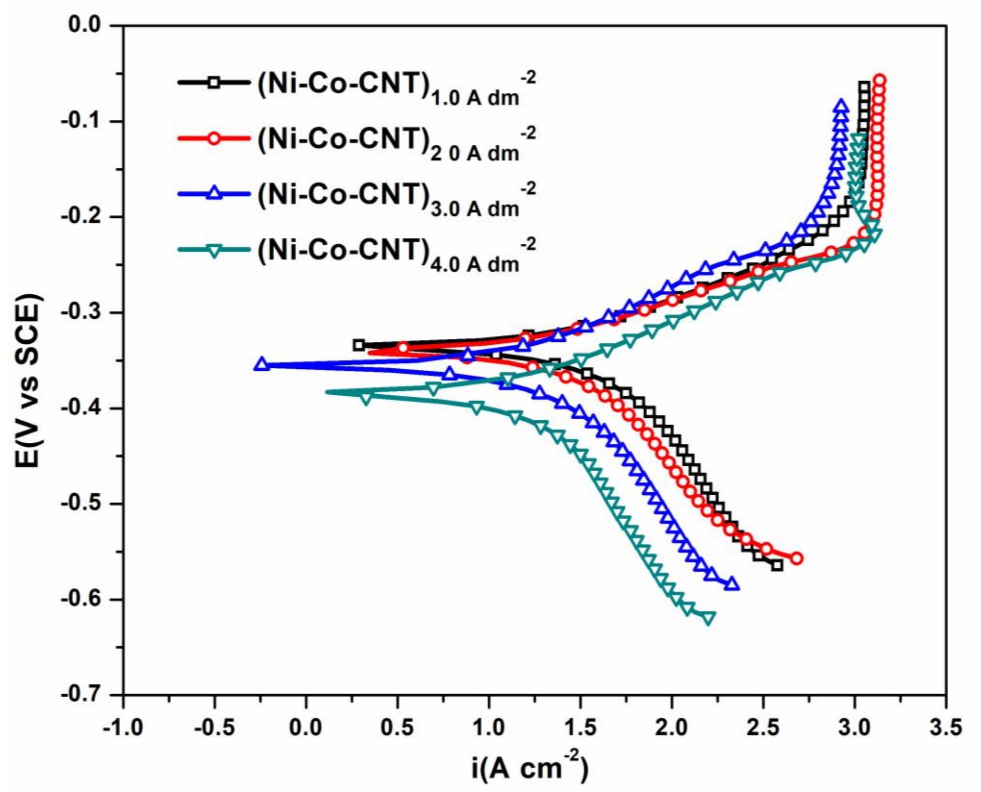

Figure 7.5-Potentiodynamic polarization behaviors of Ni-Co-CNT coatings deposited at different c.d.'s deposited from the same bath

Table 7.3- Kinetic parameters for Ni-Co-CNT alloy coating at different current densities under 1M KOH medium

Coating configuration	β_c (mV dec^{-1})	α (Symmetry factor)	i_o (mA cm^{-2})	$-\eta_c$ (mV Vs SCE)	η_a (mV Vs SCE)
(Ni-Co-CNT)$_{1.0\ \mathrm{A\ dm}^{-2}}$	65	0.91	1.707	430	300
(Ni-Co-CNT)$_{2.0\ \mathrm{A\ dm}^{-2}}$	69	0.86	1.608	450	305
(Ni-Co-CNT)$_{3.0\ \mathrm{A\ dm}^{-2}}$	72	0.78	1.504	485	310
(Ni-Co-CNT)$_{4.0\ \mathrm{A\ dm}^{-2}}$	80	0.68	1.310	500	350

7.4 WATER ELECTROLYSIS

The electrocatalytic activity of Ni-Co-CNT alloy coatings were tested through alkaline water electrolysis. The quantitative measurement of H_2 and O_2 gas evolved are made, by studying the electrolysis of water for HER and OER by following same procedure, discussed in Chapter- 6.

7.4.1 Hydrogen Evolution Reaction

The hydrogen evolution reaction was studied for all deposited composite coatings, at different current densities (1.0 Adm^{-2} - 4.0 Adm^{-2}). The discharge potentials were calculated from CV curves tangent to the X-axis. The experimental study was made using cyclic voltametry and chronopotentiometric techniques, and results are discussed.

7.4.1.1 Cyclic voltametry study

It may be recalled that the current responsible for attainment of equilibrium between attachment and detachment of hydrogen bubbles on the electrode surface is called cathodic peak current density denoted by $i_{pc,}$ and desorption of hydrogen gas at a certain potential is called onset potential.

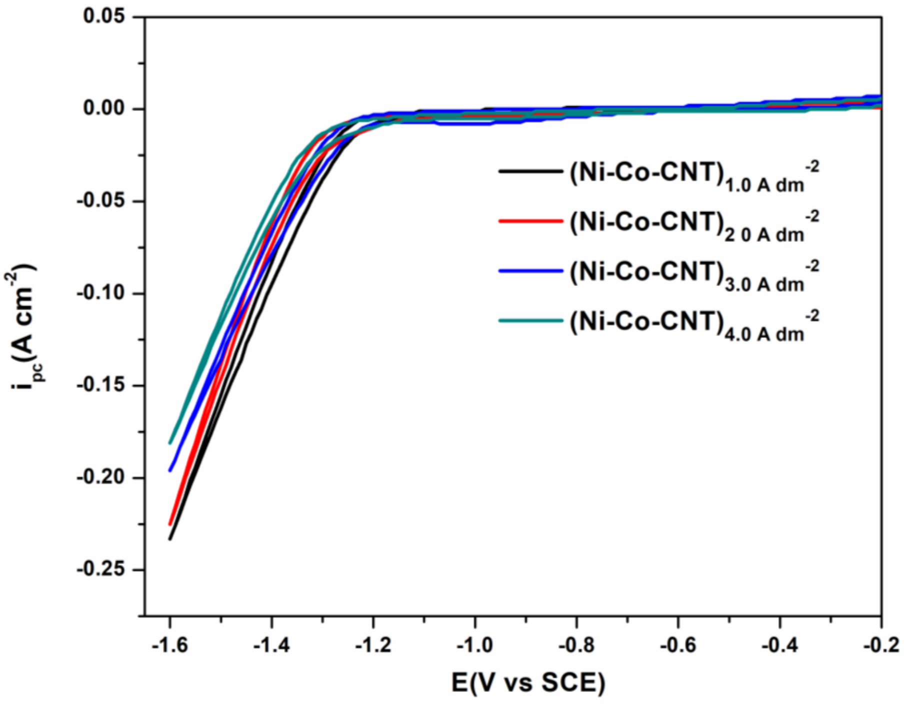

Figure7.6- CV curves of HER on the surface of Ni-Co-CNT coatings obtained at different current densities from the same bath

The electrocatalytic behavior of Ni-Co-CNT coating has been studied for HER in a potential window of 0.0V to -1.6V at 50mV/sec scan rate. The cyclic voltammograms of Ni-Co-CNT alloy coatings of different c.d.'s are shown in the Figure7.6, and corresponding data are reported in Table 7.3.From the CV curves, it may be noted that (Ni-Co-CNT)$_{1.0\ Adm}$$^{-2}$ coating showed the highest value of i_{pc} and lowest onset potential for HER, compared to all other coatings. This highest value i_{pc} of may be attributed to the highest surface roughness, Co and C content of the coatings, supported by SEM and AFM images shown in Figures 7.2 and 7.3, respectively. The highest wt.% of C corresponding to (Ni-Co-CNT)$_{1.0\ A\ dm}$$^{-2}$, reported in Table 7.2, is responsible for increase of active site for hydrogen evolution reactions. As the surface roughness increases the site for hydrogen ion reduction to evolve as hydrogen gas also increases. Thus it may be summarized that highest electro catalytic activity of (Ni-Co-CNT)$_{1.0\ A\ dm}$$^{-2}$ coating is due to the synergistic effect of transition metals, namely Ni and Co(Lee et al. 1996), with C.

7.4.1.2 Chronopotentiometric study

The Ni-Co-CNT coatings of different c.d.'s were subjected to chronopotentiometry study to test their electrocatalytic activity and stability, using them as cathode in alkaline water electrolysis. The chronopotentiograms of Ni-Co-CNT coatings were studied keeping a constant current of -300mAcm^{-2} for duration of 1800sec, and are shown in Figure 7.7. The HER parameters for electrocatalysis of Ni-Co-CNT coatings at different c.d.'s, with the volume of H_2 gas evolved for initial 300 s are given in Table 7.4.It may be noted that there is no significant increase in the volume H_2 liberated with increase of deposition c.d. from 1.0 Adm^{-2} to 4.0 Adm^{-2}, as may be seen in Figure 7.7 and Table 7.4. However, among different coatings $(Ni\text{-}Co\text{-}CNT)_{1.0\ Adm^{-2}}$ was found to be the better electrode material for HER reaction. Further, from the nature of chronopotentiogram, it is clear that reduction of hydrogen ion and evolution of hydrogen gas takes place faster in the very beginning which is indicated by sudden decrease of potential.

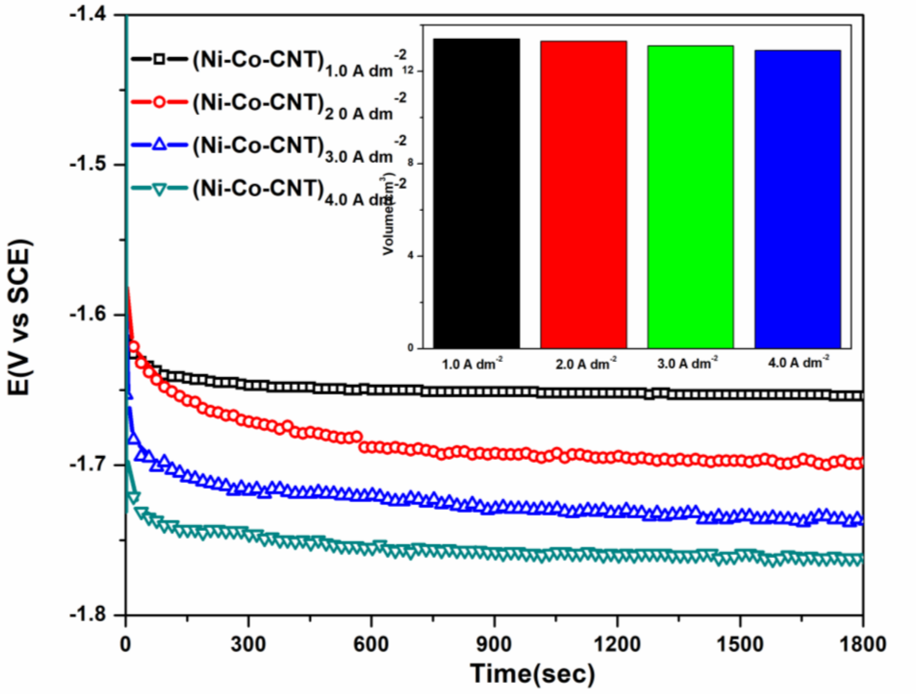

Figure 7.7- Chronopotentiogram for Ni-Co-CNT coatings deposited at different c.d.'s from the optimized bath, at impressed cathode current of -300 mAcm^{-2}

However after few minutes, a constant potential was observed as function of time indicating establishment of equilibrium. At this state, hydrogen evolution takes place continuously on the electrode surface, without any hindrance in the process.

Table 7.4- HER parameters of Ni-Co-CNT coatings of different c.d.'s, with the volume of H_2 evolved

Coating configuration Adm^{-2}	Cathodic peak c.d. (i_{pc} , Acm^{-2})	Onset potential for H_2 evolution (V vs SCE)	Volume of H_2 Evolved in 300s (cm^3)
$(Ni\text{-}Co\text{-}CNT)_{1.0\ A\ dm^{-2}}$	-0.23	-1.19	14.0
$(Ni\text{-}Co\text{-}CNT)_{2.0\ A\ dm^{-2}}$	-0.22	-1.21	13.3
$(Ni\text{-}Co\text{-}CNT)_{3.0\ A\ dm^{-2}}$	-0.19	-1.23	13.1
$(Ni\text{-}Co\text{-}CNT)_{4.0\ A\ dm^{-2}}$	-0.18	-1.25	13.0

7.4.2 Oxygen Evolution Reaction

The electrocatalytic behavior of Ni-Co-CNT coatings obtained at different c.d.'s were studied as anode in water electrolysis for OER. The cyclic voltammetry and chronopotentiometry studies were carried out in the similar line as that for HER, and results were discussed as below.

7.4.2.1 Cyclic voltametry

The cyclic voltammetric study has been made to study the electrocatalytic study of Ni-Co-CNT coatings of different c.d.'s as anode material of water electrolysis. The potential widow between 0 - 0.75 V was used, at scan rate of $50mVsec^{-1}$ for 30 cycles to get stable CV plots. The relative response of cyclic voltammograms of Ni-Co-CNT coatings of different c.d.'s are shown in the Figure7.8.The intermediates peaks observed in CV curves of all coatings is attributed to evolution of oxygen due to redox transition of interfacial oxycation between lower and higher oxidation states(Kim et al. 2012).

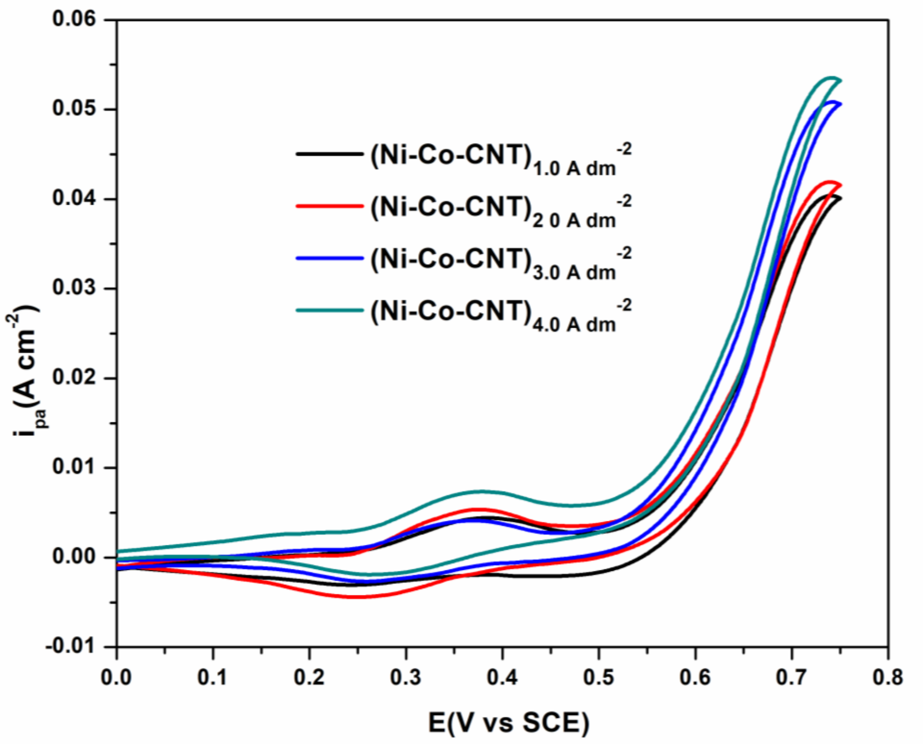

Figure 7.8- Cyclic voltammetry curves for OER on to the surface of Ni-Co-CNT coatings deposited at different current densities, while using them as anode in alkaline water electrolysis

From the graph shown in Figure 7.8, it is clear that the coating obtained at current density 4.0 Adm^{-2} showed better OER activity compared to other current density coatings. The mechanism proposed involves initial adsorption of OH^{-} ion from electrolyte solution onto the electrode surface followed by electron transfer process within the system leads to the liberation of oxygen (Lyons and Brandon 2010). The peak current shifts towards lower positive potential with increase of deposition c.d. The intermediate anodic and cathodic peaks obtained in the voltagram of Ni-Co-CNT alloys, in Figure7.8 indicates that formation and reduction of NiOOH layer. In this potential range the formed semiconducting layer NiO(H_2O) is responsible for better OER activity, due to enhanced adsorption of OH^{-} ions(Peeters et al. 2001).The Ni-Co-CNT obtained at 4.0 Adm^{-2} current density found to show the highest electrocatalytic activity towards OER. It is attributed to higher wt. % nickel in the deposit which leads to better OH^{-} adsorption for oxygen evolution. The presence of CNT in the matrix enhances the adsorption of hydroxide ion, by increasing the active site for OER.

7.4.2.2 Chronopotentiometry

The electrocatalytic stability of Ni-Co-CNT coatings of different current densities were studied by chronopotentiometry, in the same line as that for HER, except using it as anode. A positive current +300mAcm^{-2} have been applied to study the potential response of the deposits, and corresponding chronopotentiograms are shown in Figure 7.9. It may be seen that initially there exists a sudden increase of potential until the establishment of equilibrium between adsorbed OH$^-$ and liberated O$_2$.The amount of oxygen liberated on to the surface of Ni-Co-CNT coatings of different c.d., for a duration of 300 sec was found, and is given in Table 7.5. It may be seen that (Ni-Co-CNT)$_{4.0\ A\ dm}$$^{-2}$ coating showed the highest volume of oxygen evolved on its surface. This may be attributed to high wt. % Ni in the deposit, supported by data in Table 7.2. Increase of Ni content in the alloy coatings increased the OH$^-$ adsorption, which in turn increased the f O$_2$ evolution on its surface.

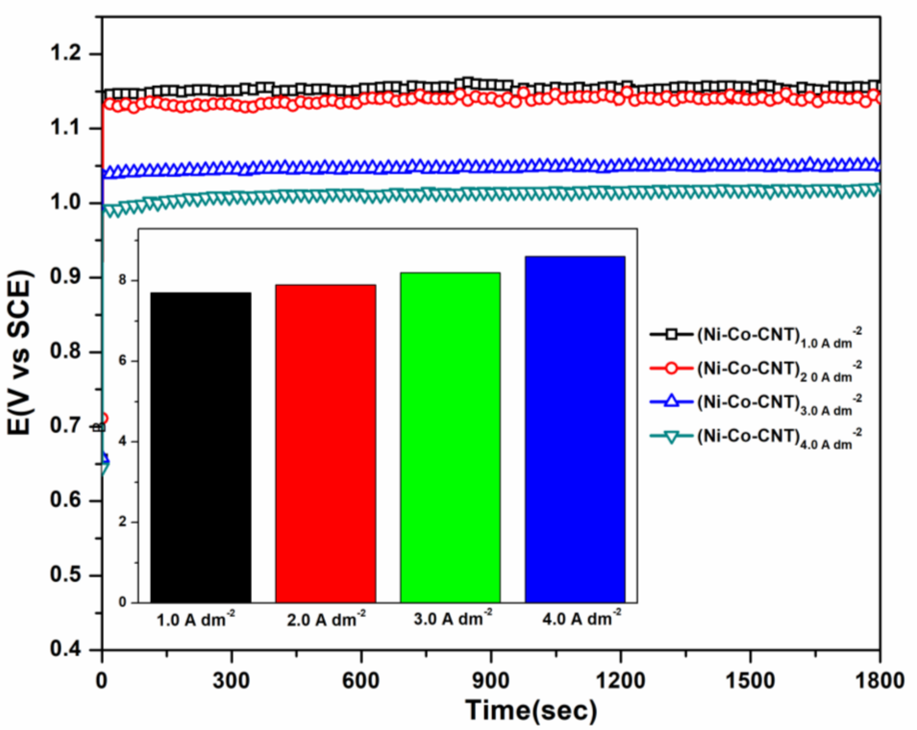

Figure 7.9- Chronopotentiogram for Ni-Co-CNT coatings deposited at different c.d.'s from the optimized bath, at impressed cathodic current of +300 mAcm^{-2}

Table 7.5- Oxygen evolution parameters for Ni-Co-CNT alloy coating obtained at different current densities

Coating configuration Adm^{-2}	Anodic peak c.d(A cm^{-2})	Onset potential for O_2 evolution (V vs SCE)	Volume of O_2 Evolved in 300s (cm^3)
$(Ni\text{-}Co\text{-}CNT)_{1.0\ A\ dm^{-2}}$	0.039	0.54	8.0
$(Ni\text{-}Co\text{-}CNT)_{2.0\ A\ dm^{-2}}$	0.042	0.53	8.3
$(Ni\text{-}Co\text{-}CNT)_{3.0\ A\ dm^{-2}}$	0.050	0.52	8.7
$(Ni\text{-}Co\text{-}CNT)_{4.0\ A\ dm^{-2}}$	0.053	0.48	9.5

7.5 MECHANISM OF HER AND OER REACTIONS

Both $(Ni\text{-}Co\text{-}CNT)_{1.0\ Adm^{-2}}$ and $(Ni\text{-}Co\text{-}CNT)_{4.0\ Adm^{-2}}$ coatings are best electrode material for HER and OER respectively, which was supported by SEM, EDX,AFM and XRD analysis. This may be explained as follows: The adsorption, desorption and recombination reaction leading to evolution of hydrogen on the Ni-Co-CNT surface. The coating at 1.0 Adm^{-2} is considered as best cathode for HER as wt.% Co and C in the deposit was found to be highest. As a result, the number of active site for hydrogen evolution increased. The Tafel slope β_c values corresponding to Ni-Co-CNT coating were determined and are reported in the Table 7.3.Tafel slopes were in the range of 60 $mVdec^{-1}$ confirming that the HER on Ni-Co-CNT coating follows Volmer- Heyrovsky mechanism (Elias and Hegde 2015), and are given as below.

1) Hydrogen adsorption(Volmer reaction)

$$H_2O + M + e^- \leftrightarrow M - H + OH^-$$

2) Hydrogen desorption(Heyrovsky reaction)

$$MH_{ads} + H_2O + e^- \leftrightarrow M + H_2 + OH^-$$

Similarly, $(Ni\text{-}Co\text{-}CNT)_{4.0\ Adm^{-2}}$ is the best electrode material for OER reaction. As the nickel content in the coating increased, the ability for formation of semiconducting layer also increases. Hence, the adsorption of OH^-on the surface helps for the liberation of oxygen.

7.6 COMPARISON OF ELECTROCATALYTIC ACTIVITY

Electrocatalytic performance of Ni-Co and Ni-Co-CNT alloy coatings were compared in terms of their ability for HER and OER. The relative response of CV curves of (Ni-Co)$_{1.0\ \mathrm{Adm}^{-2}}$ and (Ni-Co-CNT)$_{1.0\ \mathrm{Adm}^{-2}}$ coatings, when used as cathode is shown in Figure 7.10. It may be seen that on addition of CNT into alloy matrix, cathodic peak current (i_{pc}) has increased drastically indicating the fact that cathodic reaction (liberation of H_2) takes place with greater agility on the surface of (Ni-Co-CNT)$_{1.0\ \mathrm{Adm}^{-2}}$ than on the surface of (Ni-Co)$_{1.0\ \mathrm{Adm}^{-2}}$alloy. The relative response of CV curves of (Ni-Co)$_{4.0\ \mathrm{Adm}^{-2}}$and (Ni-Co-CNT)$_{4.0\ \mathrm{Adm}^{-2}}$ coatings, when used as anode is shown in Figure 7.11. It may be seen that on addition of CNT into the alloy matrix, anodic peak current (i_{pa}) has increased drastically indicating the fact that anodic reaction (liberation of O_2) takes place with greater agility on the surface (Ni-Co-CNT)$_{4.0\ \mathrm{Adm}^{-2}}$ than on the surface of (Ni-Co)$_{4.0\ \mathrm{Adm}^{-2}}$ alloy.

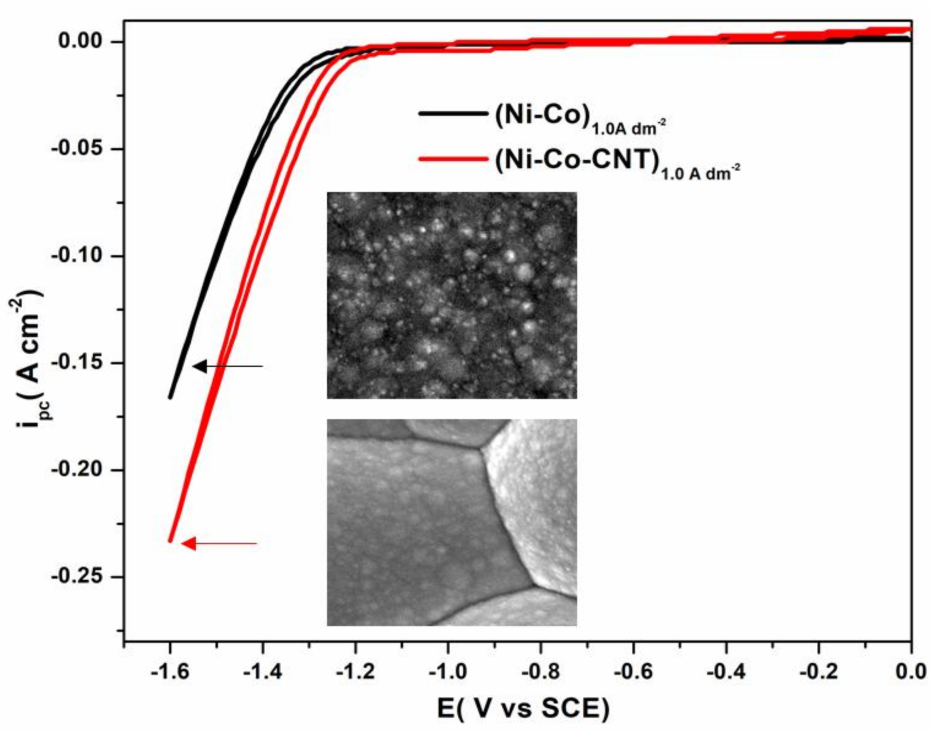

Figure 7.10 –Relative response CV curves for (Ni-Co)$_{1.0\ \mathrm{Adm}^{-2}}$ and (Ni-Co-CNT)$_{1.0\ \mathrm{Adm}^{-2}}$ coatings for HER, deposited for same duration. Inset are given their surface morphology (SEM)

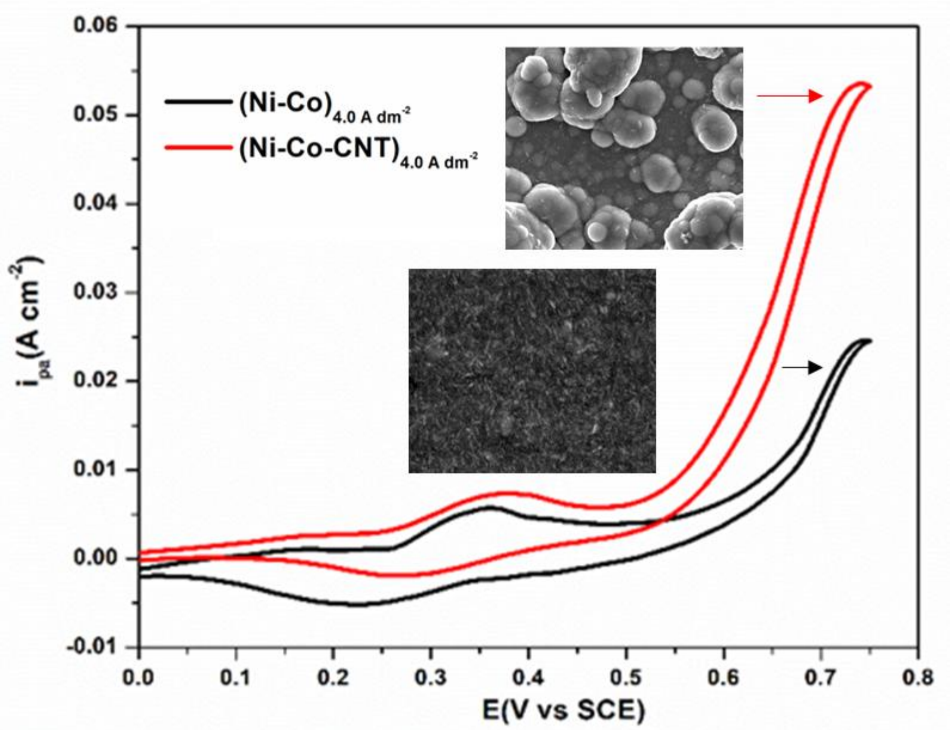

Figure 7.11- Relative response CV curves for $(\text{Ni-Co})_{4.0\ \text{Adm}^{-2}}$ *and* $(\text{Ni-Co-CNT})_{4.0\ \text{Adm}^{-2}}$ *coatings for OER, deposited for same duration. Inset are given their surface morphology (SEM)*

Thus, it may be summarized that among the Ni-Co and Ni-Co-CNT coatings deposited, $(\text{Ni-Co})_{1.0\ \text{Adm}^{-2}}$ and $(\text{Ni-Co-CNT})_{1.0\ \text{Adm}^{-2}}$, $(\text{Ni-Co})_{4.0\ \text{Adm}^{-2}}$ and $(\text{Ni-Co-CNT})_{4.0\ \text{Adm}^{-2}}$ configurations (all under optimal conditions) are the best electrode materials as cathode and anode, respectively. Further, the relative response of CV curves succinctly demonstrated that addition of CNT into the alloy matrix of Ni-Co alloy increased the electrocatalytic performance of water electrolysis of both HER and OER, depending on its composition and surface structure.

7.6 CONCLUSIONS

The Ni-Co-CNT composite coatings have been developed by addition of CNT into the sulfate bath of Ni-Co alloy. The electrocatalytic activity and stability of composite coatings have been tested by cyclic voltammetry and chronopotentiometric techniques, respectively. From the experimental results following conclusions are arrived.

1) Among different coatings deposited at different c.d.'s, (Ni-Co-CNT)$_{1.0\ \mathrm{Adm}^{-2}}$ is found to be best electrode material for HER of water splitting reactions, and (Ni-Co-CNT)$_{4.0\ \mathrm{Adm}^{-2}}$ for OER, respectively.
2) (Ni-Co-CNT)$_{1.0\ \mathrm{Adm}^{-2}}$ and (Ni-Co-CNT)$_{4.0\ \mathrm{Adm}^{-2}}$ showed the highest peak cathode current density of (i_{pc}) of –0.23Acm^{-2} and (i_{pa}) of 0.053Acm^{-2} for HER and OER, respectively, compared to coatings at other c.d.'s.
3) Better electrocatalytic activity of (Ni-Co-CNT)$_{1.0\ \mathrm{Adm}^{-2}}$ for HER is attributed to the high wt.% Co and C in the deposit, apart from increased surface roughness.
4) High electro catalytic activity of (Ni-Co-CNT)$_{4.0\ \mathrm{Adm}^{-2}}$ for OER is attributed to increase of surface roughness, due to addition of CNT and increase of Ni content in the deposit, supported by EDX, SEM, XRD and AFM analyses.
5) The relative response of CV curves succinctly demonstrated that addition of CNT into the alloy matrix of Ni-Co alloy can increase the electro catalytic performance of water electrolysis for both HER and OER by increasing the surface roughness of the deposit.

CHAPTER 8 ELECTRODEPOSITION AND CHARACTERIZATION OF Ni-Mo ALLOY COATINGS

The present chapter describes the development of Ni-Mo alloy coatings from a new citrate bath, and to explore its applications in water splitting. The effect of deposition current density (c.d.) on Ni (inducing metal) and Mo (reluctant metal) contents of the alloy coatings have been studied. The change of alloy composition on the electrocatalytic activity of water splitting of both hydrogen evolution reaction (HER) and oxygen evolution reaction have been studied using cyclic voltammetry (CV) and chronopotentiometry (CP) techniques. The practical utility of Ni-Mo alloy coatings have been tested by measuring quantitatively the amount of H_2 *and* O_2 *gas evolved, when used them as cathode and anode. The dependency of electrocatalytic activity with composition, structure, and morphology of the alloy coatings have been explained, using XRD, SEM, and EDS analyses.*

8.1 INTRODUCTION

Nowadays renewable energy sources are considered as the only remedy for global warming crisis(Bianchini and Barbaro 2009).Many researchers are working for large scale production of renewable energy sources, which are available abundantly at lesser cost, compared to fossil fuels, and this idea indirectly connects to the development of effect electrocatalytically active materials. Water electrolysis is one of the best techniques for the production of secondary energy source, where electric current is used to separate water into its basic elements as hydrogen and oxygen(Liu et al. 2009). Although water electrolysis is not the cheapest method for hydrogen production, it is preferred due to its high degree of purity. Many researchers are at work to improve the catalytic activities of the electrodes by reducing the overpotential of HER and OER. In this direction, several transition metal-based alloys have been widely used, mostly mutual alloys of transition metals, like Ni, Co, Mo, Zr and Fe. The combination of any two transition metals could indeed enhance the electrocatalytic activity compared to their individual activities, and are explained by well-known synergetic effect(Trasatti 1972). Further, the literature review reveals that electrocatalytic activity of electrode materials can be increased substantially by introducing a foreign dopant (having high surface areas or better electroactive sites) into the alloy matrix. Hence, Ni and its alloys are traditionally being used as the material of choice for electrodes to catalyse water electrolysis for both HER(Huot and Brossard 1988)and OER(Kreysa and Haakansson 1986).Among Ni-based alloys, Ni-Mo alloy is well known for its use as cathode material for HER and OER(Schulz et al. 1994).

8.2 EXPERIMENTAL

In the present study, the electrodeposition of Ni-Mo alloy coatings was carried out on copper substrate. The composition and operating parameters of the bath was arrived by Hull cell method as described in Chapter 3. The composition and operating variables of the optimized bath is given in Table 8.1.

Table 8.1-Composition and operating variables of basic bath used for development of bright Ni-Mo alloy coatings

Bath composition	Amount (gL^{-1})	Operating parameters
$NiSO_4.6H_2O$	18	Temperature : 303K (30 ºC)
Na_2MoO_4	48	Anode : Nickel, Cathode: Copper
$Na_3C_6H_5O_7$	105	c.d. range: 1.0 – 6.0 A dm^{-2}, pH = 9

The electrodepositions were carried out at over a wide range of c.d., from 2.0 to 6.0 Adm^{-2}. Electrodeposition of Ni-Mo alloy coatings were accomplished at three different c.d.’s, namely 2.0, 4.0 and 6.0 A dm^{-2}, and are conveniently represented as $(Ni\text{-}Mo)_{2.0\ Adm^{-2}}$, $(Ni\text{-}Mo)_{4.0\ Adm^{-2}}$ and $(Ni\text{-}Mo)_{6.0\ Adm^{-2}}$, respectively. The experimental procedure followed for deposition of Ni-Mo alloy coatings are same as presented in Section 6.2.The composition of coating, in terms of Ni and Mo content were determined by EDS method. The phase structure, surface morphology were characterized using advanced analytical techniques, like XRD and SEM respectively.

8.3 RESULTS AND DISCUSSIONS

8.3.1 Surface morphology and compositional analyses

The surface microstructure of Ni-Mo alloy coatings deposited at different c.d.’s are shown in Figure 8.1. It may be seen that $(Ni\text{-}Mo)_{2.0\ Adm^{-2}}$ displays the most rough surface with number of nodular structures on the surface as shown in Figure 8.1(a).

The roughness of the surface tended to be decreased with growth of c.d., and at extremely high c.d. *i.e.* at 6.0 Adm^{-2} the surface was found to be relatively smooth with small nodules on its surface, as shown in Figure 8.1(c). It is important to note that as c.d. increased, the size of nodules continuously decreased leaving the surface more smooth and uniform. Thus from SEM micrographs, it may be concluded that the surface roughness of coatings bears a close relationship with applied c.d. Further, the compositional analysis of Ni-Mo alloys, deposited at various applied c.d.'s is given in Table 8.2.

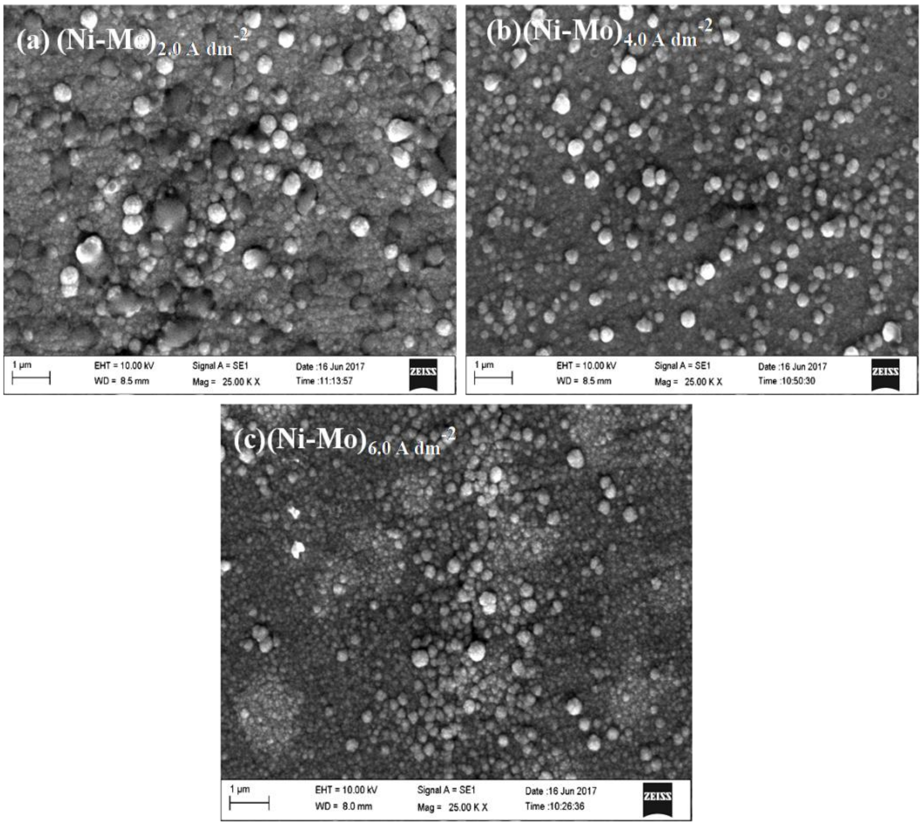

Figure 8.1-The surface morphology of Ni-Mo alloy coatings deposited from the optimized bath different c.d.'s: a) 2.0 A dm^{-2}, b) 4.0 A dm^{-2} and c) 6.0 A dm^{-2}

Porous coating having nodular structures, with high wt. % Mo was found at lower limits of c.d.'s. It is the basic characteristic of Ni-Mo alloy coatings, required for good electrocatalytic applications (Lehman et al.2012).Further, it was found that wt. % Mo started decreasing with increase of c.d., by increasing the Ni content of the deposit as shown in Table 8.2.Hence, current density influences the molybdenum content of the deposited coatings.

Table 8.2- Compositional data of Ni-Mo alloy coatings deposited at different current densities from the same bath

Coating configuration	Ni content in deposit (%)	Mo content in deposit (%)
(Ni-Mo)$_{2.0A\ dm^{-2}}$	62.53	26.01
(Ni-Mo)$_{4.0A\ dm^{-2}}$	65.18	25.52
(Ni-Mo)$_{6.0A\ dm^{-2}}$	68.25	24.54

From the data in Table 8.2, it may be observed that wt. % of Mo decreases with increase in c.d. and found to be maximum for the coating developed at 2.0 A dm^{-2} (26.0 %). From Table 8.2, it is clear that by increasing the c.d. from 2.0 to 6.0 A dm^{-2}, the molybdenum content in the deposits was reduced to 24.54%. This peculiar behaviour of Ni-Mo alloy coating, *i.e.* small variation of Mo content with substantial increase of c.d. is attributed by two factors. Firstly, due to the complexation of metal ions in the bath, where complexed metal ions affect the static potentials of the parent metals considerably. Hence, it shows less dependency with deposition c.d.(Bratoeva and Atanasov 2000). Secondly, it is due to the induced type of codeposition taking place in the bath, where reluctant metal show less response to the applied c.d.(Elias and Hegde 2015).Consequent to this, Ni content of the alloy coatings were found to be increased with c.d.as shown in Table 8.2.

8.3.2 XRD Study

XRD technique was used to see the effect of c.d. on the phase structures of Ni-Mo alloy coatings. The X-ray diffractions patterns of (Ni-Mo)$_{2.0\ Adm^{-2}}$,(Ni-Mo)$_{4.0\ Adm^{-2}}$ and (Ni-Mo)$_{6.0\ Adm^{-2}}$ alloy coatings are shown in Figure 8.2. It may be seen that there is no change in the position of XRD peaks when c.d. is changed from 2.0 to 6.0 Adm^{-2}. This constancy of scattering angle (2θ) for coatings of all c.d.'s indicates that electrodeposited coatings form the solid solution of Mo in Ni lattice(Cullity 1956). It may be seen that XRD peaks at $2\theta = 43.3°$, 50.4°, 74.03° 89.8° and 95.0° represent tetragonal $MoNi_4$ phase, corresponding to (211), (130), (420),(501) and (422) planes, respectively which is in agreement with standard patterns of $MoNi_4$ (JCPDS No. 03-065-1533). However, an increase/decrease of intensity of peaks were observed, depending on the increase/decrease of the metal contents of the alloy with change of c.d., supported by composition data in Table 8.2.The effect of change of composition of the alloy with c.d. is reflected, with increase of intensity of peaks without shifting of diffraction lines.

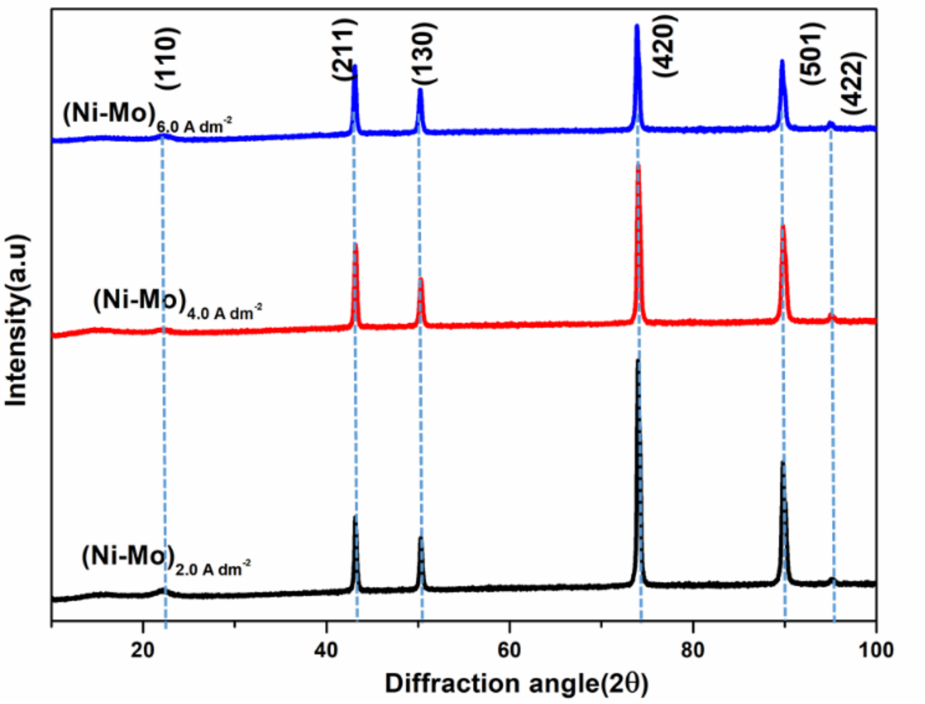

Figure 8.2- X-Ray diffraction patterns of Ni-Mo alloy coatings deposited at different c.d.'s showing the same scattering angle

It is just due to change in the lattice parameter of deposit, as shown by the perforated vertical lines, in Figure 8.2.Thus gradual increase, or decrease of intensity of peaks, corresponding to different planes of Ni-Mo alloys with deposition c.d. clearly indicates that deposition c.d. plays a crucial role on its composition, surface morphology and structural property.

8.3.3 Corrosion Stability

To assess the stability of Ni-Mo alloy coatings as an effective material for water splitting applications, they have been subjected to corrosion test in 1.0 M KOH (same medium in which water electrolysis is studied) by potentiodynamic polarization method. The polarization behavior of the coatings corresponding to different c.d.'s are shown in Figure 8.3. Tafel curves can be used to explore many valuable information pertaining to the electro catalytic applications. Accordingly, kinetic parameters of electrode reactions, like Tafel's constants, symmetry factor(α) and exchange current density(i_o) values were evaluated and are reported in Table 8.3.

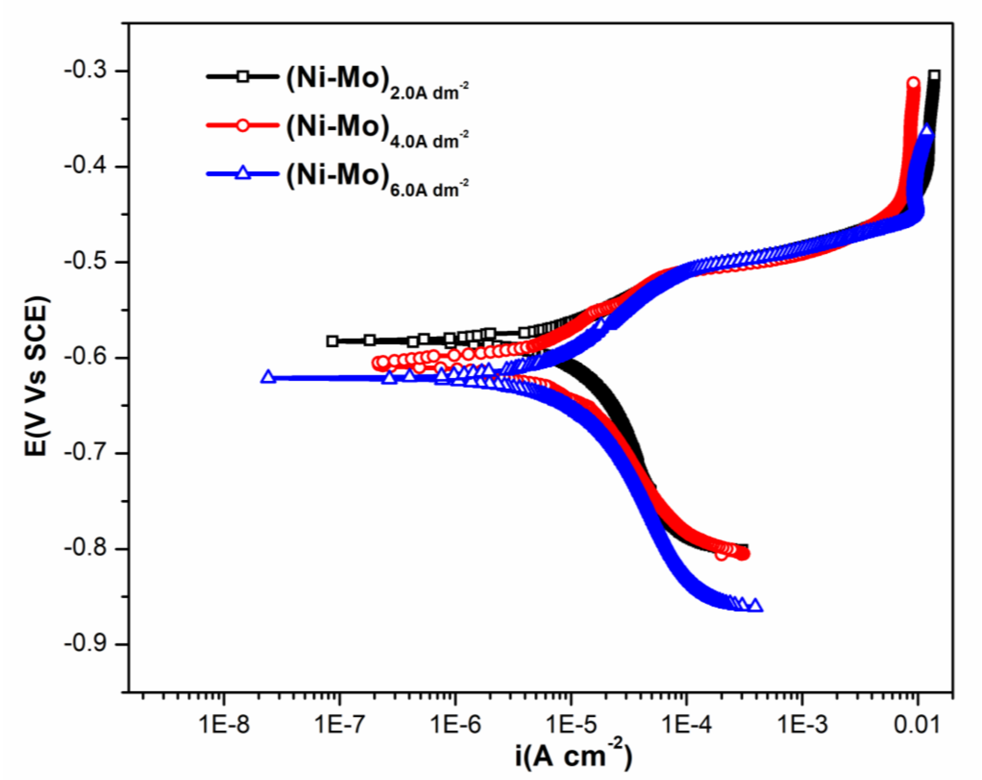

Figure 8.3-Potentiodynamic polarization behaviour of Ni-Mo alloy coatings deposited at different current densities from the same optimized bath

To investigate the electrocatalytic activity of as-deposited alloys, linear Tafel fit was performed at the cathodic and anodic region of the polarization curve. The kinetic parameters such as anodic and cathodic Tafel slopes (β), exchange current density (i_o), cathodic overpotential (η_c) and anodic overpotential (η_a) were determined from the linear part of semi-logarithmic polarization plots, and their values are given in Table 8.4. At the same time, the electron transfers coefficient (α) and i_o values need to be as large as possible(Manazoglu et al. 2016).Hence, it may be seen in Tables 8.2 and 8.4, that as wt.% Mo in the alloy is increased, values of exchange current density increased, while β_c value decreased.

Table 8.3 -Corrosion data, like E_{corr}, i_{corr} and corrosion rates of Ni-Mo alloy deposited at different c.d.'s from the optimized bath

Coating configuration	$-E_{corr}$ (mV vs SCE)	i_{corr} (µA cm^{-2})	CR×10^{-2} (mm y^{-1})
$(Ni\text{-}Mo)_{2.0\ dm^{-2}}$	580	14.4	22.0
$(Ni\text{-}Mo)_{4.0\ dm^{-2}}$	610	13.2	20.2
$(Ni\text{-}Mo)_{6.0\ dm^{-2}}$	620	11.6	17.7

The Ni-Mo alloy coatings deposited at 2.0 A dm^{-2} showed lowest value of β_c and η_c, highest value for α, i_o proving that $(Ni\text{-}Mo)_{2.0\ dm^{-2}}$ is electrocatalytically more active for HER than other coatings.

Table 8.4– Electrocatalytic kinetic parameters of Ni-Mo alloy coatings of different c.d.'s in 1M KOH medium

Coating configuration	β_c (mV dec^{-1})	α (sym. factor)	i_o (mA cm^{-2})	$-\eta_c$ (mV Vs SCE)	η_a (mV Vs SCE)
$(Ni\text{-}Mo)_{2.0\ dm^{-2}}$	191	0.31	4.653	702	548
$(Ni\text{-}Mo)_{4.0\ dm^{-2}}$	194	0.30	4.493	734	549
$(Ni\text{-}Mo)_{6.0\ dm^{-2}}$	200	0.29	3.718	746	550

8.4 ELECTROCATALYTIC STUDY

The electrodeposited Ni-Mo alloy coatings were put to test for electrocatalytic study of water electrolysis in 1M KOH medium for HER and OER, using them as cathode and anode, respectively. The experimental results are presented as below.

8.4.1 Hydrogen Evolution Reaction

8.4.1.1 Cyclic voltametry

CV is a powerful tool to explore many valuable information on the thermodynamics of redox processes and kinetics of heterogeneous electron-transfer reactions, coupled with many chemical reactions or adsorption processes. Accordingly, CV study of (Ni-

Mo)$_{2.0\ Adm^{-2}}$, (Ni-Mo)$_{4.0\ Adm^{-2}}$ and (Ni-Mo)$_{6.0\ Adm^{-2}}$ for HER is made in the potential window of 0 to -1.6V, at 50 mVs^{-1} scan rate, and is shown in Figure 8.4.It may be noted that there is no much difference in the CV response of different coatings. It may be attributed to the small compositional change of the alloy coatings with change of c.d. However, (Ni-Mo)$_{2.0\ Adm^{-2}}$ coating showed the highest value of i_{pc} and least onset potential, compare to other alloy coatings. The highest value of i_{pc}(a measure of the reduction of H^+ ions) may be attributed to the highest Mo content in the alloy, compared to remaining two alloy coatings (Table 8.5). Further, other kinetic parameters also support the fact that (Ni-Mo)$_{2.0\ Adm^{-2}}$ is good electrode material, as cathode.

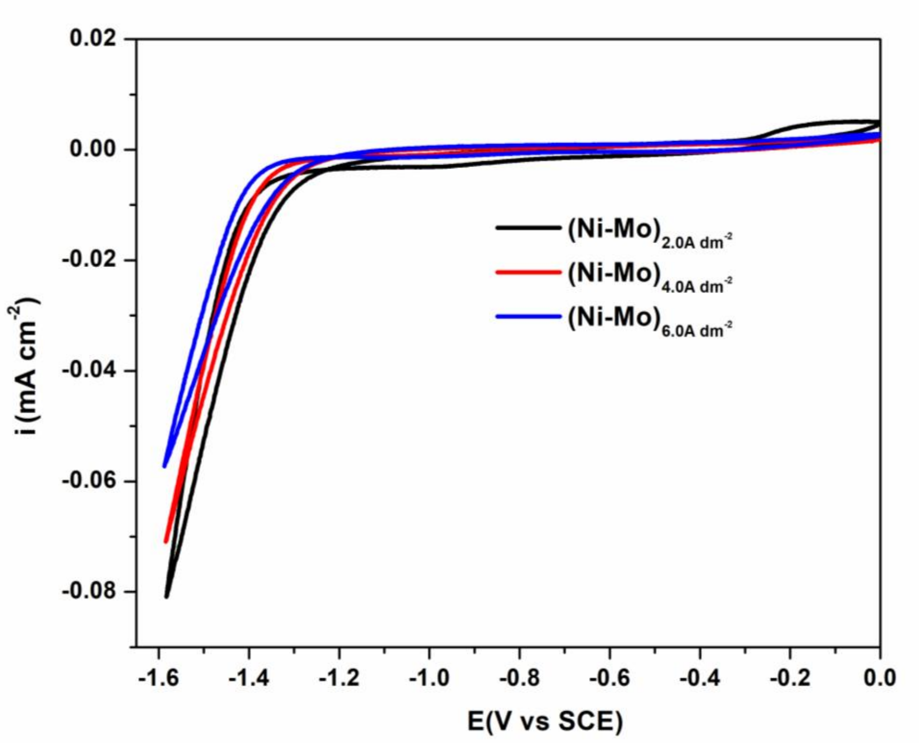

Figure 8.4- CV curves for HER on the surface of Ni-Mo coating obtained at different current densities

Further, a less onset potential for HER (towards positive direction) observed for (Ni-Mo)$_{2.0\ Adm^{-2}}$ coating confirms that the coating is more favorable for hydrogen generation with lower over potential(Table 8.4), in compliance with observation reported by Manazoglu, and co-workers. Thus, based on the surface structure and composition of (Ni-Mo)$_{2.0\ Adm^{-2}}$ coatings, evidenced by SEM and EDS study it may be concluded that its highest HER activity is attributed to the high Mo content, compared to other coatings.

Table 8.5-The electrocatalytic kinetic parameters for HER of $(Ni\text{-}Mo)_{2.0\ Adm^{-2}}$,$(Ni\text{-}Mo)_{4.0Adm^{-2}}$ and $(Ni\text{-}Mo)_{6.0\ Adm^{-2}}$ coatings deposited from the same bath

Coating configuration	Cathodic peak current density(i_{pc}) (A cm^{-2})	Onset potential for HER (V vs SCE)	Volume of H_2 evolved 300 s (cm^3)
$(Ni\text{-}Mo)_{2.0\ A\ dm^{-2}}$	-0.08	-1.22	12.9
$(Ni\text{-}Mo)_{4.0\ A\ dm^{-2}}$	-0.07	-1.24	12.5
$(Ni\text{-}Mo)_{6.0\ A\ dm^{-2}}$	-0.05	-1.26	12.1

8.4.1.2 Chronopotentiometry

The CP study of $(Ni\text{-}Mo)_{2.0\ Adm^{-2}}$,$(Ni\text{-}Mo)_{4.0\ Adm^{-2}}$ and $(Ni\text{-}Mo)_{6.0\ Adm^{-2}}$ coatings was made to analyze their efficiency towards HER by applying a constant current of -300 $mAcm^{-2}$ for the duration 1800s.The electro-catalytic activity of all three alloy compositions were assessed by measuring the volume of H_2 liberated for initial 300s (Table 8.5), and chronopotentiograms of each alloy coatings are recorded, and is shown in Figure 8.5.Experimental results showed that $(Ni\text{-}Mo)_{2.0\ Adm^{-2}}$ alloy produced a maximum amount of H_2, compared to the coatings deposited at other c.d's. This supports the fact that $(Ni\text{-}Mo)_{2.0\ Adm^{-2}}$ coating is electro-catalytically more active for HER. It is further supported by the fact that though an initial change of potential was observed in all three samples of alloy coatings immediately after the initiation of electrolysis followed by a steady-state potential response, it is less in case of $(Ni\text{-}Mo)_{2.0\ Adm^{-2}}$ coatings. This may be due to sudden depletion of electrolyzed components on the surface of the electrode, where H^+ ions from the solution undergo reduction to release H_2 gas, and eventually a state of equilibrium is established between H^+ ions and H_2 during the process. However, as the electrolysis proceeds further almost a constant potential is achieved (with time), as observed in Figure 8.5. At this stage, the evolution of hydrogen gas takes place uninterruptedly on the surface of an electrode, where the current is spent completely for conversion of H^+ ions into H_2 gas. In other words, there exist equilibrium between H^+ ions and

H_2 gas. Thus based on the experimental results of CV and CP study, it may be concluded that (Ni-Mo)$_{2.0\ Adm^{-2}}$ coatings is the most suitable for HER.

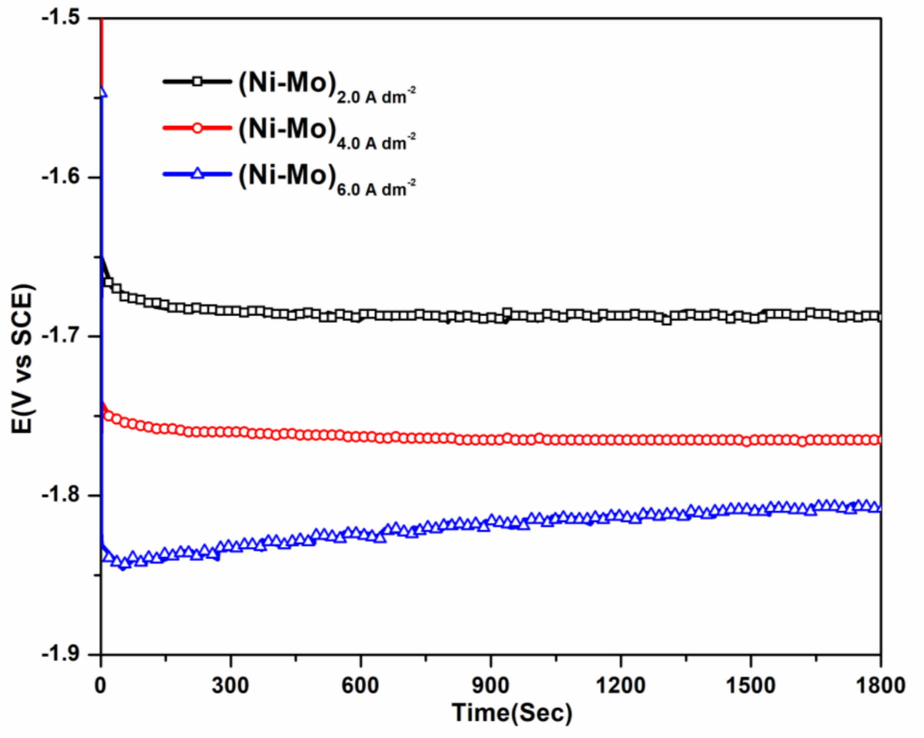

Figure 8.5- Chronopotentiograms recorded for HER on to the surface of (Ni-Mo)$_{2.0\ Adm^{-2}}$,(Ni-Mo)$_{4.0\ Adm^{-2}}$ and (Ni-Mo)$_{6.0\ Adm^{-2}}$ alloy coatings deposited from the same bath

8.4.2 Oxygen Evolution Reaction

8.4.2.1 Cyclic voltametry

The electrocatalytic behavior of (Ni-Mo)$_{2.0\ Adm^{-2}}$,(Ni-Mo)$_{4.0\ Adm^{-2}}$and (Ni-Mo)$_{6.0Adm^{-2}}$ alloy coatings for OER were analysed by CV method in a potential window 0.0 V to 0.75 V, at a scan rate of 50 mV s^{-1}, using them as anode. The CV responses showing the anodic peak current density (i_{pa}) and onset potential for O_2 evolution reaction on Ni-Mo alloy coatings of different c.d.'s are shown in Figure 8.6.It may be noted that there is no significant change in the peak anodic current(i_{pa}) as the deposition c.d. of alloy coating is changed from 2.0 Adm^{-2} to 6.0 Adm^{-2}.

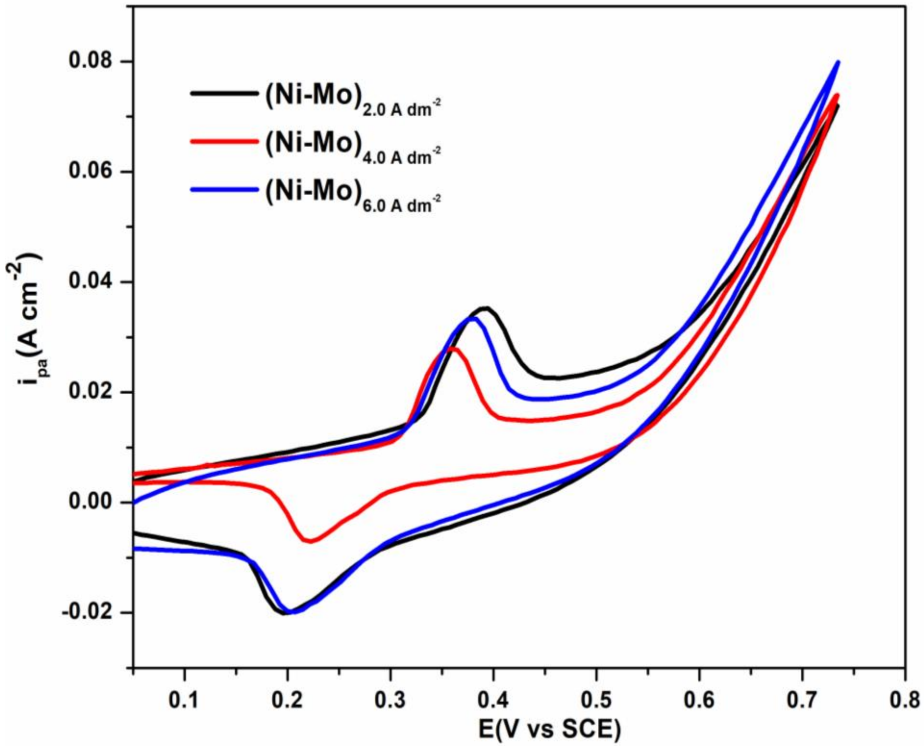

Figure 8.6- Cyclic voltammogram for OER on to the surface of (Ni-Mo)$_{2.0\ Adm^{-2}}$,(Ni-Mo)$_{4.0\ Adm^{-2}}$ and (Ni-Mo)$_{6.0\ Adm^{-2}}$ alloy coatings deposited from the same bath

Table 8.6 - Electrocatalytic kinetic parameters for OER on the surface of (Ni-Mo)$_{2.0\ Adm^{-2}}$,(Ni-Mo)$_{4.0\ Adm^{-2}}$ and (Ni-Mo)$_{6.0\ Adm^{-2}}$ alloy coatings deposited from the same bath

Coating configuration	Anodic peak current density(i_{pa}) (A cm^{-2})	Onset potential for OER (V vs SCE)	Volume of O_2 evolved 300 s (cm^3)
(Ni-Mo)$_{2.0\ A\ dm^{-2}}$	0.070	0.55	9.0
(Ni-Mo)$_{4.0\ A\ dm^{-2}}$	0.074	0.53	9.6
(Ni-Mo)$_{6.0\ A\ dm^{-2}}$	0.080	0.52	10.0

This small dependency of i_{pa} values with deposition c.d. is attributed to the small compositional change of the alloy coatings, due to inherent induced type of codeposition of the bath. However, (Ni-Mo)$_{6.0\ Adm^{-2}}$ coating showed the highest value of $i_{pa,}$ compare to other coatings.

It may be noted that Ni-Mo alloy corresponding to 6.0 A dm^{-2}, i.e. (Ni-Mo)$_{6.0\ Adm}$$^{-2}$ is the most electro catalytically active coating towards OER with highest i_{pa} and least onset potential for O_2 evolution. Hence from CV and CP study, it may be summarised that (Ni-Mo)$_{6.0\ Adm}$$^{-2}$ coatings is the most suitable for OER and corresponding electro catalytic kinetic data are reported in Table 8.6.

8.4.2.2 Chronopotentiometry

CP study was used to estimate the OER activity of Ni-Mo alloy coatings, deposited under different conditions of c.d. in the same medium, following the same procedure used for studying the HER. The chronopotentiograms for OER were recorded at a constant applied current of +300 mA cm^{-2} (anodic) and the corresponding potential obtained were plotted against the time as shown in Figure 8.7. The quantity of O_2 liberated during the study was also measured, and are reported in Table 8.6.The experimental observations revealed that maximum amount of oxygen evolved is corresponding to (Ni-Mo) $_{6.0\ Adm}$$^{-2}$, compared to other coatings. This highest i_{pa} value observed in case of (Ni-Mo)$_{6.0\ Adm}$$^{-2}$ coating may be attributed to its highest Ni content, as reported in Table 8.6. It may be further noted from the nature of chronopotentiograms that though an initial change of potential was observed in all three samples of alloy coatings immediately after the initiation of electrolysis followed by a steady-state potential response, it is less in case of (Ni-Mo)$_{6.0\ Adm}$$^{-2}$coatings. This may be due to sudden exhaustion of the electrolyzed components at the surface of the electrode, where OH^- ions from the solution undergo reduction to release O_2 gas, and ultimately a state of equilibrium is established between OH^- ions and O_2 during the process. However, as the electrolysis further proceeds, almost a constant potential is achieved as the time proceeds, as observed in Figure 8.6. At this stage, the evolution of oxygen gas takes place unabatedly on the surface of coatings, where the current applied is spent completely for conversion of OH^- ions into O_2 gas. Thus based on the experimental results of CV and CP study, it may be concluded that (Ni-Mo)$_{6.0\ Adm}$$^{-2}$ coatings is the most suitable for OER.

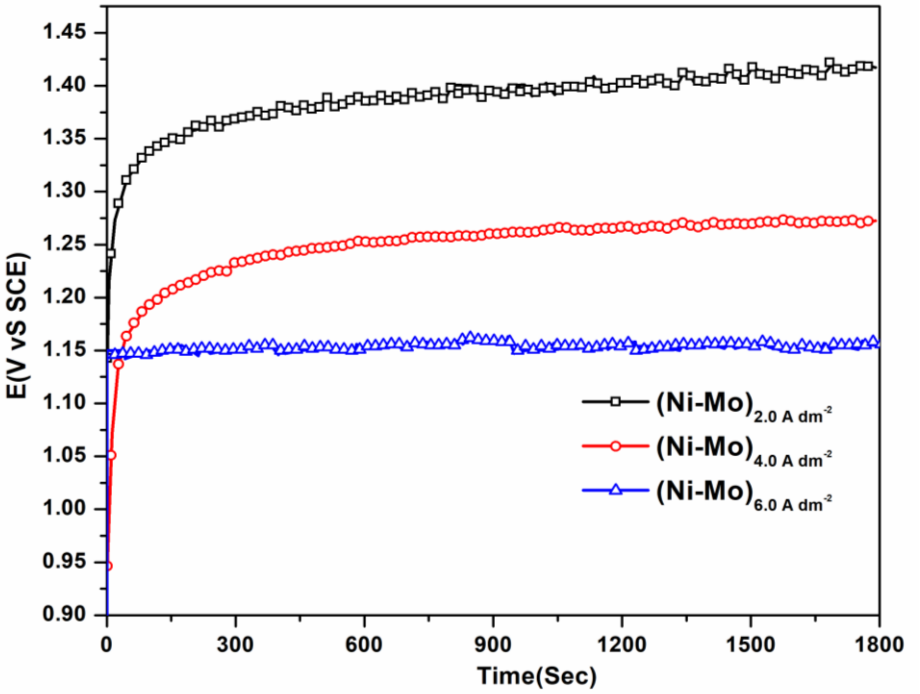

Figure 8.7-Chronopotentiograms observed for OER on $(Ni\text{-}Mo)_{2.0\ Adm^{-2}}$, $(Ni\text{-}Mo)_{4.0\ Adm^{-2}}$ *and* $(Ni\text{-}Mo)_{6.0\ Adm^{-2}}$ *alloy coatings deposited from the same bath*

8.6 MECHANISM OF HER AND OER

The electrocatalytic evolution of H_2 for HER on to the surface of Ni-Mo alloy coatings can also be explained by means of a mechanism. In basic medium, the HER pathway could follow through either the Volmer–Heyrovsky, Volmer–Tafel process or complete Tafel pathways depending on Tafel constants (Vilekar et al. 2010, Skulason et al. 2010).

1. Hydrogen adsorption(Volmer reaction)

$$H_2O + M + e^- \leftrightarrow MH_{ads} + OH^- \dots\dots (8.1)$$

2. Chemical recombination (Tafel reaction)

$$MH_{ads} + MH_{ads} \leftrightarrow 2M + H_2 \dots\dots\dots\dots (8.2)$$

The pathways include the adsorption of H_2O molecule on the surface, followed by electrochemical reduction of adsorbed H_2O into adsorbed OH^- and H atom. Further, desorption of OH^- to rejuvenate the surface, and formation of adsorbed H atom, which combine to form H_2(Gong et al. 2014).The kinetic behaviour of the Ni-Mo alloy developed under different deposition c.d.'s were evaluated by analysing their Tafel slope (β_c) values and corresponding β_c values are reported in Table 8.4. It may be noted that all slope values are in the range of -200 mV dec^{-1} confirming that the HER on these coatings follow Tafel mechanism(as given in Equn.8.1&8.2) (Choquette et al. 1990).

The OER proceeds, in alkaline media, via the steps sequentially shown below (Chekin et al. 2014).

$$OH^- \rightarrow (OH)_{ads} + e^-$$

$$OH_{ads} + OH^- \rightarrow O^-_{ads} + H_2O$$

$$O^-_{ads} \rightarrow O_{ads} + e^-$$

$$2(O)_{ads} \rightarrow O_2 \uparrow$$

This behaviour may be explained by the adsorption of comparatively large OH$^-$ ions on electrode surface, where it overlaps with other processes, like oxygen reduction reaction. Thus, enhanced OER activity of Ni-Mo coating, developed at 6.0 A dm^{-2} can be attributed to the increased OH$^-$ adsorption through the formation of a semiconducting layer in the applied potential range(Elias and Hegde 2015). Since, adsorption characteristics of the OH$^-$ can lead to the formation of NiOOH on its surface, the increase of Ni content (68.25 wt.%) of the coating, deposited at 6.0 A dm^{-2}, which favours the OER.

8.7 CONCLUSIONS

The experimental study of electrodeposition and characterization of Ni-Mo alloy coatings from the citrate bath lead to the following conclusions:

1. Ni-Mo alloy coatings electrodeposited at 2.0 Adm^{-2} (having 26.01 wt.% Mo) and 6.0 Adm^{-2} (having 68.25 wt.% Ni) shows better electrocatalytic property for water electrolysis of both HER and OER respectively, compared to other c.d.'s.
2. There is no much change in the value of both $i_{pc,}$ or i_{pa} with change of c.d. This is due to the inherent induced type of codeposition followed in the bath. In other words, change of composition of the alloy with c.d. is small.

3. The dependency of electro catalytic efficacy of Ni-Mo alloy coating with deposition c.d. was found to be poor for water electrolysis, in terms of volume of H_2 and O_2 gas produced. It is attributed by small change of composition and surface morphology of coatings with c.d., evidenced by XRD and SEM study.
4. However, comparatively better electro catalytic activity of $(Ni\text{-}Mo)_{2.0\ Adm^{-2}}$ and $(Ni\text{-}Mo)_{6.0\ Adm^{-2}}$ (for HER and OER) were attributed to high wt.% of Mo and Ni in the deposit, respectively, supported by EDX analyses.

CHAPTER 9 EFFECT OF ADDITIVES ON ELECTROCATALYTIC BEHAVIOR OF Ni-Mo ALLOY COATINGS

In this chapter the effect of nanoparticles, namely titanium dioxide (TiO_2) and cerium oxide (CeO_2) on electrocatalytic behavior of Ni-Mo alloy coatings for hydrogen evolution reaction (HER) has been studied. The enhancement in the electrocatalytic activity towards HER has been discussed in the light of changed surface morphology, phase structure and porosity of the coatings. The efficacy of the electrode for HER was explained taking advent of Electrochemical Impedance Spectroscopy (EIS) study.

9.1 INTRODUCTION

The atmosphere is polluted by plenty of greenhouse gases; SO_x, NO_x, CO_2 and CO from hydrogen production by hydrocarbon source that are fossil fuel sources which can affect seriously the ecosystem(Rashid et al. 2015).Hence the clean technology is needed for production of hydrogen that can be achieved if hydrogen is produced by renewable source, like water electrolysis and no emission of SO_x, NO_x, CO_2 and CO will be possible and to achieve hydrogen economy. There are many important non-fossil fuel based processes, like Water electrolysis, photocatalysis processes and thermochemical cycles for hydrogen productions in practice(Springer et al. 2001).The use of solar energy and wind energy are sustainable methods for hydrogen production by water electrolysis with high purity, simple and green process. The efficiency hydrogen production by water electrolysis is too low to be economically competitive. The low gas evolution rate and high energy consumption are serious problems of water electrolysis. In average 4.5–5.0kWh/m^3 H_2 energy is needed for conventional industrial electrolyzer (Wang et al. 2014). In water electrolysis for hydrogen production processes the efficiency is a very important parameter. Many researchers in their work have done for analysing the energy consumption, efficiency of hydrogen production systems. Many attempts were made to increase the electrocatalytic activity of HER by increasing its surface area, by exploiting the benefit of both specific surface area of nanoparticles and electroplating technology(Shibli and Dilimon 2007).In this direction, composite coating is one of the rapidly growing field (Low et al. 2006). The development of composite coatings with homogeneously dispersed nanoparticles can enhance the electro catalytic activity of its metal/alloy counterparts (Aal and Hassan 2009; Raj and Venkatesan 1988). Thus, there are many reports on electrocatalytic study of Ni-Mo alloy based composited coating for better electrocatalytic applications.

Therefore, in view of poor electrocatalytic response of Ni-Mo alloy coatings with deposition c.d. (Chapter-8), it has been planned to improve its performance (for HER) by incorporating the nanoparticles into its alloy matrix. The effect of addition of known amount of nanoparticles, namely $TiO_{2,}$ CeO_2 into the optimized Ni-Mo bath (Table 8.1) has been studied. The changed electrocatalytic activity of (Ni-Mo) - based composite coatings was investigated, in relation to its binary alloy matrix to confirm that improved electrocatalytic activity is due to change in the mechanism of HER, affected due to incorporation of nanoparticle into the bath. The experimental results revealed that added nanoparticles show a marked improvement in the electrocatalytic property of the coatings, affected due to changed phase structure, surface morphology, roughness and composition of the composite coatings, evidenced through XRD, SEM, AFM and EDX, respectively.

9.2 ELECTRODEPOSITION OF Ni-Mo COMPOSITE COATINGS

The electrodeposition of Ni-Mo-TiO_2 and Ni-Mo-CeO_2 electrocatalysts was accomplished on a copper substrate from an alkaline sulphate bath. The composition and operating parameters are given in Table 8.1. The electrolytic bath was prepared from analytical grade reagents (Merck, India), using double distilled water. The nanoparticles (0.5 g L^{-1}) were added into the optimised Ni-Mo bath. The electrolyte loaded with nanoparticles was agitated, ultrasonically overnight to ensure the uniform mixing of particles. The electrodeposition was carried out on the cross sectional surface area of copper rod (having of 1.0 cm^2 surface area).The deposition time was kept constant (600s), for comparison of all optimal conditions. The electrodeposition was done at c.d. equal to 2.0 Adm^{-2}, as this was the optimal c.d. at which HER was found to be the maximum (Chapter-8).Same experimental procedures, used in Chapter – 8 was used.

9.3 RESULTS AND DISCUSSION

The experimental results pertaining to the composition, phase structure, surface morphology and electrocatalytic behavior of Ni-Mo alloy coatings are already been reported in Chapter-8. The electrocatalytic behaviors of Ni-Mo-TiO_2 and Ni-Mo-CeO_2alloy coatings are discussed in the proceeding sections, with support of compositional and structural analysis carried out by different techniques.

9.3.1 Compositional Analysis

The composition of Ni-Mo, Ni-Mo-TiO_2 and Ni-Mo-CeO_2 composite coatings deposited from optimised bath (Table 8.1) at 2.0A dm^{-2} was analysed by Energy Dispersive X-ray (EDX) spectroscopy, and individual metal contents of each alloy is listed in Table 9.1.

Table 9.1- Composition data of Ni-Mo, Ni-Mo-TiO_2 and Ni-Mo-CeO_2 composite coatings deposited from the bath obtained at a c.d. of 2.0 A dm^{-2}

Coating configuration	wt.% of Ni in the deposit	wt.% of Mo in the deposit	wt.% of Ti/Ce	wt.% of O_2
$(Ni\text{-}Mo)_{2.0Adm^{-2}}$	62.53	26.01	-	11.47
$(Ni\text{-}Mo\text{-}TiO_2)_{2.0Adm^{-2}}$	53.64	29.52	2.53	14.31
$(Ni\text{-}Mo\text{-}CeO_2)_{2.0Adm^{-2}}$	31.30	30.47	22.73	15.50

It may be noted that on addition of TiO_2/CeO_2 nanoparticles into the bath, the wt. % Mo in the deposit has increased, despite of the same condition of c.d. used for deposition (2.0 Adm^{-2}).It is well known that the surface morphology of electrodeposited alloy coatings has a strong dependency on deposition conditions, like pH, current density (c.d.), temperature and type of additives used. Here, addition of nanoparticles into the Ni-Mo alloy bath, led to a non-uniform current distribution at the cathode surface, leading to increase the limiting current (i_L) of the reluctant metal Mo. As a result, the wt. % Mo in the deposit has increased from 26.01 % to 29.52 % and 30.47% as deposition is allowed to take place in presence of nanoparticles (Table 9.1). Thus this increase in wt.% Mo (reluctant metal) in the deposit is due to presence of inert nanoparticles may be attributed to the non-uniform current distribution at cathode film, as envisaged by Vayenas (Vayenas et al. 2008). Hence, it may be inferred from the data, shown in Table 9.1 that Mo content of the alloy increased (from 26.01 wt. % to 30.47 wt. %) on additions of nanoparticles into the bath.

9.3.2 SEM Analysis

The surface morphology of $(Ni\text{-}Mo)_{2.0\ Adm^{-2}}$,$(Ni\text{-}Mo\text{-}TiO_2)_{2.0\ Adm^{-2}}$ and$(Ni\text{-}Mo\text{-}CeO_2)_{2.0\ Adm^{-2}}$ coatings are examined under SEM, and their microstructures are as shown in Figure 9.1. The magnified image of the surface, showing distribution of nanoparticles in the alloy matrix is shown on the right (Figure 9.1).It may be noted that $(Ni\text{-}Mo\text{-}TiO_2)_{2.0\ Adm^{-2}}$ and $(Ni\text{-}Mo\text{-}CeO_2)_{2.0\ Adm^{-2}}$ composite coatings are found to be more non-uniform, compared to $(Ni\text{-}Mo)_{2.0Adm^{-2}}$ alloy coating. However, nanoparticles spread on the top surface are seen in SEM image. Accordingly, Figures 9.1(b) and 9.1(c) (on right) displays more non-uniform surface due to distribution of nanoparticles in the alloy matrix, compared to Figure 9.1 (a). The change of surface roughness of coatings is accompanied by the increase molybdenum (Mo) content of the composite coatings, supported by EDX data. Thus increase of surface roughness of composite coatings, in relation to bare Ni-Mo alloy coatings may be attributed to the incorporation of CeO_2 and TiO_2 nanoparticles into the alloy matrix. The incorporation of nanoparticles in the alloy matrix is considered to be responsible for increasing the effective surface area of coatings, and hence, their electrocatalytic activity.

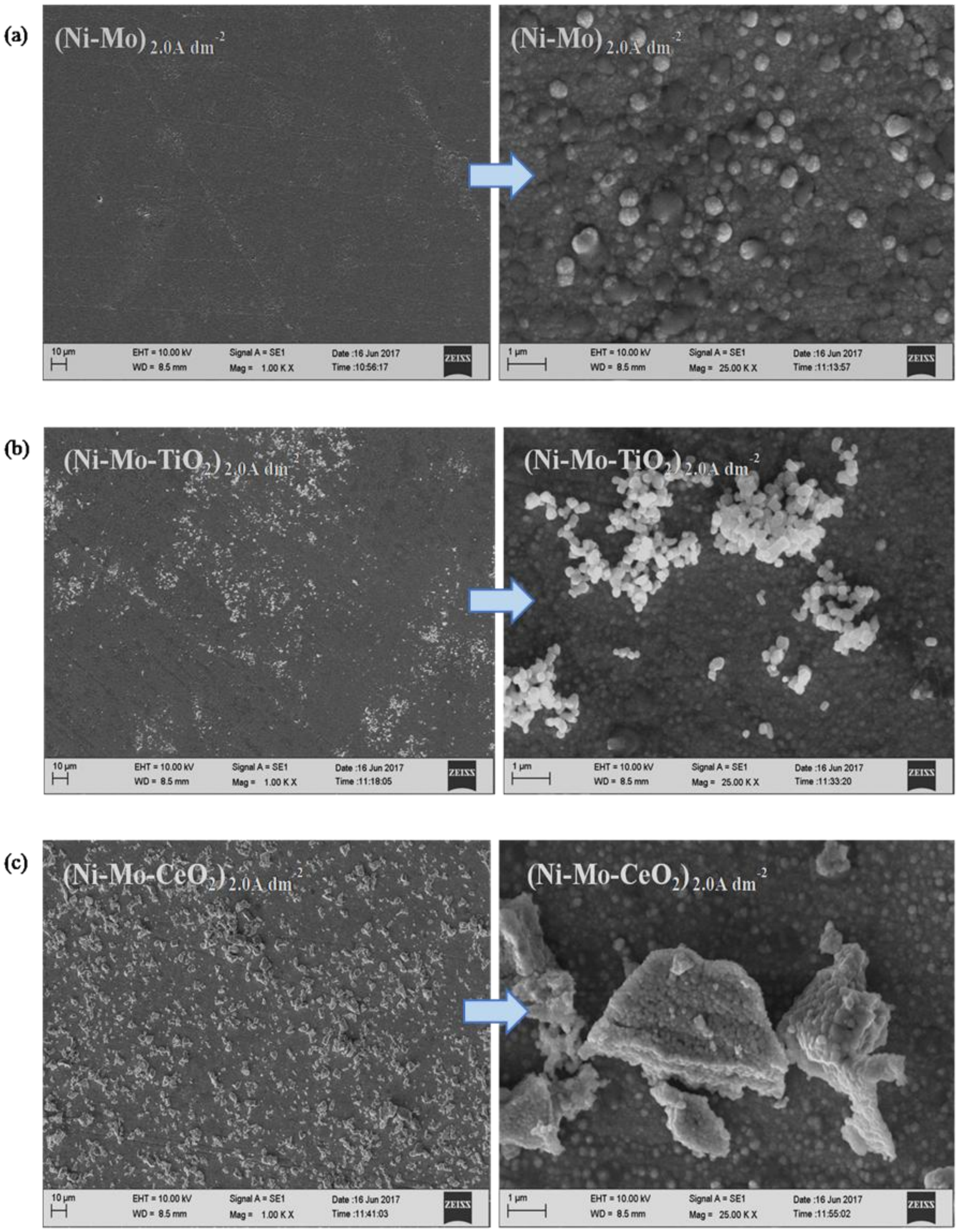

Figure 9.1- SEM image of Ni-Mo alloy coating under different conditions: a)(Ni-Mo)$_{2.0Adm}^{-2}$,b) (Ni-Mo-TiO$_2$)$_{2.0Adm}^{-2}$, and c) (Ni-Mo-CeO$_2$)$_{2.0Adm}^{-2}$ (on the right are shown their magnified image)

9.3.3 XRD Study

Figure 9.2 shows the XRD responses of $(Ni\text{-}Mo)_{2.0\ Adm^{-2}}$ alloy and $(Ni\text{-}Mo\text{-}TiO_2)_{2.0\ Adm^{-2}}$ and $(Ni\text{-}Mo\text{-}CeO_2)_{2.0\ Adm^{-2}}$ and composite coatings. It may be seen that XRD peaks corresponding to $(Ni\text{-}Mo)_{2.0\ Adm^{-2}}$ alloy coatings at $2\theta = 43.3°$, 50.4°, 74.03° and 89.8° represent tetragonal $MoNi_4$ phase, corresponding to (211), (130), (420) and (501) planes, respectively. They are in agreement with standard patterns of $MoNi_4$ (JCPDS No. 03-065-1533). The constancy of phase angles, in all three coatings indicated solid solution of Mo in Ni is formed. Further, addition of either TiO_2, or CeO_2 into the bath has not changed the positions of XRD peaks, except intensity as shown in Figure 9.2.

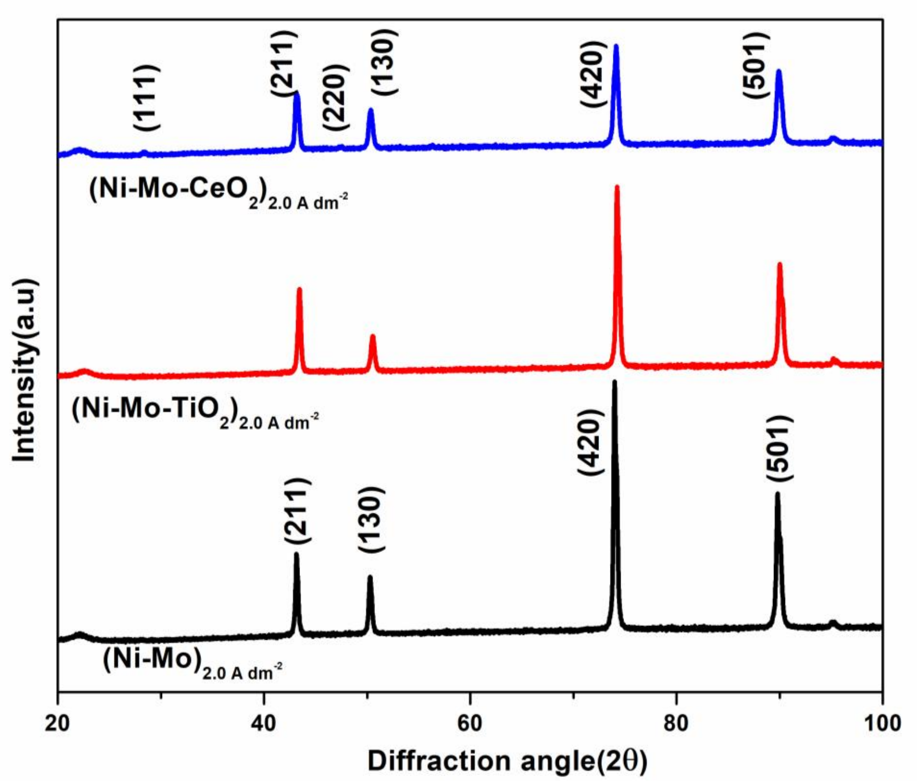

Figure 9.2- X-ray diffractograms of $(Ni\text{-}Mo)_{2.0\ Adm^{-2}}$ *alloy,* $(Ni\text{-}Mo\text{-}TiO_2)_{2.0\ Adm^{-2}}$ *and* $(Ni\text{-}Mo\text{-}CeO_2)_{2.0\ Adm^{-2}}$ *composite coating deposited from same optimized bath*

On addition of TiO_2 and CeO_2 nanoparticles the intensity of peaks, corresponding to (130), (420) and (501) planes decreased, compared to Ni-Mo alloy coating. The decrease of intensity peaks may be attributed to the increase of Mo content of the alloy, affected due to codeposition of nanoparticles. Thus added nanoparticles play an important role on both structure and composition of the alloy coatings. The peaks (111) and (220) is corresponding to incorporated CeO_2 nanoparticles into the alloy matrix (JCPDS No.81-0792). In XRD patterns, shown in Figure 9.2 there is no apparent reflection of TiO_2 was observed. Thus XRD study demonstrated that there is no much change in crystallographic orientation after the addition of nanoparticles. Decrease in the intensity of XRD peaks is attributed to the increased Mo content (or decreased Ni content), affected due to addition of CeO_2 nanoparticles. Similar observation was reported by Du et al.(2017),where it was explained that the limiting current density of the bath has an obvious effect on the composition and microstructure of the Ni-Mo alloys.

9.3.4 AFM Analysis

The three dimensional AFM image of $(Ni\text{-}Mo)_{2.0\ Adm^{-2}}$ alloy, $(Ni\text{-}Mo\text{-}TiO_2)_{2.0\ Adm^{-2}}$and $(Ni\text{-}Mo\text{-}CeO_2)_{2.0\ Adm^{-2}}$ coatings are taken, and are shown in Figures 9.3(a),(b) and (c) respectively.

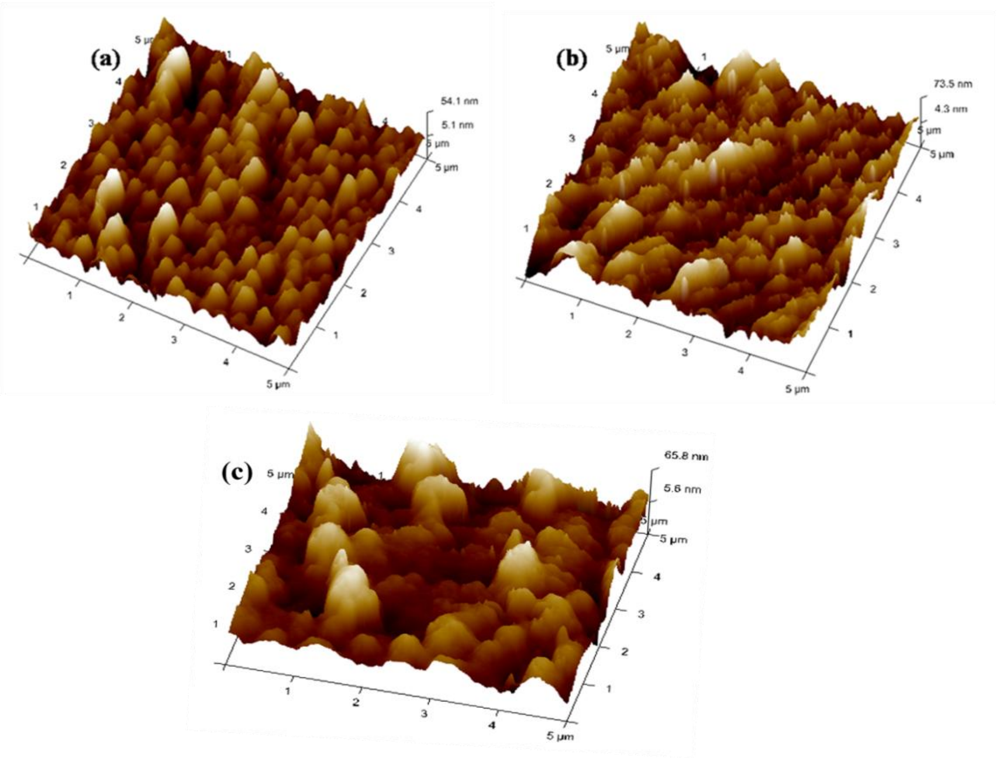

Figure 9.3-AFM image of coatings: (a) $(Ni\text{-}Mo)_{2.0Adm^{-2}}$ *(b)* $(Ni\text{-}Mo\text{-}TiO_2)_{2.0\ Adm^{-2}}$*and (c)* $(Ni\text{-}Mo\text{-}CeO_2)_{2.0\ Adm^{-2}}$ *deposited from same optimized bath*

A significant change in the surface roughness of the coating was found on incorporation of nanoparticles in the alloy matrix. Experimental data analyses showed that the average roughness of $(Ni\text{-}Mo)_{2.0\ Adm^{-2}}$ alloy coating is increased from 40.2 nm,65.6 nm and 77.7 nm on addition of TiO_2 followed by CeO_2 nanoparticles into the bath. This indicates that increased surface roughness of $(Ni\text{-}Mo\text{-}CeO_2)_{2.0\ Adm^{-2}}$ coating due to addition of CeO_2 is responsible for increase in the active surface area of coating, and hence increases in the rate of HER on its surface.

9.3.5 Corrosion Study

The corrosion study of $(Ni\text{-}Mo)_{2.0\ Adm^{-2}}$, $(Ni\text{-}Mo\text{-}TiO_2)_{2.0\ Adm^{-2}}$ and $(Ni\text{-}Mo\text{-}CeO_2)_{2.0\ Adm^{-2}}$ was carried out in 1M KOH medium by potentiodynamic polarization method, and corresponding polarization curves are shown in Figure 9.4. From the CR values, reported in Table 9.2.

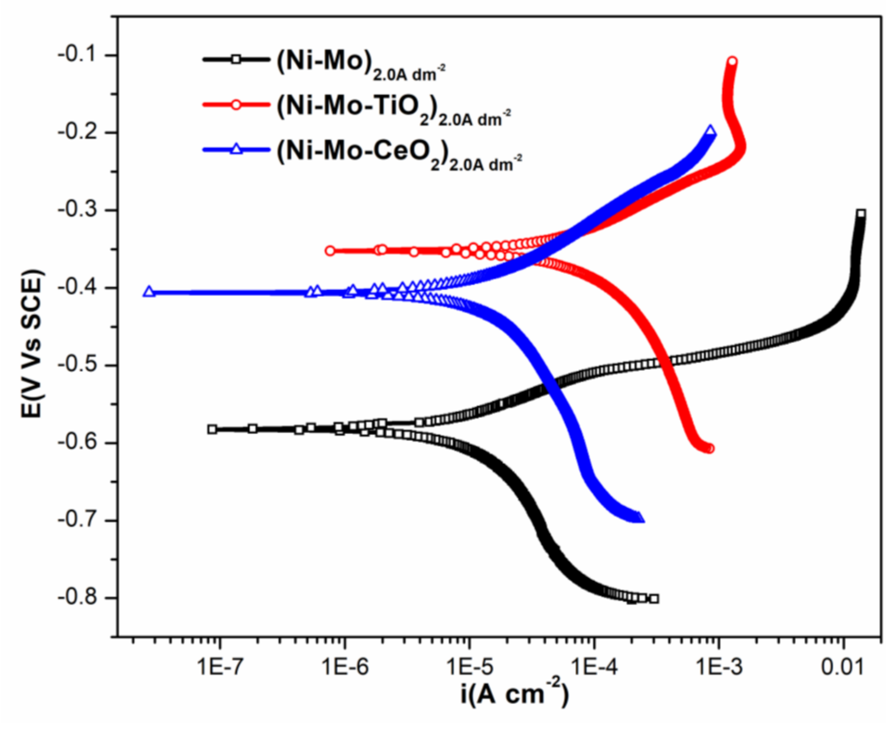

Figure 9.4-Potentiodynamic polarization curves of $(Ni\text{-}Mo)_{2.0\ Adm^{-2}}$ *,*$(Ni\text{-}Mo\text{-}TiO_2)_{2.0\ Adm^{-2}}$ *and* $(Ni\text{-}Mo\text{-}CeO_2)_{2.0\ Adm^{-2}}$ *deposited from same bath*

From the CR values reported in Table 9.2, it may be noted that corrosion protection efficacy of alloy coatings is in the order of $(Ni\text{-}Mo)_{2.0\ Adm^{-2}}$>$(Ni\text{-}Mo\text{-}TiO_2)_{2.0\ Adm^{-2}}$ >$(Ni\text{-}Mo\text{-}CeO_2)_{2.0\ Adm^{-2}}$. It is supported by their corrosion potential (E_{corr}), values as seen in Figure 9.4.The linear region of the cathodic curve corresponds to cathodic reaction of hydrogen evolution reaction (HER), in water electrolysis. Hence, electrocatalytic kinetic parameters like i_o, β_c and η_c were determined by extrapolation of Tafel plots to zero current potential. And their values are reported in Table 9.2.From the data, it can be inferred that $(Ni-Mo\text{-}CeO_2)_{2.0A\ dm^{-2}}$ alloy coating is electrocatalytically more active for HER than rest of the coatings. It can be seen that the real exchange current density for HER on the $(Ni-Mo\text{-}CeO_2)_{2.0A\ dm^{-2}}$ and $(Ni\text{-}Mo\text{-}TiO_2)_{2.0\ Adm^{-2}}$ composite coating was higher than that on $(Ni\text{-}Mo)_{2.0Adm^{-2}}$ coating, This shows that the intrinsic activity of the $(Ni-Mo\text{-}CeO_2)_{2.0A\ dm^{-2}}$ and$(Ni\text{-}Mo\text{-}TiO_2)_{2.0\ Adm^{-2}}$ composite alloy coating toward HER was remarkably higher than that of $(Ni\text{-}Mo)_{2.0\ Adm^{-2}}$ coating. This suggests that inclusion of nanoparticles into Ni–Mo alloy coatings enhances its intrinsic electro-catalytic activity for HER, due to increase in surface area. Thus, the main reason for improvement of electrocatalytic activity of Ni–Mo composite coatings toward HER arises not only from the increase of the active surface area, but also due to synergistic interaction of Ni, Mo and TiO_2/CeO_2.

Table 9.2- Electrocatalytic kinetic parameters of $(Ni\text{-}Mo)_{2.0\ Adm^{-2}}$,$(Ni\text{-}Mo\text{-}TiO_2)_{2.0\ Adm^{-2}}$ and $(Ni\text{-}Mo\text{-}CeO_2)_{2.0\ Adm^{-2}}$alloy coatings under 1M KOH medium

Coating configuration	β_c (mV dec^{-1})	α (Sym.factor)	i_o (mA cm^{-2})	η_c (mV Vs SCE)	CR×10^{-2} (mm y^{-1})
$(Ni\text{-}Mo)_{2.0\ A\ dm^{-2}}$	191	0.31	4.653	702	22.0
$(Ni\text{-}Mo\text{-}TiO_2)_{2.0\ Adm^{-2}}$	94	0.63	4.850	550	30.3
$(Ni\text{-}Mo\text{-}CeO_2)_{2.0\ Adm^{-2}}$	75	0.79	8.560	450	40.1

9.3.5 Hydrogen Evolution Reaction

9.3.5.1 Cyclic voltammetry study

The electrocatalytic behavior of $(Ni\text{-}Mo)_{2.0\ Adm^{-2}}$, $(Ni\text{-}Mo\text{-}TiO_2)_{2.0\ Adm^{-2}}$ and $(Ni\text{-}Mo\text{-}CeO_2)_{2.0\ Adm^{-2}}$ coatings were tested for HER, using them as cathode. Same experimental procedure, described in Chapter-8 was used to get cyclic voltammograms of three coatings, and is shown in Figure 9.5.

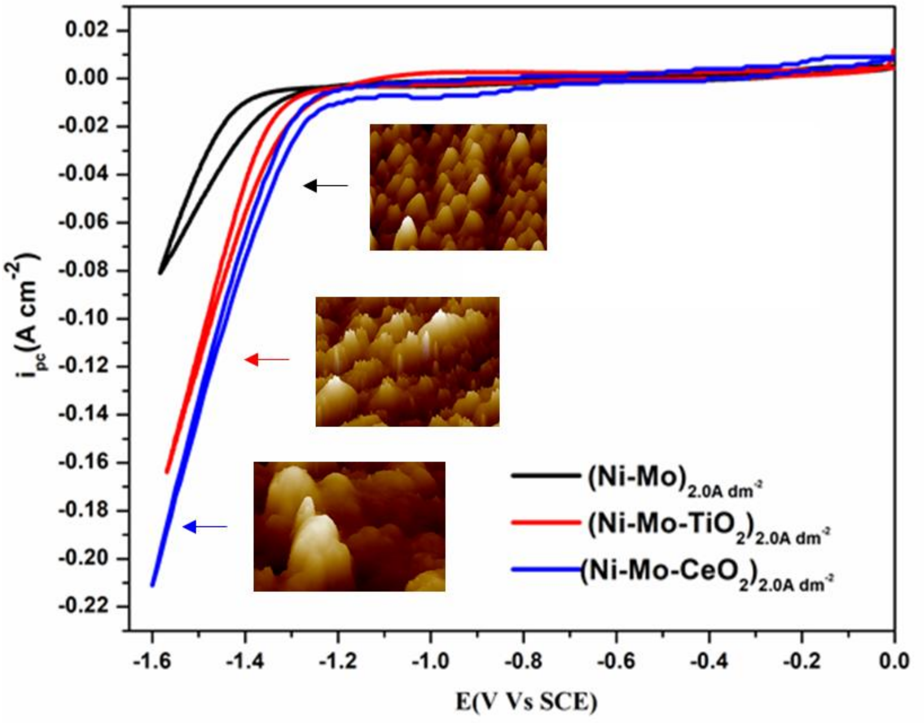

Figure 9.5– CV response of $(Ni\text{-}Mo\text{-}TiO_2)_{2.0\ Adm^{-2}}$ *and* $(Ni\text{-}Mo\text{-}\ CeO_2)_{2.0\ Adm^{-2}}$ *coatings in relation to* $(Ni\text{-}Mo)_{2.0\ Adm^{-2}}$ *coatings showing a drastic increase of cathodic peak current density* (i_{pc}) *on addition of* TiO_2 *and* CeO_2 *nanoparticles. In the inset are shown AFM images showing increase of surface roughness due addition of nanoparticles*

From the nature of CV curves, shown in Figure 9.5, it may be noted that the value of i_{pc} increased on addition of nanoparticles into the bath. This increase of i_{pc} may be attributed to the increase of surface roughness due to induction of nanoparticles in the alloy matrix. The increase of $i_{pc,}$ or electrocatalytic efficacy for HER of alloy coatings were found to have direct relation their surface roughness of the deposit. It is evident from the AFM images, shown in relation to peak cathode c.d.

(i_{pc}) in Figure 9.5. Thus, the HER intermediate product H atom can easily adsorb on Ti/Ce atom to form M-H_{ads}, due to the presence of unpaired electron present in 3d and 5d orbital of Ti/Ce metal atoms, respectively. It may be noted that $(Ni\text{-}Mo\text{-}CeO_2)_{2.0\ Adm^{-2}}$ composite coating showed maximum electrocatalytic property than $(Ni\text{-}Mo\text{-}TiO_2)_{2.0\ Adm^{-2}}$ coating, as shown in Figure 9.5.

9.3.5.2 Chronopotentiometry study

The chronopotentiometry (CP) of $(Ni\text{-}Mo)_{2.0\ Adm^{-2}}$, $(Ni\text{-}Mo\text{-}TiO_2)_{2.0\ Adm^{-2}}$ and $(Ni\text{-}Mo\text{-}CeO_2)_{2.0\ Adm^{-2}}$ coatings were studied, and their electrocatalytic stability are tested. The relative response of chronopotentiometry (CP) curves of $(Ni\text{-}Mo)_{2.0\ Adm^{-2}}$, $(Ni\text{-}Mo\text{-}TiO_2)_{2.0\ Adm^{-2}}$ and $(Ni\text{-}Mo\text{-}CeO_2)_{2.0\ Adm^{-2}}$ coatings are shown in Figure 9.6.

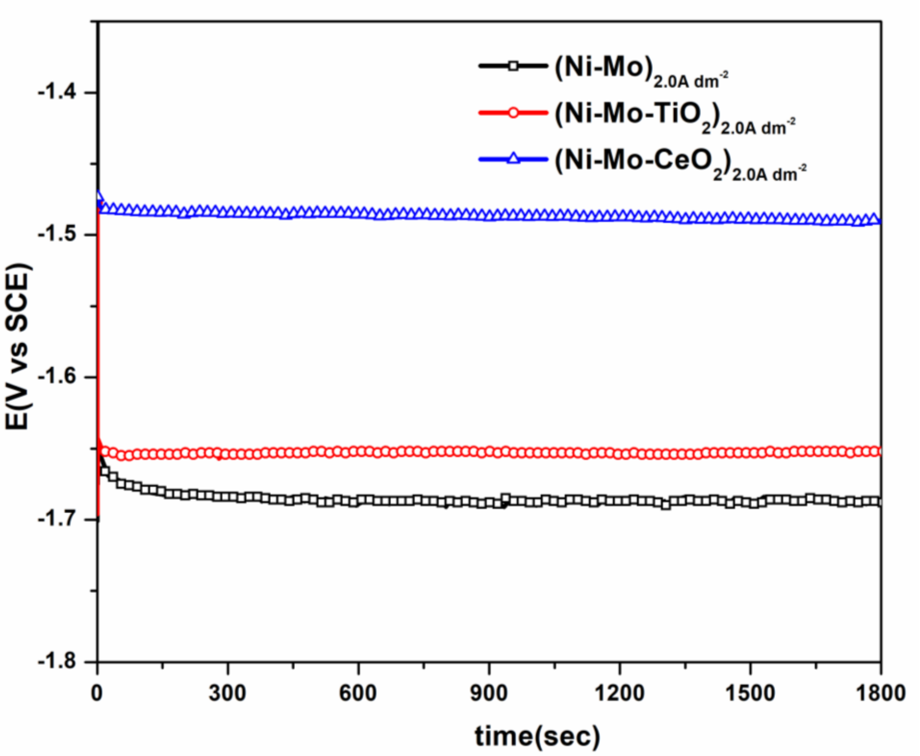

Figure 9.6- Relative response of CP curves for HER on to the surface of $(Ni\text{-}Mo)_{2.0\ A\ dm^{-2}}$*,* $(Ni\text{-}Mo\text{-}TiO_2)_{2.0\ Adm^{-2}}$ *and* $(Ni\text{-}Mo\text{-}CeO_2)_{2.0\ Adm^{-2}}$ *coatings, showing a quick state of equilibrium in* $(Ni\text{-}Mo\text{-}CeO_2)_{2.0\ Adm^{-2}}$*coating*

In this technique, the electrocatalytic behaviour of $(Ni\text{-}Mo)_{2.0\ Adm^{-2}}$,$(Ni\text{-}Mo\text{-}TiO_2)_{2.0\ Adm^{-2}}$ and $(Ni\text{-}Mo\text{-}CeO_2)_{2.0\ Adm^{-2}}$ coatings were assessed by measuring the amount of hydrogen liberated for initial 300sec. The quantity of hydrogen evolved are measured, and are tabulated in the Table 9.3. Relatively more quantity of H_2 gas was liberated on $(Ni-Mo-CeO_2)_{2.0Adm^{-2}}$, and then on $(Ni-Mo-TiO_2)_{2.0Adm^{-2}}$, when compared to $(Ni-Mo)_{2.0\ Adm^{-2}}$ coating.

Table 9.3- The value of cathodic peak current density (i_{pc}) and onset potential observed for $(Ni-Mo)_{2.0\ Adm^{-2}}$, $(Ni-Mo-TiO_2)_{2.0\ Adm^{-2}}$ and $(Ni-Mo-CeO_2)_{2.0\ Adm^{-2}}$ coatings, with amount of H_2 liberated

Electrodeposited coatings	Cathodic peak c.d. (Adm^{-2})	Onset potential for H_2 evolution (V vs SCE)	Volume of H_2 Evolved in 300s (cm^3)
$(Ni-Mo)_{2.0\ Adm^{-2}}$	-0.08	-1.28	12.9
$(Ni-Mo-TiO_2)_{2.0\ Adm^{-2}}$	-0.16	-1.16	14.2
$(Ni-Mo-CeO_2)_{2.0\ Adm^{-2}}$	-0.21	-1.09	15.5

From the data reported in Table 9.3, it may inferred that $(Ni-Mo-CeO_2)_{2.0Adm^{-2}}$ composite coating is the most effective electrode material for HER. This is attributed by the increase of active sites due to addition of CeO_2 nanoparticles, and increased Mo content of the alloy. This increase of active sites for evolution of hydrogen is found to be more, when compared to the addition of TiO_2 nanoparticles. The added CeO_2 nanoparticles increased the surface roughness of the coatings, as shown in the Figure 9.3(c).A striking difference in the electrocatalytic activity of $(Ni-Mo-CeO_2)_{2.0\ Adm^{-2}}$ for HER, compared to $(Ni-Mo)_{2.0\ Adm^{-2}}$,and $(Ni-Mo-TiO_2)_{2.0\ Adm^{-2}}$ alloy coatings is evident from the nature of chronopotentiograms shown in Figure 9.6.

9.3.6 EIS Study

The electrocatalytic efficacy of electrode materials mainly depends on its effective surface area and their intrinsic catalytic activity. Hence, to understand the reasons for increased electrocatalytic activity of (Ni-Mo) alloy coating on addition of nanoparticles (TiO_2 and CeO_2), EIS study has been carried out. From the Nyquist response of $(Ni-Mo)_{2.0\ Adm^{-2}}$, $(Ni-Mo-TiO_2)_{2.0\ Adm^{-2}}$ and $(Ni-Mo-CeO_2)_{2.0\ Adm^{-2}}$ coatings, shown in Figure 9.7. It may be inferred that $(Ni-Mo-TiO_2)_{2.0\ Adm^{-2}}$ and $(Ni-Mo-CeO_2)_{2.0\ Adm^{-2}}$ coatings offer lower charge transfer resistance (R_{ct}) value, compared to (Ni-Mo) $_{2.0\ \mathrm{Adm}^{-2}}$ coating. This confirms that composite coatings are more prone to undergo corrosion than (Ni-Mo)$_{2.0\ \mathrm{Adm}^{-2}}$. This is in agreement with their high CR values, reported in Table 9.2. The high corrosion tendency of these coatings, compared to (Ni-Mo)$_{2.0\ \mathrm{Adm}^{-2}}$ coating may be attributed to the increased surface roughness and porosity, as shown in the Figures 9.1 and 9.2.

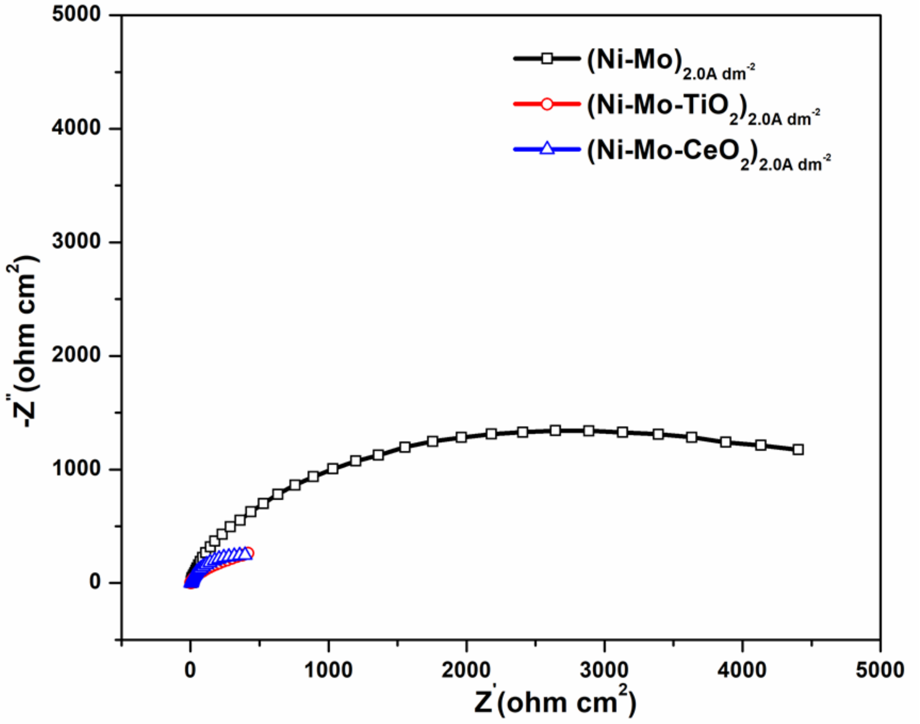

Figure 9.7-Nyquist responses of (Ni-Mo)$_{2.0\ \mathrm{Adm}^{-2}}$,(Ni-Mo-TiO$_2$)$_{2.0\ \mathrm{Adm}^{-2}}$ and (Ni-Mo-CeO$_2$)$_{2.0\mathrm{Adm}^{-2}}$ coatings showing the least charge transfer resistances (R_{ct}) corresponding to (Ni-Mo-CeO$_2$)$_{2.0\ \mathrm{Adm}^{-2}}$ coating

Further, to know the factor responsible for increased electro-catalytic activity of (Ni-Mo-TiO$_2$)$_{2.0\ \mathrm{Adm}^{-2}}$ and (Ni-Mo-CeO$_2$)$_{2.0\ \mathrm{Adm}^{-2}}$ coatings, their equivalent circuit has been simulated, and is shown in Figure 9.8(a) and (b), respectively. A close agreement between the observed and simulated impedance responses for both (Ni-Mo-TiO$_2$)$_{2.0\ \mathrm{Adm}^{-2}}$ and (Ni-Mo-CeO$_2$)$_{2.0\ \mathrm{Adm}^{-2}}$ coatings were found. The electrochemical data Response and the corresponding data are shown in Table 9.4. The charge transfers resistance (R_{ct}) and double layer capacitance (C_{dl}) values, associated in production of H_2 gas on electrode surfaces have been calculated, and are reported in Table 9.4. It may be noted that (Ni-Mo-CeO$_2$)$_{2.0\ \mathrm{Adm}^{-2}}$ demonstrating least R_{ct} and highest C_{dl} values with R_S(solution resistance), compare to its bare alloy counterpart, and is attributed to its more number of active sites on the surface, due to roughness.

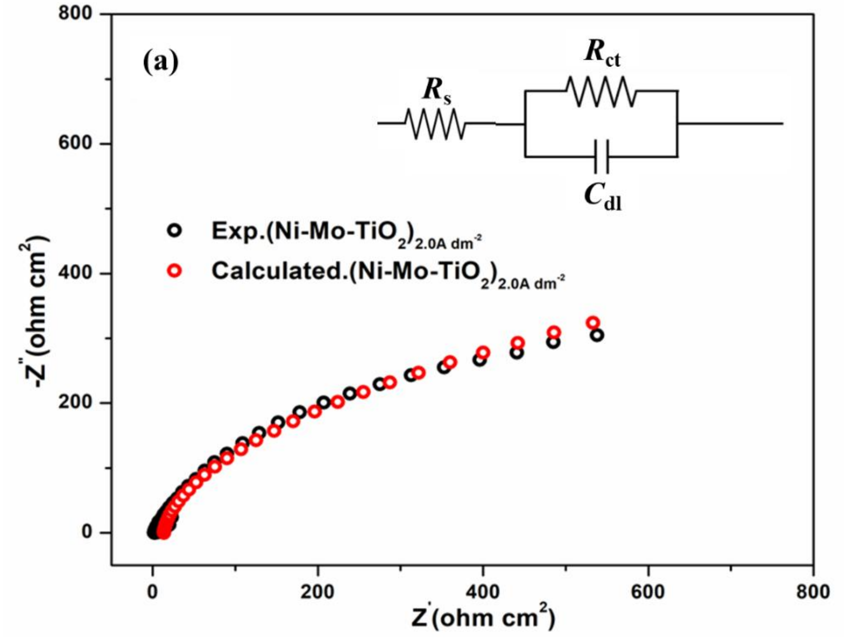

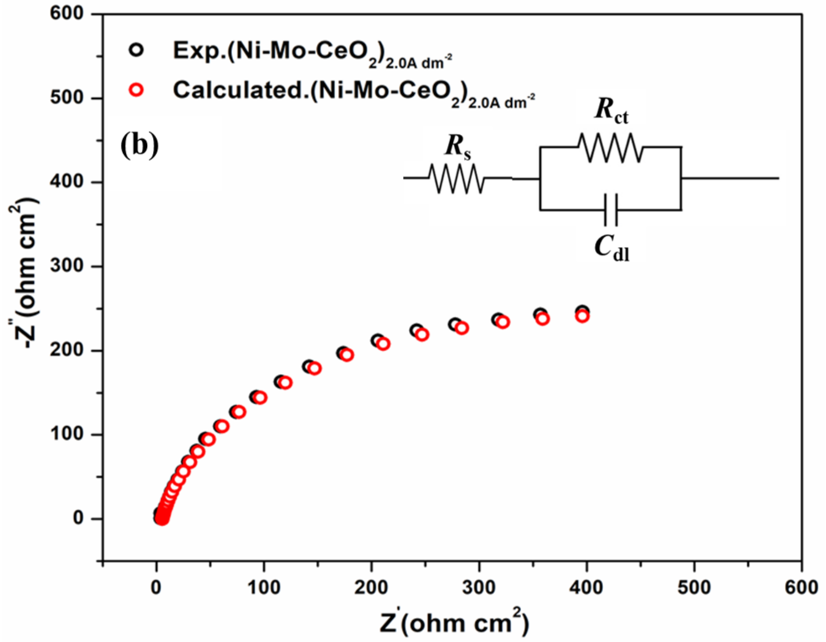

Figure 9.7- Simulation of Nyquist plots corresponding to: a) $(Ni\text{-}Mo\text{-}TiO_2)_{2.0\ Adm^{-2}}$*, and b)*$(Ni\text{-}Mo\text{-}TiO_2)_{2.0Adm^{-2}}$ *coatings with equivalent circuits having circuit components responsible for better electro catalytic property for HER*

Thus the highest electro catalytic activity of (Ni-Mo-CeO_2)$_{2.0\ Adm^{-2}}$ for HER is due to the less impedance for charge transfer process, required for the liberation of H_2, compared to that of (Ni-Mo)$_{2.0\ Adm^{-2}}$ alloy coating. Further, direct dependency of electrode roughness on the charge transfer resistance (R_{ct}) values indicates that hydrogen production is limited only by charge transfer process, not by mass transfer process(Manazoglu et al. 2016).It may be noted that C_{dl} value of the deposit increased with the surface roughness, or Mo content of the deposit. Thus, increased electrocatalytic activity Ni-Mo composite coating is due to increased active surface area, affected due to incorporation of nanoparticles (CeO_2 and TiO_2) into its matrix.

Table 9.4 - The electrochemical impedance data obtained for (Ni-Mo)$_{2.0\ Adm^{-2}}$, (Ni-Mo-TiO_2)$_{2.0\ Adm^{-2}}$and (Ni-Mo-CeO_2)$_{2.0\ Adm^{-2}}$ coatings

Coating configuration	Charge transfer resistance,(R_{ct}) (Ohm)	Capacitance(C_{dl}) (μF)
(Ni-Mo)$_{2.0\ Adm^{-2}}$	4486	69
(Ni-Mo-TiO_2)$_{2.0\ Adm^{-2}}$	532	161
(Ni-Mo-CeO_2)$_{2.0\ Adm^{-2}}$	301	391

The improved electocatalytic behaviour of composite coatings may be explained in terms of its active/effective surface area, against geometric surface area. Hence, electrochemical active surface area of electrodes, *i.e.*(Ni-Mo)$_{2.0\ Adm^{-2}}$, (Ni-Mo-TiO_2)$_{2.0\ Adm^{-2}}$ and (Ni-Mo-CeO_2)$_{2.0\ Adm^{-2}}$ were calculated, using the relation(Eqn. 9.1) (Golgovici et al. 2018).

$$A = \frac{C_{dl}}{20}(\text{cm}^2)\text{.................} \ (9.1)$$

Where A is active surface area of the electrode, and C_{dl} is calculated double-layer capacitance. The average double-layer capacitance for smooth metal surface is assumed to be equal to 20 µFcm^{-2} (Navarro-Flores et al. 2005; Wang et al. 2015).Thus, electrochemical active surface area for (Ni-Mo)$_{2.0\ Adm^{-2}}$, (Ni-Mo-TiO_2)$_{2.0\ Adm^{-2}}$ and (Ni-Mo-CeO_2)$_{2.0\ Adm^{-2}}$ coatings can be calculated using the data from Table

9.4. They are calculated to be 3.45cm^2, 8.05cm^2 and 19.55cm^2 against 1.00 cm^2 surface area (used for HER study).Hence, it may be inferred that highest electrocatalytic activity of (Ni-Mo-CeO$_2$)$_{2.0\ \mathrm{Adm}^{-2}}$ composite coating is due to the highest surface area of electrode material, affected due to addition of CeO$_2$ nanoparticles. In other words, number of active sites for H$_{ads}$ and degree of surface coverage on CeO$_2$ embedded composite electrode is more than bare Ni-Mo alloy electrode.

9.3.7 Mechanism of HER Reaction

The experimental study revealed that (Ni-Mo-CeO$_2$)$_{2.0\ \mathrm{Adm}^{-2}}$ coating is the better electrode material when compared to (Ni-Mo-TiO$_2$)$_{2.0\ \mathrm{Adm}^{-2}}$ and (Ni-Mo)$_{2.0\ \mathrm{Adm}^{-2}}$ coatings for HER, supported by SEM, AFM, EDX and XRD analyses. The HER mechanism usually follows various reaction pathways. It is due to active surface area and increased Mo content of the coating due to addition of CeO$_2$ nanoparticles into the bath, by providing more active site for hydrogen ion adsorption. The observed β_c value in the range of 94 mVdec^{-1}and 75mVdec^{-1} for (Ni-Mo-TiO$_2$)$_{2.0\ \mathrm{Adm}^{-2}}$ and (Ni-Mo-CeO$_2$)$_{2.0\ \mathrm{Adm}^{-2}}$ composite coatings, respectively confirms that the HER follows Volmer-Heyrovsky mechanism(Subramanya et al. 2015) and is shown below. The HER mechanism on (Ni-Mo)$_{2.0\ \mathrm{Adm}^{-2}}$ almost tending towards complete Tafel mechanism. Hence, HER is faster in the case of (Ni-Mo-TiO$_2$)$_{2.0\ \mathrm{Adm}^{-2}}$ and (Ni-Mo-CeO$_2$)$_{2.0\ \mathrm{Adm}^{-2}}$ coating, compared to its bare binary alloy coating.

a) Hydrogen adsorption(Volmer reaction)

$$H_2O + M + e^- \leftrightarrow MH_{ads} + OH^-$$

b) Hydrogen desorption(Heyrovsky reaction)

$$MH_{ads} + H_2O + e^- \leftrightarrow M + H_2 + OH^-$$

c) Chemical recombination (Tafel reaction)

$$MH_{ads} + MH_{ads} \leftrightarrow 2M + H_2$$

9.4 CONCLUSIONS

Ni-Mo-TiO$_2$ and Ni-Mo-CeO$_2$ composite coatings have been developed through electrodeposition method, and their electrocatalytic activity for HER has been studied, and following conclusions are drawn:

1. Both $(Ni\text{-}Mo\text{-}TiO_2)_{2.0\ Adm^{-2}}$ and $(Ni\text{-}Mo\text{-}CeO_2)_{2.0\ Adm^{-2}}$ composite coatings shows better electrocatalytic activity compared to its binary alloy counterpart. The enhanced electrocatalytic activities of composite coatings were attributed to the increased porosity and surface roughness due to addition of nanoparticles, supported by SEM and AFM study.
2. The increased surface roughness, and changed composition (Ni and Mo content) of composite coatings were attributed to the non-uniform current distribution at the cathode surface during deposition, due to addition of nanoparticles.
3. The increased electrocatalytic activity of $(Ni\text{-}Mo\text{-}TiO_2)_{2.0\ Adm^{-2}}$ and $(Ni\text{-}Mo\text{-}CeO_2)_{2.0\ Adm^{-2}}$ coating explained through decreased R_{ct} and increased C_{dl} values, in relation to its values for its binary alloy counterpart, evidenced by EIS study.
4. Higher electrocatalytic activity of $(Ni\text{-}Mo\text{-}CeO_2)_{2.0\ Adm^{-2}}$ and $(Ni\text{-}Mo\text{-}TiO_2)_{2.0\ Adm^{-2}}$ composite coatings, compared to $(Ni\text{-}Mo)_{2.0\ Adm^{-2}}$ coating is due to change of HER mechanism from Tafel's to Volmer-Heyrovsky type, supported by Tafel slope values.
5. The increased electrocatalytic activity of $(Ni\text{-}Mo\text{-}TiO_2)_{2.0\ Adm^{-2}}$ and $(Ni\text{-}Mo\text{-}CeO_2)_{2.0\ Adm^{-2}}$ as compared to $(Ni\text{-}Mo)_{2.0\ Adm^{-2}}$ is due to increase of exchange current density(i_0), symmetry factor (α) with decrease of overpotential, evidenced by Tafel plots.

CHAPTER 10 MAGENETOELECTRODEPOSITION OF (Ni-Mo-Cd) ALLOY COATINGS OF HIGH CORROSION RESISTANCE

The attractiveness of electroplating in the production of more corrosion resistant coatings is linked to the development variety of binary and ternary alloy coatings. In this direction, the present chapter unfolds in three sections. First section details the evaluation of corrosion resistance properties of electrodeposited Ni-Mo alloy coatings in 5% NaCl solution. How the corrosion resistance character of Ni-Mo alloy coating can be improved with addition of small quantity of Cd salt (into Ni-Mo bath) is reported in the second section. In the third section, how corrosion protection efficacy of Ni-Mo-Cd alloy coatings can improve further with the advent of induced magnetic field, applied parallel to deposition is explained. The experimental results of investigation on electrodeposition(ED) and magneto-electrodeposition(MED) of Ni-Mo and Ni-Mo-Cd alloy coatings are discussed, with the support of analytical data obtained from different analytical techniques, such as SEM, EDX and XRD.

10.1ELECTRODEPOSITION OF Ni-Mo ALLOY COATINGS

The electrodeposition of Ni-Mo alloy coatings was carried out from the bath, having composition reported in Table 8.1. The experimental procedure for electrodeposition was described in Chapter-8.The electrodeposited Ni-Mo alloy coatings were tested for their corrosion performance in 5% NaCl solution, and results are discussed here.

10.1.1Induced Codeposition of Ni-Mo Alloy

Electrodeposition of Ni-Mo alloy coatings was carried out at different c.d.'s (ranging from 2.0-6.0 Adm^{-2}), and their composition data is shown in Table 6.2. The composition, surface morphology and phase structures of the alloy coatings were discussed in Chapter-8.It may be noted that there is no significant variation in the Ni content of alloy with c.d. due to inherent nature of induced type of codeposition (Table 6.2).

10.1.2 Potentiodynamic polarization Method

The electrodeposited (ED) Ni-Mo alloy coatings obtained at different c.d.'s were subjected to corrosion study, in 5% NaCl medium by potentiodynamic polarization method. The potentiodynamic polarization plots are shown in Figure 10.2. The corrosion rates (CR's) obtained, on extrapolation of Tafel's curves are given in Table 10.2.

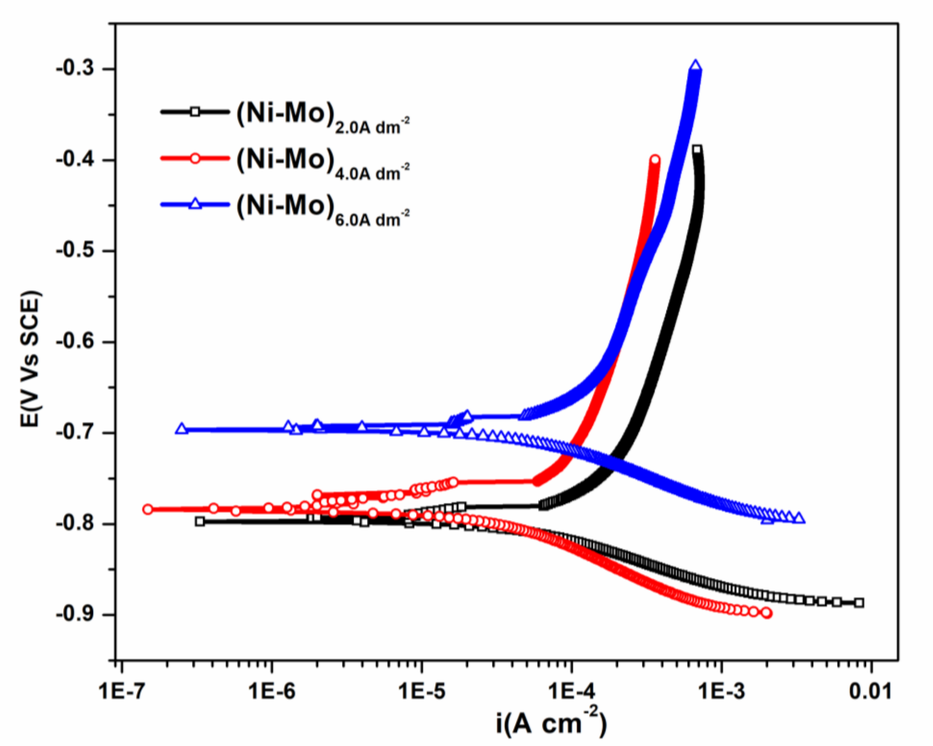

Figure 10.2- Potentiodynamic polarization behaviour of electrodeposited Ni-Mo alloy coatings in 5% NaCl medium

Table 10.2- Composition and corrosion data (in 5% NaCl medium) of Ni-Mo alloy coatings deposited at different current densities

Coating configuration	wt.% of Ni in deposit	wt.% of Mo in deposit	$-E_{corr}$ (mV vs. SCE)	i_{corr} (μA cm^{-2})	CR×10^{-2} (mm y^{-1})	R_{ct} (Ohm)
$(Ni\text{-}Mo)_{2.0A\ dm^{-2}}$	62.53	26.01	810	56.5	68.7	211
$(Ni\text{-}Mo)_{4.0A\ dm^{-2}}$	65.18	25.52	790	29.0	35.2	308
$(Ni\text{-}Mo)_{6.0A\ dm^{-2}}$	68.25	24.54	700	23.8	28.9	413

The corrosion study revealed that the Ni-Mo coatings obtained at lower limits of current density is more prone to undergo corrosion in 5% NaCl medium, whereas coating deposited at 6.0 Adm^{-2},*i.e.*, $(\text{Ni-Mo})_{6.0\text{A dm}^{-2}}$ showed the least corrosion rate (28.9×10^{-2} mm y^{-1}). This decrease of CR at higher limits of c.d. may be attributed to the increase of noble metal (Ni) content in the deposit (Huang et. al. 2015).

10.1.3 Electrochemical Impedance Study

The corrosion protection ability of ED Ni-Mo alloy coatings was studied in 5% NaCl solution, by EIS method. The impedance response of Ni-Mo alloy coatings deposited at different current densities is shown in Figure 10.2. It may be seen that the charge transfers resistance (R_{ct}) keep increasing with increase of deposition current density, indicating that the corrosion resistance has direct dependency with Ni content of the alloy, in compliance with CR values obtained by Tafel's method. The ECE fitment corresponding to $(\text{Ni-Mo})_{6.0\text{ A dm}^{-2}}$ is given in inset of Figure 10.2.The charge transfers resistance (R_{ct}) values are reported n Table 10.2

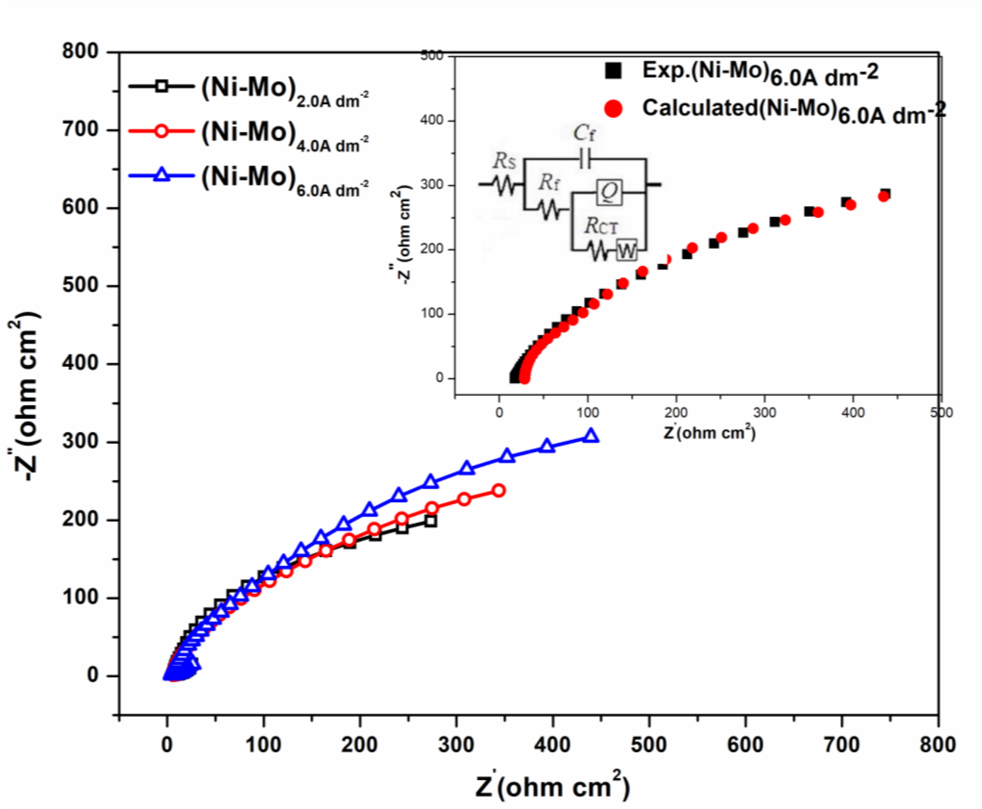

Figure 10.2- Electrochemical impedance response of Ni-Mo alloy coatings in 5% NaCl solution, deposited at different current densities

10.2 ELECTRODEPOSITION OF (Ni-Mo-Cd) ALLOY COATINGS

From the corrosion study of binary Ni-Mo alloy coatings it was arrived that, due to limitations of induced type of codeposition of Ni-Mo alloy, no further increase of Ni content in the deposit is possible. Therefore, with intention of improving the corrosion resistance of Ni-Mo alloy coating, a small quantity of $CdCl_2$ (1.0g/L) was added into Ni-Co bath. The composition and operating variables of the ternary (Ni-Mo-Cd) bath, used in the present study is given in Table 10.1.It may be noted that except addition of small quantify of $CdCl_2$ (1.0g/L), the bath composition used here is same as Ni-Mo bath (Table 6.1). $CdCl_2$ is added to see the effect of Cd^{+2} ions on the composition, surface morphology, and hence the corrosion resistivity of Ni-Mo-Cd alloy coatings.

Table 10.1-Composition and operating parameters of (Ni-Mo-Cd) bath used for deposition of Ni-Mo-Cd alloy coatings

Chemical constituents	Amount (gL^{-1})	Operating parameters
$NiSO_4.6H_2O$	18.0	Temperature:303K (30°C)
Na_2MoO_4	48.0	Anode : Nickel plate
$Na_3C_6H_5O_7$	105.0	Cathode: Copper
$CdCl_2$	1.0	c.d. range:1.0 - 6.0 Adm^{-2}
		pH = 9.0

Conventional electrodeposition of ternary Ni-Mo-Cd alloy coatings were carried out using DC power source (DC Power Analyzer, Aplab-LD3202) using optimal bath (Table 10.1).Same electrodeposition procedure, as used for binary alloys deposition was used. Ni-Mo-Cd coatings after deposition were washed in distilled water, and then air dried. The corrosion performances of ternary alloy coatings were evaluated in 5% NaCl at 303K by following the same procedure as discussed earlier. The corrosion rates (CR's) of all coatings were evaluated by Tafel's extrapolation method. For convenience, electrodeposited Ni-Mo-Cd coatings are represented as ED $(Ni\text{-}Mo\text{-}Cd)_x$ where 'x' is the current density at which deposition was carried out.

10.2.1 SEM Study

The surface morphology of ED (Ni-Mo-Cd)alloy coatings deposited at different c.d.'s (2.0-6.0 Adm^{-2}) was examined under SEM, and corresponding images are shown in Figure 10.3.It may be seen that homogeneity of the coating improved drastically with increase of the deposition c.d., *i.e*. from Figure 10.3(a) through Figure 10.3(c).

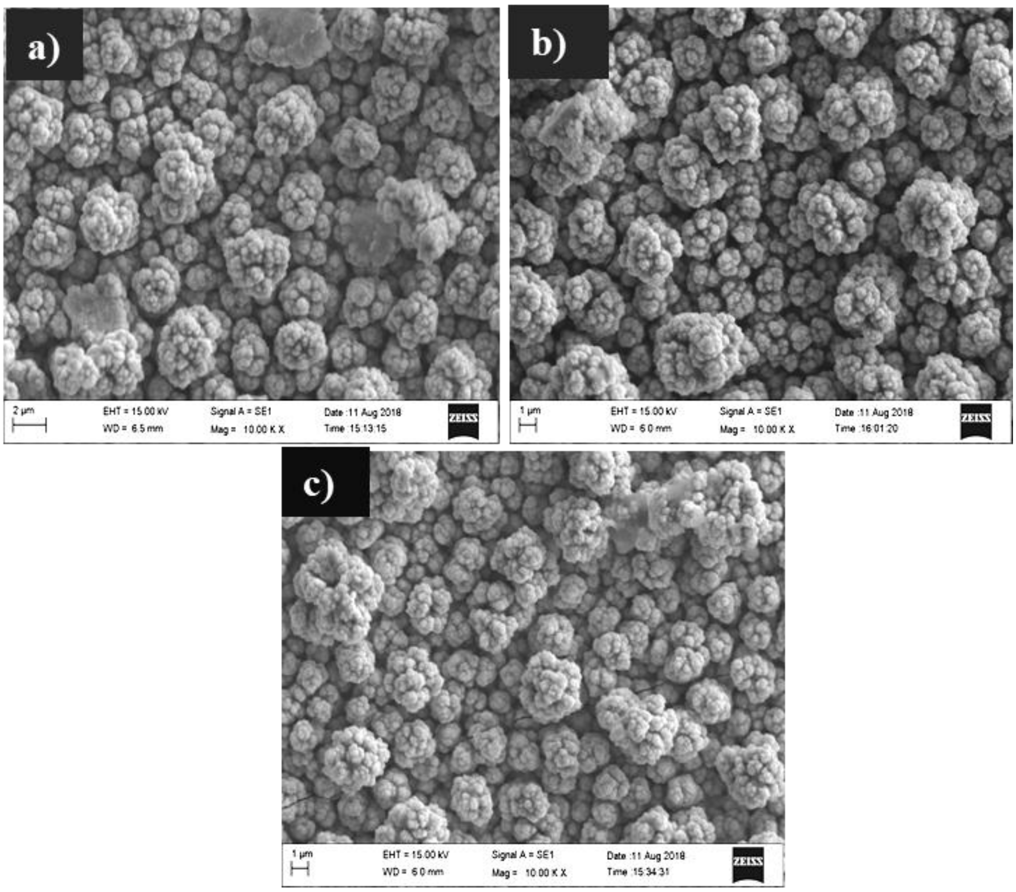

Figure 10.3- Surface morphology of different ternary alloy coatings deposited from the same bath:a) (Ni-Mo-Cd)$_{2.0\ Adm^{-2}}$*, b) (Ni-Mo-Cd)*$_{4.0\ Adm^{-2}}$*and c) Ni-Mo-Cd)*$_{6.0\ Adm^{-2}}$

Decrease in the homogeneity of coatings, with increase of c.d. is due to the effect of increased diffusion H^{+} ions towards the cathode. As the c.d. increased, diffusion of H^{+} ions leaves electrical double layer (EDL) region more acidic. This decrease of local pH, codeposition of Ni(OH)$_2$ is prevented, and consequently a relatively more uniform coating has formed(Brenner 2013). Thus the observed improvement in the homogeneity of ED (Ni-Mo-Cd) alloy coatings towards high c.d.is due to increased diffusion of H^{+} ions towards EDL, during deposition. Ternary (Ni-Mo-Cd) alloy coatings deposited at three c.d.'s are characterized by globular nodules as shown in

Figure 10.3. The size of the globular nodules decreased, as the c.d. increased from 2.0 Adm^{-2} to 6.0 Adm^{-2}.Hence, Alloy coating corresponding to 6.0 Adm^{-2} was found to be the most bright, uniform and homogeneous when compared to coatings of other c.d.'s

10.2.2 Composition Study

The composition of (Ni-Mo-Cd) alloy coating deposited at different current densities was analysed by Energy Dispersive X-ray (EDX) techniques. The metal contents of the ternary alloy at different c.d.'s is reported in Table 10.3.The Ni and Mo content of the binary Ni-Mo alloy coatings, corresponding to different c.d.'s are given in the brackets in Table 10.3, for comparison. From the composition data, it may be noted that wt.% of both Ni and Mo decreased drastically due to addition of cadmium into the bath.

Table 10.3-Composition of (Ni-Mo-Cd) ternary alloy coatings obtained at different current densities. The values given in bracket corresponding to binary Ni-Mo alloy (without Cd)

Coating configuration	wt.% of Ni	wt.% of Mo	wt.% of Cd
(Ni-Mo-Cd)$_{2.0A\ dm^{-2}}$	27.01(62.53)	5.42 (26.01)	60.82
(Ni-Mo-Cd)$_{4.0A\ dm^{-2}}$	17.14(65.18)	4.99 (25.5)	68.67
(Ni-Mo-Cd)$_{6.0A\ dm^{-2}}$	13.92(68.25)	4.41(24.54)	70.04

From the literature, it is well known that under normal condition ternary Ni-Mo-Cd bath follows normal type of codeposition with preferential deposition of more noble metal at lower limits of c.d. However, in the present bath (Table 10.1), concentration of $CdCl_2$ being very small (1g/L), the transition c.d. of Cd is too low. It may be recalled that transition current density is the current density at which the metal content of the deposit is same as that of bath (Brenner 1963). Hence increase of c.d. resulted in drastic increase of Cd content in the deposit by decreasing the noble metal content.

10.2.3 XRD Study

The change of phase structures of Ni-Mo-Cd alloy coatings with c.d. was examined by XRD technique. The XRD signals corresponding to (Ni-Mo-Cd)$_{2.0\ \mathrm{Adm}^{-2}}$,(Ni-Mo-Cd)$_{4.0\ \mathrm{Adm}^{-2}}$ and (Ni-Mo-Cd)$_{6.0\ \mathrm{Adm}^{-2}}$ coatings are shown in Figure 10.4.It may be noted that XRD peaks corresponding to (Ni-Mo-Cd)$_{2.0\ \mathrm{Adm}^{-2}}$, (Ni-Mo-Cd)$_{4.0\mathrm{Adm}^{-2}}$ and (Ni-Mo-Cd)$_{6.0\mathrm{Adm}^{-2}}$ coatings at 2θ = 43.3°, 50.4° and 89.8° represent tetragonal $\mathrm{MoNi_4}$ phase, corresponding to (211), (130) and (501) planes, respectively. They are in agreement with standard patterns of $\mathrm{MoNi_4}$ (JCPDS No. 03-065-1533). The plane (112) corresponding to added cadmium into the matrix. The grain size of the coatings was calculated using Debye -Scherrer equation (Anicai et al. 2013)(Chapter 6)**.**The XRD data analysis revealed that Ni-Mo-Cd alloy coating showed an mean grain size of 25nm.It is important to note that there is no change in the XRD patterns either with addition of Cd, or with increase of c.d.

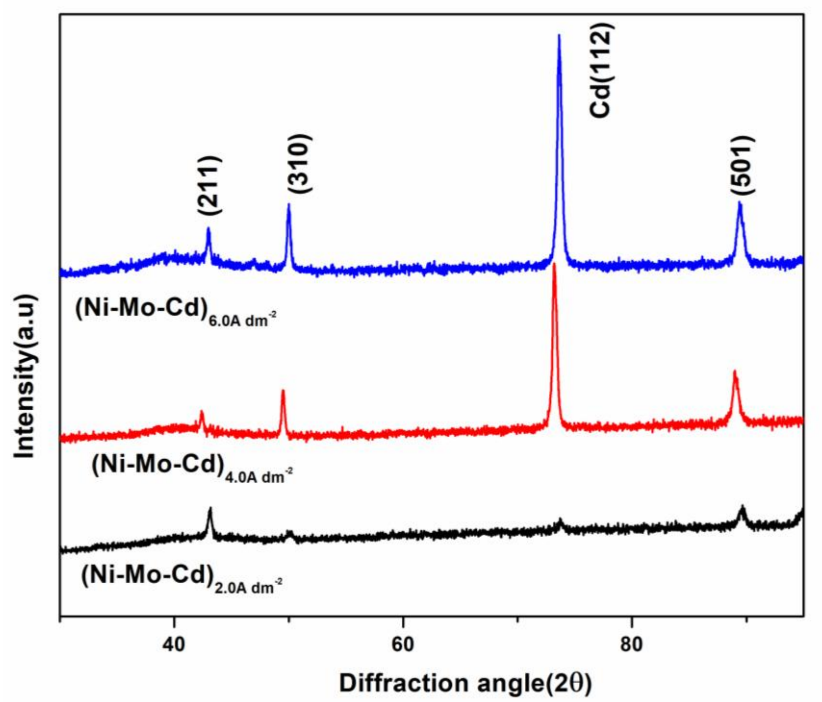

Figure 10.4- XRD patterns of Ni-Mo-Cd alloy coatings corresponding to (Ni-Mo-Cd)$_{2.0\ \mathrm{Adm}^{-2}}$, (Ni-Mo-Cd)$_{4.0\ \mathrm{Adm}^{-2}}$and (Ni-Mo-Cd)$_{6.0\ \mathrm{Adm}^{-2}}$ alloy coatings

This confirms the fact that ternary alloy forms of homogeneous solid solution of Ni, Mo and Cd in the range of composition studied. However, an increase of intensity of

XRD peak (112) is attributed to the increase of Cd content, or decrease of Ni and Mo content, affected due to addition of third salt into the bath.

10.2.4 AFM Study

The surface roughness of alloy coatings is an important parameter in relation to its performance as protective coatings against corrosion. In this regard, AFM is a powerful means to characterize the surface smoothness of coatings. Accordingly, a three dimensional AFM image of $(Ni\text{-}Mo\text{-}Cd)_{2.0\ Adm^{-2}}$ alloy and $(Ni\text{-}Mo\text{-}Cd)_{6.0\ Adm^{-2}}$ coatings are taken, and are shown in Figures 10.5(a) and (b), respectively. A significant improvement in the surface smoothness was seen when deposition c.d. is increased from 2.0 Adm^{-2} to 6.0 Adm^{-2}. Experimental data revealed that average roughness of $(Ni\text{-}Mo\text{-}Cd)_{6.0\ Adm^{-2}}$ alloy is decreased from 32.9 nm to 22.2 nm with increase of c.d, and is supported by visual observation as shown in Figure 10.5.

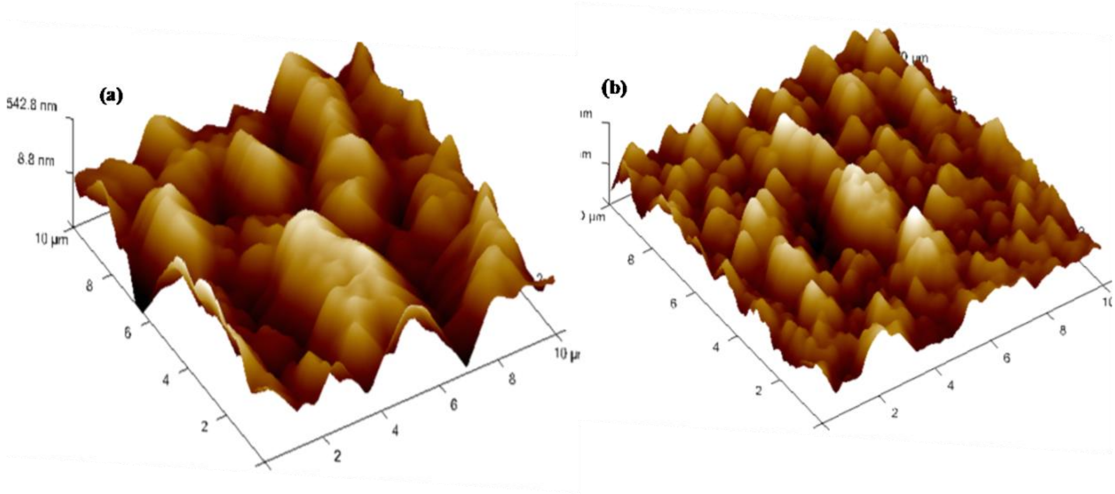

Figure 10.5- AFM image of (a) $(Ni\text{-}Mo\text{-}Cd)_{2.0\ Adm^{-2}}$ *and (b)*$(Ni\text{-}Mo\text{-}Cd)_{6.0\ Adm^{-2}}$ *alloy coatings*

10.2.5 Corrosion Study

Current density (c.d.) is the most important of all operating variables in electroplating, and no study of alloy deposition is complete without a detailed data on its variation. Moreover, the effect of c.d. is less consistent, or less predictable than that of the other operating variables, with respect to the composition of the alloy. A study on effect of c.d. on the composition of Ni-Mo-Cd alloy was undertaken, and their corrosion behaviours were evaluated.

10.2.5.1 Potentiodynamic polarization method

The electroplated coatings were subjected to the corrosion study in 5% NaCl medium. The corrosion rates were calculated by Tafel extrapolation method and values were reported as shown in the Table 10.4. A Tafel plot obtained at different current densities is as shown in the Figure 10.6. It may be noted that as the c.d. increased, corrosion rates decreased drastically. And values are listed in the Table 10.4.The composition data (Table 10.3) clearly indicates that the uniformity of ternary alloy coating increased with Cd content of the alloy. Thus from composition (Table 10.3) and corrosion data (Table 10.4), it may be inferred that ED(Ni-Mo-Cd)$_{6.0\ \mathrm{Adm}^{-2}}$ alloy coating showing the least CR is the most uniform, among all other coatings.

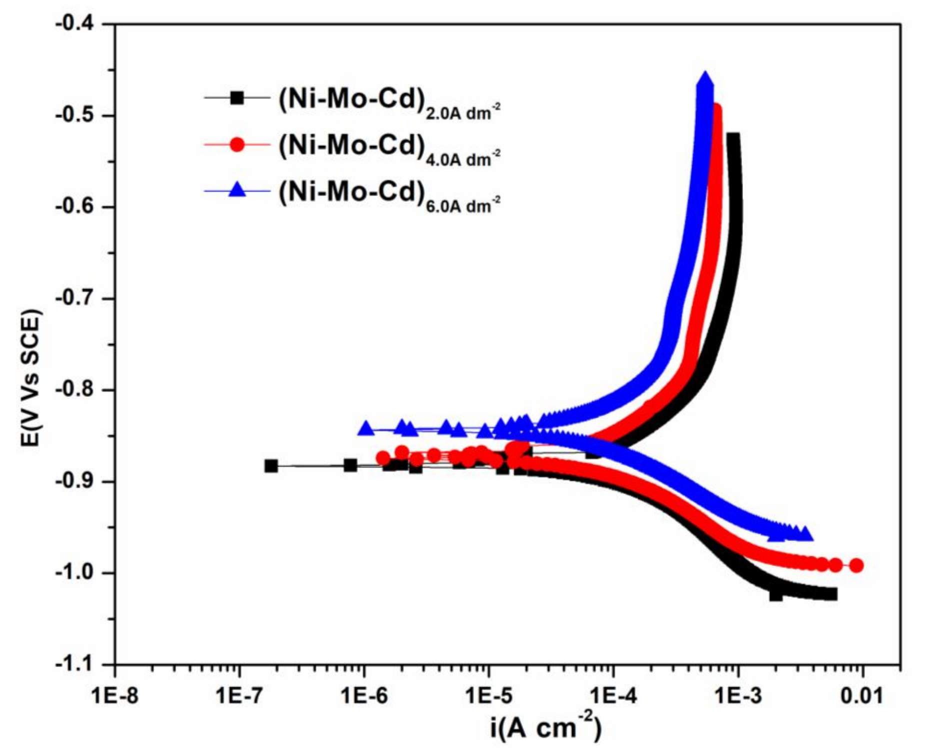

Figure 10.6-Potentiodynamic polarization behavior of Ni-Mo-Cd alloy coatings deposited at different c.d.'s deposited from optimized bath

Table10.4-Corrosion data of electrodeposited Ni-Mo-Cd alloy coating deposited at different current densities from the optimal bath

Coating configuration	$-E_{corr}$ (mV vs SCE)	i_{corr} (μA cm^{-2})	CR×10^{-2} (mm y^{-1})
$(Ni\text{-}Mo\text{-}Cd)_{2.0A\ dm^{-2}}$	880	21.6	24.4
$(Ni\text{-}Mo\text{-}Cd)_{4.0A\ dm^{-2}}$	870	11.1	16.5
$(Ni\text{-}Mo\text{-}Cd)_{6.0A\ dm^{-2}}$	840	11.0	15.4

Thus it may be summarized that on addition of small of amount of $CdCl_2$ into Ni-Mo bath, both Ni content and CR's of ternary alloy coatings decreased drastically, compare to optimal binary Ni-Mo alloy coating (Table 10.2). Further, both Ni content and CR's of ED Ni-Mo-Cd alloy coatings decreased with c.d.'s; and they reached the minimum value of 13.92 wt.% and 15.4 × 10^{-2} mm y^{-1},respectively at c.d.= 6.0 Adm^{-2}. Hence, 6.0 Adm^{-2} has been taken as optimal c.d. for further study of magnetoelectrodeposition.

10.2.5.2 Impedance study

The Nyquist response of Ni-Mo-Cd coating obtained at different current densities is as shown in the Figure 10.7.The impedance response having incomplete semi-circle of larger radius, corresponding to $(Ni\text{-}Mo\text{-}Cd)_{6.0\ Adm^{-2}}$ coating indicates that it is more corrosion resistant than other two coatings. This is compliance with least CR reported in Table 10.4.

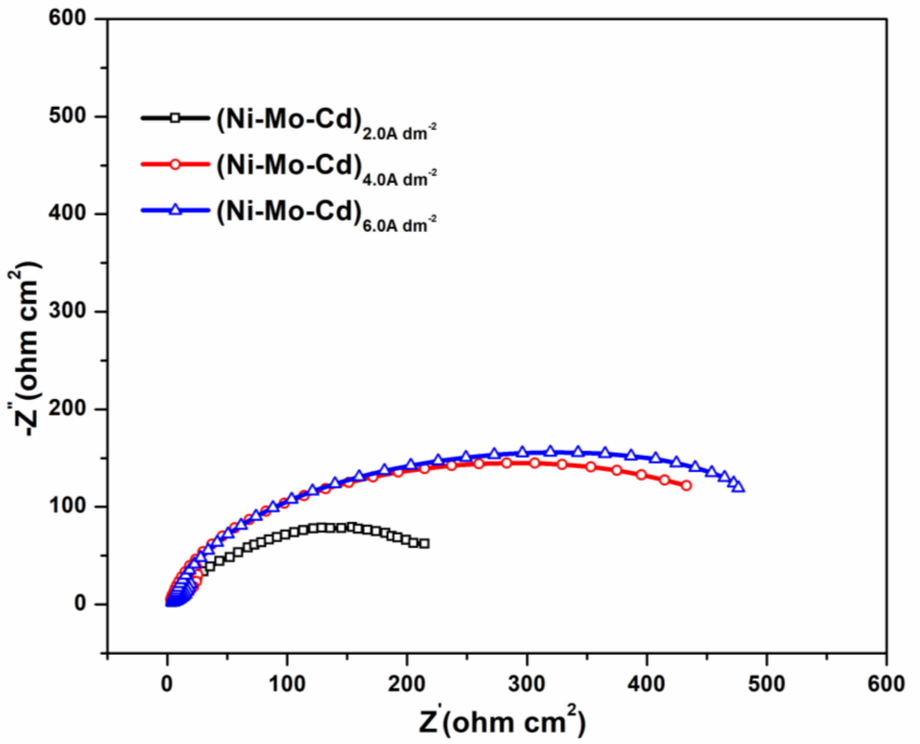

Figure 10.7-Nyquist responses of Ni-Mo-Cd alloy coatings having(Ni-Mo-Cd)$_{2.0Adm}$$^{-2}$, (Ni-Mo-Cd)$_{4.0\ Adm}$$^{-2}$, and (Ni-Mo-Cd)$_{6.0\ Adm}$$^{-2}$ *configurations*

10.3 MAGNETOELECTRODEPOSITION OF Ni-Mo-Cd ALLOY COATINGS

10.3.1 Introduction

The deposition of a metal or an alloy by electric current in conjunction with an applied magnetic field is known as magneto electrolytic deposition, or magnetoelectrodeposition (MED)(Fahidy 1983, 2001; Tacken and Janssen 1995).The introduction of magnetic field into the electrochemical reactions may lead to potential applications, and it is used as a powerful scientific tool in electrochemical reaction kinetics(Chia-Chien and Chou 1995).During electrolysis with superimposed magnetic field, a force acts on the migration of ions and induces a convective flow of electrolyte close to the electrode surface, and is governed by magnetohydrodynamic (MHD) effect.MHD effect is a physical phenomenon describing the motion of a conducting fluid (electrolyte) under the influence of an external magnetic field. The MHD convection enhances the mass transport of ionic species and changes the electrode interfacial conditions, such as the surface pH and the ionic adsorption. Natural and forced convections are important influential parameters effecting the process and properties of the electrodeposited coatings(Rabia et al. 2011). Natural convection is highly dependent on the geometric configuration of the working electrode, while stirring, rotating disc or induction of magnetic field onto the electrolytic cell are root causes of forced convection (Levesque et al. 2009). When an electric conductor flows across a magnetic field, a voltage is induced in it which produces and electric conductor; and the effect is the result of Faraday laws of electromagnetic induction. The induced EMF is given by E = $qv \times B$, where q and v are charge and velocity of the particles involved, respectively and B is the strength of magnetic field. Thus entire electromagnetic force F acting on the charged particle q moving in velocity v is through an electric field E and magnetic field B is given by Lorentz force(Bund and Ispas 2005),

$$F = q(E + v \times B) \ldots\ldots\ldots\ldots\ldots. (10.1)$$

The first term is contributed by the electric field, and the second term is the magnetic force, and has a direction perpendicular to both the velocity and the magnetic field. The magnetic force is proportional to q and to the magnitude of the vector cross product $v \times B$. In terms of the angle θ between v and B, the magnitude of the force equals qvB sin θ. When electrical field is perpendicular to B (i.e., with the angle θ between v and B of 90°), the particle will follow a circular trajectory with a radius of $r = mv/qB$. If the angle θ is less than 90°, the particle orbit will be a helix with an axis parallel to the field lines. If θ is zero, there will be no magnetic force on the particle, which will continue to move un-deflected along the field lines.

Therefore the largest MHD effect is achieved with the magnetic field oriented perpendicular to the direction of current (i.e., when the external magnetic field is oriented parallel to the electrode surface).On the contrary, when a magnetic field is applied parallel to the direction of current, Lorentz force is zero. Thus magneto hydrodynamic phenomena arise from the interaction of velocity fields with electromagnetic fields, and interesting Lorentz force is applicable to the motion of a charged particle in a uniform magnetic field(Tacken and Janssen 1995b). Besides Lorentz force, other magnetically induced forces are the magnetic gradient force and the paramagnetic force. These gradient forces depend on the magnitude of the magnetic field instead of its direction(Ebadi et al. 2010). The Lorentz forces affect significantly the usual diffusion controlled process by increasing the mass transport effect of the ions. Hence, superimposition of a magnetic field parallel to process of electrodeposition of metals and alloys can bring significant modifications on the process and properties of the deposit such as morphology, crystal texture etc.(Rabah et al. 2004; Rao et al. 2013).

As discussed in the Section 10.2, it is well known that among Ni-based alloys, Ni-Mo shows good anticorrosion behaviour, mechanical and thermal stability(Goveas et al. 2018) , by following peculiar induced codeposition mechanism with only slight variation of both noble (Ni) and reluctant (Mo) with cathodic current density (c.d.)(Brenner 1963). Our preliminary study on Ni-Mo alloy coating demonstrated that when a small amount of cadmium (Cd) is added into the bath, a significant improvement in the corrosion resistance of its ternary coating was found. Further, their CR's were found to be decreased with increase of c.d., despite the decrease of noble metal content in the deposit.

10.3.2 Magnetic Field Induced Discussion

In electroplating, mass transport resistance is the most important factor responsible for the composition of coatings. The mass transport resistance results from the depletion of the electro-active species at the cathode surface due to mass transport limitation. For simple linear diffusion, under limiting condition, the rate of mass transport is governed by the limiting current density (i_L), and is given by Eqn. 10.2(Kanani 2004).

$$i_L = \frac{nFD_z C_B}{\delta} \dots\dots\dots\dots\dots\dots\dots\dots\dots (10.2)$$

The i_L represents the highest rate at which the metal can be deposited under given experimental conditions. Therefore from Eqn. (10.2), it may be inferred that for a given electrolytic bath, i_L of metal can be increased by decreasing the thickness (δ) of EDL, which can be accomplished by imparting MHD effect in the bath, and is shown representatively in Figure 10.8a.

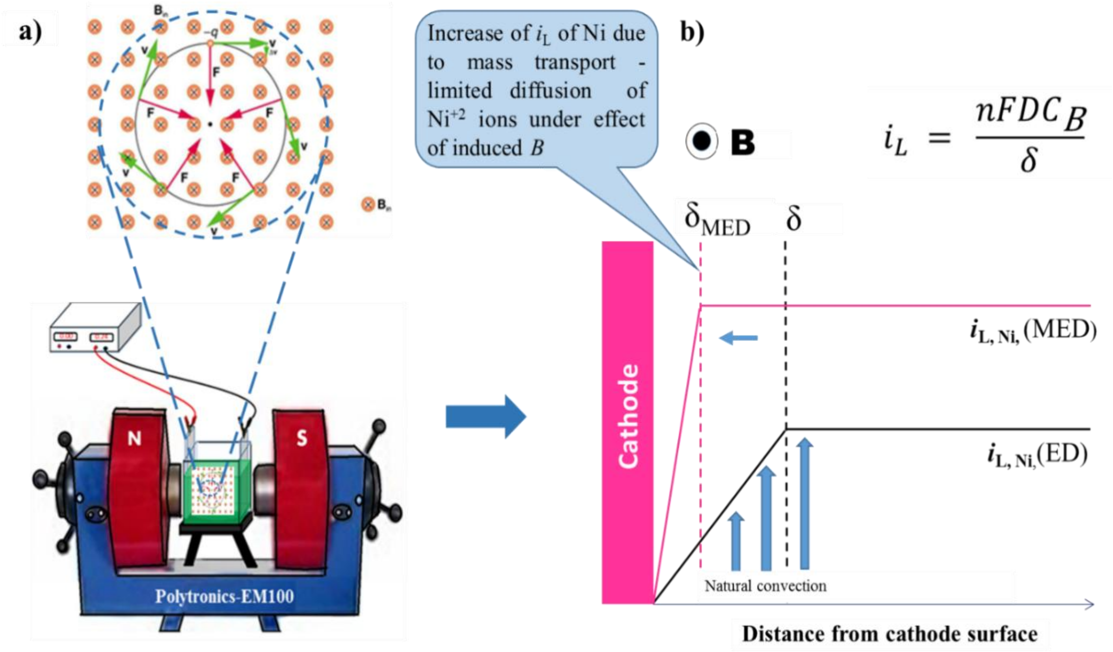

Figure 10.8- The experimental set up used for magnetoelectrodeposition of Ni-Mo-Cd alloy coatings under effect of B, showing: a) MHD effect inside the bath a), and diffusion-limited c.d. of Ni^+ *ions under conditions of natural (ED), and b) (natural + MHD effect) MED convection, responsible for reducing the thickness of EDL, and increase of* (i_L) *of Ni*

The concentration profile corresponding to diffusion-controlled mass transfer of Ni^{+2} ions during electrodepositon Ni-Mo-Cd alloy coatings, under conditions of ED (under natural convection) and MED (under natural convection + MHD effect) is shown in Figure 10.8 b. Having driven by the objective of increasing the anticorrosion performance of ternary Ni-Mo-Cd alloy coatings by taking the advent of magnetoelectrolysis; and with incentive of composition data of ED $(Ni\text{-}Mo\text{-}Cd)_{6.0\ Adm^{-2}}$ having only 13.92 wt. % Ni in the deposit, the MED coatings were tired to develop using same electrolytic bath (Table 10.1). Hence, Ni content of Ni-Mo-Cd alloy coating was tried to increase by increasing the limiting current density (i_L) of Ni, under condition of artificial convection of magnetohydrodynamic (MHD) effect, coupled with natural convection. Hence, MED Ni-Mo-Cd alloy coatings were developed by selecting 6.0 Adm^{-2} as the optimal c.d. for deposition.

10.3.3 MED of Ni-Mo-Cd Alloy Coating

As corrosion performance of alloy coatings is generally a function of its noble metal content, an attempt was made to increase the corrosion resistance of Ni-Mo-Cd alloy coating by increasing its Ni content, using the advent of magnetic field effect. Therefore, this section reports the effect of magnetic field, *B* on composition and corrosion resistance of Ni-Mo-Cd alloy coatings. The observed drastic decrease of corrosion rates (CR's) in MED (Ni-Mo-Cd) alloy coatings were discussed in the light of diffusion controlled mass transfer Ni^{+2} ions under effect of *B*. The Ni content of the deposit was found to be increased with intensity of *B* (both parallel and perpendicular) due to the combined effect of natural convection and Lorentz force. Emphasis was given to study effect of *B* on composition, surface morphology, phase structures and corrosion stability using different experimental techniques.

The experimental set up used for magnetoelectrodeposition of (Ni-Mo-Cd) alloy coatings is shown in Figure 10.9. The magnetoelectrodeposited (MED) coatings were developed under different intensity of *B*, from 0.1 to 0.4 T (Tesla), using same c.d. = 6.0 A dm^{-2}. The optimal c.d. = 6.0 A dm^{-2} was arrived based on the least CR of Ni-Mo-Cd alloy coating, deposited from bath. Electromagnet (Polytronics, Model: EM 100) and DC power source were used to source of magnetic field and electric field, respectively during magnetoelectrodeposition. MED coatings were deposited under different intensities of *B,* with respect to the plane of cathode. All depositions were carried out in a custom made glass setup of 400 mL capacity, using pre-cleaned copper plate. The cathode and anode were placed parallel at 5 cm distance, during deposition. All depositions were carried out for same duration of 10 min, at room temperature (303K) for comparison purpose. The ED and magnetoelectrodeposited (MED) were washed using distilled water, followed by air drying.

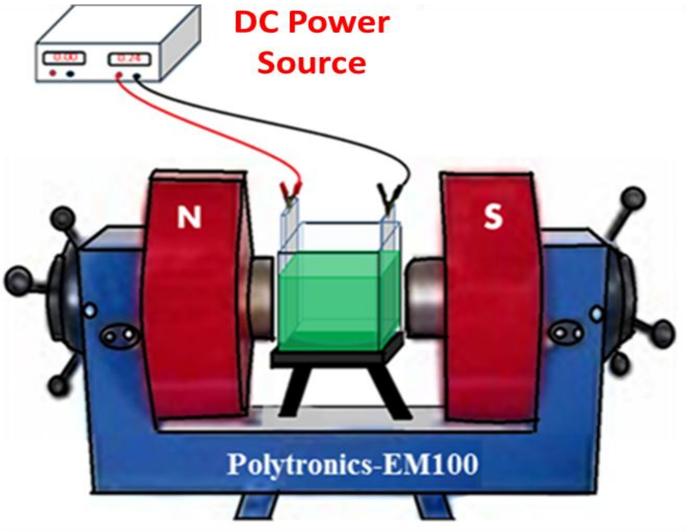

Figure 10.9- Experimental set up used for magnetoelectrodeposition of Ni-Mo-Cd alloy coating under effect of both electric and magnetic field, B (parallel)

The corrosion performances of ED and MED coatings were evaluated in 5% NaCl at 303K by electrochemical AC and DC methods using Potentiostat/Galvanostat (VersaSTAT^3, Princeton Applied Research). Electroplating specimen was used as the working electrode, and platinum electrode as counter electrode, and saturated calomel electrode (SCE) as the reference electrode. The electrochemical impedance spectroscopy (EIS) study was made in the frequency range of 100 kHz -10 mHz using a perturbing voltage of ±10 mV. No DC potential was applied during the EIS measurements. The potentiodynamic polarization study was carried out at scan rate of 1 mV s^{-1}, in a potential ramp of ±250 mV from OCP. The corrosion rates (CR's) of all coatings were evaluated by Tafel's extrapolation method. For convenience, electrodeposited Ni-Mo-Cd coatings are represented as ED $(\text{Ni-Mo-Cd})_x$ where 'x' is the current density at which deposition was carried out; and Magnetoelectrodeposited Ni-Mo-Cd coatings are represented as MED $(\text{Ni-Mo-Cd})_{y,\,z}$ where 'y' represents the intensity of *B*, and 'z' stands for orientation of cathode plane (whether parallel, or perpendicular) to the direction of *B.*

10.3.4 Effect of Induced Magnetic Field

MED coatings were developed at different conditions of *B*, in both direction (parallel and perpendicular) and intensity (from 0.1 T to 0.4 T), using same bath. The composition and corrosion data of MED coatings corresponding to different conditions of both direction and intensities of *B* are tabulated in Table 10.5. It may be noted that wt. % Ni in the deposit (in both parallel and perpendicular) has increased drastically with growing strength of *B*, upto 0.3 T, and then started decreasing. This behaviour of MED coatings may be explained by two reasons(Brenner 1963):i)Generally during electrodeposition of alloys, more noble metal is depositing first at its limiting c.d., and other metals will be deposited below this limiting c.d. density, and ii) percentage of the more readily depositable metal is increases by any alteration of the plating conditions such as increasing the agitation, temperature, or concentration of the bath that tends to oppose the depletion of metal ion in the cathode diffusion layer. In the present MED coating, electromagnetic force *F* acting on moving ions (Ni^{+2}) opposes the depletion of Ni^{+2} ions at cathode film. Hence, Ni content of the alloy increases with intensity of *B*(in both parallel and perpendicular). Thus, as the intensity of *B* increased, i_L of Ni increased, to squeeze the thickness of EDL more and more. Therefore, at $B = 0.3$ T, Ni content of the coating reached its highest value, corresponding to its $i_{L,}$ indicating that rate of deposition is maximum, and this stage is called diffusion-limited, or mass-transport-limited current density.

Thus increase of Ni content with strength of *B* is due to increase of i_L of Ni, following the principle of diffusion controlled mass transfer of Ni ions at the cathode film. Increase in i_L of Ni during MED (natural convection + MHD effect), in relation its value during ED (natural convection) is shown in Figure 10.8 b. The decrease of EDL thickness (δ), due to increase of $i_{L,}$ may also be noted, as same bath was used for both ED and MED coating. However, decrease of Ni content at high intensity of *B* (in both parallel and perpendicular) is reasoned by fact that, as magnetoelectrodeposition of any metal is limited by the rate at which (convection + MHD) effect can supply the ions to the cathode. Therefore, once Ni has attained its limiting value (i_L, MED), any intensity more than its optimal is applied, some new electrode reactions other than metal deposition can take place, like liberation of $H_{2.}$ This liberation hydrogen gas on cathode results in the decrease of Ni content in the alloy. Hence, Ni content of MED $(Ni\text{-}Mo\text{-}Cd)_{0.4T}$ coatings, of both parallel and perpendicular field effect is less than those corresponding to $B = 0.3$T.

Table 10.5- Corrosion data of MED (Ni-Mo-Cd) alloy coatings under different conditions of magnetic field effect, in relation to its electrodeposited (ED) coatings, deposited from the same bath

Coating configuration	wt.% of Ni	wt.% of Mo	wt. % of Cd	$-E_{Corr}$ (mV Vs SCE)	i_{corr} (μAcm^{-2})	CR×10^{-2} (mm y^{-1})	R_{ct} (Ohm)
ED (Ni-Mo-Cd)$_{6.0\ Adm^{-2}}$	13.92	4.41	70.04	840	11.0	15.4	418
Effect of parallel B							
MED (Ni-Mo-Cd)$_{0.1T/Par}$	28.42	4.61	57.15	810	8.4	10.8	1050
MED (Ni-Mo-Cd)$_{0.2T/Par}$	33.79	4.23	49.91	690	3.6	5.2	1170
MED (Ni-Mo-Cd)$_{0.3T/Par}$	41.12	2.23	44.90	620	2.1	2.7	1733
MED (Ni-Mo-Cd)$_{0.4T/Par}$	36.20	4.33	49.51	600	2.2	2.9	1598
Effect of perpendicular B							
MED(Ni-Mo-Cd)$_{0.1T/Per}$	38.33	3.07	50.91	510	1.2	1.7	2700
MED(Ni-Mo-Cd)$_{0.2T/Per}$	52.89	2.32	39.06	470	1.1	1.6	3978
MED (Ni-Mo-Cd)$_{0.3T/Per}$	59.34	2.15	34.04	420	0.5	0.7	6578
MED(Ni-Mo-Cd)$_{0.4T/Per}$	56.19	2.82	35.07	430	0.8	1.2	4990

Hence, it may be summarised that alloy coatings corresponding to MED (Ni-Mo-Cd)$_{0.3T/Par}$ and (Ni-Mo-Cd)$_{0.3T/Per}$ configurations showed the least CR's (2.7 ×10^{-2} mm y^{-1}and 0.7 ×10^{-2} mm y^{-1}) with having maximum Ni content (41.12 wt. % and 59.34 wt.%), respectively as shown in Table 10.5.Hence, it may be inferred that 0.3 T is the optimal intensity of *B* (both parallel and perpendicular) for development of the most corrosion resistant MED Ni-Mo-Cd alloy coatings from the optimal bath. However, lower CR of MED (Ni-Mo-Cd)$_{0.3T/Per}$ coating, compared to MED(Ni-Mo-

$Cd)_{0.3T/Par}$ coating may be attributed to the increased convection effect(Peipmann et al. 2010b), corresponding to Lorentz force in Eqn. (10.1).

10.4 CHARACTERIZATION OF MED (Ni-Mo-Cd) COATINGS

10.4.1 XRD Study

XRD technique was used to understand the change in phase structure and crystallinity of MED coatings. The XRD patterns of MED (Ni-Mo-Cd) coatings developed under induced *B*, both parallel and perpendicular at different intensities (from 0.1- 0.4T) are shown in Figures 10.10 and 10.11, respectively.

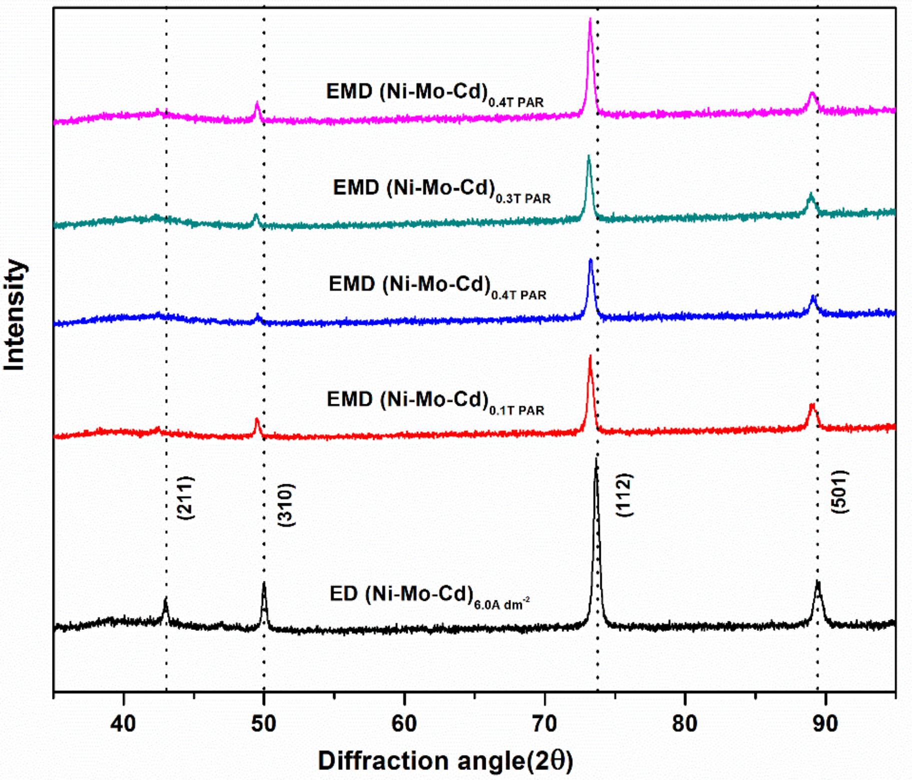

Figure 10.10 - XRD patterns of MED Ni-Mo-Cd alloy coatings deposited at different intensity of B(parallel) from the optimal bath: 0.1 T, 0.2 T,0.3 T and 0.4 T

The XRD patterns corresponding to ED coating represented as ED $(Ni\text{-}Mo\text{-}Cd)_{6.0\ Adm^{-2}}$ is also shown for comparison purpose. It may be noted that all most same type of XRD patterns were demonstrated by MED coatings, regardless of the direction and intensity of *B*. The characteristic diffraction peaks of all MED coatings (parallel and perpendicular), observed at 2θ = 43, 51°, 74° and 89°, corresponds to (211), (310), (202), (112), and (501) planes, respectively. Though there are many reports in the literature stating the significant change in the phase structure and crystallinity of MED coatings, in relation to ED coatings, our present study is not demonstrating any such changes in either in intensity or diffraction angles of XRD patterns, as may be seen in Figure 10.10 and 10.11.

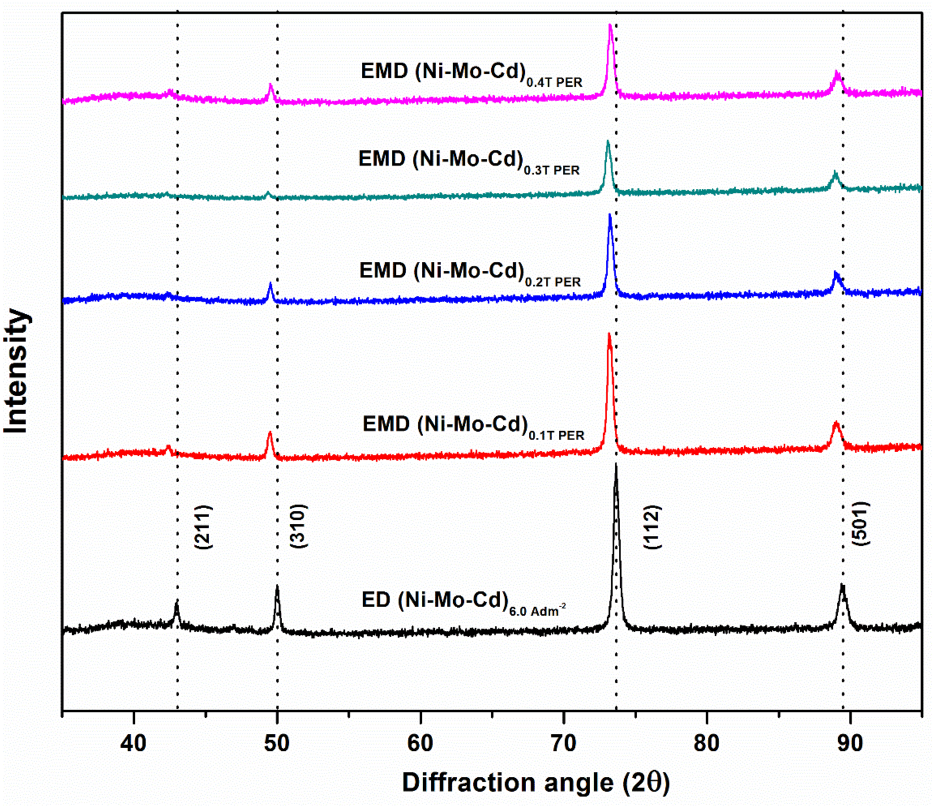

Figure 10.11- XRD patterns of MED Ni-Mo-Cd alloy coatings deposited at different intensity of B(perpendicular) from the optimized bath: 0.1 T, 0.2 T, 0.3 T and 0.4 T

The constant diffraction angle in XRD patterns of all Ni-Mo-Cd alloy coatings (both ED and MED) may be attributed to the high c.d. (6.0 Adm^{-2}) employed for electrodeposition, as the driving force for charge transfer. This is supported by fact that superimposed *B* is effective on crystallographic orientation of magnetoelectrodeposited coatings only under certain conditions of electrolyte media and applied c.d.(Brillas et al. 1999).Further, using X-ray diffraction (XRD) study Chiba et al. have concluded that the magnetic field could modify the crystal growth orientations in relation to the easy magnetization axis, and field effect is dominant at low current densities where the magnetic field effect dominates over that of the electric field(Chiba et al. 1986) .No distinct difference was observed with or without magnetic field while the crystal texture was found to be controlled by the magnetic field (Matsushima et al. 2007).Therefore, it is important to note that change in the crystallinity of MED coatings are more likely only under situation where magnetic field dominates the electric field. Since deposition c.d. is used in the present MED coating is as high as 6.0Adm^{-2}, the induced *B* is not good enough to bring change in phase structures of the coatings. Hence, XRD patterns of all MED coatings, irrespective of the direction and intensity of *B* demonstrated same diffraction peaks as ED coatings, as shown in Figure 10.10 and 10.11. The constancy of XRD peaks of Ni-Mo-Cd alloy coatings, developed with or without magnetic field *B* indicates that the crystal texture is controlled by the magnetic field. This is evidenced by increase of Ni content in the deposit with increase of intensity of *B*. Thus the constancy of diffraction angles, in XRD patterns of all Ni-Mo-Cd alloy coatings (both ED and MED may be attributed to the high c.d. (6.0 Adm^{-2}) employed for electrodeposition. Thus it may be inferred that crystal texture of all MED Ni-Mo-Cd coatings controlled by the induced magnetic field, at the c.d. selected for deposition. Further, a slight shift of XRD peaks towards lower angle was observed, in both parallel and perpendicular *B* (Figure 10.10 and 10.11), which increased with intensity of *B*. It may be attributed to residual stress inside the crystal lattice, or due to the difference in ionic radii between the main element and the dopant ion, affected during process of deposition (Cullity 1956).

10.4.2 Corrosion Study

Two electrochemical methods were used to assess the corrosion performances of ternary alloy coatings, namely electrochemical polarization and electrochemical impedance spectroscopy (EIS) methods, and are explained below with representative plots.

10.4.2.1 Potentiodynamic polarization Study

The potentiodynamic polarization behaviour of MED Ni-Mo-Cd alloy coatings, developed at different intensity of *B*(both parallel and perpendicular). The CR’s of MED coatings were evaluated by Tafel’s extrapolation method, and corresponding data are reported in Table 10.5. It may be seen that CR's of MED Ni-Mo-Cd alloy coatings is substantially less, compared to ED coatings deposited from the same bath (Table 10.1). Further, it may be noted that decrease of CR is in proportion of intensity of *B*, off course up to 0.3T indicating the effect of induced *B* in taking the Ni towards its diffusion limited c.d. The potentiodynamic polarization behaviour of MED Ni-Mo-Cd alloy coatings, developed at different intensity of *B* in parallel and perpendicular are given in Figure 10.12 and10.13 respectively.

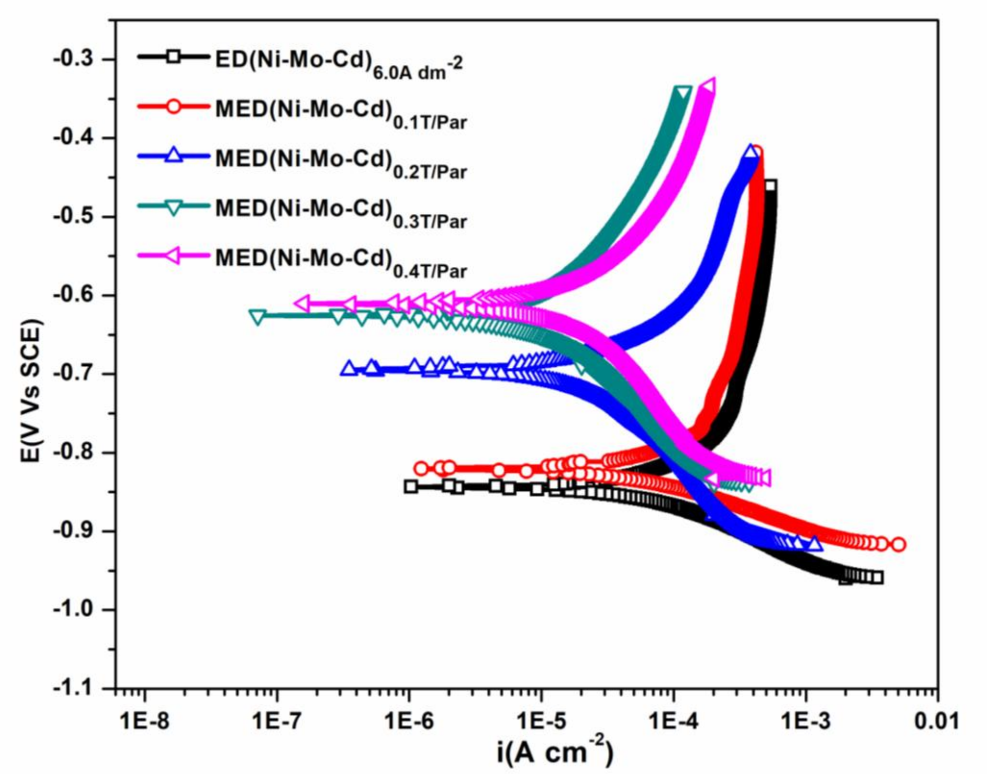

Figure 10.12- Potentiodynamic polarization behaviour of MED Ni-Mo-Cd alloy coatings deposited under different conditions of induced B (Parallel), in relation to ED coating deposited from same bath

The decrease of CR's with increase of induced *B* may be clearly seen from the nature of anodic and cathodic curves. In addition, E_{corr} values were found to be shifted towards nobler side (Figure 10.12 and 10.13), stamping the fact that corrosion protection efficacy of MED coatings are increased with intensity of *B*.

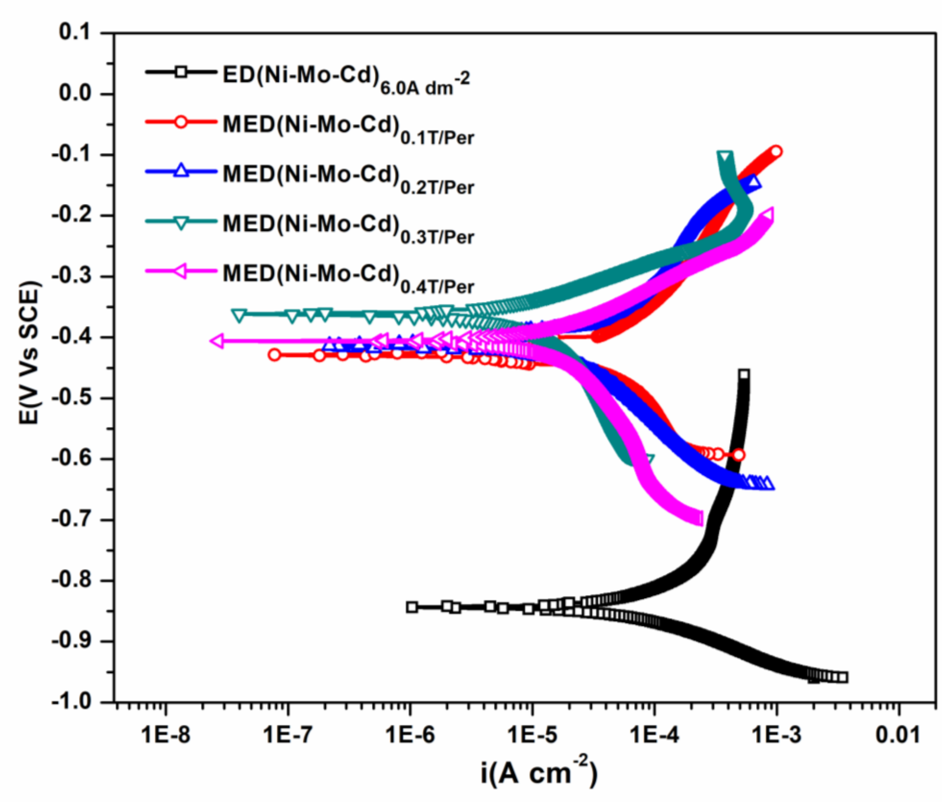

Figure 10.13- Potentiodynamic polarization behaviour of MED Ni-Mo-Cd alloy coatings deposited under different conditions of induced B (Perpendicular), in relation to ED coating deposited from same bath

10.4.2.2 Electrochemical Impedance study

EIS method is a very popular technique to acquire the valuable information in understanding the electrodic reactions, like double layer capacitance, role of inhibitors to controlling the corrosion etc. The impedance response of MED (Ni-Mo-Cd)$_{Par}$ and (Ni-Mo-Cd)$_{Per}$ coatings deposited at different intensities of *B*, in relation to ED coating from same bath is shown in Figures 10.14 and 10.15 respectively. The ECE circuit fitment for (Ni-Mo-Cd)$_{0.3T/Para}$ and(Ni-Mo-Cd)$_{0.3T/Per}$ is given in inset of Figures10.14 and 10.15 respectively. And corresponding charge transfer resistant (R$_{ct}$) values for all deposited coatings were listed in Table 10.5

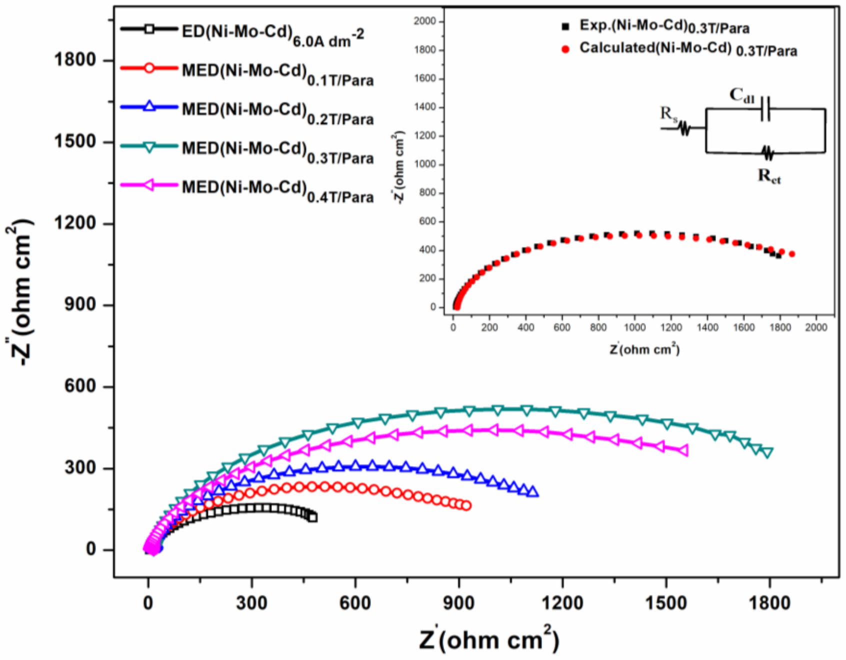

Figure 10.14- Electrochemical impedance response of MED Ni-Mo-Cd alloy coatings deposited under different conditions of induced B (Parallel), in relation to ED coating deposited from same bath

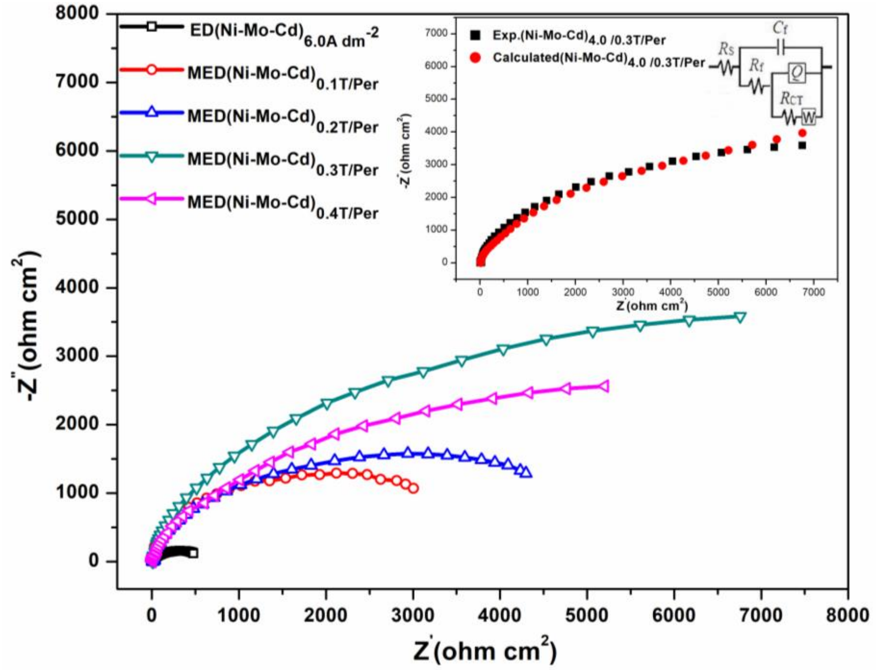

Figure 10.15- Electrochemical impedance response of MED Ni-Mo-Cd alloy coatings deposited under different conditions of induced B (Parallel), in relation to ED coating deposited from same bath

It may be noted that all coatings exhibited incomplete depressed semicircle, with consistent increase in the value of charge transfer resistance (R_{ct}), with the intensity of *B*. The axial radius of the semicircle is found to be increased with intensity of *B*, indicating that induced *B* has increased the Ni content of the alloy coatings (Table 10.5), and hence its corrosion stability.

10.4.3 SEM Study

The SEM images of MED Ni-Mo-Cd coatings conducted at different field intensities, *B*= 0.1, 0.2, 0.3and 0.4T (both parallel and perpendicular) is shown in Figures 10.16 and 10.17, respectively.

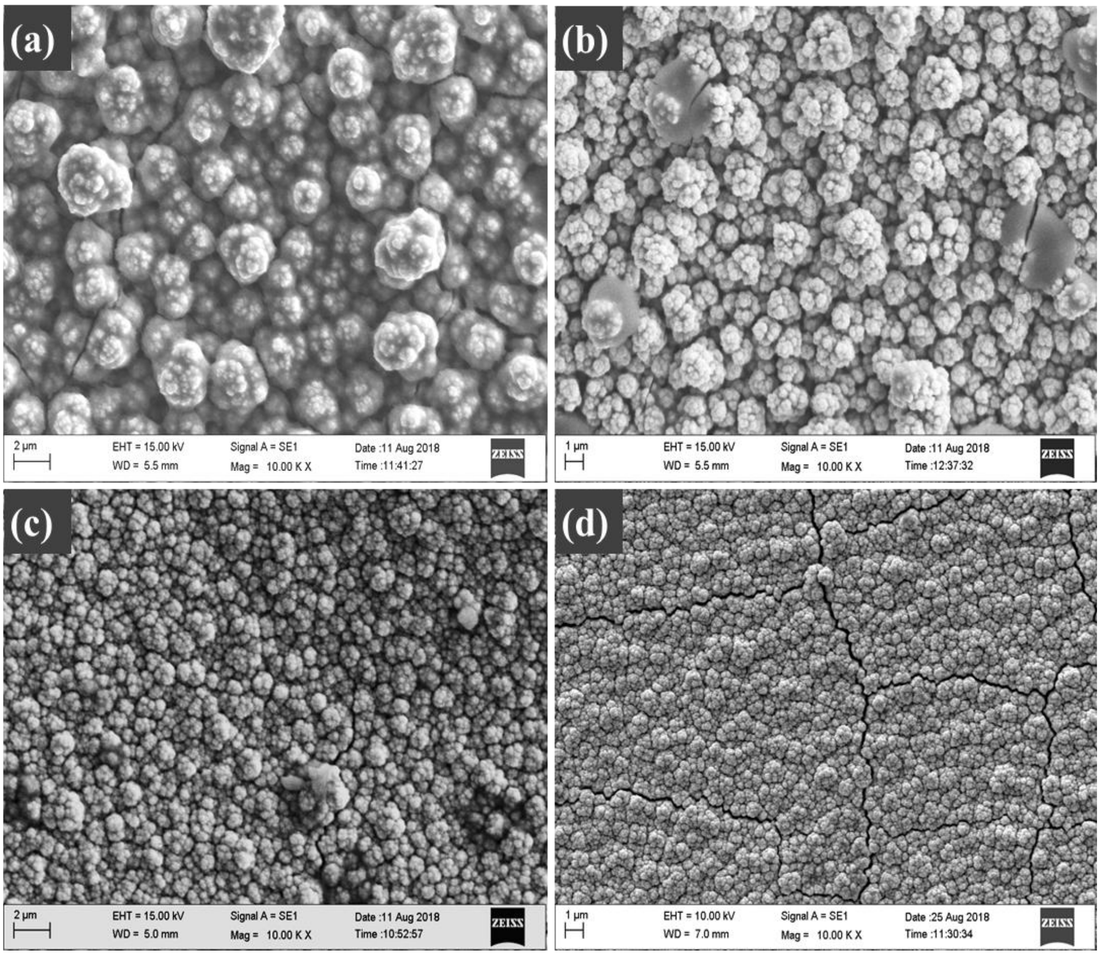

Figure 10.16-SEM images of MED Ni-Mo-Cd alloy coatings deposited at different intensity of B (parallel) from the optimized bath: (a) 0.1 T, (b) 0.2 T, (c) 0.3 T and (d) 0.4 T

A striking morphological variation was found as the intensity of *B* is changed from 0.1 T to 0.4 T, in both parallel and perpendicular field. The coatings became more smooth and fine-grained on superimposition of *B*, which further improved with intensity of *B* in both parallel and perpendicular field. The nodular structure of coatings started to change into more uniform coating, in both parallel and perpendicular *B* as shown in Figures 10.16 and 10.17. There are many reports documented in the literature that in electrodeposition, surface morphology of the coatings can be modified by induction of *B*.

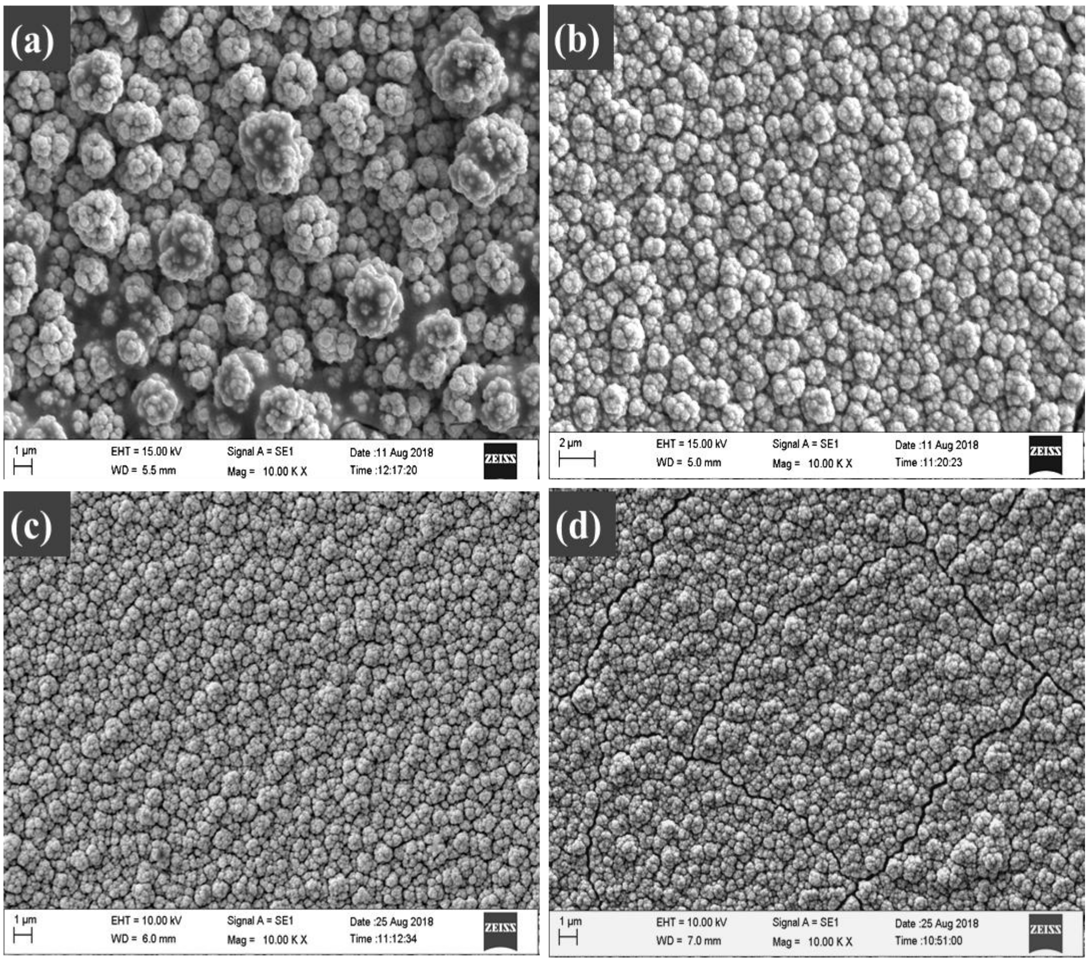

Figure 10.17- SEM images of MED Ni-Mo-Cd alloy coatings deposited at different intensity of B(perpendicular) from the optimized bath: (a) 0.1 T, (b) 0.2 T, (c) 0.3 T and (d) 0.4 T

The change in morphology of MED coatings with intensity of *B* is reasoned by two factors (Uhlemann et al. 2005): i) Induced *B* is acting on the ions in the electrolyte to generate an additional convection to form more nuclei, and to reduce rate of nucleation. Thus observed improvement in uniformity of MED coatings with increase of intensity of *B,* in Figures 10.16 and 10.17 may be attributed to the increased rate of nucleation, affected due to increased MHD effect. ii) Electroplating is usually overlapped by the reduction of hydrogen ions during reduction of less noble metal ions. This normally leads to a large increase of the pH value close to the electrode surface and to a change of the deposition behaviour and the properties of the deposits. But the enhanced convection, due to induced *B* increases the mass transport of electroactive species towards the electrode, alongside the H^+ ions from bulk solution. Under above possibility, it is expected that the hydrogen evolution reaction is affected similarly and consequently pH close to the surface is influenced(Monzon and Coey 2014b). Therefore, when intensity of *B* is increased, more H^+ ions have diffused towards cathode surface, and decreased the pH at EDL. This decrease of pH at cathode solution interface reduced the possibility of codeposition of $Ni(OH)_2$, responsible for non-uniform deposition, like in Figures 10.16(a) and 10.17(a). Therefore, the uniformity of coatings improved as the intensity of *B* increased (in both parallel and perpendicular) as seen in Figures 10.16 and 10.17 (from a through d). Thus it may be summarised that gradual improvement in the uniformity of MED coatings with increase of intensity of *B* (both parallel and perpendicular) may be attributed to the gradual increase in the rate of nucleation, and decrease of local pH (due to more diffusion of H^+ ions) on the surface of cathode, due to gradually increasing Lorentz force.

However, micro-cracks observed on the coatings, corresponding to $B = 0.4$ T, in both Figures 10.16 and 10.17 may be attributed to the internal stresses, resulting from liberation of hydrogen, after attainment of i_L Ni. Thus, surface morphology of the optimal coatings, under condition of both parallel and perpendicular *B*, *i.e.,* correspond to MED $(Ni\text{-}Mo\text{-}Cd)_{0.3T/Par.}$ and MED$(Ni\text{-}Mo\text{-}Cd)_{0.3T/Per.}$ are shown in Figures 10.16(c) and 10.17(c) respectively.

10.4.4 AFM Analysis

The three dimensional AFM image of MED (Ni-Mo-Cd)$_{0.3T/Par,}$ and MED(Ni-Mo-Cd)$_{0.3T/Per}$ coatings are taken, and are shown in Figure 10.18(a) and (b), respectively. The surface roughness is an important parameter in relation to the corrosion of coatings. In this regard, AFM is a powerful technique to support the surface smoothness, and hence AFM image of representative coatings was taken.

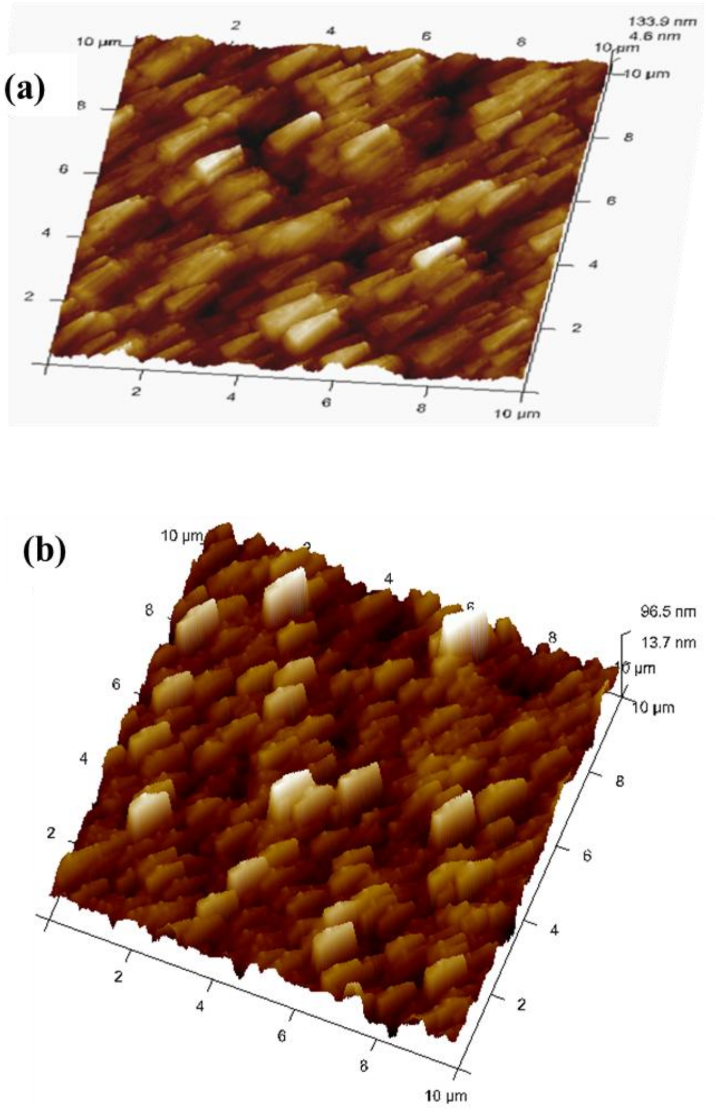

Figure 10.18- Comparison of AFM image of MED coatings: (a) MED (Ni-Mo-Cd)$_{0.3T/Par}$ and MED (Ni-Mo-Cd)$_{0.3T/Per}$ alloy coatings deposited from same bath

Accordingly, AFM image corresponding to (Ni-Mo-Cd)$_{0.3T/Par}$ and (Ni-Mo-Cd)$_{0.3T/Per}$ alloy coatings are taken, and are shown in Figures 10.18(a) and (b), respectively. A significant change in the surface roughness of the coating was found, with change of direction of induced magnetic field intensity. Experimental data analyses showed that the average roughness of $(Ni\text{-}Mo\text{-}Cd)_{0.3T/Per}$ alloy coating is decreased from 20.2 nm to 15.2 nm on change of direction of magnetic field intensity from parallel to perpendicular. This indicates that decreased surface roughness of $(Ni\text{-}Mo\text{-}Cd)_{0.3T/Per}$ coating is responsible for decrease of corrosion rate of the deposited coating and hence increases in the corrosion resistance on its surface.

10.5 EFFECT OF INDUCED *B* ON Ni CONTENT

The purpose of this research was to decrease the CR of ternary Ni-Mo-Cd alloy coating by increasing its Ni content with the advent of induced *B*. The change in the wt.% of Ni in Ni-Mo-Cd alloy coatings, deposited under different conditions of *B* is shown in Figure 10.19. The metal content of ED Ni-Mo-Cd alloy coating ($B = 0$ T), deposited at 6.0 Adm^{-2} (optimal c.d.) is shown by horizontal lines, showing only 13.9 wt.% Ni in the deposit.On superimposition of both parallel and perpendicular *B*, the Ni content of the alloy coatings have increased drastically, compared to its ED coatings as shown in Figure 10.19. It may be seen that at optimal intensity (0.3T), for parallel and perpendicular *B* the Ni content of alloy increased to 41.1 wt.% and 59.3 wt. %, respectively, from 13.9 wt.% corresponding to conventional ED coating. Further, MED $(Ni\text{-}Mo\text{-}Cd)_{0.3T/Par}$ and $(Ni\text{-}Mo\text{-}Cd)_{0.3T/Per}$ configurations showed the least CR's (2.7×10^{-2} mm y^{-1} and 0.7×10^{-2} mm y^{-1}), respectively.

Therefore, it may be inferred that the effect of *B* is more pronounced in case of perpendicular *B* compared to the parallel field, and it is due to increased Ni content of the alloy, affected due to increased convection. The change of Ni content with intensity of *B*, shown in Figure 10.19 indicates that 0.3T is the limiting field intensity (i_B) of the bath (for both parallel and perpendicular field), for development of coatings showing best performance against corrosion. The effect of limiting current density on normal electrodeposition and magnetoelectrodeposition are graphically represented in Figure 10.20.

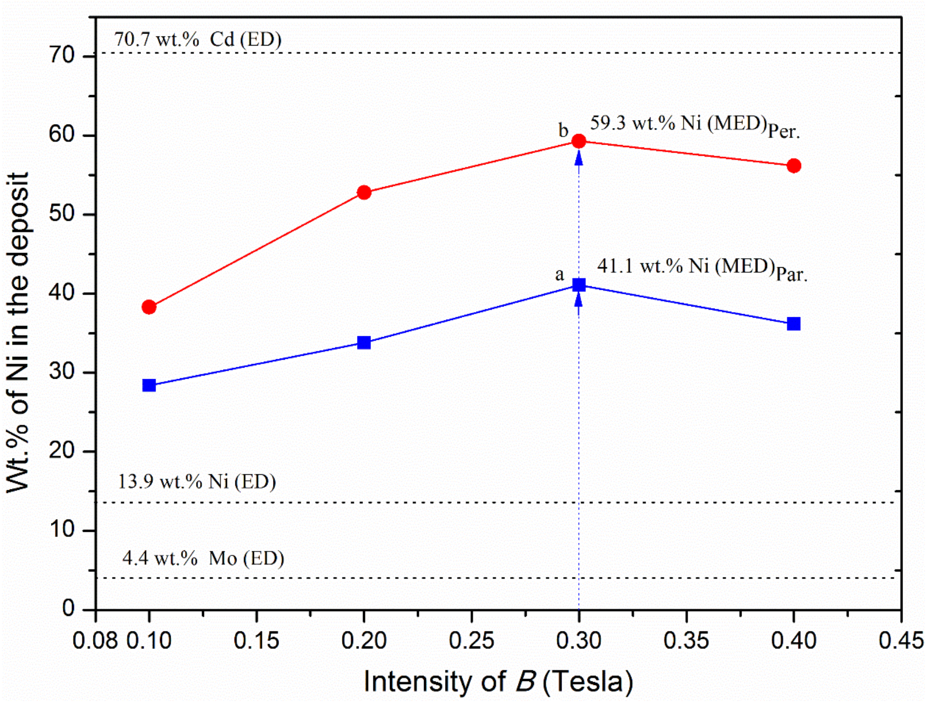

Figure 10.19- Change in wt.% of Ni in MED Ni-Mo-Cd alloy coatings, under different conditions of induced magnetic field, B. The perforated line indicates wt. % of individual metals in the ED Ni-Mo-Cd alloy

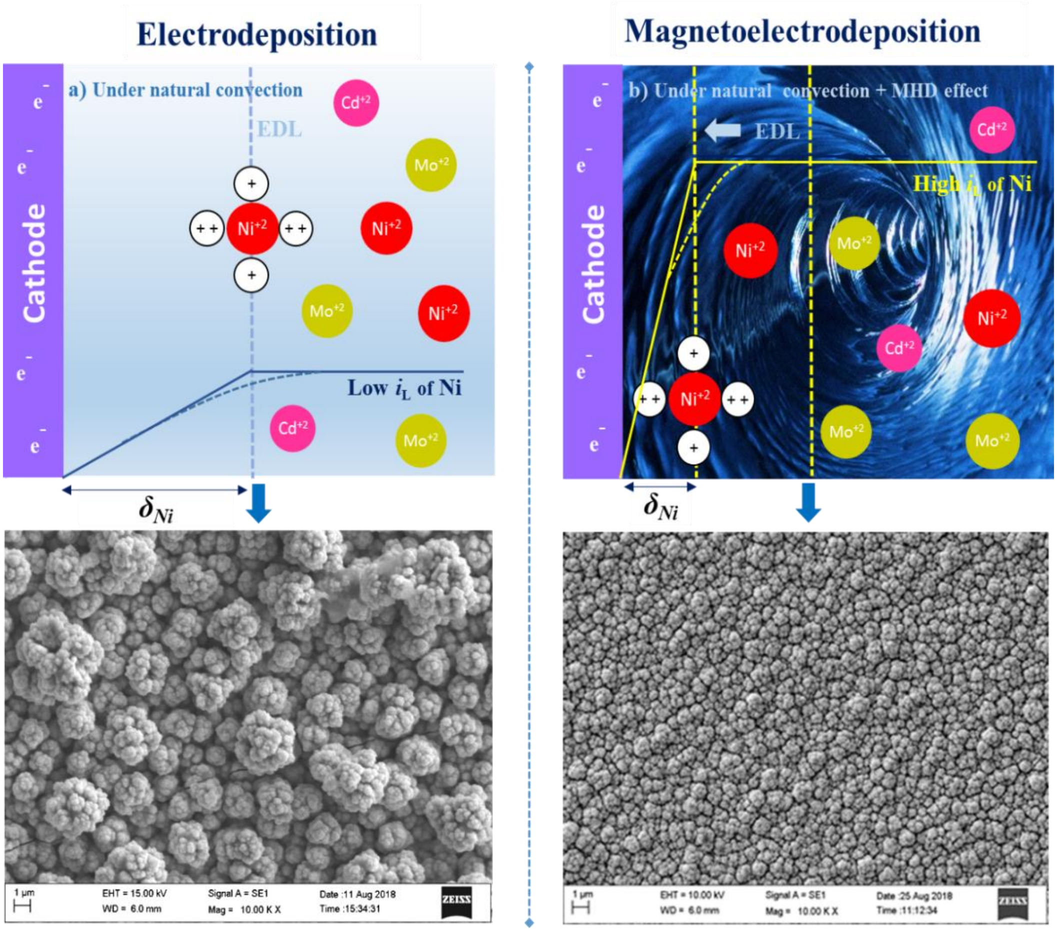

Figure 10.20- Diagrammatic representation showing the increase of limiting current density (i_L) of Ni due to change of electrodeposition from: a) natural convection to b) combined effects of natural convection and MHD resulting in drastic decrease of EDL thickness (δ). Below are the surface morphology of Ni-Mo-Cd alloy coatings developed by electrodeposition (ED) and magneto-electrodeposition (MED) methods

10.6 COMPARISON OF ED AND MED COATINGS

The corrosion performance of any coating largely depends on the surface morphology and their phase structures. The microstructure of ED (Ni-Mo-Cd)$_{6.0\mathrm{Adm}^{-2}}$, MED (Ni-Mo-Cd)$_{0.3\mathrm{T/Par.}}$ and MED (Ni-Mo-Cd)$_{0.3\mathrm{T/Per.}}$ alloy coatings, showing the highest corrosion resistances (optimal) are shown in Figure 10.21.It may be seen that homogeneity of coatings, responsible for better corrosion resistance has improved as the mode of deposition is changed from conventional type to magnetoelectrodeposition type. MED coating, deposited under perpendicular B, represented as MED (Ni-Mo-Cd) $_{0.3\mathrm{T/Per.}}$ is found to be most uniform compared to all other coatings. Further, XRD patterns of ED and MED coatings (optimal) shown in Figure 10.21 displays almost same signals, due to reasons discussed in preceding sections. Except compositions (hence CR's), other properties like surface morphology and phase structures of MED coatings were not found to vary much with direction and intensity of *B*. It may be due to high c.d. of 6.0 Adm^{-2}, used for deposition.

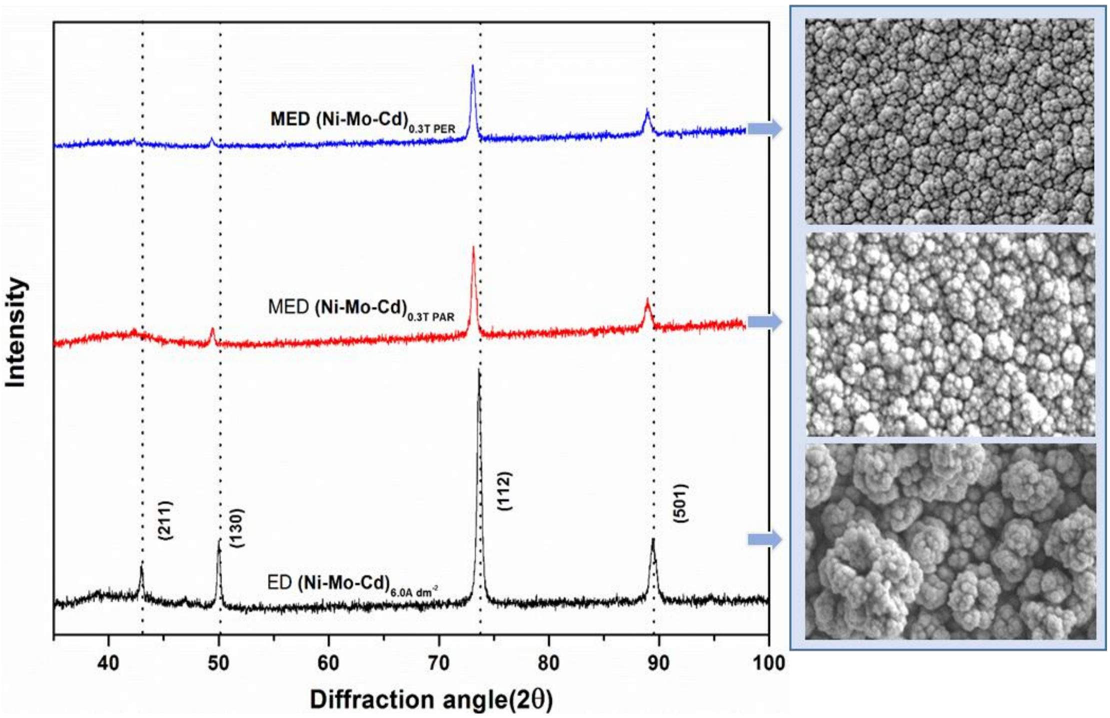

Figure 10.21- Phase structures and surface morphology and of optimal MED (Ni-Mo-Cd) alloy coatings, both parallel and perpendicular B in relation to ED(Ni-Mo-Cd)$_{6.0\ Adm}^{-2}$ alloy coating, deposited from same bath

10.7 COMPARISON OF CORROSION BEHAVIORS

The corrosion protection efficacy of ED (Ni-Mo-Cd)$_{6.0\ Adm}^{-2}$, MED (Ni-Mo-Cd)$_{0.3T/Par.}$ and MED (Ni-Mo-Cd)$_{0.3T/Per.}$ coatings showing the least CR (optimal) are shown in Figure 10.22. The potentiodynamic polarization plots clearly demonstrate a distinct difference between coatings, in terms of their both i_{corr} value, and E$_{corr}$ values. The relative response of their EIS plots are also shown in the inset of Figure 10.22. Thus from the data it may be summarized that, if ED(Ni-Mo-Cd)$_{0.6\ Adm}^{-2}$ alloy coating, having 13.9 wt.% Ni showed CR = 15.4×10^{-2} mm y^{-1},MED coatings having configuration MED (Ni-Mo-Cd)$_{0.3T/Par}$ and (Ni-Mo-Cd)$_{0.3T/Per}$ having, respectively 41.1 wt. % and 59.3 wt. % showed CR's = 2.7 ×10^{-2} mm y^{-1}and 0.7 ×10^{-2} mm y^{-1}, respectively. This drastic improvement in the corrosion performance of MED coatings are supported by Tafel's and impedances responses shown in Figure 10.22.

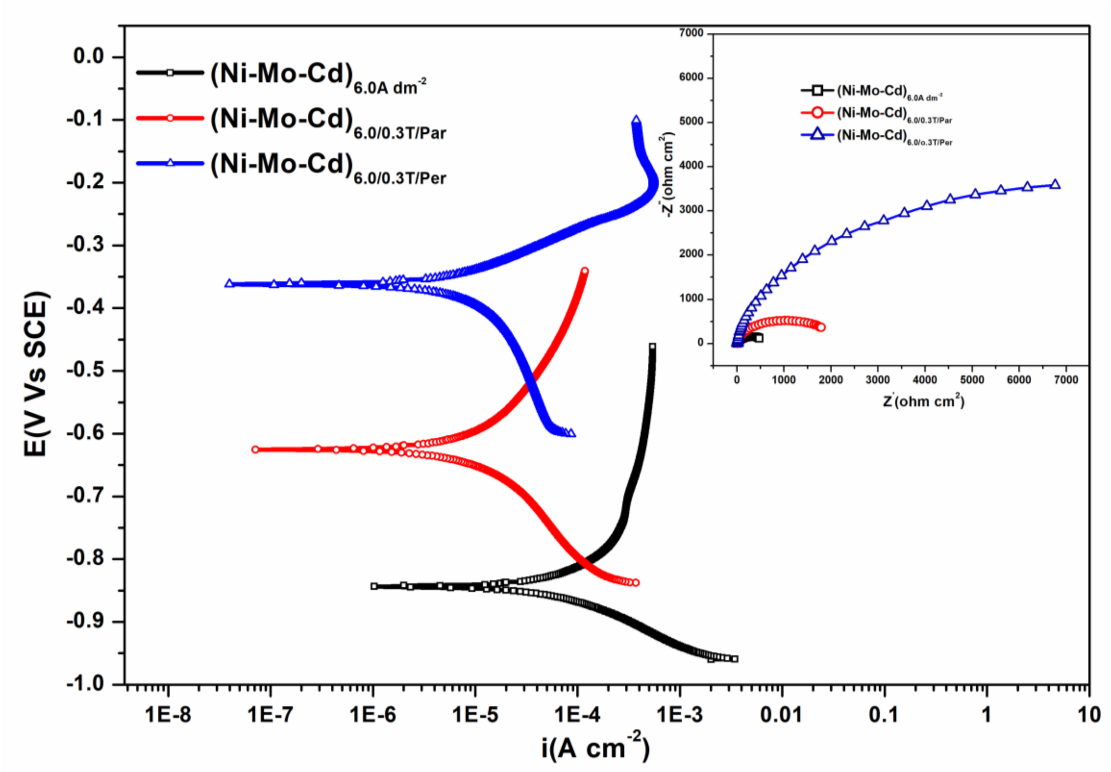

Figure 10.22- Comparison of polarization response of MED (Ni-Mo-Cd)$_{0.3T/Par}$ and (Ni-Mo-Cd)$_{0.3T/Per}$ coatings in relation of ED(Ni-Mo-Cd) coating deposited from same bath (under optimal condition)

The decrease of corrosion rates with change of coating configurations, *i.e*, from binary to ternary, and then to magnetoelectrodeposition method is shown by a histogram, in Figure 10.23. It may be noted that the corrosion protection efficacy are in the order that (Ni-Mo-Cd)$_{0.3T/Per.>}$(Ni-Mo-Cd)$_{0.3T/Par}$>(Ni-Mo-Cd)>(Ni-Mo) alloy coatings. Thus,(Ni-Mo-Cd)$_{0.3T/Per.}$ is the most corrosion resistant coating, with CR = 0.7 ×10^{-2} mm y^{-1} compare to all other coatings.

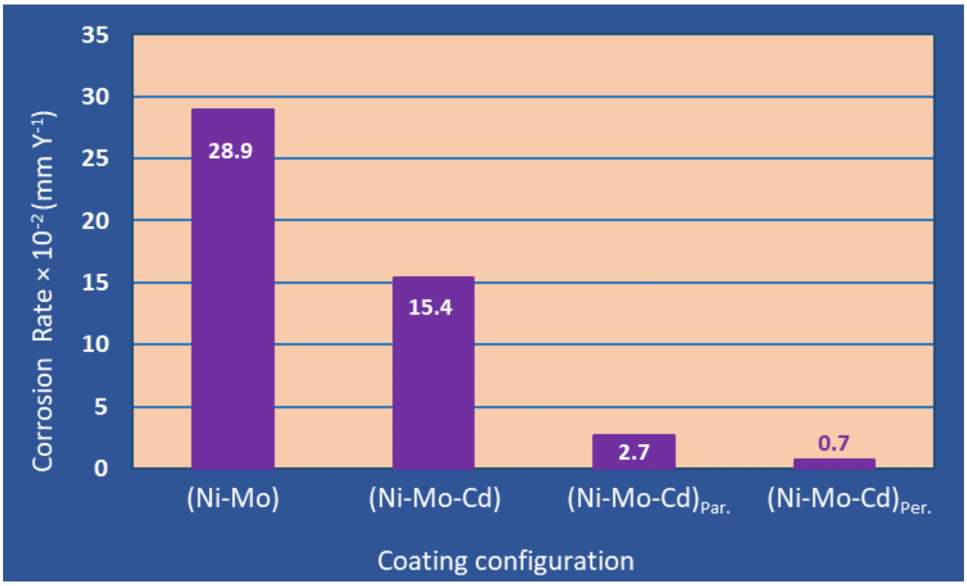

Figure 10.23- Histogram showing the corrosion rates (CR's) of electrodeposited alloy coatings of different configurations (all corresponds to optimal condition)

10.8 CONCLUSIONS

In the experimental research on magnetoelectrodeposition of Ni-Mo-Cd alloy coating for better corrosion resistance following observations were made as conclusions:

1. High corrosion rates (CR's) of ternary Ni-Mo-Cd alloy coatings, limited by the inherent limitation of induced type of codeposition is successfully resolved by magnetoelectrodeposition approach.
2. Both parallel and perpendicular *B* reduced the corrosion rates (CRs) of MED (Ni-Mo-Cd) alloy coatings to drastically. However, the effect is more pronounced in case of perpendicular *B*, due to effect of Lorentz force.
3. Low CR's of MED (Ni-Mo-Cd) alloy coatings are attributed by increased Ni content of the alloy, affected due to diffusion-controlled mass transfer of Ni^{+2} ions under condition of applied magnetic field.
4. CR's MED coatings decreased with intensity of field only up to 0.3T (optimal intensity), and then started increasing. This increase is due to decrease in the Ni content of the alloy.
5. Gradual improvement in the uniformity of MED coatings with increase of intensity of *B* was attributed to the gradual increase in the rate of nucleation

and decrease of local pH on cathode surface, affected due to increasing Lorentz force.

6. The constancy of diffraction peaks of ED, and MED Ni-Mo-Cd coatings of all configurations indicated that crystallinity of the coating is controlled by induced *B*, at given c.d.
7. Experimental investigation revealed that (Ni-Mo-Cd)$_{0.3T/Per.}$ is the most corrosion resistant coating, with CR = 0.7 $\times 10^{-2}$ mm y^{-1}, compare to all other coating

CHAPTER 11 SUMMARY AND CONCLUSIONS

This chapter summarizes the experimental results of investigation on electrodeposition (electroplating) and characterization of (Ni-Co) and (Ni-Mo) alloy coatings for improved corrosion protection and electrocatalytic activity, through different methods of electroplating reported in the thesis. The electrodeposition conditions were optimized for peak performance of their intended purposes, either corrosion protection, or electrocatalytic activity. Improved performance of alloy coatings were explained through the changed composition, surface morphology and phase structure of coatings, depending on the c.d. used for electroplating. The effect of forced convections, like ultrasound and magnetic field (B) effects on mass transport process, and hence corrosion performance have been compared. The advent of sonoelectrodeposition (SED) and magnetoelectrodeposition (MED), over the conventional electrodeposition (ED) are compared and discussed. The effect of addition of Cd, into (Ni-Mo) alloy matrix on corrosion performance were studied. The effect of c.d., and addition of nanoparticles on electrocatalytic behavior of alloy coatings were tested, and results are discussed. Conclusions arrived on the titled thesis is presented at the end.

11.1 STRUCTURE OF THE THESIS

The research work presented in the thesis emphasise on the electrodeposition and characterization of (Ni-Co) and (Ni-Mo) alloy coatings. The depositions were carried out using different modern approaches with the intention of improving both corrosion resistance and electrocatalytic activity of their conventional monolayer alloy coatings. The flow chart of the research work carried out in titled thesis is presented in Figure 11.1.

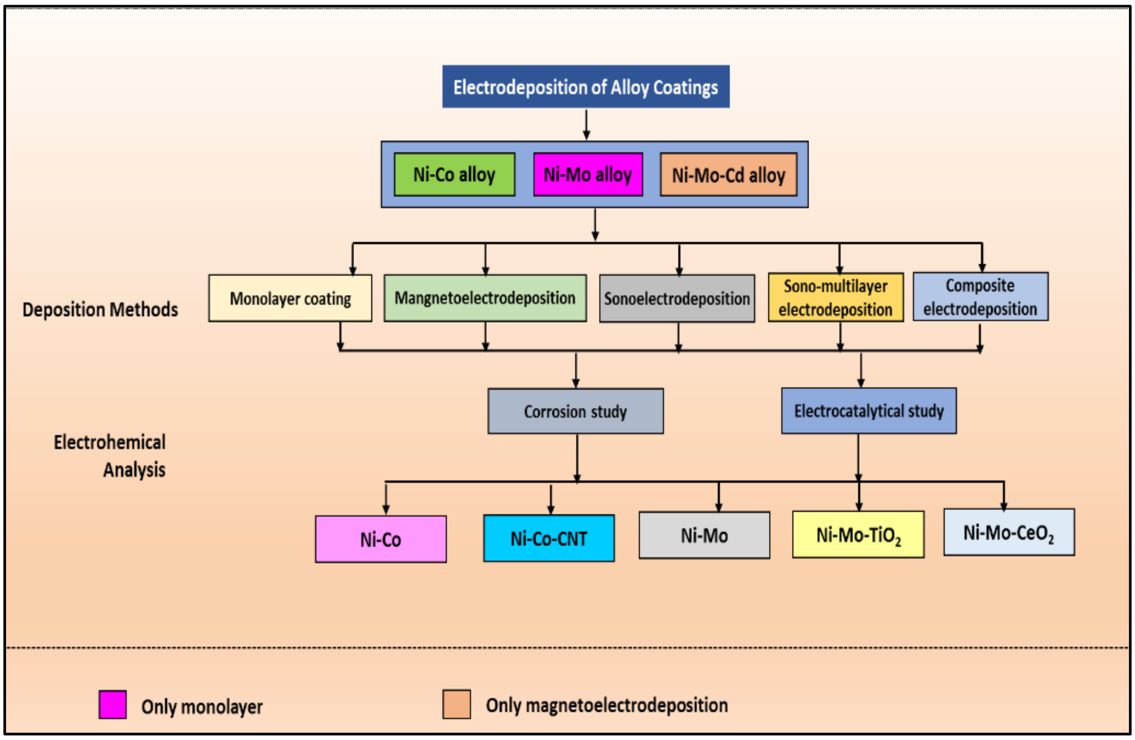

Fig. 11.1- The flow chart of the research work presented in the thesis

11.2 EXPERIMENTAL

The optimal conditions necessary to obtain quality electrodeposits of (Ni-Co) and (Ni-Mo)alloy coatings were achieved using Hull cell method (Kanani 2004). The various deposition techniques adopted for the development of alloy/composite coatings from optimised (Ni-Co) and (Ni-Mo) plating baths are schematically represented in Figure 11.2. All depositions were carried out in a rectangular PVC vessel of 250 mL capacity by keeping pure Ni anode and copper cathode (substrate) parallel, at 5 cm distance. Depositions of alloy and composite coatings were carried out for the same duration of time (10 min), for comparison purpose using computer-controlled DC Power Analyser (Agilent Technologies, Model: N6705), as the power source. The MED alloy coatings were accomplished at desired c.d. in conjunction with induced *B*, using DC power source and an electromagnet (Polytronics, Model: EM 100), respectively. The corrosion behaviours and electrocatalytic activities of alloy coatings were tested using electrochemical methods. Potentiodynamic polarization and electrochemical impedance spectroscopy (EIS) methods were used for evaluating the corrosion behaviours of the alloy coatings, in 5% NaCl medium.

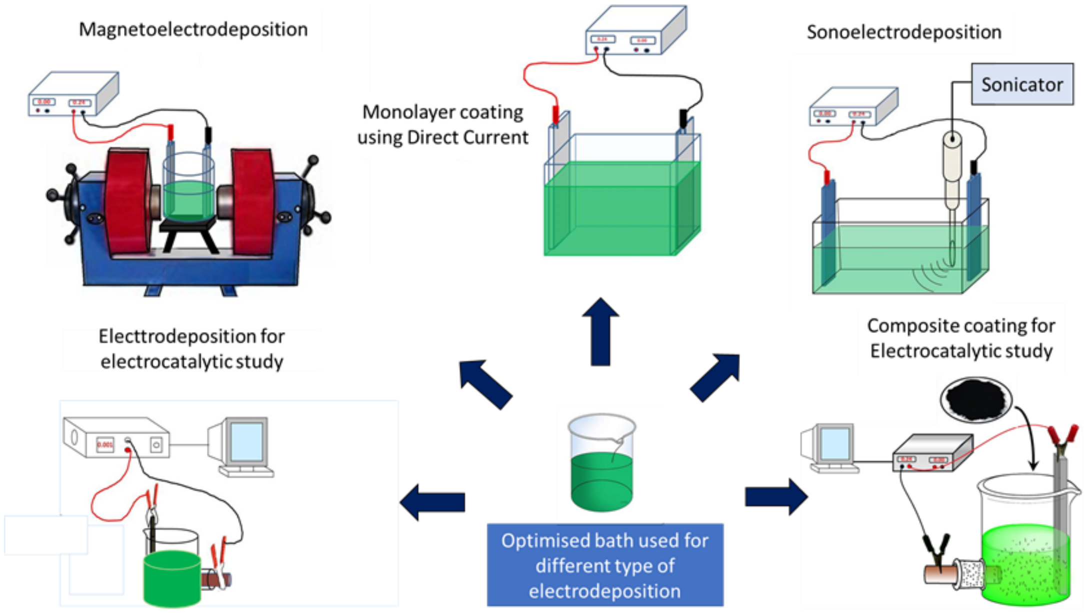

Fig. 11.2- Schematic of the various deposition techniques used for development of different binary/ternary alloy coatings

The electrocatalytic activity of the alloys, and their nanocomposite coatings were assessed through cyclic voltammetry (CV) and chronopotentiometry (CP) techniques, in 1.0 M KOH medium. All electrochemical measurements were made using computer controlled potentiostat/galvanostat (VersaSTAT^3, Princeton Applied Research Laboratory, USA). Apart from the electrochemical characterizations, coatings were analyzed for their morphology, composition and structure, using scanning electron microscopy (SEM), energy dispersive spectroscopy (EDS) and X-ray diffraction (XRD), respectively. The new class of materials, called composition modulated multilayer alloy (CMMA), or simply multilayer coatings, have been developed electrolytically, using optimised baths(Kanani 2004; Krishnan et al. 2002). The corrosion behaviour of monolayer alloy coatings (developed using direct current) was tried to increase by depositing in multilayers, by pulsing the ultrasound, parallel to the process of deposition. The deposition was carried out using ultrasound generator(SONICVibra-CellTM-VC750,20kHz,maximumpower 750W,sonoelectrode, with cylindrical rod having 13mm tip diameter), at different power densities measured in Wcm^{-2}, coupled with DC power source.

11.3 SUMMARY

Electroplating is an extremely important technology, concerned with covering inexpensive and widely available base materials with plated layers of different metals/alloys having superior properties; consequently they can be used to explore their application which is otherwise prohibitively expensive. Generally, electrodeposited alloys have a better appearance than the parent metals, being smoother, brighter, and finer grained. It is further asserted that relative to the single metal involved, alloy deposits can have different properties in certain composition ranges. They can be denser, harder, more corrosion resistant, more protective of the underlying base metal, tougher and stronger, more wear resistant, superior with respect to magnetic properties, more suitable for subsequent electroplate overlays and conversion chemical treatment, and superior in antifriction applications etc. Off late, the subject of alloy plating is growing in both evolutionally and revolutionary ways and it is supported by ever increasing number of publications. The reason for this is due to the vastness of the number of possible alloy combinations, and concomitant possible practical applications.

Thus keeping wide industrial applications of alloy plating, two electrolytic baths, namely (Ni-Co) and (Ni-Mo) were optimized through standard Hull Cell method. The composition and operating variables of optimized (Ni-Co) and (Ni-Mo) alloy baths are shown in Table 11.1. The electrodeposition was carried out at different c.d.'s on copper substrate for same time duration, for comparison purpose. The electroplated monolayer coatings were characterized for their corrosion behavior and electrocatalytic activity of water electrolysis. Corrosion performance of alloy coatings were evaluated through electrochemical methods using 5% NaCl, as common medium of reference. Corrosion resistance of alloy coatings were improved by modulating the mass transfer process at the cathode, during plating. Accordingly, monolayer/multilayer Ni-based alloy coatings have been developed under effect of ultrasound/magnetic field, using them as a tool to modify the mass transfer at cathode layer.

Table 11.1-Composition and operating parameters of optimized binary/ternary alloy baths used for electrodeposition and characterization of different alloys

Composition and operating variables of different baths used			
Bath Constituents	**(Ni-Co) bath (g/L)**	**(Ni-Mo) bath (g/L)**	**(Ni-Mo-Cd) (g/L)**
Cobalt sulfate	14.0	-	-
Nickel sulphate	131.0	18.0	18.0
Sulphanilic acid	0.74	-	-
Ascorbic acid	2.4	-	-
Boric acid	30.0	-	-
Glycerol	14 mL/L	-	-
Sodium molybdate	-	48.0	48.0
Sodium citrate	-	105.0	105.0
Cadmium chloride	-	-	1.0
Operating parameters			
c.d. range	1.0-4.0 Adm^{-2}	1.0-6.0 Adm^{-2}	1.0-6.0 Adm^{-2}
Temperature	303K	303K	303K
Anode	Ni plate	Ni plate	Ni plate
Cathode (substrate)	Copper	Copper	Copper

Taking the general principle that, periodic modulation of mass transfer at cathode layer leading to the development of coatings on its surface, in multilayers. Thus multilayer coatings, having different number/thickness of layers have been developed by pulsing the ultrasound, during deposition. The effectiveness of alloy coating, developed under different conditions were tested for their electrocatalytic activity. Electrodeposited coatings were used as electrode material for water splitting reaction of HER and OER in 1.0 M KOH medium, through electrochemical CV and CP methods. The effect of addition of nanoparticles (into the alloy matrix) on corrosion and electro catalytic performance of their bear-alloy coatings were studied. The experimental results are compared, and discussed, with support of data from different analytical techniques, like SEM, EDX, AFM and XRD etc.

11.4 CORROSION STUDY OF ALLOY COATINGS

11.4.1. Conventional Monolayer Alloy Coatings

In the thesis, two binary alloy baths, namely (Ni-Co) and (Ni-Mo) alloy were optimized, and electrodeposition of monolayer (conventional) alloy coatings were carried out using direct current. A ternary (Ni-Mo-Cd) alloy bath was formulated by adding 1g/L of $CdCl_2$ to improve the corrosion protection efficacy of (Ni-Mo) alloy coating. Electrodeposition of alloy coatings were carried out from the optimized baths for same duration of time (10 min), and their corrosion behaviors were studied in 5% NaCl solution.

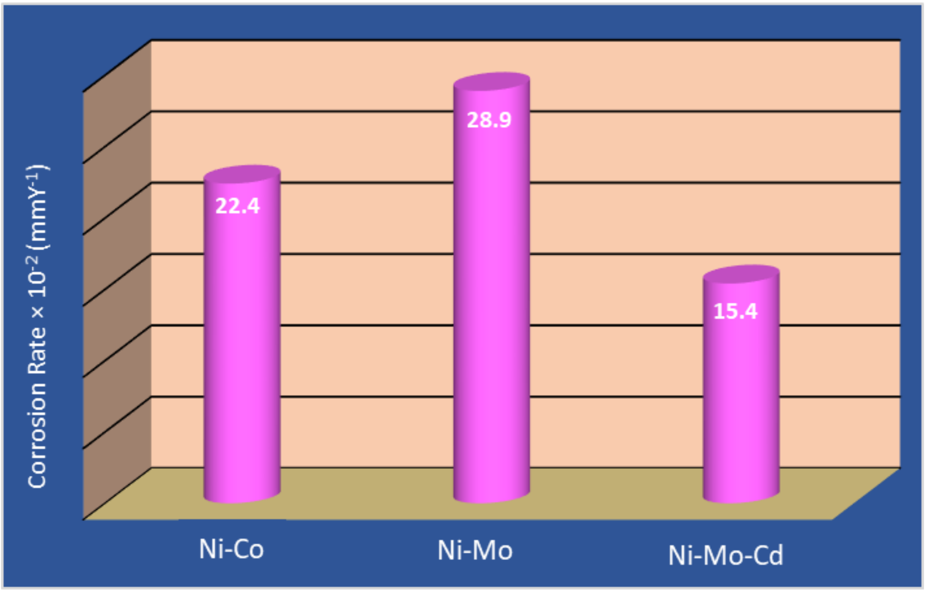

Figure 11.3-Bar diagram showing the corrosion rates of (Ni-Co), (Ni-Mo) and (Ni-Mo-Cd) alloy coatings studied in 5% NaCl solution (all at optimal condition)

Accordingly, monolayer binary and ternary (Ni-Co), (Ni-Mo) and (Ni-Mo-Cd) alloy coating was carried out at different c.d.'s and their optimal conditions were identified. The current density (c.d.) at which alloy coating showed the least corrosion rate (CR) was considered as the optimal c.d., and coating is considered as the optimal configuration of the coating. The corrosion rates of (Ni-Co), (Ni-Mo) and (Ni-Mo-Cd) alloy coatings, deposited from their baths (all under optimal condition)are summarized as bar diagram, shown in Figure 11.3.From the diagram shown in Figure 11.3, it is clear that (Ni-Mo-Cd) coating is more corrosion resistant, with least CR than other two binary alloy coatings.

11.4.2 Corrosion Behavior of MED, SED and SMD (Ni-Co) Alloy Coatings

To improve the corrosion resistance property of conventional monolayer (Ni-Co) alloy coatings, electrodeposition was carried out through other three approaches.

11.4.2.1 MED (Ni-Co) alloy coating

Monolayer (Ni-Co) alloy coatings were developed with advent of superimposed magnetic field *B*, parallel to the process of deposition, keeping the c.d. (optimal) constant. The magnetoelectrodeposition (MED) was carried out at different intensities of *B*, applied both parallel and perpendicular to the direction of flow of ions. Experimental investigation proved that corrosion resistance of (Ni-Co) alloy coatings can be increased by many folds, by superimposing the magnetic field *B*, parallel to the electrodeposition. Hence, significant increase in corrosion resistance exhibited by MED coatings (under both parallel and perpendicular *B*) is attributed to the increase of limiting current density of Co. This enhances the mass transfer process at the cathode, and improves the surface properties. Further, MED coating developed under perpendicular *B* was found to show superior properties over the coatings developed under parallel. The enhanced characteristics of MED coatings were attributed to the maximum MHD effect, due to Lorentz force. Since, this force is maximum when magnetic field applied is perpendicular to movement of ions. An optimum condition was arrived, and is abbreviated as MED (Ni-Co) alloy.

11.4.2.2 SED (Ni-Co) alloy coating

The corrosion property of the (Ni-Co) has been improved with advent of power ultrasound effect, applied parallel to the process of deposition. Monolayer (Ni-Co) alloy coatings were developed under different conditions of ultrasound power densities. An optimum condition (power density) for development of sonoelectrodeposited (Ni-Co) coating, showing highest corrosion resistance was identified, and is represented as SED (Ni-Co) alloy.

11.4.2.3 SMD(Ni-Co) alloy coating

The corrosion protection efficacy of SED (Ni-Co) alloy coating was enhanced further through multilayer approach by pulsing alternatively the ultrasound frequency, during deposition. The alloy coatings obtained through this approach was called sono-multilayer deposited (SMD) alloy coatings, abbreviated as SMD (Ni-Co) alloy coatings. An optimum condition (in terms of number and thickness of each layers) for development of SMD (Ni-Co) coating, showing highest corrosion resistance was identified, and is represented as SMD(Ni-Co) alloy. SMD (Ni-Co) alloy coatings were found to show many folds better corrosion resistance, compared to its monolayer counterpart developed from same bath. Drastic improvement in the corrosion protection efficacy of SMD (Ni-Co) alloy coatings was found, and is attributed to increase in number of interfaces, separating layers of alloys having different morphology, composition and phase structures. Thus the corrosion protection efficacy of (Ni-Co) alloy coatings obtained through different approaches of electrodeposition, namely MED(Ni-Co), SED(Ni-Co) and SMD(Ni-Co) alloy coatings are shown by a bar chart, in Figure 11.4. It may be noted that sono-multilayer deposition (Ni-Co) alloy coatings showed the least CR compare to other two coatings.

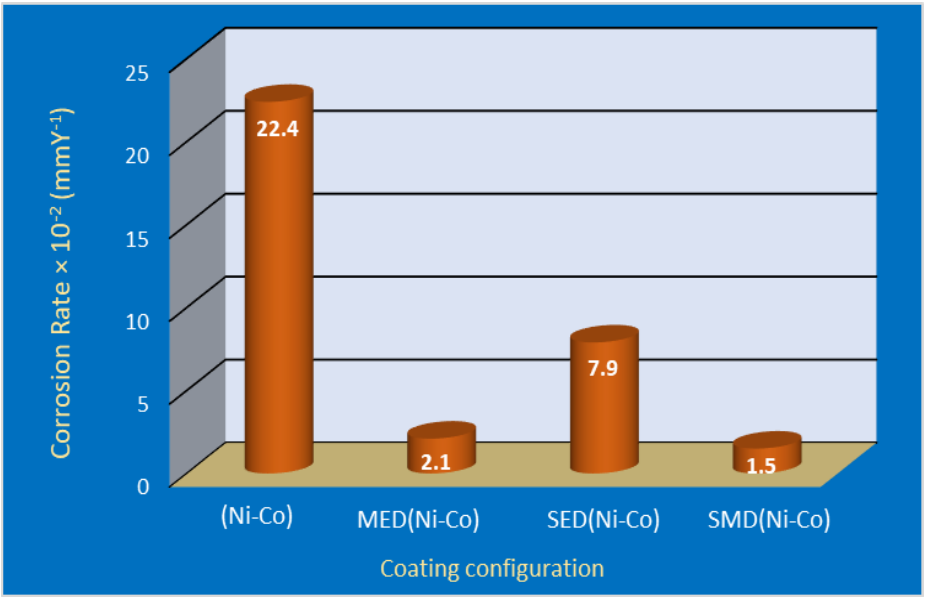

Figure 11.4-Comparision of corrosion rate (CR's) of (Ni-Co) alloy coatings developed through different mode of electrodeposition, using same bath (under optimal condition

11.4.3 Corrosion Behavior of (Ni-Mo), (Ni-Mo-Cd) and MED (Ni-Mo-Cd) Alloy Coatings

The (Ni-Mo) bath, following induced type of codeposition showing the less dependency of plating variables, particularly c.d. on the composition of alloy, was optimized. As a result, no much variation in the CR's of the coatings were found with change of c.d. Hence, to improve the corrosion resistance property of (Ni-Mo) coatings, a small quantity of $CdCl_2$(1g/L) was added into the bath to get ternary alloy of (Ni-Mo-Cd). A drastic decrease of CR was found, due to marked change in the composition of alloy. The electrodeposition of (Ni-Mo-Cd) alloy was carried out at different c.d.'s, and optimal configuration of (Ni-Mo-Cd) alloy coating was arrived. Then, corrosion protection ability of (Ni-Mo-Cd) alloy coatings was improved further by magneto-electrodeposition approach. The magnetic field of different intensity *B* was induced, both parallel and perpendicular direction to the flow of ions, and change of CR's were studied. The experimental results revealed that MED (Ni-Mo-Cd) coating is much more corrosion resistant than all other coatings. Further, MED (Ni-Mo-Cd) alloy coating obtained under condition of perpendicular *B* is the more corrosion resistant, compared to the parallel one. This was explained on the basis of increased magneto-convection effect.Thus the corrosion study of (Ni-Mo) alloy coatings, deposited under different condition, *i.e.* ternary (Ni-Mo-Cd) and MED(Ni-Mo-Cd) alloy coatings are shown by the bar chart, in Figure 11.5.It may be noted that among the Mo - based alloy coatings,MED(Ni-Mo-Cd) is the most corrosion resistant compare to all other coatings, giving indication that magnetic field can be used as additional tool to improve their properties and performances.

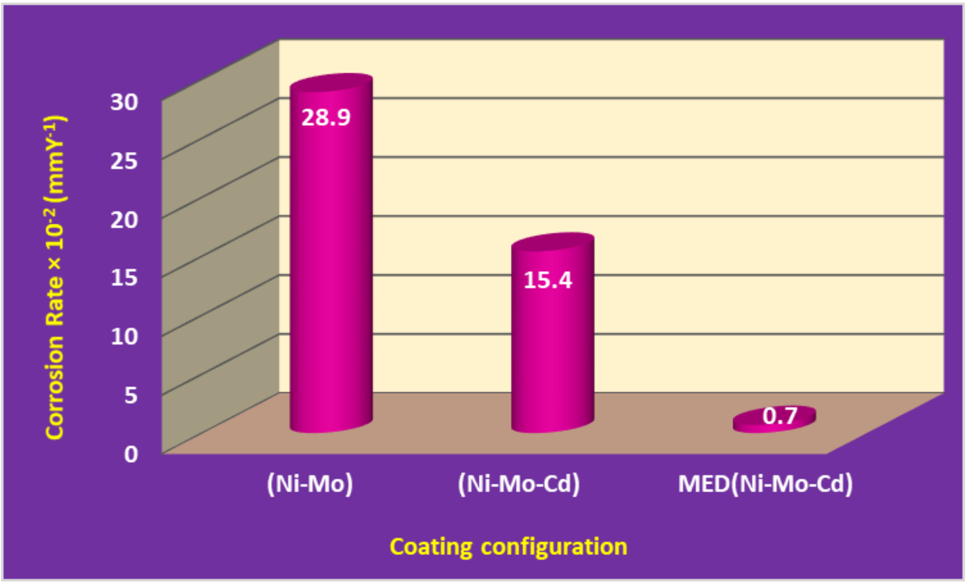

Figure 11.5- Relative performance of (Ni-Mo),(Ni-Mo-Cd) and MED(Ni-Mo-Cd) alloy coatings against corrosion in 5% NaCl medium (all under optimal conditions)

To summarize, with objective of developing a better corrosion resistant Ni-based alloy coatings from two baths, namely (Ni-Co) and (Ni-Mo), using different modern methods of electrodeposition, like magnetoelectrodeposition, sonoelectrodeposition, multilayer deposition and ternary alloy deposition a good degree of success was achieved. The corrosion performance of all coatings, deposited for same duration (10 min) were evaluated in common corrosion medium (5% NaCl solution). The corrosion rates (CR’s) of all alloy coatings are shown in a relative scale Figure 11.6.

On comparing the corrosion protection efficacy of both Co and Mo -based alloy coatings, it may be seen that the superimposition of ultrasound/magnetic field effect has significant effect on their composition, and hence corrosion behaviors. The compositional change, responsible for better corrosion protection ability is attributed to the change in the diffusion controlled convection of metal ions, at the electrical double layer. Thus, it may be concluded that among all alloy coatings, MED(Ni-Mo-Cd)$_{6.0//0.3T,Per.}$ is the most corrosion resistant.

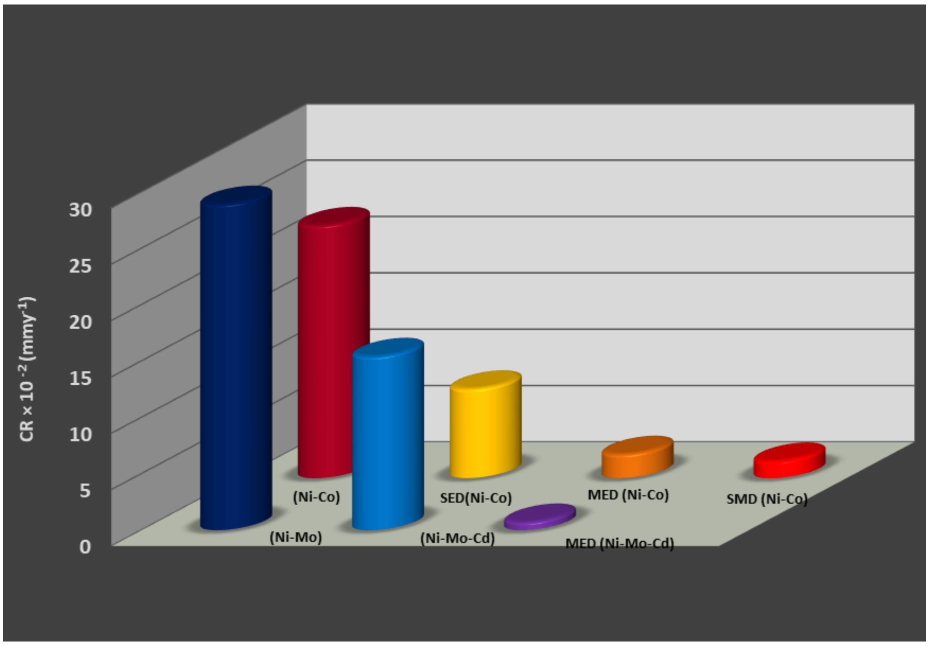

Figure 11.6-Histogram showing the corrosion rates (CR) of alloy coatings of different combination achieved through different approaches of electrodeposition in relation to the CR of (Ni-Co) and (Ni-Mo) alloy coatings, deposited from same bath for same duration of time

11.5 ELECTROCATALYTIC STUDY OF ALLOY COATINGS

Alkaline water electrolysis is one of the best and easiest method for hydrogen evolution (HER) and oxygen evolution (OER) reactions. Though this method is simple, reducing energy consumption, increase durability and safety of these systems are the main challenges. Hence, electro catalytic activity (Ni-Co) and (Ni-Mo) alloy coatings, deposited from their optimised baths have been tested. The effect of addition of different nanoparticles, like carbon nanotubes (CNT), TiO_2 and CeO_2 were also examined. To begin with (Ni-Co),(Ni-Mo)alloy coatings were electrodeposited from their optimised baths, at different current densities, and their electro catalytic activity for alkaline water electrolysis were studied in 1.0 M KOH, using them as both anode and cathode. The experimental conditions used for electro-catalytic study of different coatings are shown in Table 11.5.

Table 11.5- The experimental conditions employed for electro-catalytic study of (Ni-Co), (Ni-Mo) and for their nanocomposite coatings

Operating parameters	*Working conditions*
Working electrode	(Ni-Co) and (Ni-Mo) alloy and its composite coatings
Reference electrode	Saturated calomel electrode
Counter electrode	Platinized platinum
Medium	1M KOH
Potential range for CV(HER)	0 to -1.6V
Potential range for CV(OER)	0 to 0.75V
Constant current applied for HER during CP analysis	$^{-}$ 300 mAcm^{-2}
Applied constant current value for OER in CP analysis	+300 mAcm^{-2}

Electrocatalytic efficacy, in terms of hydrogen evolution reaction (HER) and oxygen evolution reaction (OER) have been studied by measuring quantitatively the amount of H_2 and O_2 evolved. The electrocatalytic stability of alloy coatings, in the medium of water electrolysis (1 M KOH) have also been studied, by electrochemical AC and DC methods. Electrocatalytic activity of alloy coatings, deposited at different c.d.'s are tested as electrode material for water electrolysis of HER and OER in 1 M KOH. A mutually opposite electrocatalytic activity of (Ni-Co) and (Ni-Mo) alloy coatings towards HER and OER, with deposition c.d.'s was observed. It was attributed to the change in composition of the alloy, in terms of the constituting metals content, in the deposit. The effect of CNT on electrocatalytic activity of (Ni-Co) alloy coating was tested for both HER and OER. In addition to this, the effect of addition of TiO_2 and CeO_2nanoparticles, into the optimal bath of (Ni-Mo) on the electrocatalytic behaviour was studied, and results are discussed. Electrocatalytic kinetic parameters for HER were calculated by studying cyclic voltammetry and chronopotentiometry in 1M KOH medium. The optimal c.d. corresponding to different alloy coatings, showing the highest electrocatalytic activity (in terms of H_2 and O_2 evolved) are reported in Table 11.6.

Table 11.6-Amount of H_2 and O_2 evolved (measure of electrocatalytic activity)on the surface of electrodeposited alloy coatings during water electrolysis in 1M KOH medium

Coating configuration	Optimal c.d. for HER (Adm^{-2})	Volume of H_2 evolved in 300s(cm^3)	Optimal c.d for OER ($A\ dm^{-2}$)	Volume of O_2 evolved in 300s (cm^3)
(Ni-Co)	1.0	12.8	4.0	7.6
(Ni-Co-CNT)	1.0	14.0	4.0	9.5
(Ni-Mo)	2.0	12.9	6.0	10.0
(Ni-Mo-TiO_2)	2.0	14.2	-	-
(Ni-Mo-CeO_2)	2.0	15.9	-	-

From the data, it is clear that (Ni-Co) and (Ni-Mo) coating obtained at lower current density limits can be used as the best electrode material for hydrogen evolution reaction. At the same time, coating obtained at higher current density limits is the most suitable for OER activity.Optimizing the conditions for the development of advanced electrode materials is a crucial issue for improving the efficiency of water electrolysis, and to reduce the power consumption. Hence, efforts are made to reduce overpotential for HER activity in order to increase electrocatalytic activity. In this regard, incorporation of nanoparticle into the alloy matrix are tried to enhance the electrocatalytic activity of (Ni-Co) and (Ni-Mo) alloy coatings. Accordingly, Ni-based nanocomposite coatings of Co and Mo were developed, and were used as cathode in electrocatalytic study of HER. The H_2 and O_2 gases evolved on surface of different alloy coatings were measured, and are given in Table 11.6.The nanocomposite coatings showed better electrocatalytic activity when compared to (Ni-Co) and (Ni-Mo) alloy coatings. This is attributed to increase in surface area of alloy coatings for hydrogen and oxygen evolution reaction, due to addition of nanoparticle into the alloy matrix, which in turn increased the surafce area,number active site for evolution of hydrogen gas.

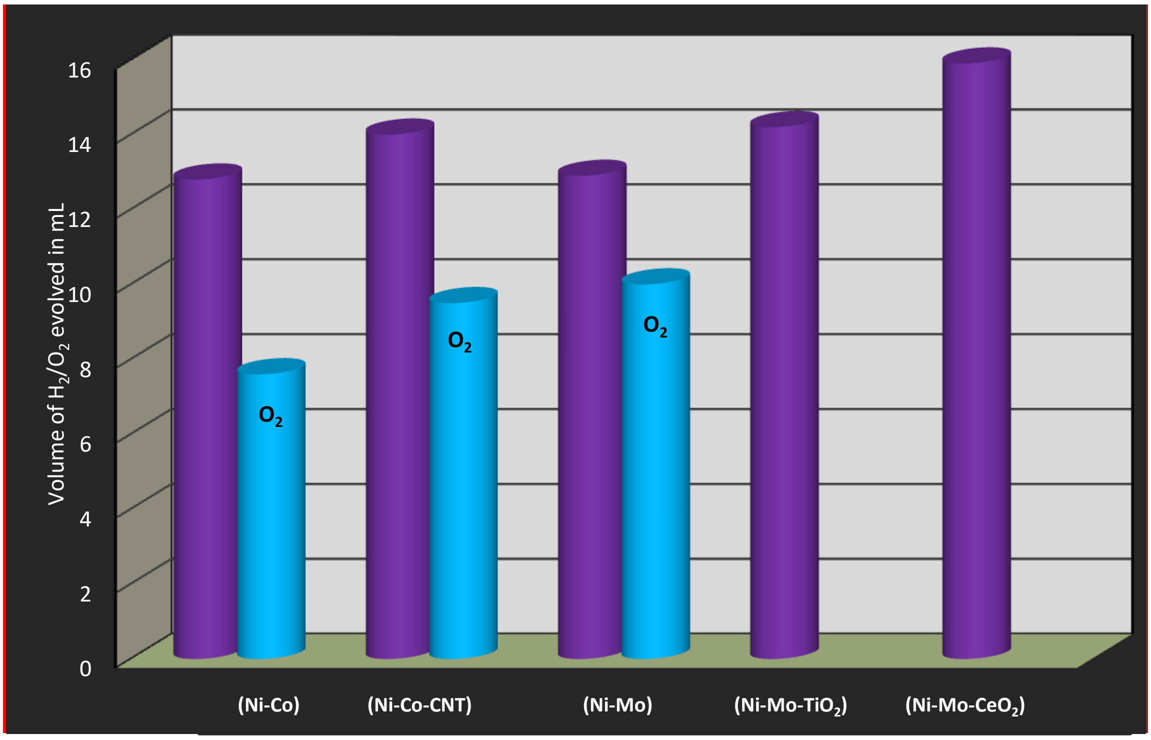

Figure 11.7-Diagrammatic representation showing the relative performance of Ni-based alloy coatings of different configurations as electro-catalyst for HER and OER (deposited for same duration of time)

To summarize, electrocatalytic activity of different electrode materials have been measured, interms of amount of hydrogen and oxygen evolved during the reaction. The relative performance of different alloy coatings, for HER and OER of water electrolysis are shown diagrammatically in Figure 11.7. From both the Table

11.6 and Figure 11.7, it is clear that (Ni-Mo) deposit and (Ni-Mo-CeO_2) composite coatings are the best electrode material for HER and OER, respectively among all other coatings.

11.6 CONCLUSIONS

Based on experimental investigation carried out on electrodeposition of (Ni-Co) and (Ni-Mo) alloy coatings, through different methods for better corrosion performance and electro-catalytic activity, the following conclusion are drawn:

1. The (Ni-Co) and (Ni-Mo) alloy baths were found to follow anomalous (sometime normal type, depending upon the concentration of metal ions in the bath) and induced type of codeposition, respectively.
2. The corrosion performance of monolayer (Ni-Co) alloy coatings was improved through magneto-electrodeposition method, by superimposing the magnetic field B (both parallel and perpendicular), during process of deposition.
3. The effect of perpendicular B is more pronounced, than parallel field due to increased magneto-convection controlled mass transfer process.
4. The corrosion resistance property of monolayer (Ni-Co) alloy coating was increased substantially with advent of ultrasound induced mass transfer, called sonoelectrodeposition method.
5. Sono-multilayer (Ni-Co) alloy coatings of high corrosion protection was developed by pulsing the power ultrasound periodically, parallel to the process of electrodeposition.
6. The corrosion performance of (Ni-Mo) has been improved drastically on addition of small quantity of cadmium chloride (1 g/L) into the bath, affected due to change in the composition of the deposit. Further, corrosion protection efficacy of (Ni-Mo-Cd) alloy coatings has been increased to many folds through magneto-electrodeposition approach.
7. The electrocatalytic study of electrodeposited (Ni-Co), (Ni-Mo) and their composite coatings revealed that composite coatings can be used as efficient electrode materials for alkaline water electrolysis of HER and OER.
8. A mutually opposite electrocatalytic activity of both (Ni-Co) and (Ni-Mo) alloy coatings towards HER and OER, with deposition c.d.’s was observed. It was

attributed to the change in composition of alloys, in terms of their constituting metals content, in the deposit.

9. The experimental investigation on corrosion behavior of different alloy coatings, magnetoelectrodeposited (Ni-Mo-Cd) alloy coating, represented as $(\text{Ni-Mo-Cd})_{6.0/0.3\text{T}}$ showed the least corrosion rate, compared to all other coatings.
10. The electro-catalytic efficacy of many electrodeposited alloy coatings, having different configurations demonstrated that $(\text{Ni-Mo-CeO}_2)_{2.0\ \text{Adm}^{-2}}$ and $(\text{Ni-Mo})_{6.0\ \text{Adm}^{-2}}$ alloy coatings are the most active electrode material for HER and OER, respectively.

11.7 SCOPE FOR FUTURE WORK

- To use other non-noble metals in Ni-based alloycoatings to achieve higher corrosion resistance and electrocatalytic activity
- To study increased electrical and optical property of (Ni-Co) alloy coatings with advent of sono-electrodeposition and magneto-electrodeposition
- To develop multilayer coatings of high performance of corrosion resistance by pulsing the magnetic field effect during deposition
- To study the effect of doping of other nanoparticles in the alloy matrix for improved electro-catalytic activity

REFERENCES

Aaboubi, O., and Msellak, K. (2017). “Magnetic field effects on the electrodeposition of CoNiMo alloys.” *Appl. Surf. Sci.*, 396, 375–383.

Aal, A. A., and Hassan, H. B. (2009). “Electrodeposited nanocomposite coatings for fuel cell application.” *J. Alloys Compd.*, 477(1–2), 652–656.

Abd El-Halim, A. M., and Khalil, R. M. (1986). “Some characteristics of Ni-Co alloy powders electrodeposited from dilute sulphate baths.” *Surf. Coat. Technol.*, 27(2), 103–115.

Abuin, G., Coppola, R., and Diaz, L. (2019). “Ni-Mo Alloy Electrodeposited over Ni Substrate for HER on Water Electrolysis.” *Electrocatalysis*, 10(1), 17–28.

Akiyama, T., and Fukushima, H. (1992). “Recent Study on the Mechanism of the Electrodeposition of Iron-group Metal Alloys.” *ISIJ Int.*, 32(7), 787–798.

Anicai, L., Petica, A., Costovici, S., Prioteasa, P., and Visan, T. (2013). “Electrodeposition of Sn and NiSn alloys coatings using choline chloride based ionic liquids—Evaluation of corrosion behavior.” *Electrochimica Acta*, 114, 868–877.

Bagotzky, V. S., Osetrova, N. V., and Skundin, A. M. (2003). “Fuel Cells: State-of-the-Art and Major Scientific and Engineering Problems.” *Russ. J. Electrochem.*, 39(9), 919–934.

Bahadormanesh, B., and Dolati, A. (2010). “The kinetics of Ni–Co/SiC composite coatings electrodeposition.” *J. Alloys Compd.*, 504(2), 514–518.

Bakhit, B., and Akbari, A. (2013). “Nanocrystalline Ni–Co alloy coatings: electrodeposition using horizontal electrodes and corrosion resistance.” *J. Coat. Technol. Res.*, 10(2), 285–295.

Bang, J. H., and Suslick, K. S. (2010). “Applications of ultrasound to the synthesis of nanostructured materials.” *Adv. Mater.*, 22(10), 1039–1059.

Banks, C. E., and Compton, R. G. (2003). “Ultrasonically Enhanced Voltammetric Analysis and Applications: An Overview.” *Electroanalysis*, 15(5–6), 329–346.

Bianchini, C., and Barbaro, P. (2009). *Catalysis for sustainable energy production*. Wiley-Vch.

Bockris, J. O. (1998). *Modern electrochemistry 2B: electrodics in chemistry, engineering, biology and environmental science*. Springer Science & Business Media.

Bouzit, F. Z., Nemamcha, A., Moumeni, H., and Rehspringer, J. L. (2017). "Morphology and Rietveld analysis of nanostructured Co-Ni electrodeposited thin films obtained at different current densities." *Surf. Coat. Technol.*, 315, 172–180.

Bratoeva, M., and Atanasov, N. (2000). "Effect of sulfamate-citrate electrolyte pH on the Ni-W alloy electrodeposition." *Russ. J. Electrochem.*, 36(1), 60–63.

Brenner, A. (1963). *Electrodeposition of Alloys: Practical and specific information*. Academic Press.

Brenner, A. (2013). *Electrodeposition of alloys: principles and practice*. Elsevier.
Brillas, E., Rambla, J., and Casado, J. (1999). "Nickel electrowinning using a Pt catalysed hydrogen-diffusion anode. Part I: Effect of chloride and sulfate ions and a magnetic field." *J. Appl. Electrochem.*, 29(12), 1367–1376.

Brooman, E. W. (2000). "Corrosion behavior of environmentally acceptable alternatives to cadmium and chromium coatings: Cadmium. Part I." *Met. Finish.*, 98(4), 42–50.

Bund, A., and Ispas, A. (2005). "Influence of a static magnetic field on nickel electrodeposition studied using an electrochemical quartz crystal microbalance, atomic force microscopy and vibrating sample magnetometry." *J. Electroanal. Chem.*, 575(2), 221–228.

Burchardt, T. (2000). "The hydrogen evolution reaction on NiPx alloys." *Int. J. Hydrog. Energy*, 25(7), 627–634.

Cardoso, D. S. P., Amaral, L., Santos, D. M. F., Šljukić, B., Sequeira, C. A. C., Macciò, D., and Saccone, A. (2015). "Enhancement of hydrogen evolution in alkaline water electrolysis by using nickel-rare earth alloys." *Int. J. Hydrog. Energy*, 40(12), 4295–4302.

Carlin, R. L., and De Jongh, L. J. (1986). "Structural and magnetic properties of transition metal complexes of pyridine N-oxide." *Chem. Rev.*, 86(4), 659–680.

Chekin, F., Tahermansouri, H., and Besharat, M. R. (2014). "Nickel oxide nanoparticles prepared by gelatin and their application toward the oxygen evolution reaction." *J. Solid State Electrochem.*, 18(3), 747–753.

Chen, D., Sharma, S. K., Mudhoo, A., Sharma, S. K., and Mudhoo, A. (2011). *Handbook on Applications of Ultrasound : Sonochemistry for Sustainability*. CRC Press.

Chen, W. X., Tu, J. P., Wang, L. Y., Gan, H. Y., Xu, Z. D., and Zhang, X. B. (2003). “Tribological application of carbon nanotubes in a metal-based composite coating and composites.” *Carbon*, 41(2), 215–222.

Chen, Z., Ma, Z., Song, J., Wang, L., and Shao, G. (2016). “Novel one-step synthesis of wool-ball-like Ni-carbon nanotubes composite cathodes with favorable electrocatalytic activity for hydrogen evolution reaction in alkaline solution.” *J. Power Sources*, 324, 86–96.

Chia-Chien, L., and Chou, T.-C. (1995). “Effects of magnetic field on the reaction kinetics of electroless nickel deposition.” *Electrochimica Acta*, 40(8), 965–970.

Chiba, A., Kitamura, K., and Ogawa, T. (1986). “Magnetic field effects on the electrodeposition of nickel from a high pH watt’s bath.” *Surf. Coat. Technol.*, 27(1), 83–88.

Choquette, Y., Brossard, L., Lasia, A., and Ménard, H. (1990). “Investigation of hydrogen evolution on Raney-Nickel composite-coated electrodes.” *Electrochimica Acta*, 35(8), 1251–1256.

Chuang, H.-C., Jiang, G.-W., and Sanchez, J. (2020). “Study on the changes of ultrasonic parameters over supercritical Ni-Co electroplating process.” *Ultrason. Sonochem.*, 60, 104805.

Chung, C. K., and Chang, W. T. (2009). “Effect of pulse frequency and current density on anomalous composition and nanomechanical property of electrodeposited Ni–Co films.” *Thin Solid Films*, 4th International Conference on Technological Advances of Thin Films and Surface Coatings, 517(17), 4800–4804.

Cohen, U., Koch, F. B., and Sard, R. (1983). “Electroplating of Cyclic Multilayered Alloy (CMA) Coatings.” *J. Electrochem. Soc.*, 130(10), 1987–1995.

Correia, A. N., Machado, S. A., and Avaca, L. A. (1999). “Studies of the hydrogen evolution reaction on smooth Co and electrodeposited Ni–Co ultramicroelectrodes.” *Electrochem. Commun.*, 1(12), 600–604.

Correia, A. N., and Machado, S. A. S. (2000). “Electrodeposition and characterisation of thin layers of Ni□ Co alloys obtained from dilute chloride baths.” *Electrochimica Acta*, 45(11), 1733–1740.

Cullity, B. D. (1956). *Elements of X-ray Diffraction*. Addison-Wesley Publishing.
Daltin, A. L., Benaissa, M., and Chopart, J. P. (2018). "Nucleation and crystal growth in magnetoelectrodeposition." *MS&E,* 424(1), 012022.

Daneshvar-Fatah, F., and Nasirpouri, F. (2014). "A study on electrodeposition of Ni-noncovalnetly treated carbon nanotubes nanocomposite coatings with desirable mechanical and anti-corrosion properties." *Surf. Coat. Technol.,* 248, 63–73.

Danilov, F. I., Tsurkan, A. V., Vasil'Eva, E. A., and Protsenko, V. S. (2016). "Electrocatalytic activity of composite Fe/TiO2 electrodeposits for hydrogen evolution reaction in alkaline solutions." *Int. J. Hydrog. Energy,* 41(18), 7363–7372.

Darband, Gh. B., Aliofkhazraei, M., Rouhaghdam, A. S., and Kiani, M. A. (2019). "Three-dimensional Ni-Co alloy hierarchical nanostructure as efficient non-noble-metal electrocatalyst for hydrogen evolution reaction." *Appl. Surf. Sci.*, 465, 846–862.

Del Campo, F. J., Coles, B. A., Marken, F., Compton, R. G., and Cordemans, E. (1999). "High-frequency sonoelectrochemical processes: mass transport, thermal and surface effects induced by cavitation in a 500 kHz reactor." *Ultrason. Sonochem.,* 6(4), 189–197.

Devos, O., Aaboubi, O., Chopart, J.-P., Merienne, E., Olivier, A., and Amblard, J. (1998). "Magnetic Field Effects on Nickel Electrodeposition: II. A Steady-State and Dynamic Electrochemical Study." *J. Electrochem. Soc.*, 145(12), 4135.

Dini, J. W. (1993). *Electrodeposition*. Noyes Publications,.Donten, M., Cesiulis, H., and Stojek, Z. (2000). "Electrodeposition and properties of Ni- W, Fe-W and Fe- Ni-W amorphous alloys. A comparative study." *Electrochimica Acta*, 45(20), 3389–3396.

Du, J., Xie, S., Li, N., and Xu, L. (2017). "Influence of technological conditions on microstructure, surface topography and electrocatalytic hydrogen evolution of Ni–Mo alloy films." *J. Nanosci. Nanotechnol.*, 17(7), 5104–5108.

Ebadi, M., Basirun, W. J., and Alias, Y. (2010). "Influence of magnetic field on the electrodeposition of Ni-Co alloy." *J. Chem. Sci.*, 122(2), 279–285.

El-Feky, H., Negem, M., Roy, S., Helal, N., and Baraka, A. (2013). "Electrodeposited Ni and Ni-Co alloys using cysteine and conventional ultrasound waves." *Sci. China Chem.,* 56(10), 1446–1454.

Elias, L., Bhat, K. U., and Hegde, A. C. (2016). "Development of nanolaminated multilayer Ni–P alloy coatings for better corrosion protection." *RSC Adv.*, 6(40), 34005–34013.

Elias, L., and Hegde, A. C. (2015). "Electrodeposition of laminar coatings of Ni–W alloy and their corrosion behaviour." *Surf. Coat. Technol.*, 283, 61–69.

Elias, L., and Hegde, A. C. (2017). "Effect of magnetic field on corrosion protection efficacy of Ni-W alloy coatings." *J. Alloys Compd.*, 712, 618–626.

Fahidy, T. Z. (1983). "Magnetoelectrolysis." *J. Appl. Electrochem.*, 13(5), 553–563.
Fahidy, T. Z. (2001). "Characteristics of surfaces produced via magnetoelectrolytic deposition." *Prog. Surf. Sci.*, 68(4), 155–188.

Fan, C., Piron, D. L., and Paradis, P. (1994). "Hydrogen evolution on electrodeposited nickel-cobalt-molybdenum in alkaline water electrolysis." *Electrochimica Acta*, 39(18), 2715–2722.

Fang, X., Cui, X. F., Jin, G., and Wang, Y. (2017). "Effect of magnetic field on brush plating Ni–Co alloy." *Surf. Eng.*, 33(2), 142–148.

Ganesh, V., Vijayaraghavan, D., and Lakshminarayanan, V. (2005a). "Fine grain growth of nickel electrodeposit: effect of applied magnetic field during deposition." *Appl. Surf. Sci.*, 240(1–4), 286–295.

Gao, M. Y., Yang, C., Zhang, Q. B., Zeng, J. R., Li, X. T., Hua, Y. X., Xu, C. Y., and Dong, P. (2017). "Facile electrochemical preparation of self-supported porous Ni–Mo alloy microsphere films as efficient bifunctional electrocatalysts for water splitting." *J. Mater. Chem. A*, 5(12), 5797–5805.

Gawne, D. T., and Ma, U. (1988). "Engineering properties of chromium plating and electroless and electroplated nickel." *Surf. Eng.*, 4(3), 239–249.

Golgovici, F., Pumnea, A., Petica, A., Manea, A. C., Brincoveanu, O., Enachescu, M., and Anicai, L. (2018). "Ni–Mo alloy nanostructures as cathodic materials for hydrogen evolution reaction during seawater electrolysis." *Chem. Pap.*, 72(8), 1889–1903.

Gong, M., Li, Y., Wang, H., Liang, Y., Wu, J. Z., Zhou, J., Wang, J., Regier, T., Wei, F., and Dai, H. (2013). "An advanced Ni–Fe layered double hydroxide electrocatalyst for water oxidation." *J. Am. Chem. Soc.*, 135(23), 8452–8455.

Gong, M., Zhou, W., Tsai, M.-C., Zhou, J., Guan, M., Lin, M.-C., Zhang, B., Hu, Y., Wang, D.-Y., Yang, J., Pennycook, S. J., Hwang, B.-J., and Dai, H. (2014). "Nanoscale nickel oxide/nickel heterostructures for active hydrogen evolution electrocatalysis." *Nat. Commun.*, 5(1), 4695.

González-Buch, C., Herraiz-Cardona, I., Ortega, E., García-Antón, J., and Pérez-Herranz, V. (2013). “Synthesis and characterization of macroporous Ni, Co and Ni–Co electrocatalytic deposits for hydrogen evolution reaction in alkaline media.” *Int. J. Hydrog. Energy*, 38(25), 10157–10169.

Gorobets, O. Yu., Gorobets, V. Yu., Derecha, D. O., and Brukva, O. M. (2008). “Nickel Electrodeposition under Influence of Constant Homogeneous and High-Gradient Magnetic Field.” *J. Phys. Chem. C*, 112(9), 3373–3375.

Goveas, J. J., Shetty, S., Mascarenhas, N. P., Hegde, A. C., and Gonsalves, R. A. (2018). “Corrosion inhibiting action of Ni–Mo alloy coatings in the presence of mixed metal oxide nanocomposites.” *New J. Chem.*, 42(16), 13660–13666.

Grimaud, A., Demortière, A., Saubanère, M., Dachraoui, W., Duchamp, M., Doublet, M.-L., and Tarascon, J.-M. (2016). “Activation of surface oxygen sites on an iridium-based model catalyst for the oxygen evolution reaction.” *Nat. Energy*, 2(1), 1–10.

Gu, C., Lian, J., and Jiang, Z. (2006). “High Strength Nanocrystalline Ni-Co Alloy with Enhanced Tensile Ductility.” *Adv. Eng. Mater.*, 8(4), 252–256.

Guan, S., and Nelson, B. J. (2005). “Electrodeposition of low residual stress CoNiMnP hard magnetic thin films for magnetic MEMS actuators.” *J. Magn. Magn. Mater.*, 292, 49–58.

Hassani, Sh., Raeissi, K., and Golozar, M. A. (2008). “Effects of saccharin on the electrodeposition of Ni–Co nanocrystalline coatings.” *J. Appl. Electrochem.*, 38(5), 689–694.

Herraiz-Cardona, I., Ortega, E., Antón, J. G., and Pérez-Herranz, V. (2011). “Assessment of the roughness factor effect and the intrinsic catalytic activity for hydrogen evolution reaction on Ni-based electrodeposits.” *Int. J. Hydrog. Energy*, 36(16), 9428–9438.

Hinds, G., Spada, F. E., Coey, J. M. D., Ní Mhíocháin, T. R., and Lyons, M. E. G. (2001). “Magnetic Field Effects on Copper Electrolysis.” *J. Phys. Chem. B*, 105(39), 9487–9502.

Huang, P.-C., Hou, K.-H., Wang, G.-L., Chen, M.-L., and Wang, J.-R. (2015). “Corrosion resistance of the Ni-Mo alloy coatings related to coating’s electroplating parameters.” *Int J Electrochem Sci*, 10, 4972–4984.

Huot, J. Y., and Brossard, L. (1988). “In situ activation of cobalt cathodes in alkaline water electrolysis.” *J. Appl. Electrochem.*, 18(6), 815–822.

Idris, J., Christian, C., and Gaius, E. (2013). "Nanocrystalline Ni-Co Alloy Synthesis by High Speed Electrodeposition." *J. Nanomater.*, 2013, 1–8.

Imanian Ghazanlou, S., Farhood, A. H. S., Ahmadiyeh, S., Ziyaei, E., Rasooli, A., and Hosseinpour, S. (2019). "Characterization of Pulse and Direct Current Methods for Electrodeposition of Ni-Co Composite Coatings Reinforced with Nano and Micro ZnO Particles." *Metall. Mater. Trans. A*, 50(4), 1922–1935.

Iragar, V. V., Mendon, S., Acharya, S., Sujaya, Sujana, Anjana Pai, V., Rashmi, D., and Pavithra, G. P. (2020). "Electrodeposition and Corrosion Analysis of Ni-Mo Alloy Coatings." *Adv. Mater. Process.*, Lecture Notes in Mechanical Engineering, S. Singh, C. Prakash, S. Ramakrishna, and G. Krolczyk, eds., Singapore: Springer, 67–75.

Jiang, W., Shen, L., Xu, M., Wang, Z., and Tian, Z. (2019). "Mechanical properties and corrosion resistance of Ni-Co-SiC composite coatings by magnetic field-induced jet electrodeposition." *J. Alloys Compd.*, 791, 847–855.

Johnson, C. J., and Pohlman, S. L. (1983). *Proceedings of the Symposia on Corrosion in Batteries and Fuel Cells and Corrosion in Solar Energy Systems*. Electrochemical Society.

Jones, D. A. (1996). *Principles and prevention of corrosion. 2*. Prentice Hall.

Kanani, N. (2004). *Electroplating: Basic Principles, Processes and Practice*. Elsevier.

Kaninski, M. P. M., Nikolic, V. M., Tasic, G. S., and Rakocevic, Z. L. (2009). "Electrocatalytic activation of Ni electrode for hydrogen production by electrodeposition of Co and V species." *Int. J. Hydrog. Energy*, 34(2), 703–709.

Karimzadeh, A., Aliofkhazraei, M., and Walsh, F. C. (2019). "A review of electrodeposited Ni-Co alloy and composite coatings: Microstructure, properties and applications." *Surf. Coat. Technol.*, 372, 463–498.

Kasai, S. (2014). "Hydrogen electrical energy storage by high-temperature steam electrolysis for next-millennium energy security." *Int. J. Hydrog. Energy*, 39(36), 21358–21370.

Khorsand, S., Raeissi, K., Ashrafizadeh, F., Arenas, M. A., and Conde, A. (2016). "Corrosion behaviour of super-hydrophobic electrodeposited nickel–cobalt alloy film." *Appl. Surf. Sci.*, 364, 349–357.

Kim, K. H., Zheng, J. Y., Shin, W., and Kang, Y. S. (2012). “Preparation of dendritic NiFe films by electrodeposition for oxygen evolution.” *Rsc Adv.*, 2(11), 4759–4767.

Kiuchi, D., Matsushima, H., Fukunaka, Y., and Kuribayashi, K. (2006). “Ohmic resistance measurement of bubble froth layer in water electrolysis under microgravity.” *J. Electrochem. Soc.*, 153(8), E138.

Krause, A., Uhlemann, M., Gebert, A., and Schultz, L. (2004). “The effect of magnetic fields on the electrodeposition of cobalt.” *Electrochimica Acta*, 49(24), 4127–4134.

Kreysa, G., and H\aakansson, B. (1986). “Electrocatalysis by amorphous metals of hydrogen and oxygen evolution in alkaline solution.” *J. Electroanal. Chem. Interfacial Electrochem.*, 201(1), 61–83.

Krishnan, K. R., Srinivasan, K., and Mohan, S. (2002). “Electrodeposition of Compositionally Modulated Alloys—An Overview.” *Trans. IMF*, 80(2), 46–48.

Kritzer, P., Boukis, N., and Dinjus, E. (2000). “Review of the Corrosion of Nickel-Based Alloys and Stainless Steels in Strongly Oxidizing Pressurized High-Temperature Solutions at Subcritical and Supercritical Temperatures.” *CORROSION*, 56(11), 1093–1104.

Kuang, D., Xu, L., Liu, L., Hu, W., and Wu, Y. (2013). “Graphene–nickel composites.” *Appl. Surf. Sci.*, 273, 484–490.

Lasia, A., and Rami, A. (1990). “Kinetics of hydrogen evolution on nickel electrodes.” *J. Electroanal. Chem. Interfacial Electrochem.*, 294(1–2), 123–141.

Laszczyńska, A., Tylus, W., Winiarski, J., and Szczygieł, I. (2017). “Evolution of corrosion resistance and passive film properties of Ni-Mo alloy coatings during exposure to 0.5M NaCl solution.” *Surf. Coat. Technol.*, 317, 26–37.

Laszczyńska, A., Winiarski, J., Szczygieł, B., and Szczygieł, I. (2016). “Electrodeposition and characterization of Ni–Mo–ZrO2 composite coatings.” *Appl. Surf. Sci.*, 369, 224–231.

Lee, Y.-S., Hu, C.-C., and Wen, T.-C. (1996). “Oxygen Evolution on Co-Cu-Zn Ternary Spinel Oxide-Coated Electrodes in Alkaline Solution: Integration of Statistical, Electrochemical, and Textural Approaches.” *J. Electrochem. Soc.*, 143(4), 1218.

Levesque, A., Chouchane, S., Douglade, J., Rehamnia, R., and Chopart, J.-P. (2009). “Effect of natural and magnetic convections on the structure of electrodeposited zinc–nickel alloy.” *Appl. Surf. Sci.*, 255(18), 8048–8053.

Li, B., Zhang, W., Zhang, W., and Huan, Y. (2017). “Preparation of Ni-W/SiC nanocomposite coatings by electrochemical deposition.” *J. Alloys Compd.*, 702, 38–50.

Li, D., Wu, C., Wang, Q., Chopart, J.-P., He, J., Franczak, A., and Levesque, A. (2016). “Effects of High Magnetic Field Postannealing on Microstructure and Properties of Pulse Electrodeposited Co-Ni-P Films.” *Adv. Mater. Sci. Eng.*, <https://www.hindawi.com/journals/amse/2016/3816972/> (Jan. 30, 2020).

Li, J., Jiang, J., He, H., and Sun, Y. (2002). “Synthesis, microstructure, and mechanical properties of TiO 2/Ni nanocomposite coatings.” *J. Mater. Sci. Lett.*, 21(12), 939–941.

Li, W., Hao, J., Mu, S., and Liu, W. (2020). “Electrochemical behavior and electrodeposition of Ni-Co alloy from choline chloride-ethylene glycol deep eutectic solvent.” *Appl. Surf. Sci.*, 507, 144889.

Li, Z. H., Wang, X. Q., Wang, M., Wang, F. F., and Ge, H. L. (2006). “Preparation and tribological properties of the carbon nanotubes–Ni–P composite coating.” *Tribol. Int.*, 39(9), 953–957.

Liu, J., Watanabe, H., Fuji, M., and Takahashi, M. (2009). “Electrocatalytic evolution of hydrogen on porous alumina/gelcast-derived nano-carbon network composite electrode.” *Electrochem. Commun.*, 11(1), 107–110.

Liu, X., Liu, W., Ko, M., Park, M., Kim, M. G., Oh, P., Chae, S., Park, S., Casimir, A., Wu, G., and Cho, J. (2015). “Metal (Ni, Co)-Metal Oxides/Graphene Nanocomposites as Multifunctional Electrocatalysts.” *Adv. Funct. Mater.*, 25(36), 5799–5808.

Liu, Y., Lu, H., and Kou, X. (2019). “Electrodeposited Ni-Co-Sn alloy as a highly efficient electrocatalyst for water splitting.” *Int. J. Hydrog. Energy*, 44(16), 8099–8108.

Low, C. T. J., Wills, R. G. A., and Walsh, F. C. (2006). “Electrodeposition of composite coatings containing nanoparticles in a metal deposit.” *Surf. Coat. Technol.*, 201(1–2), 371–383.

Luo, Q., Peng, M., Sun, X., Luo, Y., and Asiri, A. M. (2016). “Efficient electrochemical water splitting catalyzed by electrodeposited NiFe nanosheets film.” *Int. J. Hydrog. Energy*, 41(21), 8785–8792.

Luo, S., Fan, J., Liu, W., Zhang, M., Song, Z., Lin, C., Wu, X., and Chu, P. K. (2006). "Synthesis and low-temperature photoluminescence properties of SnO2nanowires and nanobelts." *Nanotechnology*, 17(6), 1695–1699.

Lupi, C., Dell'Era, A., and Pasquali, M. (2014). "In situ activation with Mo of Ni–Co alloys for hydrogen evolution reaction." *Int. J. Hydrog. Energy*, 39(5), 1932–1940.

Lyons, M. E., and Brandon, M. P. (2008). "The oxygen evolution reaction on passive oxide covered transition metal electrodes in aqueous alkaline solution. Part 1-Nickel." *Int J Electrochem Sci*, 3(12), 1386–1424.

Lyons, M. E. G., and Brandon, M. P. (2010). "A comparative study of the oxygen evolution reaction on oxidised nickel, cobalt and iron electrodes in base." *J. Electroanal. Chem.*, 641(1), 119–130.

Ma, Z. S., Zhou, Y. C., Long, S. G., and Lu, C. (2012). "Residual stress effect on hardness and yield strength of Ni thin film." *Surf. Coat. Technol.*, 207, 305–309.

Mahalingam, T., Raja, M., Thanikaikarasan, S., Sanjeeviraja, C., Velumani, S., Moon, H., and Kim, Y. D. (2007). "Electrochemical deposition and characterization of Ni–P alloy thin films." *Mater. Charact.*, XIV International Materials Research Congress: Symposium 7, 58(8), 800–804.

Mahboob, S., Haghighi, M., and Rahmani, F. (2017). "Sonochemically preparation and characterization of bimetallic Ni-Co/Al_2O_3-ZrO_2 nanocatalyst: Effects of ultrasound irradiation time and power on catalytic properties and activity in dry reforming of CH4." *Ultrason. Sonochem.*, 38, 38–49.

Manazoğlu, M., Hapçı, G., and Orhan, G. (2016). "Electrochemical deposition and characterization of Ni-Mo alloys as cathode for alkaline water electrolysis." *J. Mater. Eng. Perform.*, 25(1), 130–137.

Manazoğlu, M., Hapçı, G., and Orhan, G. (2016). "Effect of electrolysis parameters of Ni–Mo alloy on the electrocatalytic activity for hydrogen evaluation and their stability in alkali medium." *J. Appl. Electrochem.*, 46(2), 191–204.

Masdek, N. R. N., and Alfantazi, A. (2010). "Review of Studies on Corrosion of Electrodeposited Nanocrystalline Metals and Alloys." *ECS Trans.*, 28(24), 249.

Matsushima, H., Ispas, A., Bund, A., Plieth, W., and Fukunaka, Y. (2007). "Magnetic field effects on microstructural variation of electrodeposited cobalt films." *J. Solid State Electrochem.*, 11(6), 737–743.

Matsushima, J. T., Trivinho-Strixino, F., and Pereira, E. C. (2006). “Investigation of cobalt deposition using the electrochemical quartz crystal microbalance.” *Electrochimica Acta*, 51(10), 1960–1966.

McCafferty, E. (2010). *Introduction to Corrosion Science*. Springer Science & Business Media.

Meng, X., Wang, X., Zhang, D., Luo, H., Xu, C., and Liu, S. (2020). “Electrodeposition of Ni-Mo/TiO2 Nanocomposite Coatings on Low-Carbon Steels for Improving Corrosion Resistance.” *Int J Electrochem Sci*, 15, 6198–6206.

Mirkova, L., Pashova, V. P., and Monev, M. H. (2011). “Study of hydrogen evolution reaction on Ni/Co3O4 composite electrode in alkaline solution.” *ECS Trans.*, 35(21), 77.

Mohanta, S., and Fahidy, T. Z. (1978). “Hydrodynamic and mass transport phenomena in a multiple-electrode magnetoelectrolytic cell.” *J. Appl. Electrochem.*, 8(1), 5–10.

Monzon, L. M., and Coey, J. M. D. (2014a). “Magnetic fields in electrochemistry: The Lorentz force. A mini-review.” *Electrochem. Commun.*, 42, 38–41.

Moriguchi, N. (1934). “The effect of supersonic waves on chemical phenomena,(III). The effect on the concentration polarization.” *J Chem Soc Jpn*, 55, 749–750.

Navarro-Flores, E., Chong, Z., and Omanovic, S. (2005). “Characterization of Ni, NiMo, NiW and NiFe electroactive coatings as electrocatalysts for hydrogen evolution in an acidic medium.” *J. Mol. Catal. Chem.*, 226(2), 179–197.

Obradović, M., Stevanović, J., Despić, A. R., Stevanović, R., and Stoch, J. (2001). “Characterization and corrosion properties of electrodeposited Ni-W alloys.” *J. Serbian Chem. Soc.*, 66(11–12), 899–912.

Pan, Y., Jiang, S., Dai, C.-Y., Tang, T., Zhou, Z.-F., and Zhou, Y.-C. (2007). “Preparation and characterization of jet-electrodeposited nanocrystalline nickel coatings.” *Trans. Nonferrous Met. Soc. China*, 17(s1B), s770–s775.

Parthasaradhy, N. V. (1989). *Practical Electroplating Handbook*. Englewood Cliffs, N.J: Prentice Hall.

Parthasarathy, N. V. (1992). *Electroplating Handbooks*. Prentice Hall.

Paseka, I., and Velicka, J. (1997). “Hydrogen evolution and hydrogen sorption on amorphous smooth Me-P(x) (Me-Ni, Co and Fe-Ni) electrodes.” *Electrochimica Acta,* 42(2), 237–242.

Paunovic, M., and Schlesinger, M. (2000). *Modern electroplating*. John Wiley.

Paunović, P., Popovski, O., Dimitrov, A., Slavkov, D., Lefterova, E., and Jordanov, S. H. (2006). “Improvement of performances of complex non-platinum electrode materials for hydrogen evolution.” *Electrochimica Acta,* 52(4), 1810–1817.

Pavithra, G. P., and Hegde, A. C. (2013). “Development of nanostructure multilayer Co-Ni alloy coatings for enhanced corrosion protection.” *Anal Bioanal Electrochem,* 5(1), 59–73.

Peeters, P., Hoorn, G. V. D., Daenen, T., Kurowski, A., and Staikov, G. (2001). “Properties of electroless and electroplated Ni–P and its application in microgalvanics.” *Electrochimica Acta,* 47(1–2), 161–169.

Peipmann, R., Lange, R., Kubeil, C., Mutschke, G., and Bund, A. (2010a). “Magnetic field effects on the mass transport at small electrodes studied by voltammetry and magnetohydrodynamic impedance measurements.” *Electrochimica Acta,* 56(1), 133–138.

Pentland, N., Bockris, J., and Sheldon, E. (1957). “Hydrogen evolution reaction on copper, gold, molybdenum, palladium, rhodium, and iron: mechanism and measurement technique under high purity conditions.” *J. Electrochem. Soc.,* 104(3), 182.

Pérez-Alonso, F. J., Adán, C., Rojas, S., Peña, M. A., and Fierro, J. L. G. (2014). “Ni/Fe electrodes prepared by electrodeposition method over different substrates for oxygen evolution reaction in alkaline medium.” *Int. J. Hydrog. Energy,* 39(10), 5204–5212.

Peters, D. (1996). “Ultrasound in materials chemistry.” *J. Mater. Chem.,* 6(10), 1605–1618.

Pletcher, D. (1984). “Electrocatalysis: present and future.” *J. Appl. Electrochem.,* 14(4), 403–415.

Pollet, B. G. (2012). “Power ultrasound in electrochemistry.” *Wiley Online Libr.*
Pollet, B. G., and Ashokkumar, M. (2019). *Introduction to Ultrasound, Sonochemistry and Sonoelectrochemistry*. Springer Nature.

Prather, M. J. (2003). “An environmental experiment with H2?” *Science*, 302(5645), 581–582.

Pu, Z., Wei, S., Chen, Z., and Mu, S. (2016). “Flexible molybdenum phosphide nanosheet array electrodes for hydrogen evolution reaction in a wide pH range.” *Appl. Catal. B Environ.*, 196, 193–198.

Rabah, K. L., Chopart, J.-P., Schloerb, H., Saulnier, S., Aaboubi, O., Uhlemann, M., Elmi, D., and Amblard, J. (2004). “Analysis of the magnetic force effect on paramagnetic species.” *J. Electroanal. Chem.*, 571(1), 85–91.

Rabia, J., Tajamal, H., Saliha, S., and Shahid, A. M. (2011). “Magnetic field effects on the microstructural variation of electrodeposited nickel film.” *J. Mater. Sci. Eng. A*, 1(4A), 481.

Ragsdale, S. R., Grant, K. M., and White, H. S. (1998). “Electrochemically generated magnetic forces. Enhanced transport of a paramagnetic redox species in large, nonuniform magnetic fields.” *J. Am. Chem. Soc.*, 120(51), 13461–13468.

Raj, I. A. (1993). “Nickel-based, binary-composite electrocatalysts for the cathodes in the energy-efficient industrial production of hydrogen from alkaline-water electrolytic cells.” *J. Mater. Sci.*, 28(16), 4375–4382.

Raj, I. A., and Vasu, K. I. (1990). “Transition metal-based hydrogen electrodes in alkaline solution—electrocatalysis on nickel based binary alloy coatings.” *J. Appl. Electrochem.*, 20(1), 32–38.

Raj, I. A., and Vasu, K. I. (1992). “Transition metal-based cathodes for hydrogen evolution in alkaline solution: electrocatalysis on nickel-based ternary electrolytic codeposits.” *J. Appl. Electrochem.*, 22(5), 471–477.

Raj, I. A., and Venkatesan, V. K. (1988). “Characterization of nickel-molybdenum and nickel-molybdenum-iron alloy coatings as cathodes for alkaline water electrolysers.” *Int. J. Hydrog. Energy*, 13(4), 215–223.

Rao, V. R., Bangera, K. V., and Hegde, A. C. (2013). “Magnetically induced electrodeposition of Zn–Ni alloy coatings and their corrosion behaviors.” *J. Magn. Magn. Mater.*, 345, 48–54.

Rashid, M. M., Al Mesfer, M. K., Naseem, H., and Danish, M. (2015). “Hydrogen production by water electrolysis: a review of alkaline water electrolysis, PEM water electrolysis and high temperature water electrolysis.” *Int J Eng Adv Technol*, 4(3), 2249–8958.

Reddy, S., Du, R., Kang, L., Mao, N., and Zhang, J. (2016). "Three dimensional CNTs aerogel/MoSx as an electrocatalyst for hydrogen evolution reaction." *Appl. Catal. B Environ.*, 194, 16–21.

Roger, I., Shipman, M. A., and Symes, M. D. (2017). "Earth-abundant catalysts for electrochemical and photoelectrochemical water splitting." *Nat. Rev. Chem.*, 1(1), 1–13.

Rosalbino, F., Delsante, S., Borzone, G., and Angelini, E. (2008). "Electrocatalytic behaviour of Co–Ni–R (R= Rare earth metal) crystalline alloys as electrode materials for hydrogen evolution reaction in alkaline medium." *Int. J. Hydrog. Energy*, 33(22), 6696–6703.

Roy, S. (2009). "Electrochemical fabrication of nanostructured, compositionally modulated metal multilayers (CMMMs)." *Electrochem. Nanoscale*, Springer, 349–376.

Safizadeh, F., Ghali, E., and Houlachi, G. (2015). "Electrocatalysis developments for hydrogen evolution reaction in alkaline solutions–a review." *Int. J. Hydrog. Energy*, 40(1), 256–274.

Sakai, S., Nakanishi, S., and Nakato, Y. (2006). "Mechanisms of Oscillations and Formation of Nano-Scale Layered Structures in Induced Co-Deposition of Some Iron-Group Alloys (Ni−P, Ni−W, and Co−W), Studied by an In Situ Electrochemical Quartz Crystal Microbalance Technique." *J. Phys. Chem. B*, 110(24), 11944–11949.

Sapountzi, F. M., Gracia, J. M., Fredriksson, H. O., and Niemantsverdriet, J. H. (2017). "Electrocatalysts for the generation of hydrogen, oxygen and synthesis gas." *Prog. Energy Combust. Sci.*, 58, 1–35.

Schulz, R., Huot, J., Trudeau, M. L., Dignard-Bailey, L., Yan, Z. H., Jin, S., Lamarre, A., Ghali, E., and Van Neste, A. (1994). "Nanocrystalline Ni-Mo alloys and their application in electrocatalysis." *J. Mater. Res.*, 9(11), 2998–3008.

Schwarzacher, W. (2006). "Electrodeposition: A Technology for the Future." *Electrochem. Soc. Interface*, 4.

Shervedani, R. K., Alinoori, A. H., and Madram, A. R. (2008). "Electrocatalytic activities of nickel-phosphorous composite coating reinforced with codeposited graphite carbon for hydrogen evolution reaction in alkaline solution." *J New Mater Electrochem Syst*, 11(4), 259–265.

Shetty, S., and Hegde, A. C. (2017). "Electrodeposition of Sn-Ni alloy coatings for water-splitting application from alkaline medium." *Metall. Mater. Trans. B*, 48(1), 632–641.

Shetty, S., Sadiq, M. M. J., Bhat, D. K., and Hegde, A. C. (2016). “Development of multilayer Sn–Ni alloy coating by pulsed sonoelectrolysis for enhanced corrosion protection.” *RSC Adv.*, 6(81), 77465–77473.

Shibli, S. M. A., and Dilimon, V. S. (2007). “Effect of phosphorous content and TiO2-reinforcement on Ni–P electroless plates for hydrogen evolution reaction.” *Int. J. Hydrog. Energy*, 32(12), 1694–1700.

Simunovich, D., Schlesinger, M., and Snyder, D. D. (1994). “Electrochemically layered Copper-Nickel nanocomposites with enhanced hardness.” *J. Electrochem. Soc.*, 141(1), L10.

Slavcheva, E., Mokwa, W., and Schnakenberg, U. (2005). “Electrodeposition and properties of NiW films for MEMS application.” *Electrochimica Acta*, 50(28), 5573–5580.

Springer, T. E., Rockward, T., Zawodzinski, T. A., and Gottesfeld, S. (2001). “Model for polymer electrolyte fuel cell operation on reformate feed: effects of CO, H; 2 dilution, and high fuel utilization.” *J. Electrochem. Soc.*, 148(1), A11.

Spyrellis, N., Pavlatou, E. A., Spanou, S., and Zoikis-Karathanasis, A. (2009). “Nickel and nickel-phosphorous matrix composite electrocoatings.” *Trans. Nonferrous Met. Soc. China*, 19(4), 800–804.

Srivastava, M., Ezhil Selvi, V., William Grips, V. K., and Rajam, K. S. (2006). “Corrosion resistance and microstructure of electrodeposited nickel–cobalt alloy coatings.” *Surf. Coat. Technol.*, 201(6), 3051–3060.

Stansbury, E. E., and Buchanan, R. A. (2000). *Fundamentals of Electrochemical Corrosion*. ASM International.

Steinbach, J., and Ferkel, H. (2001). “Nanostructured Ni-Al2O3 films prepared by DC and pulsed DC electroplating.” *Scr. Mater.*, 44(8–9), 1813–1816.

Subramanya, B., Ullal, Y., Shenoy, S. U., Bhat, D. K., and Hegde, A. C. (2015). “Novel Co–Ni–graphene composite electrodes for hydrogen production.” *RSC Adv.*, 5(59), 47398–47407.

Suen, N.-T., Hung, S.-F., Quan, Q., Zhang, N., Xu, Y.-J., and Chen, H. M. (2017). “Electrocatalysis for the oxygen evolution reaction: recent development and future perspectives.” *Chem. Soc. Rev.*, 46(2), 337–365.

Sun, T., Cao, J., Dong, J., Du, H., Zhang, H., Chen, J., and Xu, L. (2017). “Ordered mesoporous NiCo alloys for highly efficient electrocatalytic hydrogen evolution reaction.” *Int. J. Hydrog. Energy*, 42(10), 6637–6645.

Tacken, R. A., and Janssen, L. J. J. (1995a). “Applications of magnetoelectrolysis.” *J. Appl. Electrochem.*, 25(1), 1–5.

Taniguchi, T., Sassa, K., Yamada, T., and Asai, S. (2000). “Control of crystal orientation in zinc electrodeposits by imposition of a high magnetic field.” *Mater. Trans. JIM*, 41(8), 981–984.

Tench, D., and White, J. (1984). “Enhanced tensile strength for electrodeposited nickel-copper multilayer composites.” *Metall. Trans. A*, 15(11), 2039–2040.

Thangaraj, V., Eliaz, N., and Hegde, A. C. (2009). “Corrosion behavior of composition modulated multilayer Zn–Co electrodeposits produced using a single-bath technique.” *J. Appl. Electrochem.*, 39(3), 339.

Thiemig, D., and Bund, A. (2008). “Characterization of electrodeposited Ni–TiO2 nanocomposite coatings.” *Surf. Coat. Technol.*, 202(13), 2976–2984.

Tian, L., Xu, J., and Xiao, S. (2011). “The influence of pH and bath composition on the properties of Ni–Co coatings synthesized by electrodeposition.” *Vacuum*, 86(1), 27–33.

Toghraei, A., Shahrabi, T., and Barati Darband, Gh. (2020). “Electrodeposition of self-supported Ni-Mo-P film on Ni foam as an affordable and high-performance electrocatalyst toward hydrogen evolution reaction.” *Electrochimica Acta*, 335, 135643.

Trasatti, S. (1972). “Work function, electronegativity, and electrochemical behaviour of metals: III. Electrolytic hydrogen evolution in acid solutions.” *J. Electroanal. Chem. Interfacial Electrochem.*, 39(1), 163–184.

Trotochaud, L., Young, S. L., Ranney, J. K., and Boettcher, S. W. (2014). “Nickel–iron oxyhydroxide oxygen-evolution electrocatalysts: the role of intentional and incidental iron incorporation.” *J. Am. Chem. Soc.*, 136(18), 6744–6753.

Tudela, I., Zhang, Y., Pal, M., Kerr, I., Mason, T. J., and Cobley, A. J. (2015). “Ultrasound-assisted electrodeposition of nickel: Effect of ultrasonic power on the characteristics of thin coatings.” *Surf. Coat. Technol.*, 264, 49–59.

Uhlemann, M., Krause, A., Chopart, J. P., and Gebert, A. (2005a). "Electrochemical deposition of Co under the influence of high magnetic fields." *J. Electrochem. Soc.*, 152(12), C817–C826.

Ullal, Y., and Hegde, A. C. (2014). "Electrodeposition and electro-catalytic study of nanocrystalline Ni–Fe alloy." *Int. J. Hydrog. Energy*, 39(20), 10485–10492.

Vargas-Uscategui, A., Mosquera, E., Chornik, B., and Cifuentes, L. (2015). "Electrocatalysis of the hydrogen evolution reaction by rhenium oxides electrodeposited by pulsed-current." *Electrochimica Acta*, 178, 739–747.

Vayenas, C. G., White, R. E., and Gamboa-Aldeco, M. E. (2008). *Modern Aspects of Electrochemistry 42*. Springer Science & Business Media.

Walker, C. T., and Walker, R. (1977). "Hardening effect of ultrasonic agitation on copper electrodeposits." *J. Electrochem. Soc.*, 124(5), 661.

Wang, C. B., Wang, D. L., Chen, W. X., and Wang, Y. Y. (2002). "Tribological properties of nanostructured WC/CoNi and WC/CoNiP coatings produced by electro-deposition." *Wear*, 253(5–6), 563–571.

Wang, H., Lee, H.-W., Deng, Y., Lu, Z., Hsu, P.-C., Liu, Y., Lin, D., and Cui, Y. (2015). "Bifunctional non-noble metal oxide nanoparticle electrocatalysts through lithium-induced conversion for overall water splitting." *Nat. Commun.*, 6(1), 1–8.

Wang, L., Gao, Y., Xue, Q., Liu, H., and Xu, T. (2005). "Microstructure and tribological properties of electrodeposited Ni–Co alloy deposits." *Appl. Surf. Sci.*, 242(3), 326–332.

Wang, M., Wang, Z., Gong, X., and Guo, Z. (2014). "The intensification technologies to water electrolysis for hydrogen production–A review." *Renew. Sustain. Energy Rev.*, 29, 573–588.

Wang, Y., Pu, Y., Ma, Z., Pan, Y., and Sun, C. Q. (2016). "Interfacial adhesion energy of lithium-ion battery electrodes." *Extreme Mech. Lett.*, 9, 226–236.

Wasekar, N. P., Verulkar, S., Vamsi, M. V. N., and Sundararajan, G. (2019). "Influence of molybdenum on the mechanical properties, electrochemical corrosion and wear behavior of electrodeposited Ni-Mo alloy." *Surf. Coat. Technol.*, 370, 298–310.

Waskaas, M., and Kharkats, Y. I. (1999). "Magnetoconvection Phenomena: A Mechanism for Influence of Magnetic Fields on Electrochemical Processes." *J. Phys. Chem. B*, 103(23), 4876–4883.

Wassef, O., and Fahidy, T. Z. (1976). “Magnetoelectrolysis in the presence of bubble formation at the cathode.” *Electrochimica Acta*, 21(10), 727–730.

Webb, P. R., and Robertson, N. L. (1994). “Electrolytic Codeposition of Ni-γAl2 O 3 Thin Films.” *J. Electrochem. Soc.*, 141(3), 669.

Wilcox, G. D., and Gabe, D. R. (1993). “Electrodeposited zinc alloy coatings.” *Corros. Sci.*, 35(5–8), 1251–1258.

Wu, G., Li, N., Dai, C. S., and Zhou, D. R. (2004). “Electrochemical preparation and characteristics of Ni–Co–LaNi5 composite coatings as electrode materials for hydrogen evolution.” *Mater. Chem. Phys.*, 83(2–3), 307–314.

Wu, M., Liu, G., Li, M., Dai, P., Ma, Y., and Zhang, L. (2010). “Magnetic field-assisted solvothermal assembly of one-dimensional nanostructures of Ni–Co alloy nanoparticles.” *J. Alloys Compd.*, 491(1), 689–693.

Xia, M., Lei, T., Lv, N., and Li, N. (2014). “Synthesis and electrocatalytic hydrogen evolution performance of Ni–Mo–Cu alloy coating electrode.” *Int. J. Hydrog. Energy*, 39(10), 4794–4802.

Xu, C., Zhou, J., Zeng, M., Fu, X., Liu, X., and Li, J. (2016). “Electrodeposition mechanism and characterization of Ni–Mo alloy and its electrocatalytic performance for hydrogen evolution.” *Int. J. Hydrog. Energy*, 41(31), 13341–13349.

Yogesha, S., Bhat, R. S., Venkatakrishna, K., Pavithra, G. P., Ullal, Y., and Hegde, A. C. (2011). “Development of nano-structured Zn-Ni multilayers and their corrosion behaviors.” *Synth. React. Inorg. Met.-Org. Nano-Met. Chem.*, 41(1), 65–71.

Yogesha, S., and Hegde, A. C. (2010). “Electrodeposition of high performance multilayer coatings of Zn–Co using triangular current pulses.” *Trans. IMF*, 88(6), 317–323.

Yogesha, S., Udupa, K. R., and Hegde, A. C. (2012). “Surface modification by multilayered Zn–Co alloy coatings.” *Surf. Eng.*, 28(1), 49–56.

You, B., Jiang, N., Sheng, M., Gul, S., Yano, J., and Sun, Y. (2015). “High-performance overall water splitting electrocatalysts derived from cobalt-based metal–organic frameworks.” *Chem. Mater.*, 27(22), 7636–7642.

Yuan, X.-Z. R., Song, C., Wang, H., and Zhang, J. (2009). *Electrochemical impedance spectroscopy in PEM fuel cells: fundamentals and applications*. Springer Science & Business Media.

Zamani, M., Amadeh, A., and Lari baghal, S. M. (2016). “Effect of Co content on electrodeposition mechanism and mechanical properties of electrodeposited Ni–Co alloy.” *Trans. Nonferrous Met. Soc. China*, 26(2), 484–491.

Zeng, K., and Zhang, D. K. (2011). “Recent progress in alkaline water electrolysis for hydrogen production and applications (vol 36, pg 307, 2010).” *Prog. Energy Combust. Sci.*, 37(5), 631–631.

Zheng, Z., Li, N., Wang, C.-Q., Li, D.-Y., Zhu, Y.-M., and Wu, G. (2012). “Ni–CeO_2 composite cathode material for hydrogen evolution reaction in alkaline electrolyte.” *Int. J. Hydrog. Energy*, 37(19), 13921–13932.

Zimmerman, A. F., Palumbo, G., Aust, K. T., and Erb, U. (2002). “Mechanical properties of nickel silicon carbide nanocomposites.” *Mater. Sci. Eng. A*, 328(1–2), 137–146.

Zou, X., and Zhang, Y. (2015). “Noble metal-free hydrogen evolution catalysts for water splitting.” *Chem. Soc. Rev.*, 44(15), 5148–5180.

LIST OF PUBLICATIONS

- Shetty, A.R. and Hegde, A.C. (2016). “Ultrasound induced co-deposition of Ni-Co alloy for better corrosion protection.” *Int. J. Innov. Res. Dev.*, 5(1), 207-211.
- Shetty A.R. and Hegde, A.C. (2017). “Study on the Effect of Current Density on Electrocatalytic Behavior of Ni–Co Alloy.” *International Journal of Chemical Engineering and Processing.*, 3(1), 9-23.
- Shetty, A.R. and Hegde, A.C.(2017). “Electrofabrication of Ni-Co-CNT composite coatings for hydrogen energy.” *Nanohybrids and composites*, 17,149-155.
- Shetty, A.R. and Hegde, A.C.(2017). “Development of multilayer Ni-Co alloy coatings by pulsed sonoelectrodeposition for better corrosion protection.” *Int. j. adv. chem. sci. appl.;*,5(1)9-15.
- Shetty, A.R. and Hegde, A.C. (2017). “Ultrasound induced multilayer Ni-Co alloy coatings for better corrosion protection.” *Surf. Coat. Technol.,* 322, 99-107.
- Shetty, A.R. and Hegde, A.C.(2018). “Effect of TiO_2 on electrocatalytic behavior of Ni-Mo alloy coating for hydrogen energy.” *Materials Science for Energy Technologies*; 1(2), 97-105.
- Shetty, A.R. and Hegde, A.C. (2018). “Electrodeposition of Ni-Mo alloy coatings for water splitting reaction.” In *AIP Conference Proceedings*; 1943(1), 020108. AIP Publishing.
- Shetty, A.R. and Hegde, A. C. (2020). “Effect of cadmium on corrosion performance of Ni-Mo alloy coating.” *Mater.Sci.Eng.* (under review).
- Shetty, A.R. and A. Chitharanjan Hegde(2021). “Magnetoelectrodeposition of Ni-Mo-Cd alloy coating for improved corrosion resistance.” *Chem. Data Collect.* 32,100639

LIST OF CONFERENCES ATTENDED

- Shetty, A.R. and Hegde, A.C.(2016). “Electrocatalytic behavior of Co -W alloy for hydrogen energy.”National Conference on Recent Trends in

Chemical Sciences (NCRTCS-2016), held at MIT Manipal, Karnataka on January 11-12, 2016.

- Shetty, A.R. and Hegde, A.C.(2016).“Electrofabrication of Ni-Co-CNT composite coatings for hydrogen energy.”International conference on nanoscience and nanotechnology for energy applications (EApp-2016), held at Satyabama University, Chennai on June 27-29, 2016.
- Shetty, A.R. and Hegde, A.C.(2016). “Ultrasound induced co-deposition of Ni-Co alloy for better corrosion protection.”National Conference on Recent Advances in industrial engineering and applied chemistry (NCRAIEAC-2016), held at SSIT, Tumkur on October 21-22, 2016.
- Shetty, A.R. and Hegde, A.C.(2017). “Development of multilayer Ni-Co alloy coatings by pulsed sonoelectrodeposition for better corrosion protection.” International conference on Recent Advance in Material Chemistry (ICRAMC 2017) , held at SRM university, Chennai. On February 15-17, 2017.
- Shetty, A.R. and Hegde, A.C.(2017). “Study of magnetic field effect on electrodeposition of Ni-Co alloy for improved corrosion protection.” International conference on Emerging Trends in Chemical Sciences (ICETCS 2017) , held at MIT, Manipal. September 14-16, 2017.
- Shetty, A.R. and Hegde, A.C (2018). “Electrodeposition of Ni-Mo alloy coatings for water splitting reaction.” International conference on Design, Materials and Manufacture (IcDeM 2018), held at NITK, Surathkal. January 29-31, 2018.
- Shetty, A.R. and Hegde, A.C (2018). “Two day workshop on metal finishing technologies On electroplating -2018”held at IISC Bangalore, February 1-2, 2018.
- Shetty, A.R. and Hegde, A.C (2018). “Effect of TiO_2 on electrocatalytic behavior of Ni-Mo Alloy boating for water splitting reaction.” International Conference on Electrochemistry in Advanced Materials, Corrosion and Radiopharmaceuticals (CEAMCR-2018) held at BARC, Mumbai 15-17, 2018.

- Shetty, A.R. and Hegde, A.C (2018). “Effect of CeO_2 on electrocatalytic behavior of Ni-Mo alloy coating for Hydrogen Energy.” International Conference on Sustainable Chemistry for Health Environment and Materials held at IICT-CSIR Laboratory, Hyderabad, and August 5-8, 2018.
- Shetty, A.R. and Hegde, A.C (2019). “Electrocatalytic Behavior of Ni-Mo-CeO_2 composite coating for Hydrogen Energy.”International conference on Nanoscience and nanotechnology (ICONN 2019), held at SRM University, Chennai on January 28-30, 2019.

BIODATA

PERSONAL DATA

Full Name : AKSHATHA R SHETTY

Date of Birth : 21 JANUARY 1993

Permanent Address : Sanjeevi Nilaya, Vaddameshwara, Perdoor Post-576124

Marital status : Married

Contact No. : 8722701182

e-mail id : 01akshathashetty@gmail.com

ACADEMIC CREDENTIALS

Doctor of Philosophy in Chemistry (Ph.D)(2015-2020)

Institution : National Institute of Technology Karnataka (NITK), Surathkal

Title : Electrofabrication of Ni based alloy coatings for Corrosion protection and water electrolysis

Supervisor : Prof. A Chitharanjan Hegde

PERIOD	QUALIFICATION	INSTITUTION	AGGREGATE (%)	RANK
2013-2015	Master of Science (Chemistry)	National Institute of Technology Karnataka, Surathkal	9.64 (CGPA)	I Rank with Gold medal
2010-2013	Bachelor of Science (PCM)	MGM College, Udupi	92.00	I Class with Distinction

RESEARCH EXPERIENCE

(1) Project in “ Synthesis and Characterization of phenothiazine based derivatives for DSSC application”, Dept. of Chemistry, NITK Surathkal (2015)

(2) IAS Sponsored project entitled “Synthesis and characterization of MBH adducts of bis(4-formylphenyl)amine”, Oraganic

Laboratory, C.L.R.I., Chennai (CSIR lab) (summer research-2014).

(3) VGST Bangalore Sponsored project entitled “Preparation of Chitosan based biodegradable polymers”, Dept. of Chemistry MGM College, Udupi (2012-2013).

RESEARCH PUBLICATION

- **Akshatha R Shetty** and A. Chitharanjan Hegde (2016) “Ultrasound induced co-deposition of Ni-Co alloy for better corrosion protection.”*International Journal of Innovative Research and Development.*, 5(1), 207-211.
- **Akshatha R Shetty** and A. Chitharanjan Hegde.(2017) “Study on the Effect of Current Density on Electrocatalytic Behavior of Ni–Co Alloy.” *International Journal of Chemical Engineering and Processing.*, 3(1), 9-23.
- **Akshatha R Shetty** and A. Chitharanjan Hegde (2017). “Electrofabrication of Ni-Co-CNT composite coatings for hydrogen energy.” *Nanohybrids and composites.*, 17,149-155.
- **Akshatha R Shetty** and A. Chitharanjan Hegde (2017).“Development of multilayer Ni-Co alloy coatings by pulsed sonoelectrodeposition for better corrosion protection.”*International Journal of advanced chemical science and Applications,*5(1),9-15.
- **Akshatha R Shetty** and A. Chitharanjan Hegde (2017). “Ultrasound induced multilayer Ni-Co alloy coatings for better corrosion protection.”*Surf. Coat. Technol.,*322,99-107.
- **Akshatha R Shetty** and A. Chitharanjan Hegde(2018).“Effect of TiO_2 on electrocatalytic behavior of Ni-Mo alloy coating for hydrogen energy.” *Materials Science for Energy Technologies*, *1*(2), 97-105.
- **Akshatha R Shetty** and A. Chitharanjan Hegde (2018). “Electrodeposition of Ni-Mo alloy coatings for water splitting reaction. In *AIP Conference Proceedings* (Vol. 1943, No. 1, p. 020108). AIP Publishing.
- C Shamitha, **Akshatha R Shetty**, Ampar Chitharanjan Hegde and Srinivasan Anandhan(2019).“Sol-gel electrospun ZnMn₂O₄ nanofibers as bifunctional electrocatalysts for hydrogen and oxygen evolution reactions.” *Mater. Res. Express* ,doi:10.1088/2053-1591/ab51aa

- B. Sachin Kumar, Kartick Tarafder, **Akshatha R Shetty**, A. Chitharanjan Hegde, Visweswara C. Gudla, Rajan Ambat, Sreeram K. Kalpathy and S. Anandhan(2019). "Polymorph nickel titanate nanofibers as bifunctional electrocatalysts towards hydrogen and oxygen evolution reactions." *Dalton Trans.*,48, 12684-12698.

LIST OF CONFERENCES/WORKSHOP ATTENDED

- **Akshatha R Shetty** and A. Chitharanjan Hegde(2019). "Electrocatalytic Behavior of Ni-Mo-CeO_2 Composite Coating for Hydrogen Energy."International conference on Nanoscience and nanotechnology(ICONN 2019),held at SRM University, Chennai on January 28-30,2019.
- **Akshatha R Shetty** and A. Chitharanjan Hegde (2018). "Electrodeposition of Ni-Mo Alloy Coatings For Water Splitting Reaction."International conference on Design, Materials and Manufacture (IcDeM 2018), held at NITK, Surathkal. January 29-31,2018.
- Akshatha R Shetty and A. Chitharanjan Hegde (2018). "Two day workshop on metal finishing technologies On electroplating -2018"held at IISC Bangalore, February 1-2, 2018.
- **Akshatha R Shetty** and A. Chitharanjan Hegde (2018)."Effect of TiO_2 on Electrocatalytic Behavior of Ni-Mo Alloy Coating for Water Splitting Reaction." International Conference on Electrochemistry in Advanced Materials, Corrosion and Radiopharmaceuticals (CEAMCR-2018) held at BARC, Mumbai 15-17, 2018.
- **Akshatha R Shetty** and A. Chitharanjan Hegde (2018). "Effect of CeO_2 on Electrocatalytic Behavior of Ni-Mo Alloy Coating for Hydrogen Energy." International Conference on Sustainable Chemistry for Health Environment and Materials held at IICT-CSIR Laboratory, Hyderabad, August 5-8, 2018.
- **Akshatha R Shetty** and A.Chitharanjan Hegde.(2017). "Development of multilayer Ni-Co alloy coatings by pulsed sonoelectrodeposition for better corrosion protection." International conference on Recent Advance in Material

Chemistry (ICRAMC 2017) , held at SRM university, Chennai. On February 15-17,2017.

- **Akshatha R Shetty** and A.Chitharanjan Hegde.(2017). “Study of magnetic field effect on electrodeposition of Ni-Co alloy for improved corrosion protection.” International conference on Emerging Trends in Chemical Sciences (ICETCS 2017) , held at MIT, Manipal. September 14-16, 2017.
- **Akshatha R Shetty** and A.Chitharanjan Hegde (2016) **“**Electrocatalytic behaviour of Co -W alloy for hydrogen energy.”National Conference on Recent Trends in Chemical Sciences (NCRTCS-2016), held at MIT Manipal, Karnataka on January 11-12, 2016.
- **Akshatha R Shetty** and A.Chitharanjan Hegde (2016).“Electrofabrication of Ni-Co-CNT composite coatings for hydrogen energy.”International conference on nanoscience and nanotechnology for energy applications (EApp-2016), held at Satyabama university, Chennai on June 27-29,2016.
- **Akshatha R Shetty** and A. Chitharanjan Hegde (2016). “Ultrasound induced co-deposition of Ni-Co alloy for better corrosion protection.”National Conference on Recent Advances in industrial engineering and applied chemistry (NCRAIEAC-2016), held at SSIT, Tumkur on October 21-22, 2016.

AWARDS AND ACHIEVMENTS

1. Won “Rula Research Ratna Awards 2019” as a Best Researcher in Electrocatalysis” awarded by Rula awards and powered by World research Council at Trichy, Tamilnadu.
2. Best poster award in ICETCS-2017, International conference on Emerging Trends in Chemical Sciences, held at MIT, Manipal. September 14-16, 2017.
3. Won Institute Medal and Prof. G. H. Kulkarni Gold Medal-2015, in Master of Science of science at NITK, Surathkal.

Languages Known **:** English, Hindi, Kannada, Tulu

Interests and Hobbies: Reading books, Listening music, Singing, Shuttle Badminton, Jogging.

REFERENCES

1. **Prof.A.Chitharanjan Hegde**

   Professor and Former Head
   Department of Chemistry
   National Institute of Technology Karnataka, Surathkal
   Srinivasnagar-575 025. INDIA.
   Mobile: 9980360242

2. **Prof. A. Nityananda Shetty**

   Department of Chemistry
   National Institute of Technology Karnataka, Surathkal
   Srinivasnagar-575 025. INDIA.
   Mobile: 9448779922

DECLARATION

I hereby declare that the information furnished above is true to the best of my Knowledge.

Yours Sincerly,
Mrs.Akshatha R Shetty